OCTOBER 9, 2019

Multiple Molecular Mechanisms Contribute Towards *In Vitro* Resistance to Tyrosine Kinase Inhibitors In Chronic Myeloid Leukaemia

BENJAMIN LEOW
LEUKAEMIA RESEARCH LABORATORY, SAHMRI
School of Medicine, Faculty of Health Sciences, University of Adelaide

i. Abstract

Resistance to therapeutic drugs is detrimental to treatment efficacy in chronic myeloid leukaemia (CML). CML is driven by the constitutive activity of the tyrosine kinase, Bcr-Abl, and has been treated effectively, in the majority of patients, using tyrosine kinase inhibitor (TKI) therapy. However, therapeutic TKI resistance often results in suboptimal treatment response. The molecular mechanisms of TKI resistance include: overexpression of Bcr-Abl; perturbed activity of cell membrane influx/efflux transporters; amino acid substitutions in the Bcr-Abl kinase domain precluding TKI binding (known as kinase domain mutations); and loss of dependence on Bcr-Abl kinase activity, via the gain of alternate driver function (known as Bcr-Abl independence). There is a temporal order to the acquisition of resistance mechanisms, with shifts in clonal architecture over time and treatment altering therapy sensitivity. This thesis explores the emergence of resistance to the TKIs dasatinib and ponatinib with regard to CML, investigating the molecular mechanisms of TKI resistance, to identify novel therapeutic strategies for circumventing resistance and improving treatment outcomes.

The initial experiments described development of a leukaemic cell model of TKI resistance. Using gradually increasing concentrations of the TKI dasatinib, TKI resistance was induced. A dasatinib resistant K562 cell line was established by culture in increasing concentrations of dasatinib over several months. Intermediate cell line samples were harvested over the course of TKI dose escalation and were interrogated for TKI sensitivity by TKI-induced cell death assay and phospho-CrkL IC50. Results indicated the loss of dasatinib and ponatinib sensitivity and efficacy with prolonged dasatinib exposure. The expression of *BCR-ABL1* gene transcript and protein levels were analysed, demonstrating *BCR-ABL1* overexpression as an early occurring resistance mechanism. The Bcr-Abl kinase domain mutation, T315I, was observed emerging late in dasatinib dose escalation, conferring complete dasatinib resistance. Dose escalation intermediates were further examined by transcriptome sequencing. By interrogating global gene expression perturbation and genetic structural rearrangements, putative resistance mechanisms were identified: a) overexpression of the drug transporter ABCG2, and b) expression of the rare *BCR-ABL1* transcript isoform, e6a2.

The identification of *ABCG2* expression in mRNAseq experiments was validated by assays to demonstrate ABCG2 function and involvement in TKI resistance, confirming ABCG2 overexpression as a critical early resistance mechanism. Cell death and IC50 assays were performed in the presence of the ABCG2 inhibitor, Ko143, which sensitised ABCG2 overexpressing cells to TKI-based inhibition. It was demonstrated, for the first time, that ABCG2 is able to confer decreased ponatinib sensitivity. Interestingly, the loss of ABCG2 expression coincided with the gain of T315I, demonstrating the competitive advantage of T315I-positive cells.

The role of the e6a2 *BCR-ABL1* fusion transcript in TKI resistance was investigated. *BCR-ABL1* e6a2 gene expression was quantified in dasatinib resistant cells using RT-qPCR and DNA qPCR, demonstrating a transient peak in expression, followed by a distinct reduction. Intriguingly, this reduction in *BCR-ABL1* expression coincided with the gain of ABCG2. To determine whether e6a2 was less sensitive to TKI than the typical e14a2 (p210) or e1a2 (p190) Bcr-Abl fusions, these were cloned into a Ba/F3 pro-B cell line. All isoforms were able to transform cells to IL-3 independence, demonstrating the leukaemia driving activity of Bcr-Abl. TKI-induced cell death experiments determined that e6a2 expressing cells were less sensitive to dasatinib than Ba/F3 cells harbouring the e14a2 isoform. Overall, several resistance mechanisms were identified and explored, however more may remain undetected. Results suggest a model of selective pressure in drug resistance, whereby leukaemic cells expressing the most efficient drug resistance mechanisms are selected for, eventually becoming the predominant cell population. These data and conclusions have bearing on the treatment of Bcr-Abl driven leukaemia, guiding the development of better therapeutic targets and strategies.

ii. Declaration

I certify that this work contains no material which has been accepted for the award of any other degree or diploma in my name in any university or other tertiary institution and, to the best of my knowledge and belief, contains no material previously published or written by another person, except where due reference has been made in the text. In addition, I certify that no part of this work will, in the future, be used in a submission in my name for any other degree or diploma in any university or other tertiary institution without the prior approval of the University of Adelaide and where applicable, any partner institution responsible for the joint award of this degree.

I give permission for the digital version of my thesis to be made available on the web, via the University's digital research repository, the Library Search and also through web search engines, unless permission has been granted by the University to restrict access for a period of time.

Benjamin Leow

iii. Scholarships and awards

Australian Postgraduate Award

Awarded February 2015

$25849 per annum for 42 months

Florey Medical Research Foundation Travel Grant

Awarded October 2015

$250 one time

SAHMRI Research Office Travel Scholarship

Awarded January 2016

$1500 one time

Institute of Molecular Bioscience Travel Scholarship

Awarded June 2016

$300 one time

Cancer Council Beat Cancer Project Supplementary Scholarship

Awarded July 2016

$5000 per annum for 24 months

iv.   Presentation of work

23rd Congress of EHA: The European Hematology Association

14th-17th June 2018

Poster presentation: 'Clonal Selection Determines Resultant Dominance of Tyrosine Kinase Inhibitor-Resistant Cells in CML'.

Leow B, Eadie L, Pagani I, Yeung D, Hughes T, White D

EMBL Postgraduate Research Symposia

3rd-5th November 2017

Oral presentation: 'Exploring TKI Resistance in CML'.

Leow B, Yeung D, Eadie L, White D.

Florey Postgraduate Research Conference

29th September 2016

Poster presentation: 'Detection of a Rare e6a2 Bcr-Abl Variant in a Dasatinib-Resistant CML Cell Population'.

Leow B, Kok C, Pagani I, Eadie L, White D.

HAA Annual Scientific Meeting

18th-21st October 2015

Oral presentation: 'Elucidating the Role of the T315I Mutation in CML'.

Leow B, Eadie LN, Leclercq T, White DL.

ASMR Annual Scientific Meeting

3rd June 2015

Oral presentation: 'The T315I Bcr-Abl mutation in CML and ALL: A mere case of altered drug binding?'

Leow B, Saunders V, Eadie L, Leclercq T, Hughes T, White D.

v. Acknowledgements

To those who have helped me finish this work, I owe my sincere gratitude. If I continue studying the health sciences in the future, it will be because of the caring, inquisitive, and generally brilliant souls that it attracts.

To my supervisors, Deb, Laura, and David, thank you for undertaking the immense task of supervising me. The scientific and personal guidance you provided stopped me slipping through the cracks when it was hard. Laura, from day one you've been showing me the ropes in and out of the lab; I've learned countless techniques and tips from you. The fine-toothed comb to which you subjected to my work and drafts showed me the rigour and detail required of science, and I regret that I didn't take on some of your organisational habits sooner. Thanks David, for the astute critique of my drafts, keeping my work focussed on the clinically relevant and useful. Deb, having your experience and knowledge on hand was critical in shaping the direction of my project, and over my time with the leukaemia group, you've been a supportive lab ~~mum~~ nan, who has always had my back. Additionally, Tam for supervising me during the beginning of my candidature, I owe my sincere appreciation.

The leukaemia research lab at SAHMRI has been an enjoyable group to work with for the past 5 years, and I've always felt looked after during my time here, never struggling to find someone to help with any challenges. Steph, Bron, and Janey, the support you've given organising administrative aspects of my project was invaluable to me, and I would certainly still be lost in a maelstrom of paper if it were not for your help. Chung, thank you for being a driving force with identification the e6a2 fusion, for assistance and training with data analysis, and for many valuable discussions of science and statistics. Tim, it was great to have your expertise on hand for feedback and during lab meetings. Thanks Ilaria for help following up on e6a2 and generally being a PCR wizard. Thank you Barb, your assistance with the bacterial cloning was invaluable. Cheers Randall, not just for the sage flow advice and assistance, but also for providing me with half my wardrobe, most of my shoe rack, and my bike pedals to boot. To Kate, thank you for your help with the retroviral work, and for your friendship. Verity, cheers for all of your help in the lab, for saving so many of my gels and other potential lab

vi. Acronyms

Acronym	Expansion
7-AAD	7-aminoactinomycin D
Abl	Abelson murine leukaemia viral homolog (protein)
ABL1	Abelson murine leukaemia viral homolog (gene)
ADP	Adenosine diphosphate
AGRF	Australian Genome Research Facility
ALL	Acute lymphoblastic leukaemia
AML	Acute myeloid leukaemia
ATP	Adenosine triphosphate
BAM	Binary alignment map
BCR	Breakpoint cluster region (gene)
Bcr	Breakpoint cluster region (protein)
bp	Base pair
BSA	Bovine serum albumin
CMV	Cytomegalovirus
DEPC	Diethyl pyrocarbonate
DMEM	Dulbecco's modified Eagle's medium
DMSO	Dimethyl sulfoxide
DNA	Deoxyribonucleic acid
eGFP	Green fluorescent protein
ERK	Extracellular signal-related kinases
FACS	Flow assisted cell sorting
FCS	Foetal calf serum
FISH	Fluorescence *in situ* hybridisation
GAP	GTPase activating protein
GDP	Guanine diphosphate
GEF	Guanine exchange factor
GMO	Genetically modified organism
Grb2	Growth factor receptor-bound protein 2
GTP	Guanine triphosphate
HBSS	Hank's balanced salt solution
HEPES	4-(2-hydroxyethyl)-1-piperazineethanesulfonic acid
IBC	Institutional Biosafety Committee
IMDM	Iscove's modified Dulbecco Medium
IUR	Intracellular uptake and retention
JAK	Janus kinase
JNK	Jun N-terminal kinases
kbp	Kilo base pairs
kDa	Kilo Dalton
MAPK	Mitogen activated protein kinases
MMR	Major molecular response

mTOR	Mammalian target of rapamycin
NCS	Newborn calf serum
OGTR	Office of Gene Technology Regulation
PBS	Phosphate buffered saline
PCR	Polymerase chain reaction
PDGF	Platelet derived growth factor
PDGFR	Platelet derived growth factor receptor
Ph	Philadelphia chromosome
PIP2	Phosphotidyl inositol (4,5)-bisphosphate
PIP3	Phosphotidyl inositol (3,4,5)-trisphosphate
PMSF	Phenylmethylsulfonyl fluoride
PVDF	Polyvinyline difluoride
qPCR	Quantitative polymerase chain reaction
RCF	Relative centrifugal force
RO	Reverse osmosis
rpm	Revolutions per minute
RPMI-1640	Roswell Park Memorial Institute medium
RT-qPCR	Reverse transcriptase-quantitative polymerase chain reaction
SDS	Sodium dodecyl sulfate
SILAC	Stable isotope labelling with amino acids in cell culture
SOS1	Son of Sevenless homolog 1
STAR	Spliced transcripts alignment to a reference
STAT	Signal transduction and activation of transcription
STRING	Search tool for the retrieval of interacting genes/proteins
TBS	Tris buffered saline
TBST	Tris buffered saline +Tween20

1 Introduction

1.1 Chronic Myeloid Leukaemia

The first recorded case of chronic myeloid leukaemia (CML) was described in 1845 by physician and pathologist, John Hughes Bennett (1). Though the cause was unknown, Bennett described symptoms of spleen, liver and lymph node enlargement, and material resembling thick pus exuded from cut veins (2). The patient, treated with purgatives, potassium iodide, and the application of leeches, died from the disease three months following diagnosis. Death was attributed to "the presence of purulent matter in the blood" (3). Today, the World Health Organization describes CML as "a myeloproliferative disorder affecting the hematopoietic stem cell compartment" (4). As its name suggests, chronic myeloid leukaemia is a cancer of the granulocytic lineage cells, including neutrophils, eosinophils, basophils, and their stem cell precursors. The overproduction of these cells in the bone marrow and peripheral blood results in disease (5, 6), and can be seen in Figure 1.1. Affecting around 1-2 per 100,000 adults, CML accounts for ~15% of newly diagnosed leukaemia in adults, and there are approximately 340 new patients diagnosed in Australia each year (7, 8). Little is known of CML risk factors, although exposure to ionising radiation increases rates of CML (9).

In patients with CML, anaemia, thrombocytosis and neutrophilia can result in patient fatigue, immunosuppression, and propensity to bleed and bruise easily. However, ~50% of CML cases are asymptomatic, and disease diagnosis occurs following routine physical examination or blood tests (7). As the disease progresses, splenomegaly can lead to abdominal discomfort as the excess leukocytes overflow to lymphatic tissue (8). The disease is often indolent. However, without effective treatment, CML is almost universally fatal. CML is typically identified in its less aggressive chronic phase, progressing over 5-8 years through an accelerated phase and ultimately to blast crisis (7). Blast crisis is characterised by a block in cellular differentiation, resulting in an increase in the proportion of immature blast cells in the bone marrow and peripheral blood. As genetic abnormalities accumulate in the leukaemic cell, symptoms worsen, and patients typically succumb to the disease (10).

1.2 The molecular biology of CML

1.2.1 The Philadelphia chromosome and Bcr-Abl

Much is now known about the genetic and molecular basis of the disease. There is a consistent genetic abnormality underlying the malignant transformation in patients with CML. Nowell and Hungerford identified the Philadelphia (Ph) chromosome in patient leukaemic cells; a genetic hallmark associated of CML, named for the place of its discovery (11). Using improved cytogenetic Giemsa banding techniques, Janet Rowley expanded on their research, elucidating the origins of the Ph chromosome: a translocation between chromosomes 9 and 22 (t(9;22)(q34;q11) (Figure 1.2) (12). The translocation is thought to arise due to a double strand break of the two DNA molecules, followed by aberrant DNA repair joining the chromosomes, and sequencing of the Ph breakpoint location has identified Alu repeat sequences which could facilitate DNA strand end joining (13). The Ph chromosome is consistently observed in the leukaemic cells of CML and ALL patients, providing a genetic identifier for CML cells as determined by FISH or other cytogenetic analysis (5).

As a result of the translocation event, two genes are fused together: the breakpoint cluster region (*BCR*) gene on chromosome 22, with the Abelson murine leukaemia viral oncogene homolog 1 (*ABL1*) gene on chromosome 9, giving rise to the *BCR-ABL1* fusion gene. *BCR-ABL1* is an oncogene; enforced expression in the murine haematopoietic cell line, Ba/F3, results in a rapid malignant transformation (14, 15), and the introduction of *BCR-ABL1* into haematopoietic cells in murine models induces a myeloproliferative disease (16-18). Such a specific marker of disease allowed for development of molecular assays that measure *BCR-ABL1* gene transcript expression using RT-qPCR, for disease diagnosis and monitoring (19). The fusion of *BCR* to *ABL1* removes the 5' regulatory elements of the *ABL1* gene, relegating transcriptional control to the constitutive *BCR* promoter region (20, 21). Thus, the fusion gene is transcribed and translated as a fusion protein, with both *ABL1* and *BCR* sequences contributing important functional elements to its oncogenic activity. In the majority of patients, a fusion from intron 13 or 14 of *BCR*, to a region within the ~300 kb breakpoint region in intron 1 of *ABL1*, gives rise to a 210 kD protein product known as Bcr-Abl p210 (5). However, several transcript and protein isoforms have been identified in CML: genomic *BCR* breakpoints are found in introns 1 to 19, and genomic *ABL1* breakpoints are available within

introns 1 and 2 (Figure 1.3) (22). These are transcribed as a number of different *BCR-ABL1* transcripts. The Ph chromosome and *BCR-ABL1* transcript is also associated with other leukaemias; a breakpoint fusing *BCR* exon 1 to *ABL1* exon 2 (e1a2 transcript, giving rise to the p190 protein) is associated with ~30% of adult acute lymphoblastic leukaemia (ALL) cases, known as Ph+ ALL (23, 24).

The different *BCR* and *ABL1* breakpoints can result in translation of a range of protein isoforms which harbour varying functional domains. However, regardless of the isoform present, it is the tyrosine kinase activity of the translated Bcr-Abl protein, derived from the Abl kinase domain region, which is the primary driver of the disease phenotype (25). The physiological properties of both Abl and Bcr are relevant for understanding the oncogenic properties of the fused Bcr-Abl variant isoforms, and will be discussed below.

1.2.2   Structure and function of Abelson kinase

The highly conserved and ubiquitously expressed wildtype *ABL1* proto-oncogene encodes a non-receptor tyrosine kinase, Abl, which phosphorylates specific tyrosine residues on protein cofactors and is an important mediator of proliferative growth factor signalling. Abl kinase activation has been demonstrated following stimulation by platelet derived growth factor (PDGF), members of the epidermal growth factor (EGF) family, and transforming growth factor-ß (TGF-ß) cytokines (26). Canonical signal transduction downstream of Abl kinase occurs through induction of extracellular signal regulated kinase 5 (ERK5), Janus kinase/signal transduction and activation of transcription (Jak2/STAT5), and c-Jun N-terminal kinase (JNK) proteins, which permit activation of downstream effector, the proto-oncogenic transcription factor Myc (26).

The Abl protein contains three nuclear localisation domains and one nuclear export signalling domain, which shuttle the protein between the nucleus and cytosol. Abl contains protein binding SH2 and SH3 domains, as well as a catalytic tyrosine kinase domain (27). Proline rich regions of Abl bind and interact with the SH3 domains of protein scaffolding cofactors, such as Crk (28). Physiologically, Abl plays an important role in leukocyte, cardiomyocyte and osteoblast development, acting as mediators of growth factor signal transduction. Disruption of the *ABL1* gene transcript in C57BL/6J murine models results in a ~50% loss of neonate

viability, with gene knockout resulting in splenic and thymic atrophy, impaired lymphoid development, cardiac abnormality, and defective osteoblast proliferation (26, 29).

In addition to CML, the dysregulated and aberrant activity of Abl kinase has been implicated in several malignancies, including breast, lung, ovarian, skin, bladder, colorectal, and renal cell carcinomas (30). Aberrant Abl kinase activation has also been identified in other blood cancers, including acute myeloid leukaemia, and both B- and T-cell ALL (30). In addition to acting as a proliferative driver, Abl activity is known to regulate epithelial cell polarity and tumour epithelial-mesenchymal transition, leading to increased cell invasion and metastasis (30).

The kinase activity of native Abl is tightly regulated through multiple mechanisms. Principle kinase activity moderation occurs via an autoinhibitory mechanism, mediated by its N-terminal cap (31). Crystallographic studies of Abl have demonstrated the presence of a hydrophobic pocket within the catalytic kinase domain, which, when bound to the myristoylated N-terminal region of Abl, results in an inhibitory conformational change whereby the SH2 and SH3 domains bind distal regions in the kinase domain, losing an activating phosphorylated tyrosine residue at position 245 (27, 32). Thus, native Abl is typically not kinase active. In CML, the 5' fusion of *BCR* replaces the N-terminal cap region, resulting in Bcr-Abl autophosphorylation, constitutive kinase activity, and disease.

1.2.3 Structure and function of the Bcr protein

The *BCR* gene also encodes a protein kinase, alternatively spliced to yield a 130 or 160 kDa serine-threonine kinase (33, 34). Native Bcr harbours three major functional domains: a serine/threonine kinase domain, a Dbl-homologous (DH) guanidine exchange factor (GEF) domain, and a C-terminal Rac GTPase activating protein (GAP) domain (Figure 1.4) (34). A central pleckstrin homology (PH) domain is able to bind PIP2 and PIP3 molecules, localising Bcr to plasma membranes. Additionally, an N-terminal coiled-coil oligomerisation domain mediates protein homodimerisation and kinase-activating autophosphorylation. Immunoprecipitation of Bcr and its interacting proteins recovers a 650 kDa protein complex, demonstrating the protein's extensive scaffolding and cofactor recruitment (33). It is likely that signalling through the Bcr protein complex is involved in haematopoiesis and cell

differentiation. Through protein-protein interactions of its DH domain, Bcr has been demonstrated to stimulate GTP binding to RhoA, Rac1, Rac2, and Cdc42 (35). The members of the Rho/Rac family of GTPases coordinate diverse cellular functions, and importantly, are central to the development and differentiation of haematopoietic cells (36). It is possible that Bcr activity is involved with mitogenesis and cell cycle control, through interactions with Myc (37), and the tumour suppressor Bap-1 (38). Recently, Bcr was demonstrated to play a role in activation of inflammatory NF-κB signalling, through interactions with casein kinase II (39). The diverse cell signalling roles and extensive protein scaffolding interactions of Bcr are important for the oncogenic signalling profile of the Bcr-Abl fusion protein.

1.2.4   Oncogenic kinase signalling of p210 Bcr-Abl

With both Abl and Bcr independently regulating several aspects of cellular signalling and haematopoiesis, the fusion of the two proteins produces a potent oncogenic entity, which is independently capable of driving the CML phenotype. The phosphorylation cascade of signal activation induced by the aberrant, constitutive kinase activity of Bcr-Abl impacts several proliferative pathways (Figure 1.5). Tyrosine kinase activity is performed by the Abl kinase domain, however the signalling pathway activation profile of Bcr-Abl is more complex than that of Abl alone. Bcr-Abl tetramerisation, mediated by the Bcr oligomerisation domain, is critical for full tyrosine kinase activation (40-42). Canonical Abl signalling occurs through activation of the mitogen activated protein kinase (MAPK) and Jak/STAT pathways. These pathways are also activated by Bcr-Abl, however, the kinase interactions are more diverse than that of native Abl. Within Bcr, the phosphorylated tyrosine 177 forms critical interactions with the Grb2 adaptor protein, which in turn recruits the Son of Sevenless homolog 1 (SOS1) protein via its SH3 domain. The Bcr-Abl/Grb2/SOS1 complex is able to stimulate conversion of GDP to GTP on the Ras protein, potently activating the proliferative MAPK signalling pathway (43, 44). Grb2 also mediates Bcr-Abl activation of the Src family kinases Hck and Lyn, which are important transducers of growth factor signalling (45). Src kinase activation can in turn mediate the downstream activation of STAT5 (46).

In addition to canonical pathway activation through Jak proteins, the direct phosphorylation of STAT1 and STAT5 proteins by Bcr-Abl has been described, independent of Jak

phosphorylation (47). Often upregulated in several cancer types, the dimerization and nuclear translocation of phosphorylated STAT5 results in activation of Myc, D-type cyclins, Bcl-2, Bcl-xL, and several other genes involved in cell cycle, chromatin remodelling, and protection from apoptosis (48, 49). Each signalling pathway activated contributes to CML oncogenesis; it has been demonstrated that functional cooperation of STAT, PI3K/Akt and MAPK pathway activation is required for the full oncogenic transformation potential of Bcr-Abl (50).

Additionally, Bcr-Abl p210 is a potent activator of the PI3K/Akt signalling pathway (51), promoting cell survival through activation of mammalian target of rapamycin (mTOR) signalling and downstream gene expression changes (43, 44). Bcr-Abl kinase activity results in the repression of apoptotic signalling, through inhibitory phosphorylation of the pro-apoptotic Bad protein (52). Bcr-Abl is also known to be a potent activator of Myc signalling, through multiple overlapping pathways. Expression of Myc is regulated by PI3K/Akt signalling, and phosphorylation of Myc by Jak2 is associated with the loss of proteasomal Myc degradation, resulting in increased Myc activation (53-55). Interestingly, it has been demonstrated that *BCR* and *BCR-ABL1* gene expression is upregulated by Myc activation, leading to a positive feedback loop of proliferative and oncogenic signalling. Bcr-Abl activity has been also demonstrated to increase genomic instability (10, 56). This occurs both directly, with Bcr-Abl increasing reactive oxygen species and DNA mutation(s) (57), but also indirectly with downstream signalling pathway activation protecting leukaemic cells from apoptosis, allowing DNA damage to accrue (58, 59). CML progression to blast crisis coincides with the gain of multiple genetic abnormalities, and the increased mutation rate caused by Bcr-Abl signalling may be central to disease propagation.

1.3 The contribution of alternate Bcr structure to Bcr-Abl oncogenesis

1.3.1 Bcr-Abl structure diversity and leukaemic phenotype

Approximately 95% of the *BCR-ABL1* breakpoints in CML patients occur between exons 12 and 16 of *BCR*, and within intron 1 of *ABL1*, in a region known as the 'major' breakpoint cluster region, M-bcr (Figure 1.3). Approximately half of the CML *BCR-ABL1* transcript breakpoints occur immediately 3' of exon 14, resulting in an 8.5 kb transcript known as e14a2 (formerly

b3a2) (60, 61). Normal *BCR-ABL1* fusion transcript nomenclature joins the *BCR* 3' breakpoint location (e.g. *BCR* exons 1-14: e14) with the *ABL1* 5' breakpoint location (e.g. *ABL1* exons 2-14: a2). Another ~30% of *BCR-ABL1* breakpoints in CML result in fusion of *BCR* exon 13 with *ABL1* exon 2, generating the e13a2 (formerly b2a2) transcript. Both the e14a2 and e13a2 transcripts are translated as the typical p210 Bcr-Abl protein.

However, several other BCR breakpoints have been identified in CML patients, ranging from *BCR* exon 1 to exon 19 (61). The e1a2 fusion transcript is translated as the smaller p190 Bcr-Abl protein isoform (62). As previously stated, this isoform is most commonly associated with Ph+ ALL; an aggressive, often fatal disease (62). These patients typically have less favourable treatment response and a fast disease progression (63, 64). There is conjecture as to whether the p190 isoform is a result of, or causative of, the more aggressive ALL phenotype (61). Conversely, the e19a2 transcript is translated as a 230 kDa protein. This p230 isoform is associated with a more benign leukaemic phenotype, characterised by a higher mature granulocyte and platelet count; it has been hypothesised that this is due to the leukaemic cells retaining the capacity for normal neutrophilic granulocyte differentiation (61). Conversely, Pane *et al* hypothesised that disease indolence was due to p230 having a lower intrinsic kinase activity (22), with other studies describing lower levels of transcript expression associated with the e19a2 *BCR-ABL1* fusion (65).

Following identification of the e1a2 chromosomal fusion in cases of Ph+ ALL, several studies investigated the differences in disease phenotype associated with different Bcr-Abl isoforms. Melo reviewed the contribution of the Bcr sequence, observing that while p210-induced CML is characterised by expansion of granulocytic and megakaryocytic lineages, p190 associated disease presents with monocytosis and variable basophilia (66). Cell line and animal model studies concluded that the p190 Bcr-Abl isoform confers a more aggressive malignancy than the one induced by p210. A bone marrow reconstitution leukaemogenesis model demonstrated both e14a2 and e1a2 isoforms induce similar haematological disease, however, transformation with e1a2 resulted in a shorter disease latency period than e14a2 (67). Other studies demonstrated that the e1a2 isoform induced a B-lymphocyte malignancy, in contrast with e14a2, which conferred a mixed B-, T- and myeloid cell disease with a long latency period (68). When transduced into myeloid 32D and lymphoid Ba/F3 cells, p210, p190

and p230 each transform cells to IL-3 independent growth, and induce a CML-like disease in recipient mice; transduction of p190 resulted in a higher leukaemic cell proliferative rate than p210 or p230, and had increased potency for induction of B-lymphoid leukaemia (17). Conversely, the p230 isoform conferred an indolent disease phenotype. Taken together, these studies demonstrate that the Bcr-Abl isoform expressed by the leukaemic cell is causative of the associated disease.

1.3.2   Rare Bcr-Abl isoforms: e6a2 and e8a2

In addition to p210, p190 and p230, alternate isoforms of Bcr-Abl have been identified in rare cases of CML. The *BCR-ABL1* e6a2 fusion transcript has been documented in over 20 clinical case reports, of CML (69-79), AML (80, 81), chronic myelomonocytic leukaemia (82), B- and T-ALL (83-85), and basophilic myeloid leukaemia (86-88). While the patient outcomes have been variable, the e6a2 association with several leukaemic phenotypes suggests that presence of this fusion does not exclusively confer a particular cell fate or disease outcome However, Colla *et al* suggested that the presence of e6a2 results in a more aggressive disease and poorer patient outcome (71, 74, 89). The functional mechanisms behind this disease phenotype remain to be elucidated.

Similar to the Bcr-Abl e6a2 fusion, the e8a2 fusion transcript has been identified in rare cases of CML (90-95). While patients with the e8a2 fusion have responded to therapy, investigators have described an aggressive disease phenotype and poorer prognosis associated with e8a2 (91, 92, 95). Both the e6a2 and e8a2 fusions result in truncation of the PH domain in the central Bcr region, while keeping intact the N-terminal serine/threonine kinase domain and RhoGEF DH domain. In contrast, the e1a2 fusion completely lacks the DH and PH domains (Figure 1.3). The importance of the Bcr region on Abl kinase activity, leukaemic phenotype, and potential therapy resistance, is yet to be fully explored, and is expanded on in Chapter 4.

1.4 Therapeutic options for treatment of CML

1.4.1   Methods for monitoring of disease and treatment response

Regardless of the therapy used, the measurement of CML disease burden is essential for both diagnosis and evaluation of treatment response. As previously mentioned, initial diagnosis is

primarily made based on disease symptoms and diagnostic assays. Haematological analysis provides a description of the white blood cell counts, with a reduction in their levels indicating remission. However, with increasing understanding of the underlying molecular biology of CML, molecular methods for measuring treatment response are now available to most first world clinicians. Using cytogenetic techniques such as G banding or FISH, Ph positive cells are detected in the peripheral blood and bone marrow (96). Analysis of Ph positive cells allows determination of cytogenetic response and remission. Using more sensitive RT-qPCR based methods, quantitation of *BCR-ABL1* transcripts is the current Australian standard of care for monitoring of CML (97, 98). A ratio of *BCR-ABL1* transcripts in patient samples is calculated, quantitated and compared with a standard curve of reference genes, typically *ABL1*, *BCR*, or *GUSB* (99). Molecular assessment typically occurs at diagnosis and in the months following induction of therapy. The international exchange of patient samples across CML laboratories allowed development of an international reporting scale (IS) and designation of molecular response (MR) targets (98, 100). A deep molecular response is associated with a 4-log reduction in $BCR\text{-}ABL1^{\text{IS}}$ transcripts from diagnosis levels to below 0.01% (MR^4) (100). The timely achievement of a deep molecular response is associated with high rates of progression-free survival, and following treatment success, some of these patients are able to discontinue therapy without disease recurrence (101). In these patients, the sensitive detection of residual disease may be important for predicting leukaemic cell expansion following treatment discontinuation.

1.4.2   Non-targeted CML therapies

Prior to the development of current kinase inhibition therapies, the most successful treatments for CML were not particularly targeted to the leukaemic cell. Allogeneic stem cell therapy utilises high dose chemotherapy and/or radiotherapy to deplete the leukaemic cell population, followed by bone marrow or peripheral blood stem cell transplantation from a HLA matched donor (102). While being potentially curative, stem cell transplant is not always suitable. Chemotherapy side effects are significant, and can be associated with secondary malignancies. The procedure often results in patient mortality as the engrafted cells attack the new host, known as graft-versus-host disease. Furthermore, the requirement for a HLA matched donor, often a sibling or other relative, is often prohibitive (103). Nevertheless,

transplant can be curative, and remains a treatment option for patients with advanced disease or following the failure of other therapies.

Interferon-α is a naturally occurring human protein secreted by many cell types, including lymphocytes, macrophages and endothelial cells, and is used as a therapy for CML. The current understanding of how interferon-α exerts its antileukaemic effect is incomplete (104). Interferon-α treatment *in vitro* is known to inhibit cell proliferation, promote cell differentiation and apoptosis, and induce an immunomodulatory response, possibly activating the patient's immune system. Interferon-α treatment was once considered standard of care in CML (105). The common flu-like side effects are relatively mild, however neurological effects can be debilitating, and poor response rates have largely relegated it to being a historical treatment. Nevertheless, interferon-α is still indicated when more modern therapies cannot be used due to intolerance or failure (104).

1.4.3   Imatinib and the introduction of tyrosine kinase inhibitor therapy

In 1996, Druker *et al* described the *in vitro* efficacy of the first clinically available tyrosine kinase inhibitor (TKI), imatinib (Gleevec™, formally STI571, Novartis International AG). Imatinib effectively impeded the proliferation and survival of the K562 Bcr-Abl positive cell line at low nanomolar concentrations (106). A derivative of 2-phenylaminopyrimidine, imatinib was synthesised along with a series of other compounds, designed to compete for the ATP binding site in the kinase domain of Abl (Figure 1.6) (25, 107, 108). By downregulating Bcr-Abl kinase signalling, imatinib not only prevents the proliferation of leukaemic cells, but also induces apoptosis through downregulation of BCL family regulators of apoptosis (109). In addition to Bcr-Abl, imatinib also potently inhibits the kinase activity of native Abl, PDGFR, and c-Kit tyrosine kinases (110, 111). The IRIS clinical trial, comparing imatinib against interferon-α + cytarabine, demonstrated imatinib was significantly more effective than the contemporaneous standard of care (112). In that study, response to treatment was defined as having normal peripheral blood counts with <5% bone marrow blast cells, between 1-3 months following treatment induction, which was termed haematological remission (113); remarkably, oral dosing over 300 mg daily resulted in haematological remission in 53/54 CML patients (114). After demonstrating clinical efficacy for the treatment of CML, imatinib was further used in trials of Ph+ ALL (115), and other malignancies driven by PDGFR and c-Kit

activation (110). Compared with traditional chemotherapy, imatinib has proven to be remarkably safe with relatively few adverse effects. Follow up studies demonstrated the long lasting efficacy of imatinib, with 83% event free survival after 5 years (116). Incredibly, overall survival after 14 years was 87%, approaching survival rates of healthy, age-matched populations (117). Today, durable remission on imatinib therapy is common, and some patients are able to cease treatment (101). Imatinib remains one of the great success stories of molecular biology and targeted drug design.

While most patients treated with imatinib are able to achieve deep and durable remissions, imatinib treatment is not without its shortcomings. Analysis of the IRIS patient samples found that although most patients on imatinib achieved good haematological response, 32% of patients failed to achieve the more sensitive complete cytogenetic response (112). Imatinib failure rates are significantly higher in patients with advanced disease (113). Additionally, imatinib therapy is not always tolerated by patients, and while side effects are usually minimal, patients are typically required to be on therapy indefinitely, significantly affecting lifestyle (101). Most importantly, imatinib resistance in leukaemic cells can result in secondary resistance and therapy failure, even following successful therapy and remission (113). Indeed, even after successful imatinib induction therapy, *BCR-ABL1* gene expression remains detectable in 95% of patients even following 12 months of treatment. Elucidating why some leukaemic cells are resilient to imatinib and other TKIs is of clear clinical importance for improving patient outcomes.

1.4.4   2nd generation TKIs: nilotinib, dasatinib and bosutinib

Following the success of imatinib, several other TKIs were developed for clinical use (Figure 1.6). Newer TKIs were designed for several reasons, including increasing drug potency, specificity and tolerance. However, the principle function of second and third generation TKIs is to overcome leukaemic cell resistance to imatinib, which would otherwise result in therapy failure. Crystallographic studies of the Abl kinase domain demonstrated that imatinib binding stabilises a kinase inactive state of Abl, whereby the activation loop motif mimicked peptide substrate binding (118). However, mutations in the Abl kinase domain can result in loss of imatinib binding and drug efficacy (further discussed in Section 1.5). Using structural knowledge of Abl-imatinib binding, a number of 2nd generation TKIs were developed,

including nilotinib (formerly AMN107, Tasigna™, Novartis International AG), dasatinib (formerly BMS-354825, Sprycel™, Bristol-Myers Squibb), and bosutinib (formerly SKI-606, Bosulif™, Pfizer Inc.) (119, 120).

Nilotinib was designed on the structural backbone of imatinib, and binds and stabilises Abl in the inactive conformation. However, nilotinib is significantly more potent than imatinib at inducing antiproliferative activity in Bcr-Abl positive cell lines (121, 122). Like imatinib, nilotinib demonstrates inhibition of Abl, c-Kit, and PDGFR kinases (123). Trialled in CML and Ph+ ALL patients, nilotinib was active in many otherwise imatinib refractory cases (124). When compared with imatinib in newly diagnosed CML patients, nilotinib is significantly more likely to induce molecular response, and responses are deeper and faster (125). The drug is generally well tolerated, however can induce neutropenia, thrombocytopenia, and vascular toxicity (124). Nevertheless, nilotinib remains an important front line clinical therapeutic option for CML.

Unlike imatinib and nilotinib, dasatinib was designed to bind and inhibit the active Abl conformation, as well as members of the Src family of kinases (126). *In vitro* data demonstrated that dasatinib is over 300 times more potent than imatinib in antileukaemic activity (123, 127). However, the structure of dasatinib also results in reduced specificity of kinase binding and increased off target effects (128). Therefore, more severe adverse side effects are noted with dasatinib treatment, and can include fluid retention, haemorrhage, pleural effusion, dyspnea and diarrhoea, as well as neutropenia and thrombocytopenia (123, 129, 130). Nevertheless, a phase 1 clinical trial in imatinib resistant CML and Ph+ ALL patients found dasatinib was able to overcome almost all imatinib resistance mutations (131), and the drug is now available both as a frontline and salvage therapy following imatinib or nilotinib failure (132). The thesis presented here interrogates the cellular mechanisms granting resistance to dasatinib in a cell line model, in order to identify ways to circumvent drug resistance.

1.4.5 The 3rd generation TKI: ponatinib

A single nucleotide mutation in *BCR-ABL1* is able to confer resistance to imatinib, nilotinib, bosutinib and dasatinib. The T315I 'gatekeeper' mutation was identified in TKI-resistant CML

and Ph+ ALL patients, and several efforts have been made to synthesise inhibitors of T315I-mutated Bcr-Abl. The importance of the T315I mutation will be further discussed in Section 1.5.3. One clinically available compound targeting T315I-mutated Bcr-Abl is ponatinib (formerly AP24534, Iclusig™, Ariad Pharmaceuticals), currently used as salvage therapy for patients harbouring a T315I Bcr-Abl mutation (133). Ponatinib was designed to bind the inactive conformation of Bcr-Abl, and uses a carbon triple bond to straighten out its structure, accommodating the steric bulk of isoleucine 315 while excluding the hydrogen bond requisite for the binding of other 1st and 2nd generation TKIs (Figure 1.6) (134, 135). It has been shown to be effective in clinical trials, inducing haematological and molecular responses where previous TKI therapy had failed (136). Unfortunately, ponatinib also has increased off target inhibition of several other kinases, including PDGFR, VEGFR, and Src family kinases (137). This purportedly induces several possible adverse effects, such as pancreatitis, arterial thrombotic events, hepatotoxicity, and drug induced rashes (135). Concerns about cardiac toxicity resulted in ponatinib being temporarily withdrawn from the market, and it is now available with a black box warning. Furthermore, certain single nucleotide or compound mutations dramatically alter the protein structure, and are able to confer ponatinib resistance (138). Resistance to ponatinib severely limits patient treatment options, and therefore the ponatinib resistance and cross resistance mechanisms investigated in this study have direct clinical relevance.

1.4.6   Other future therapies

While most Bcr-Abl TKIs were designed to bind the ATP binding site in the kinase domain of Abl, others have been designed to inhibit Abl by stabilising the inactive kinase conformation. These small molecules bind to the allosteric binding site, where the myristate moiety usually sits to autoinhibit native c-Abl (139, 140). Recently, the allosteric inhibitor asciminib (ABL001, Novartis International AG) entered phase 1 clinical trials, where it demonstrated efficacy against several Bcr-Abl kinase domain mutants (141). However, some leukaemic cells are able to evade Bcr-Abl inhibition via a different spectrum of kinase domain mutations (139), or drug efflux mediated by membrane transporters ABCB1 and ABCG2 (142). Asciminib resistance may be circumvented by co-treatment with conventional ATP binding site TKIs, marking novel strategies simultaneously overcoming toxicity and resistance (143).

1.5 TKI resistance mechanisms and next generation TKI design

The selective pressure of TKI therapy in CML patients has resulted in the emergence of TKI resistant leukaemic cells, which expand in the leukaemic cell population and result in disease relapse and patient mortality. TKI resistance mechanisms can be broadly defined by four distinct groups: overexpression of Bcr-Abl and its cellular signalling, lowering of leukaemic cell intracellular TKI concentrations, loss of TKI binding and inhibition of Bcr-Abl, and loss of leukaemic cell dependence on Bcr-Abl kinase activity for proliferation. Additionally, there are patient specific reasons for the loss of TKI effectiveness, extrinsic to changes in the leukaemic cell.

1.5.1 Increases in Bcr-Abl expression and kinase activation

CML cells are reliant on Bcr-Abl kinase activity for maintaining cell proliferation, and CML cells often overcome TKI treatment by compensatory upregulation of Bcr-Abl expression and kinase activation. In order for imatinib to effectively restrain growth of the CML cell population, Bcr-Abl kinase activity must be inhibited in each tumour cell. Several studies have generated *in vitro* models with CML cell lines resistant to imatinib and other TKIs, and many of these cell lines display similar characteristics to patient study samples. In these studies, authors demonstrated that TKI resistant leukaemic cells expressed significantly more Bcr-Abl protein and gene transcript levels than TKI sensitive cells; this has the net effect of increasing the oncogenic signalling pathway activation, while titrating the amount of available intracellular TKI (144-146). This effect is clinically relevant, and has been identified in imatinib resistant patients (147). Bcr-Abl overexpression is associated with disease progression, and is a common resistance mechanism to all therapeutics targeting Bcr-Abl kinase activity (148). Overexpression of the Bcr-Abl protein often results from increases in *BCR-ABL1* gene transcript expression. The increases in transcript expression can be driven by duplication of the Ph chromosome, or genomic amplification of the *BCR-ABL1* locus by tandem duplication or expansion on extrachromosomal elements such as double minutes (149-151). However, like other proteins, increased Bcr-Abl levels have been detected in the absence of gene overexpression or DNA amplification, indicating multiple dynamic levels of Bcr-Abl protein expression control (145).

1.5.2 Bcr-Abl kinase mutations

The most commonly detected mechanism of resistance to TKIs is the emergence of mutations in the kinase domain of Bcr-Abl, and are identified in most patients who fail to achieve responses to TKI treatment. Detected via sequencing of *BCR-ABL1* mRNA transcripts, over 100 nucleotide mutations have been identified (Figure 1.7). These result in the substitution of amino acid residues, affecting the drug-protein interaction and resulting in a loss of TKI efficacy (146, 152). Protein crystallography studies have identified the conformational changes caused by Abl kinase domain mutations, and how these result in the loss of TKI binding (118). Several of these mutations cluster around the P-loop of Abl kinase (Figure 1.6), and increase the level of kinase phosphorylation, increasing activation (153). Interestingly, mutations occur not only at the site of TKI binding, but also at more distant regions, forcing the protein into a conformational state which prevents drug access (152). Kinase domain mutations vary widely in both the level of resistance conferred, as well as the frequency detected in patients (113, 152, 154). However, detection of a kinase domain mutation during imatinib treatment is almost always accompanied by clinical resistance (155).

1.5.3 The T315I 'gatekeeper' kinase domain mutation, and development of ponatinib

Despite several treatment options available to clinicians, there remains an Achilles heel in TKI therapy. The first report of clinical imatinib resistance in CML patients by Gorre *et al* identified a single amino acid exchange occurring in over half of the TKI refractory patients (146). Known as the 'gatekeeper' mutation, a cytosine to thymine mutation at *ABL1* position 944 leads to a threonine-to-isoleucine substitution at amino acid position 315, in the kinase domain of the Abl protein. Interaction of imatinib with the ATP binding site of Bcr-Abl is mediated through hydrogen bonding to the threonine hydroxyl group; substitution with the non-polar isoleucine residue abrogates this interaction, while the physical bulk of isoleucine protects the binding site by steric hindrance (156, 157). T315I mutant CML and Ph+ ALL cells are thus completely resistant to all 1st and 2nd generation TKIs (158). Crystallographic studies of the Abl kinase domain have demonstrated that mutation of the gatekeeper residue results in stabilisation of the active kinase conformation, restoring constitutive Bcr-Abl activity leading to Ba/F3 cell transformation (159). Azam *et al* further demonstrated that the T315I mutation results in stronger ATP binding, and confers further increases in Bcr-Abl kinase activation and transformation potential compared with unmutated Bcr-Abl (159). Griswold *et al*

demonstrated that T315I imposed a significant growth advantage to Bcr-Abl harbouring cells (160), postulating that this was due to alterations in adaptor protein binding and kinase substrate phosphorylation (153). Furthermore, a study by Härtel *et al* demonstrated that unlike native Bcr-Abl, Bcr-Abl harbouring T315I exhibits compensatory MAPK pathway activation in response to TKI treatment (161). Indeed, significant differences in gene expression have been identified in cells harbouring the T315I mutation (162). Thus, even in the absence of TKI therapy, T315I may confer kinase activating transformations, functional alterations, and an altered disease phenotype. That said, T315I rarely emerges clinically in the absence of TKI based selection, and unpublished observations in our laboratory indicate that in the absence of TKI, T315I harbouring cells do not outcompete wildtype Bcr-Abl cells, suggesting that the altered kinase activity associated with T315I is only advantageous under the selective pressure of TKI exposure.

1.5.4   Lowering of intracellular TKI concentrations: ABCB1 and ABCG2

In addition to absolute Bcr-Abl levels, the amount of intracellular TKI available to bind Bcr-Abl also affects the proliferation of CML cells. Being highly water soluble, imatinib does not readily diffuse through the lipid bilayer of the cell membrane, requiring active import to mediate its effects. Lowered leukaemic cell activity of the organic cation transporter 1 (OCT1), a cell membrane small molecule importer, has been associated with primary resistance to imatinib, and the activity of OCT1 is predictive of imatinib response in CML patients (163, 164). In addition to lowered TKI import, increased drug export from the leukaemic cell is known to confer therapeutic resistance. The most well studied of the drug efflux transporters are the members of the ATPase binding cassette (ABC) transporter superfamily.

The ABC transporters are responsible for translocating a wide variety of substrates across the cellular lipid membrane. With both cellular export and import function, they are expressed by eukaryotes, prokaryotes and archaea (165, 166). Within the human genome, there are at least 49 distinct ABC transporter genes divided into 7 subfamilies, expressed predominantly in the liver, kidneys, intestines and at the blood-brain barrier (165, 167). ABC transporters have several critical functions in cellular homeostasis and physiology, transporting a wide array of substrates, including metal ions, peptides, sugars and hydrophobic compounds across cell lipid bilayers (167). While the function and sequences of human ABC transporters

are highly diverse, there are structural and mechanistic attributes common to members of the transporter superfamily. All members rely on ATP binding and hydrolysis for transporter function; two conserved nucleotide binding domains contain a catalytic core responsible for the hydrolysis of ATP. Two variable transmembrane domains form a translocation pathway through the plasma membrane, and a short α helix couples the conformational change from nucleotide binding to allow alternating transmembrane access (168).

The prototypical ABC transporter, ABCB1 (P-glycoprotein, MDR-1), was the first demonstration of an ABC transporter contributing to altered cell membrane drug permeability (169) and chemotherapy resistance (170). Overexpression of ABCB1 is associated with resistance to several cytotoxic chemotherapeutics (171), and is often induced following exposure to single agent therapy. Its broad substrate transport specificity can result in cross-resistance to several chemotherapeutics, known as a multidrug resistant phenotype (172). Commonly associated with therapeutic resistance in colon, kidney, liver and adrenal carcinomas, ABCB1 also contributes to poor therapy response in several leukaemic subtypes (172-175). In the CML setting, cell line models have identified ABCB1 as a transporter of imatinib (176, 177), and ABCB1 overexpression as a significant contributor to TKI resistance (144, 175, 178, 179). In CML patients, high ABCB1 expression is significantly associated with imatinib failure (180), and poor response upon switching to nilotinib (181). ABCB1 overexpression has been also observed in cell line models as a result of exposure to nilotinib (182) and dasatinib (183, 184). However, TKIs have also been demonstrated to act as inhibitors of ABCB1 activity. Several studies have reported the inhibition of ABCB1 substrate transport in ABCB1 expressing lines treated with imatinib (178, 185, 186), nilotinib (186, 187), and dasatinib (186). The contrasting nature of TKIs as both substrate and inhibitor is often TKI concentration dependent, highlighting the complex nature of drug-transporter interactions (173).

The ABCG2 transporter (formerly known as breast cancer resistance protein, Bcrp1) was first identified in 1998 (188). ABCG2 has been implicated in chemotherapy resistance in several cancer types and has a promiscuous substrate transport profile, ferrying both hydrophobic and anionic compounds across the phospholipid bilayer. Several cancer therapeutics are transported by ABCG2, and ABCG2 overexpression has been associated with poor outcome

and chemotherapy failure in the myeloid malignancy, AML (189), as well as several solid tumours (190). The functional ABCG2 complex consists of one nucleotide binding domain and six transmembrane helices, dimerising to form a ~144 kDa functional transporter (191). McDevitt *et al* demonstrated the existence of a higher order tetrameric complex of ABCG2 homodimers, forming an aqueous central region to facilitate transport (192). The binding of ATP to ABCG2 switches the ABCG2 complex from inward facing to outward facing, transporting its small molecule cargo; the subsequent loss of bound ATP reverts the conformational change, exposing the substrate binding site to the inner leaflet of the plasma membrane, to again recruit a transported molecule (193). Recently, Jackson *et al* described the structure of ABCG2 bound to the ABCG2 inhibitor, Ko143, demonstrating that the compound binds to the central cavity of the inward-facing molecule, blocking substrate access and preventing ATP hydrolysis (194). This compound was used in the current study to inhibit ABCG2 function, following the identification of ABCG2 overexpression in the described dasatinib resistance model (Chapter 5).

The interaction of ABCG2 with imatinib, dasatinib, and nilotinib has been previously demonstrated, with the TKIs functioning both as transported substrate and transporter inhibitor. Studies have identified ABCG2 overexpression in TKI-resistant cell populations (173, 195-197). Imatinib efflux is mediated by ABCG2, while at higher concentrations imatinib inhibits ABCG2 transport activity (198). The overexpression of ABCG2 is associated with poor imatinib response, and poor response to salvage therapy with 2nd generation TKIs (199). Studies have also demonstrated the selective advantage conferred by ABCG2 overexpression during TKI treatment. Gromicho *et al* described the increase of ABCG2 expression in K562 cells following prolonged culture in imatinib (200). Interestingly, mRNA expression did not increase linearly with TKI exposure, instead peaking early in dose escalation before significantly falling with increasing TKI concentration, likely due to the selection for clones harbouring alternate TKI resistance mechanisms. In our own laboratory, we have demonstrated that overexpression of ABCG2 in K562 cells does not significantly decrease the intracellular concentrations of imatinib or nilotinib, nor does inhibition of ABCG2 decrease the cytotoxic sensitivity to these TKIs (201). The body of evidence for imatinib-ABCG2 interactions demonstrates a marked complexity, with function of ABCG2 differing depending on cell type, imatinib concentration, and the analytical methods used.

Studies of dasatinib-ABCG2 interactions have been less comprehensive and conclusive. Our laboratory first described significantly lower intracellular dasatinib in cells overexpressing ABCG2 compared with parental cell line controls, which was reversible upon treatment with the ABCG2 inhibitor, Ko143 (184). Similarly, dasatinib uptake was significantly increased in ABCG2-overexpressing K562 cells, when treated with Ko143. Consistent with these data, Bcr-Abl kinase sensitivity to dasatinib was decreased in K562-ABCG2 cells, and was significantly reduced with Ko143 treatment. ABCG2 has subsequently been demonstrated to confer resistance to both nilotinib and dasatinib (183). However, higher concentrations of dasatinib have an inhibitory effect on ABCG2 function, though only above clinically relevant levels (183, 186). The emergence of ABCG2 overexpression has also been described following dasatinib dose escalation in a K562 cell model similar to the study described here (200). A study of CML patients resistant to imatinib and subsequently treated with dasatinib salvage therapy, identified ABCG2 expression contributing to failure to achieve molecular response on dasatiib, and to shorter progression-free survival (202).

1.5.5 Bcr-Abl independent leukaemic cell growth

The gain of an alternate driver mutation can override the requirement for Bcr-Abl activity, granting the leukaemic cell Bcr-Abl independent growth. Some studies of imatinib resistant cells have demonstrated the loss of dependence on Bcr-Abl, with cellular proliferation instead driven by other proliferative drivers, such as Lyn kinase (203). Lyn has previously been implicated in TKI resistance (182, 204-206), providing a potential mechanism for differential resistance through kinase activation. Mahon *et al* also demonstrated that a relative increase in the expression of Lyn was associated with failure of imatinib and nilotinib (207). Authors also suggested that the TKI resistant CML patients with overexpression of Src family kinases be treated with dasatinib, due to its dual function as Bcr-Abl and Src kinase inhibitor. Furthermore, Bcr-Abl independent growth has been associated with increases in MAPK pathway activation, which can be therapeutically targeted (208, 209). The compensatory upregulation of proliferative signalling pathways regardless of Bcr-Abl activity inhibition demonstrates the need to confirm the leukaemic cell's reliance on continued Bcr-Abl activity.

1.5.6   Leukaemic cell extrinsic TKI resistance mechanisms

As with most other cancer therapies, the efficacy of TKI treatment is influenced by several factors independent of the leukaemic cell. Pharmacokinetic factors are known to significantly influence treatment response. The oral bioavailability of imatinib is ~98%, and a long half-life of 18 h allows effective once daily dosing regimens in the majority of patients (210, 211). The main metabolite of imatinib, N-desmethyl imatinib (CGP74588), is also known to have anti-leukaemic potency *in vitro* (212). Nevertheless, genetic polymorphisms in gastrointestinal and liver drug transporters are known to affect the uptake and clearance of most TKIs (211). As a substrate of the cytochrome P450 3A4 (CYP3A4) enzyme, inducers of CYP3A4 result in lowered imatinib exposure, and as always care must be taken by clinicians to maintain adequate drug dosing (210, 211). Additionally, the leukaemic stem cell population can repopulate the malignancy following TKI treatment (213, 214). Residing in the bone marrow, the cytokine laden microenvironment can support the ongoing maintenance of leukaemic cells, further complicating the absolute elimination of the malignancy (215). Hiwase *et al* described the protective effect of the cytokines granulocyte-macrophage colony-stimulating factor (GM-CSF) and granulocyte colony-stimulating factor (G-CSF) under TKI exposure on leukaemic cells, and TKI sensitisation following inhibition of the cytokine's main effector, Jak (216). Paracrine signalling effects have also been reported; a study by Liu *et al* demonstrated that the increased production of IL-3 by dasatinib resistant DA1-3b murine leukaemic cells conferred a TKI protective effect on co-cultured leukaemic cells, which were otherwise sensitive in monoculture (217).

1.5.7   Selective pressures in the context of TKI resistance

While the use of TKI therapy in CML has been clinically effective, the therapy provides a selective pressure, which shapes the evolution of the cell population (174). If the CML cell population is not completely eliminated, TKI exposure selects out the most adaptive, TKI-resistant cells (218). The genetic instability, fast proliferation rate, diverse initial genetic heterogeneity, and vast initial pool of cancer cells, can facilitate the rapid clonal evolution of leukaemic cells to a resistant phenotype (219, 220). The common targeting of Bcr-Abl to elicit antileukaemic effects, in addition to the structural homogeneity of the TKI molecules, often results in multidrug resistance. This is exemplified by the T315I mutation or overexpression of ABCB1, whereby the gained resistance to one TKI can result in failure of secondary TKI

treatments (221). In this context, the potency and timeliness of the therapy becomes critical. With prolonged culture, stochastic variances in the cancer cell population can spontaneously develop into pro-survival characteristics (218). This makes the study of TKI resistance in CML not a simple listing of identified individual resistance mechanisms, but an investigation of how the tumour subpopulations interact with each other. Several previous studies have generated TKI resistant cells, comparing them directly against TKI naïve cells, while ignoring the fluctuations in the resistance mechanisms which occur over time and drug treatment. Thus, this thesis aims to investigate the longitudinal aspects of TKI resistance generation.

1.6 Research questions, hypotheses and approach

To further investigate the molecular mechanisms of TKI resistance in CML, several research questions were posed, which served to direct investigative procedure. These were mostly centred around a cell line model of induced dasatinib resistance, which was previously generated in our laboratory. The cell line, here named K562 DasR, overexpresses Bcr-Abl p210 (e14a2), and in the later stages of dasatinib dose escalation, harbours the T315I mutation (205). However, there remained several unexplored aspects of the TKI resistance mechanisms present, and indeed, entirely undiscovered resistance mechanisms at play. This thesis serves to explore deeper into the resistance mechanisms present, and how they contribute towards the gain of total TKI therapy resistance. To gain further understanding of how TKI resistance was mediated, the following research aims and hypotheses were posed:

• To explore the factors altering the propensity for leukaemic cells to develop the T315I mutation under dasatinib selection

o Hypothesis: Prior to the acquisition of T315I, subpopulations of leukaemic cells harbour and express alternate resistance mechanisms, allowing cells to evade TKI treatment

• To determine how cellular adaptations conferring resistance to dasatinib affect response to the salvage therapy TKI, ponatinib

o Hypothesis: Resistance mechanisms arising in response to dasatinib exposure can provide leukaemic cells a means to evade ponatinib treatment

- To determine how drug resistance mechanisms can be circumvented and overcome

o Hypothesis: Targeting of the individual drug resistance mechanisms will allow re-sensitisation to TKI treatment

To investigate the cellular adaptations involved in dasatinib and ponatinib resistance, dasatinib dose escalation intermediates of the K562 DasR cell line were subjected to a combination of genetic, transcriptomic, protein and functional analysis. Previously established resistance mechanisms (e.g. *BCR-ABL1* overexpression and the T315I mutation) were validated using RT-qPCR, western blotting and transcript sequencing, and aspects of these resistance mechanisms were further explored with DNA qPCR and cytogenetic analysis, which determined the origin and outcome of *BCR-ABL1* gene overexpression. Dasatinib resistance was determined in dose escalation intermediates using the TKI induced cell death and phospho-CrkL IC50 assays; cross resistance to ponatinib was determined using the same method. To determine alternate resistance mechanisms, transcriptome sequencing of selected K562 DasR dose escalation intermediates was performed, and was interrogated to identify changes in gene expression and the formation of genetic alterations (nucleotide variants, indels and genetic fusions). The overexpression of ABCG2 was identified in certain K562 DasR dose escalation intermediates, and its functional role in TKI resistance was determined. It was demonstrated that ABCG2 expression contributes to dasatinib resistance, and for the first time, to ponatinib cross resistance. Furthermore, genetic fusion analysis detected a rare *BCR-ABL1* fusion associated with TKI resistance, e6a2, which was, for the first time to our knowledge, cloned into a Ba/F3 cell line to determine its effects on dasatinib susceptibility. Finally, analysis of the fluctuations in each of the different TKI resistance mechanisms gave insight into the selective advantages each mechanism provided, which provided evidence for a model of TKI resistance accrual, governed by the cellular energy efficiency of the individual resistance mechanisms.

The data and interpretation presented here has added significantly to the understanding of drug resistance in CML, not only in identification of individual TKI resistance mechanisms, but also how each mechanism contributes to the evolution of resistance, allowing prediction of which cell populations will end up predominating under TKI selection, and suggesting how

these cell populations may be effectively targeted. This improved understanding will guide translational research approaches to improve patient care.

1.7 Chapter 1: Figures
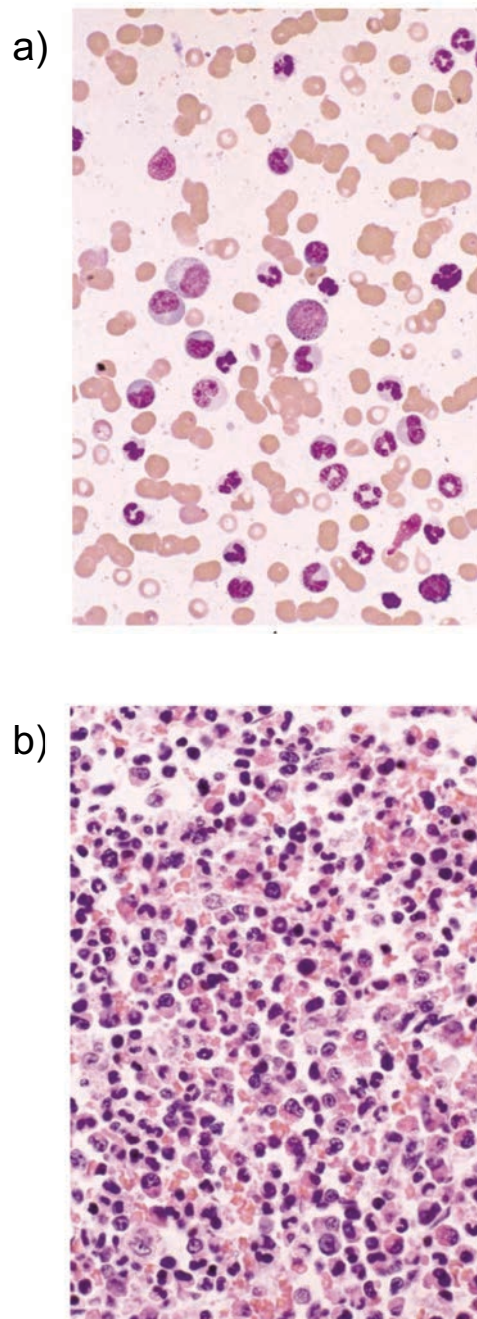
Figure 1.1: a) Peripheral blood smear (Wright's stain, 40x) and b) bone marrow biopsy smear (hematoxylin and eosin stain, 160x) from a patient with CML. Both slides demonstrate the marked myeloid hyperplasia typically associated with CML. From New England Journal of Medicine, Sawyers CL, Chronic Myeloid Leukemia, Volume 340(17), pages 1330-40. Copyright © (1999) Massachusetts Medical Society. Reprinted with permission.
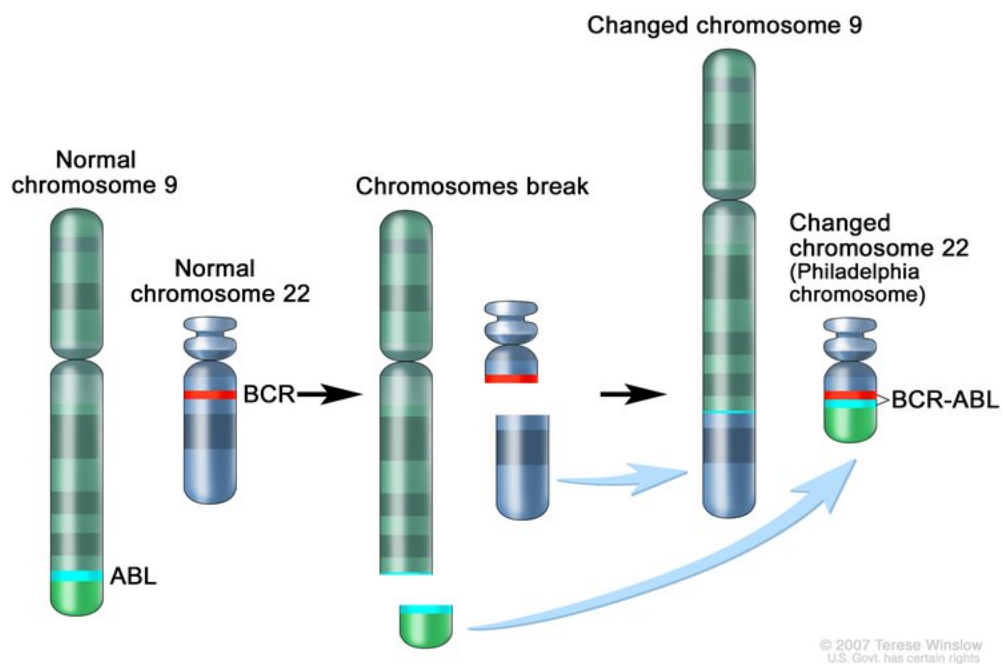
Figure 1.2: Representation of the Philadelphia chromosome translocation event. Translocation between chromosomes 9 and 22 brings the *BCR* and *ABL1* genes into juxtaposition. For the National Cancer Institute © (2007) Terese Winslow LLC, U.S. Govt. has certain rights. Permission granted to: Benjamin Leow.
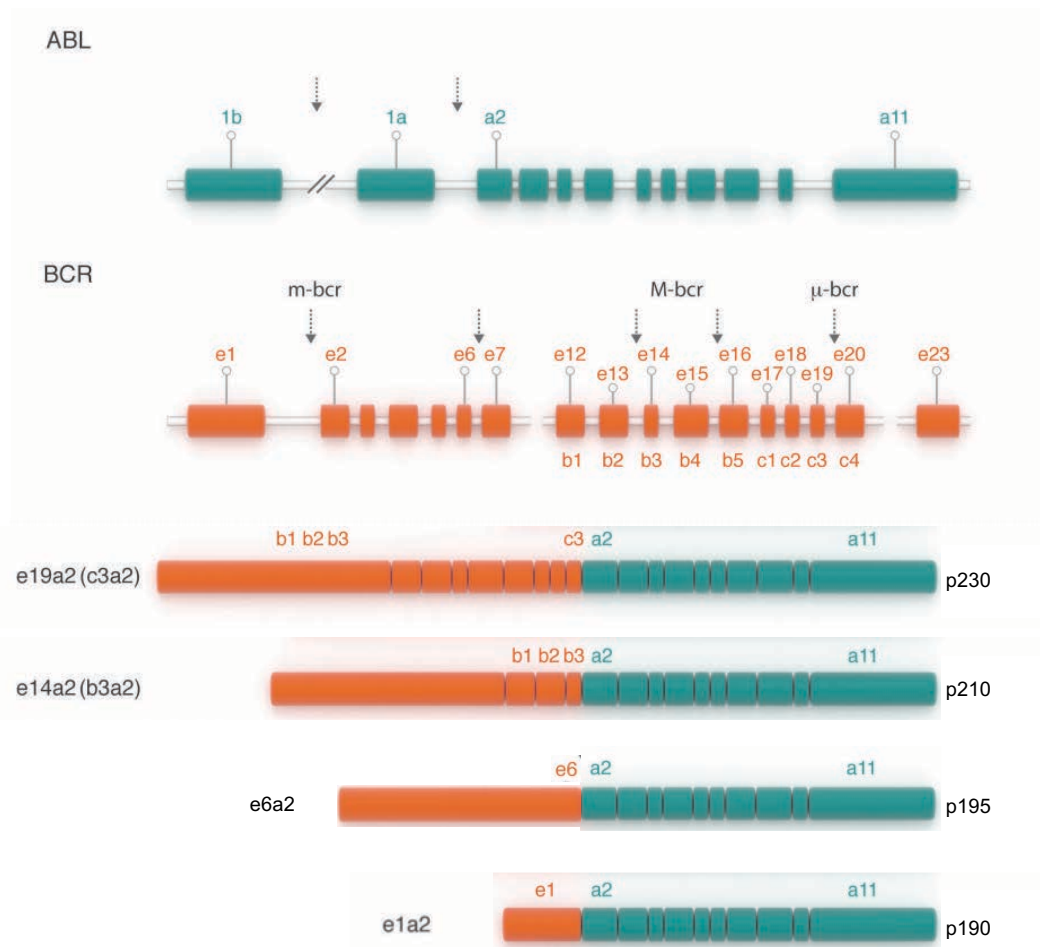
Figure 1.3: A diagrammatic representation of *ABL1* (green) and *BCR* (red) exon and intron locations, and how they break to form transcript isoforms of *BCR-ABL1*. Most transcripts have the same 5' exonic *ABL1* breakpoint, beginning at exon a2. However, several differ in the length and content of the *BCR* portion, such as e6a2, which likely confers functional differences. The major (M), minor (m), and micro (µ) *BCR* breakpoints are shown, which give rise to p210, p190, and p230 Bcr-Abl proteins, respectively.

Adapted from Haematologica, Mughal TI *et al*. Chronic myeloid leukemia: reminiscences and dreams (222).
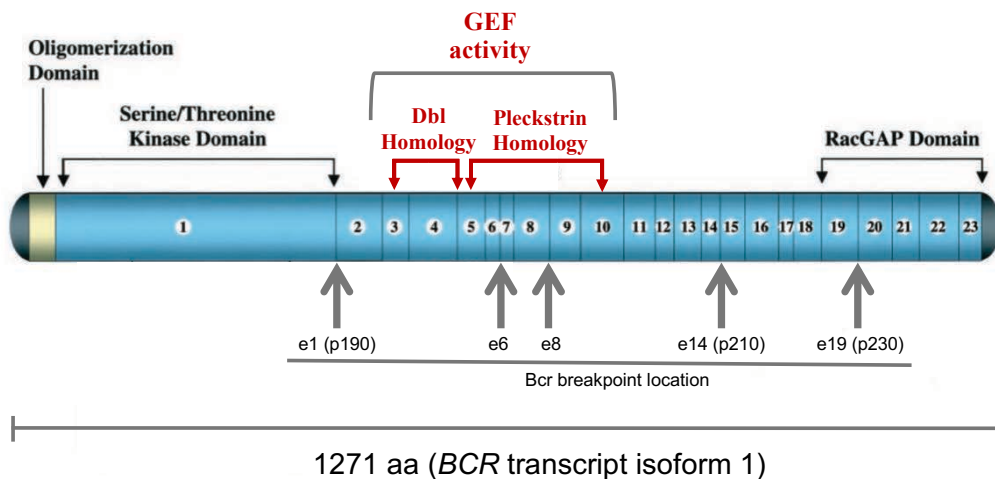
Figure 1.4: A schematic representation of the Bcr protein. Exon locations are shown, as well as common Bcr breakpoints. The Bcr portion of all Bcr-Abl isoforms contain oligomerisation and serine/threonine kinase domains, while only some contain the guanine exchange factor (GEF) regions. None of the Bcr-Abl isoforms contain the N-terminal Bcr GTPase activating protein (GAP) domain. The existence of different Bcr regions is likely to confer functional variance.

Figure adapted from Cancer Research, Laurent E *et al*. The BCR gene and Philadelphia chromosome-positive leukemogenesis (223).

Figure 1.5: A diagram of the signalling pathways activated by Bcr-Abl. These include the MAPK (orange), JAK/STAT (pink), PI3K/AKT (blue), and Src family kinase (yellow) pathway members. Important scaffolding proteins (purple) mediate interactions with several effector proteins. Phosphorylated amino acid residues (dark blue P's) are crucial for signalling pathway activation, which leads to increases in cell survival and proliferation, and loss of apoptotic signalling.

Adapted from Haematologica, Mughal TI *et al*. Chronic myeloid leukemia: reminiscences and dreams (222).

(a)

(b)
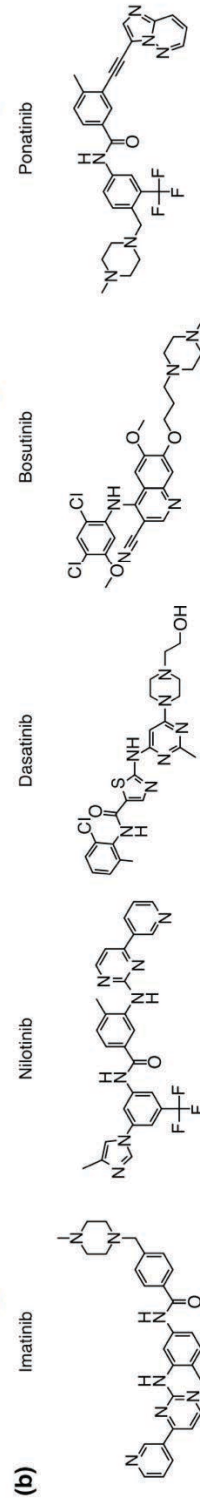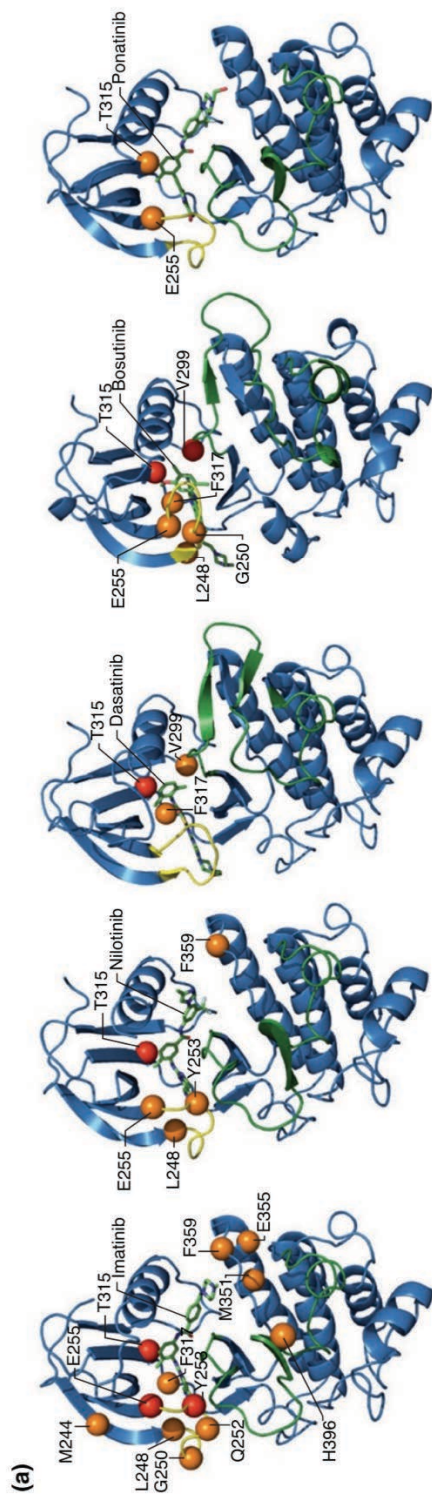
Figure 1.6: a) Crystal structure of the Abl kinase domain in complex with clinically available TKIs. The yellow region indicates the phosphate binding P-loop, and green the kinase activation loop. Highlighted amino acid residues indicate point mutation locations which can confer resistance to the TKI. b) The structure of the TKIs determines the binding conformation to Bcr-Abl, critical amino acid interactions, and drug potency.

Reproduced from Genome Biology, Eiring AM, Deininger MW. Individualizing kinase-targeted cancer therapy: the paradigm of chronic myeloid leukemia (215).
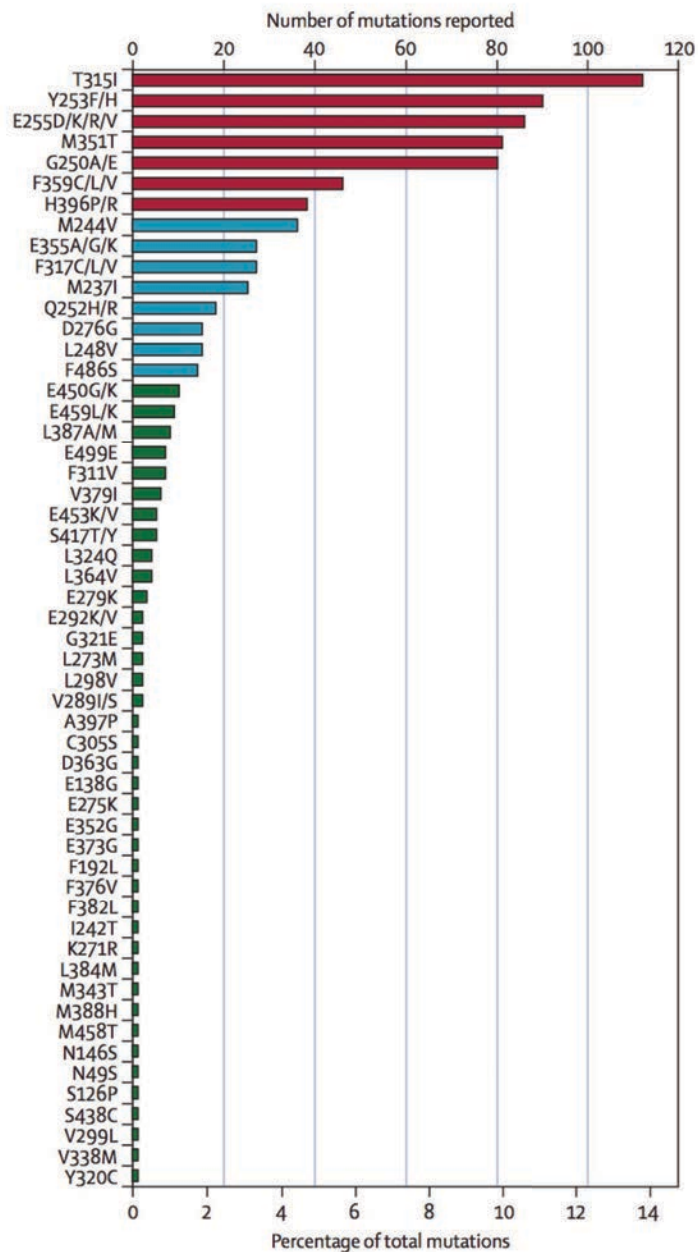
Figure 1.7: A listing of the most common imatinib resistance mechanisms and their relative frequency. While there is a great deal of diversity in TKI resistance mutations, the most important kinase domain mutation for all 1st and 2nd generation TKIs is T315I, conferring complete TKI resistance. Adapted from The Lancet Oncology, Apperley JF. Part I: Mechanisms of resistance to imatinib in chronic myeloid leukaemia (113).

2 Methods and Materials

2.1 Reagent sourcing

Reagent	Supplier	Part number
7-Aminoactinomycin D (7-AAD)	Life Technologies	A1310
ABCB1 PE antibody	Beckman Coulter	PN IM 2370U
ABCG2 PE antibody	R & D Systems	FAB995P
Agarose (for gel electrophoresis)	Sigma-Aldrich	A6013-100G
Ampicillin	Sigma-Aldrich	A5354-10ML
Annexin-V PE	Becton Dickinson	556421
Aprotinin	Sigma-Aldrich	A1153-5MG
BCR-ABL TaqMan Gene Expression Assay for e1-a2	Applied Biosystems	Hs03024844
BenchMark Protein Ladder	Life Technologies	10748010
Bovine serum albumin (BSA)	Sigma-Aldrich	A9418-500G
Bromophenol blue	Sigma-Aldrich	114405-5G
Buffer saturated phenol	Life Technologies	15513039
Chloroform	Sigma-Aldrich	C2432-1L
Colcemid	Thermo Fisher Scientific	15210-040
Complete protease inhibitor cocktail	Sigma-Aldrich	4693124001
Criterion TGX precast gel	Bio-Rad	assorted
Custom oligos	Sigma-Aldrich	VC00021
Dasatinib	Selleckchem	S1021
DC Protein Assay	Bio-Rad	500-0116
DEPC-treated water	Thermo Fisher Scientific	ICN821739
Dimethyl sulfoxide (DMSO)	Sigma-Aldrich	1029522500
DNA Hydration Solution	Qiagen	158914
Donkey anti-mouse-IRDye-800CW antibody	Li-Cor Biosciences	926-32212
Donkey anti-rabbit-IRDye-680LT antibody	Li-Cor Biosciences	926-68023
ECF substrate	Bio-strategy	RPN5785
Ethanol	Thermo Fisher	AJA726-20L
Expand Long Template PCR System	Sigma-Aldrich	11681842001
Foetal calf serum (FCS)	Fisher Biotec	FBS-AU-015
Glycerol	Sigma-Aldrich	G5516-1L
Glycine	Sigma-Aldrich	G8898-1KG
Glycogen (for RNA/DNA extraction)	Sigma-Aldrich	10901393001
Hank's balanced salt solution (HBSS)	Sigma-Aldrich	H9394
HEPES	Sigma-Aldrich	H0887-100ML
Imatinib mesylate	Sapphire Bioscience	G407002
Iscove's modified Dulbecco medium (IMDM)	Sigma-Aldrich	I3390-500ML
Isopropanol	Chem Supply	PA013-2.5L-P
Kanamycin	Life Technologies	15160054
Ko143	Sigma-Aldrich	K2144-5MG
L-glutamine	Sigma-Aldrich	G7513-100ML
Leupeptin	Sigma-Aldrich	L0649-5MG
Lipofectamine	Life Technologies	11668019
Luria broth base	Thermo Fisher Scientific	12795-084
Marabu Fixo Gum rubber cement	Leica Biosystems Amsterdam	LK-071A
Methanol	Chem supply	MA004-20L-P
Mouse anti-Abl (c-, v-, Bcr-) clone 24-21 antibody	Merck Millipore	MABT203
Mouse anti-IgG2a PE antibody	Agilent Technologies	X0950

Mouse anti-IgG2b PE antibody	Agilent Technologies	X0951
Newborn calf serum	Sigma-Aldrich	12023C-500ML
NEXTFlex Rapid Directional RNA Seq Library Prep Kit	Geneworks	BIOO-5138-10
Nilotinib	Sapphire Bioscience	N465303
NP-40	Thermo Fisher Scientific	85124
One Shot® MAX Efficiency® DH5α™-T1R Competent Cells	Life Technologies	12297016
Opti-MEM reduced serum media	Life Technologies	51985034
Penicillin-Streptomycin	Sigma-Aldrich	P4333-100ML
Phenylmethanesulfonyl fluoride (PMSF)	Sigma-Aldrich	78830
Phosphate buffered saline (PBS), 10x	Life Technologies	14200-166
Polybrene	Thermo Fisher	SC-134220
Polyvinylidene fluoride (PVDF)	Adelab	MIL-IPVH00010
Ponatinib	Sapphire BioScience	S1490
Precision Plus Protein Kaleidoscope Standards	Bio Rad	1610395
Proteinase K	Sigma-Aldrich	3115887001
Q5 Site-Directed Mutagenesis Kit	Genesearch	E0554S
QIAGEN Plasmid Plus Midi Kit	Qiagen	12643
QIAprep Spin Miniprep Kit	Qiagen	27104
QIAquick Gel Extraction Kit	Qiagen	28706
Rabbit anti-CrkL (C-20) antibody	Santa Cruz Biotechnology	sc-319
Rabbit anti-IgG antibody (alkaline phosphatase conjugated)	Santa Cruz Biotechnology	sc-2007
Rabbit anti-phospho-Bcr (Tyr177)	Cell Signalling Technology	3901
Rabbit anti-phospho-c-Abl (Tyr245)	Cell Signalling Technology	2861S
Rabbit anti-phospho-STAT5 antibody (Tyr 694)	Cell Signalling Technology	9359S
Rabbit anti-STAT5 antibody	Cell Signalling Technology	94205S
Rabbit anti-β-Tubulin (9F3) antibody	Cell Signalling Technology	2128
RNase A	Qiagen	19101
RPMI-1640	Sigma-Aldrich	R0883-500ML
Select Agar (For solid microbial growth media)	Thermo Fisher Scientific	30391-023
Sodium azide	Sigma-Aldrich	S2002
Sodium chloride	Thermo Fisher Scientific	AJA465-2.5KG
Sodium dodecyl sulfate (SDS)	Sigma-Aldrich	75746-1KG
Sodium fluoride	Sigma-Aldrich	S7920-100G
Sodium orthovanadate	Sigma-Aldrich	S6508
Sodium pyrophosphate	Sigma-Aldrich	P8010-500G
ß-mercaptoethanol	Sigma-Aldrich	M6250-100ML
SuperScript II Reverse Transcriptase Kit	Life Technologies	18064014
SureSelect XT Target Enrichment System	Integrated Sciences	5190-9491
SYBR® Green Real-Time PCR Master Mix system	Qiagen	330503
TOPO XL-2 Complete Cloning Kit	Life Technologies	K8050-10
Tris	Sigma-Aldrich	252859-500G
TRIzol reagent	Life Technologies	15596018
Trypan Blue	Sigma-Aldrich	T0776
UltraPure Phenol:Chloroform:Isoamyl Alcohol (25:24:1, v/v)	Thermo Fisher Scientific	15593031
Vectashield Antifade Mountin Medium with DAPI	Abacus	VEH1200
Vysis LSI BCR/ABL Dual Color Translocation Probe	Abbott Molecular Inc	05J77-0011

2.2 Reagent recipes

Reagents were made up by myself or members of the Leukaemia Research Laboratory, as needed. Final molar concentrations are shown, and/or volumes added in typical recipes made. Stock concentrations and pH are shown in brackets.

2.2.1   Cell culture medium

RPMI 1640 medium – 500 mL

10% FCS – 50 mL

25000 Units penicillin-streptomycin (5000 U/mL) – 5 mL

2 mM L-glutamine (200 mM) – 5 mL

Media made sterile and stored at 4˚C, and warmed to 37˚C in a water bath before use.

2.2.2   Ba/F3 (naïve and empty vector control) cell culture medium

Cell culture medium from 2.1.1 – 47.5 mL

5% WEHI-3B conditioned media – 2.5 mL

Media made sterile and stored at 4˚C, and warmed to 37˚C in a water bath before use.

2.2.3   HEK293T cell culture medium

Dulbecco's modified Eagle's medium (DMEM) – 500 mL

10% FCS – 50 mL

25000 Units penicillin (5000 U/mL) – 5 mL

25000 µg/mL streptomycin (5000 µg/mL) – 5 mL

2 mM L-glutamine (200 mM) – 5 mL

Media made sterile and stored at 4˚C, and warmed to 37˚C in a water bath before use.

2.2.4   WEHI-3B conditioned medium (source of murine IL-3)

Conditioned media from WEHI-3B murine monomyelocytic leukaemia cells was used as a source of murine IL-3 for stimulation of Ba/F3 cells. WEHI-3B cells were subcultured at $2x10^5$

cells/mL in 200 mL cell culture medium for 48 h or until confluent. Conditioned media was harvested and frozen in 50 mL aliquots at -20˚C until needed, and sterile filtered before use.

2.2.5   Minimal media

Iscove's modified Dulbecco's medium (IMDM) – 500 mL

1% w/v bovine serum albumin (BSA) – 5 g

2 mM L-glutamine (200 mM) – 5 mL

BSA was dissolved in IMDM with L-glutamine by agitation at room temperature, then filter sterilised and stored at 4˚C, and warmed to 37˚C in a water bath before use.

2.2.6   HBSS + HEPES (final concentration)

Hanks balanced salt solution (HBSS)

200 mM HEPES

2.2.7   Freeze solution (final concentrations)

70% HBSS + HEPES

20% FCS

10% DMSO

Fresh solution was prepared ice cold as needed.

2.2.8   Binding buffer

HBSS + HEPES – 47.5 mL

100 mM $CaCl_2$ – 2.5 mL

2.2.9   Annexin V / 7-AAD staining solution (per sample)

Binding buffer – 50 µL

Annexin-V PE – 1 µL

7-AAD stock – 0.1 µL

2.2.10 FACS fixative

PBS – 500 mL

Formaldehyde (40% w/v) – 5 mL

D-glucose – 10 g

Sodium azide – 0.1 g

Prepared, sterile filtered and stored at 4°C.

2.2.11 Laemmi's lysis buffer (final concentrations)

50 mM Tris-HCl (pH 6.8)

10% glycerol

2% SDS

5% ß-mercaptoethanol

0.1% bromophenol blue

1 mM sodium orthovanadate

10 mM sodium fluoride

The buffer was prepared and stored in 1 mL aliquots at -20°C, and briefly thawed in a 95°C heat block before use.

2.2.12 4x loading buffer

Tris HCl (2M, pH 6.8) – 1.25 mL

SDS – 0.8 g

Glycerol – 4 mL

ß-mercaptoethanol – 2 mL

Bromophenol blue – 500 μL

MilliQ H_2O up to 10 mL

The buffer was prepared and stored in 1 mL aliquots at -20°C, and briefly thawed in a 95°C heat block before use.

2.2.13 NP40 lysis buffer

Tris-HCl (1M, pH 7.4) – 10 µL

Sodium chloride (1M) – 137 µL

Glycerol – 100 µL

1% NP-40 (10%) – 100 µL

MilliQ H_2O – 415 µL

ß-glycerol phosphate (1M) – 10 µL

Sodium vanadate (0.1 M) – 20 µL

Sodium fluoride (0.5M) – 4 µL

PMSF (0.2M in ethanol) – 10 µL

Sodium pyrophosphate (0.25M) – 10 µL

Leupeptin (1 mg/mL) – 1 µL

Aprotinin (1.7 mg/mL) – 3 µL

1x Complete™ protease inhibitor cocktail (1x tablet in 1 mL MilliQ H_2O) - 100 µL

The buffer prepared ice cold as needed, immediately before use.

2.2.14 Tris buffer A

MilliQ H_2O – 500 mL

1.5 M Tris-HCl (pH 8.8) – 90.885 g

2.2.15 Tris buffer B

MilliQ H_2O – 500 mL

0.5 M Tris-HCl – 30.285 g (pH 6.8)

2.2.16 10x SDS-PAGE running buffer

250 mM Tris-HCl (pH 8.3) – 30.26 g

1.92 M glycine – 144.13 g

1% SDS – 10 g

Dissolved in 750 mL RO H_2O and made up to 1 L. Diluted to 1x in RO H_2O before use.

2.2.17 Tris buffered saline (TBS), 10x stock

200 mM Tris-HCl – 24.2 g (pH 7.5)

1.5 M NaCl – 87.6 g

Dissolved in 750 mL RO H_2O and adjusted to pH 7.5 with HCl, then filled to 1 L. Diluted to 1x in RO H_2O before use.

2.2.18 1x Tris buffered saline + Tween20 (TBST)

10x TBS stock – 100 mL

0.1% Tween20 – 1mL

RO H_2O – 900 mL

2.2.19 10x Transfer buffer stock

Glycine – 144.414 g

Tris – 30.26 g

RO-H_2O – 950 mL

2.2.20 1x Transfer buffer

10x Transfer buffer stock – 100 mL

Methanol – 200 mL

RO-H_2O – 700 mL

2.2.21 2.5% skim milk

2.5% non-fat milk powder – 12.5g

1x TBST – 500 mL

2.2.22 dNTP set (25 mM stock)

40 μL of each 100 mM dNTP stock, stored at -20˚C.

2.2.23 Luria broth agar plates

Luria broth was prepared according to manufacturer's directions, with the addition of 1.2% Select Agar. This was made in 500 mL Schott glass bottles and autoclaved at the SAHMRI washing facility.

2.2.24 Carnoy's fixative

Methanol – 75 mL

Glacial acetic acid – 25 mL

Prepared fresh and kept on ice.

2.2.25 DNA Lysis Buffer

10 mM Tris (pH 8.0)

10 mM NaCl

10 mM EDTA (pH 8.0)

2.2.26 Tyrosine kinase inhibitors

Dasatinib and ponatinib were dissolved into DMSO to prepare a 10 mM stock, which was stored at -20˚C and diluted in DMSO as needed.

2.3 Cell culture and generation of cell lines

2.3.1 General cell culture

All sterile cell culture was performed in a laminar flow cabinet. For cell maintenance, filter capped flasks were stored in a CO_2 incubator at 37˚C in 5% CO_2 at 100% relative humidity. To account for spontaneous mutations associated with long term subculture, cells were maintained under 30 passages post thawing, at which point they were discarded. Cells were maintained at cell density appropriate for cell type to ensure exponential growth, typically between $1 \times 10^5 - 1 \times 10^6$ cells/mL. To assess cell density and viability, trypan blue dye exclusion was performed every 2-4 days, depending on cell type. Trypan blue dye was mixed 1:1 with cell suspension and counted on a Neubauer haemocytometer.

2.3.2 Thawing of cells

Cells were thawed and cultured from liquid nitrogen storage as required. Briefly, cells were retrieved from liquid nitrogen storage and thawed rapidly in a 37°C water bath. The cell suspension was transferred to a conical centrifuge tube, and cell culture medium (Chapter 2.2.1) was added dropwise to 10 mL total volume, with constant mixing. Cells were pelleted by centrifugation and supernatant discarded, and media addition was repeated to remove residual DMSO from the freeze solution. Following this, cells were resuspended in cell culture medium as required.

2.3.3 Cryopreservation of cells

Cell ampoules were cryopreserved in the liquid nitrogen storage facility in SAHMRI, Adelaide. To prepare cells for preservation, 5-10 x 10^6 cells were harvested by centrifugation and resuspended in 1.5 mL freeze solution (Chapter 2.2.7). 1.5 mL ampoules were chilled first to -80°C in a Mr Frosty freezing container, before transfer to liquid nitrogen storage. Listings of cell lines generated are located in SAHMRI leukaemia laboratory databases.

2.3.4 Generation of the K562 dasatinib resistant cell lineage (K562 DasR)

The dasatinib resistant K562 leukaemic cell line, K562 200 nM Das (herein named K562 DasR), was previously developed by our laboratory (205). K562 cells were obtained from American Type Culture Collection (ATCC) and cultured in the presence of dasatinib, increasing from 0.5 to 200 nM over 9.5 months. Over this period, cell ampoule samples were stored at various stages of dasatinib resistance (dose escalation intermediates). A K562 vehicle control line, K562 DMSO, was concurrently generated by culture in 0.02% DMSO. To assess the resistant characteristics of these cell populations, samples were thawed, and interrogated in various experiments. These cells were cultured in the dasatinib concentration to which they had been made resistant during experimentation (e.g. the K562 15 nM Das cell line was cultured in 15 nM dasatinib).

2.3.5 Single cell cloning of K562 200 nM Das cell line

In efforts to assess the genetic and phenotypic heterogeneity within the K562 200 nM Das resistant cell line, single cell cloning of the line was performed. Previously, the line was

demonstrated to express both 'wildtype' *BCR-ABL1* transcripts, as well as those harbouring the T315I mutation. Single cell clones were generated by limiting dilution into 96 well plates, followed by clonal expansion over 30 days. Cell populations with two distinct genotypes were identified, one expressing ~50% T315I mutated *BCR-ABL1* transcripts, and another with no measurable T315I mutation by kinase domain Sanger sequencing. Both of these populations were demonstrated to be similarly resistant to dasatinib and ponatinib; this has been described in my honours thesis (University of Adelaide, BHSc Honours). To further investigate differences in their transcriptional profile, three T315I negative clones (A8, C10 and G5) and two T315I positive clones (B9 and E2) were thawed and used in RNAseq transcriptional profiling experiments.

2.3.6   The HL60 *BCR-ABL1* and HL60 T315I cell lines

HL60 cell lines transduced with *BCR-ABL1* were previously generated by Dr Jane Engler. Briefly, lentiviral particles containing co-expressing eGFP and *BCR-ABL1* in a pHIV-1SDm-based lentiviral vector were kindly provided by Professor John Rasko and Dr Charles Bailey, (Centenary Institute, Sydney, Australia). Vectors contained 5'- and 3'- HIV-1 long terminal repeat, Rev response element, CMV promoter and a woodchuck hepatitis virus posttranscriptional regulatory element. These were transduced into the acute promyelocytic leukaemia cell line, HL60. Cells were FACS sorted for eGFP expression as required to maintain high *BCR-ABL1* expression.

2.4 Cloning of *BCR-ABL1* sequences into Ba/F3 cell lines

2.4.1   Plasmid DNA preparation techniques

Plasmid DNA was expanded, stored in, and extracted from transformed *E. coli* DH5α chemically competent cells. Cells were streaked onto antibiotic selection Luria broth plates, and single colonies were picked for overnight expansion in Luria broth. Glycerol stocks were made as needed using 500 μL of culture mixed with 500 μL of 80% glycerol, and stored at -80˚C.

To expand, extract and purify plasmid DNA from *E. coli* expression cells, miniprep and midiprep were used, as per the amount of DNA required. Transformation of plasmid DNA into

E. coli was performed by heat shock at 42°C for 40 seconds. A single colony culture was expanded in Luria broth. For purification of up 20 µg of DNA, plasmid was prepared using QIAprep Spin Miniprep Kit, according to manufacturer's protocol. For midiprep above these volumes, plasmid midiprep was used with QIAGEN Plasmid Midi Kit, according to manufacturer's protocol.

To isolate DNA bands of specific sizes following gel electrophoresis, DNA products were electrophoresed in a 2% agarose gel at 100V until differentiated by size, and purified using the QIAquick Gel Extraction Kit, according to manufacturer's protocols.

2.4.2 Acquisition and modification of *BCR-ABL1* sequences

The *BCR-ABL1* cDNA sequences, e14a2 and e6a2, were procured from the online plasmid repository, Addgene (224), following unsuccessful attempts at cloning directly from the K562 DasR line in which they originated. An outline of the cloning procedure and methodology can be found in Supplementary Data (Figure S1). The Bcr/Abl P210-pLEF plasmid, deposited by Professor Nora Heisterkamp (Figure S2, #38158), was selected for further experimentation, and has previously been used by Kweon *et al*, for determining the activity of the BCR Rho GTPase domain (225). This was received by stab culture under Materials Transfer Agreement for Addgene order #331443. GMO work was performed under SAHMRI IBC ID: BC07/2016. Cells were expanded under ampicillin selection, plasmid was extracted by miniprep. Extracted plasmid DNA was digested using EcoRI and BamHI to test for the correct digest products (Figure S3) and the *BCR-ABL1* portion was sequenced for validation.

All *BCR-ABL1* full length sequencing of plasmid DNA was performed by AGRF, according to their PD+ protocol, using the following sequencing primers:

BCR-ABL1 seq F1: 5'-GAG GGT TCT CCG GGT AAG GC-3'

BCR-ABL1 seq F2: 5'-CTA CCA GAG CAT CTA CGT CGG G-3'

BCR-ABL1 seq F3: 5'-CAT TGA TGA CTC GCC CTC CTC A-3'

BCR-ABL1 seq F4: 5'-GAG AAC CTG AGA GCC AGA AGC A-3'

BCR-ABL1 seq F5: 5'-GCT GGA CGC TTT GAA GAT CAA GA-3'

BCR-ABL1 seq F6: 5'-GCT GGA CCC AGT GAA AAT GAC C-3'

BCR-ABL1 seq F7: 5'-AGC CCA CTG TCT ATG GTG TGT C-3'

BCR-ABL1 seq F8: 5'-GGT AGC TGA TTT TGG CCT GAG C-3'

BCR-ABL1 seq F9: 5'-CTG AGA TGC CTC ACT CCA AGG G-3'

BCR-ABL1 seq F10: 5'-GCT TCC TGC GCT CTT GCT C-3'

BCR-ABL1 seq F11: 5'-AGG GAG GGA CAA GGG GAA ATT G-3'

BCR-ABL1 seq F12: 5'-CTA GGA ACT CCG AGC AGA TGG C-3'

BCR-ABL1 seq R1: 5'-ATC GCT GCC GGT CAT AGC TC-3'

BCR-ABL1 seq R2: 5'-TTC AAC TCG GCG TCC TCG TAG-3'

BCR-ABL1 seq R3: 5'-CAT CGT TGG GCC AGA TCT GC-3'

BCR-ABL1 seq R4: 5'-CTT CTG GAA GAG GTC GCC CAC-3'

BCR-ABL1 seq R5: 5'-AGT CAT ACT GCT GCG TTT TGC C-3'

BCR-ABL1 seq R6: 5'-TGG CTG AGT GGA CGA TGA CAT T-3'

BCR-ABL1 seq R7: 5'-GCT TGC CAT CAG AAG CAG TGT T-3'

BCR-ABL1 seq R8: 5'-TGA CGA GAT CTG AGT GGC CAT G-3'

BCR-ABL1 seq R9: 5'-TGT TTC CCC AGC TCC TTT TCC A-3'

BCR-ABL1 seq R10: 5'-CAC TGC CCT TTC CAG CTT CTT C-3'

BCR-ABL1 seq R11: 5'-CCG AAG AGA CAC TCG GGT TGA T-3'

BCR-ABL1 seq R12: 5'-TGT CAC TGA TTT CCT TCA CCG A-3'

The sequencing chromatogram files were analysed using Benchling (California, USA), aligning to *BCR* and *ABL1* sequences curated from the Ensembl through the Benchling web application.

In order to minimise the size of the plasmid construct for cloning work, the *BCR-ABL1* e14a2 sequence was cloned from the 7400 bp pLEF vector backbone into the 3960 bp pCR-XL-2-TOPO vector using the TOPO XL-2 Complete Cloning Kit. The *E. coli* line harbouring Bcr/Abl P210-pLEF was expanded from the stab culture under ampicillin selection and used as a template for PCR amplifying the *BCR-ABL1* sequence (Figure S5). This was performed using the SuperFi PCR kit supplied with the TOPO XL-2 Complete Cloning Kit, used with the following primers (bolded region indicates *BCR-ABL1* alignment):

Forward: 5'-GCA TGA ATT CAC C**AT GGT GGA CCC GGT GGG CTT C**-3'
Reverse: 5'-GCA TCA TAT G**CT ACC TCT GCA CTA TGT CAC TGA TTT CCT TCA C**-3'

PCR was performed under the following cycling conditions:

Cycle	Temp (˚C)	Time	Cycles
1	98	30 sec	x1
2	98	10 sec	X28
	66	30 sec	
	72	4 min	
3	72	5 min	x1
4	4	infinity	x1

A ~6 kb PCR product was gel purified and cloned into the pCR-XL-2-TOPO vector as per the manufacturers protocol. The plasmid was transformed into competent *E. coli* DH5α for expansion under kanamycin selection, and *BCR-ABL1* portion was sequenced, and colonies with successful cloning were expanded and stored as glycerol stocks (Figure S6). To generate the e6a2 fusion from the e14a2 construct, site directed mutagenesis was performed using the Q5 Site-Directed Mutagenesis Kit (NEB). A PCR mutagenesis reaction was performed as per manufacturer's instructions, using the following primers:

Forward: 5'-TTT CCA GAG AGT TCT TGG TCG TTG GAT C-3'
Reverse: 5'-AAG CCC TTC AGC GGC CAG TAG CAT-3'

This was performed under the following PCR conditions:

Cycle	Temp (˚C)	Time	Cycles
1	98	30 sec	x1
2	98	10 sec	X25
	69	30 sec	
	72	4 min	
4	72	4 min	x1
5	4	infinity	x1

Concurrently, the e1a2 fusion was also generated by site directed mutagenesis under the same PCR conditions, using the following primers:

Forward: 5'-CTG CGT CTC CAT GGA AGG C-3'

Reverse: 5'-AAG CCC TTC AGC GGC CAG-3'

The template and mutagenised plasmids were digested with EcoRI to ensure correct band sizes (Figure S7). The e6a2 and e1a2 mutagenised plasmids were ligated and transformed into *E. coli* DH5α cells for plasmid expansion and EcoRI test digest (Figures S8/S9). The pCR-XL-2-TOPO *BCR-ABL1* e6a2 and e1a2 mutagenised plasmids were sequenced over the *BCR-ABL1* fusion breakpoint, and colonies with successful mutagenesis were expanded and stored as glycerol stocks. The mutagenised *BCR-ABL1* sequences were then cloned into the pRuf-iG2 retroviral expression vector. The pCR-XL-2-TOPO vector was digested with EcoRI and separated by gel electrophoresis, and the *BCR-ABL1* sequences were excised and gel extracted (Figure S10/S11). The *BCR-ABL1* sequence was cloned into the pRuf-iG2 vector, kindly provided by Professor Andrew Zannettino (University of Adelaide), via the EcoRI site (Figure S12). The e14a2, e6a2 and e1a2 vectors were transformed into *E. coli* DH5α cells under ampicillin selection, and restriction digested using EcoRI and electrophoresed to determine the size of the ligated sequence (Figure S13). Sequencing was performed over the insertion site to determine the correct orientation of the insert. *BCR-ABL1* sequences inserted in the correct orientation were then sequenced in full. No additional single nucleotide or insertion-deletion mutations were identified (data not shown).

2.4.3   Retroviral transduction of *BCR-ABL1* sequences

The Ba/F3 murine pro-B cell line is often used for assessment of the potency and downstream signalling of kinase oncogenes. Ba/F3 cells are typically dependent on supplementation with IL-3 for ongoing proliferation and survival, however transformation with an oncogenic kinase allows growth factor independent proliferation (226). This, coupled with the co-expression of green fluorescent protein (GFP), allowed the purification of *BCR-ABL1* transduced cells.

For expression of *BCR-ABL1* sequences in the Ba/F3 cell lines, retroviral particles were produced by expansion in HEK293T cells. 1×10^6 HEK293T cells were seeded in 5 mL of HEK293T cell culture medium for 24 h. A DNA lipofection solution was prepared with 500 µL Opti-MEM reduced serum media, 4 µg of the pRuf-iG2 expression construct, and 4 µg of pEQ-

Eco viral packaging plasmid (227). Separately, a lipofectamine solution was prepared with 500 µL Opti-MEM media and 20 µL Lipofectamine and incubated for 10 minutes. These two solutions were combined and incubated for 2 h at room temperature, before dropwise addition to the HEK293T cell flasks and incubation for 24 h. Media was refreshed and cells incubated a further 24 h, after which viral supernatant was collected by centrifugation and filtered through a 0.45 µm syringe filter. Polybrene was added to viral supernatant to give a final concentration of 4 µg/mL. Ba/F3 cells were pelleted by centrifugation and resuspended in 3.5 mL of viral supernatant from *BCR-ABL1* e14a2, e6a2, e1a2, or the pRuf-iG2 empty vector control. Cells were transduced by spinfection at 1800 rpm for 1 h in a 6 well culture plate. Following a 24 h incubation at 37°C in viral supernatant, cells were expanded in fresh media and FACS sorted for GFP fluorescence, attaining a pure population of *BCR-ABL1* expressing cells. To ascertain the malignant transformation of the Ba/F3 cells by Bcr-Abl kinase activity, WEHI-3B conditioned media was withdrawn from Ba/F3 cell culture medium, and phosphorylation of CrkL was determined by western blotting.

2.5 Quantitation of TKI resistance

2.5.1 TKI-induced cytotoxicity assay

To determine and quantify the level of resistance to kinase inhibitors, K562 and Ba/F3 cell lineages were subjected to the TKI-induced cytotoxicity assay. Cells were cultured in a concentration gradient of a TKI, with an appropriate vehicle control, in 1 mL volume of minimal media (Chapter 2.2.5) in a sterile 24-well cell culture plate. Following 72 h incubation at 37°C / 5% CO_2, cells from 200 µL of culture medium were harvested by centrifugation at 1400 rpm for 5 min, washed with 200 µL binding buffer, and stained with 50 µL Annexin V / 7-AAD staining solution for 20 min at room temperature. 7-AAD can penetrate the plasma membranes of dead cells, intercalating into double stranded DNA. Annexin-V PE is a phycoerythrin conjugated phospholipid protein that binds to the inverted inner surface of the cell membrane, on the outer surface of dying cells. Staining for both allows the determination of the live, dead, and dying fractions of a cell population. Single stained (Annexin V only or 7-AAD only) and unstained controls were simultaneously performed, using a mix of live and dead cells. Following addition of 200 µL binding buffer, cells were analysed on either a BD FACSCanto™ II or BD LSRFortessa X-20 at the SAHMRI Flow Cytometry Core Facility, with the

assistance of Dr Randall Grose. FCS file processing was performed using either FCS Express version 4.07.0019 (De Novo Software, California, USA) or FlowJo version 9 (FlowJo LLC, Oregon, USA), adjusting compensation based on single stained and unstained controls.

2.5.2 Phospho-CrkL IC50 analysis of Bcr-Abl kinase activity

To quantify the level of cellular Bcr-Abl activity in the presence of TKI, the phospho-CrkL IC50 was performed as previously described (228). This uses the phosphorylation of the Bcr-Abl target, CrkL, as a measure of Bcr-Abl kinase activity. An IC50, the half maximal inhibitory concentration, can be calculated following culture in a TKI concentration gradient. Briefly, 2×10^5 cells were washed with RPMI 1640 medium and resuspended 10 mL of RPMI 1640 + 10% NCS + 0.5% DMSO in a 50 mL centrifuge tube. Nine concentrations of TKI were identically set up, which spanned the expected IC50 concentration. These experiments were also performed in the presence of the ABCG2 inhibitor, Ko143, in order to determine the role of ABCG2 in TKI transport. Cells were incubated at 37˚C / 5% CO_2 for 2 h, before being pelleted by centrifugation, washed in 5 mL ice cold PBS, transferred to a 1.7 mL microfuge tube, and lysed in 20 μL of Laemmli's lysis buffer in a 100˚C heat block for 12 min. Lysates were clarified by brief centrifugation and stored at -20˚C.

CrkL and pCrkL were visualised by western blot. Frozen protein lysates were heated in a 100˚C heat block for 12 mins, then separated on a denaturing 10% polyacrylamide gel for ~2 hours at 20 V per gel at 4˚C, until pCrkL separated from CrkL. Protein was transferred to PVDF membrane in transfer buffer overnight at 50 mA. Membrane was blocked with 2.5% skim milk powder in TBST for 1 h and probed with 1:1000 anti-CrkL antibody for 2 h. Membrane was washed 3x in TBST for 5 min, then probed with 1:2000 anti-rabbit IgG alkaline phosphatase antibody for 1 h. Membrane was finally washed 3x in TBST and 3x in TBS for 5 min, then treated with ECF substrate for 90 sec and analysed on a ChemiDoc Gel Imaging System (Bio-Rad Laboratories Inc., California, USA). Scan files were analysed using provided Image Lab software version 5 build 8, to perform band densitometry. Relative CrkL/pCrkL band intensities were plotted in Microsoft Excel version 16.17, to determine an IC50 concentration.

2.6 Genetic analysis of resistance mechanisms

2.6.1 RNA extraction and cDNA synthesis

RNA used for cDNA synthesis and subsequent RT-qPCR analyses was extracted and purified from cell lines using TRIzol reagent extraction. Using $2x10^6$ cells per 1 mL of TRIzol, cells were mixed and lysed by pipetting, at which point they were optionally stored at -80˚C for later extraction. Phase separation was performed with the addition of 200 μL of chloroform and mixed by shaking for ~10 sec and incubation for 3 minutes at room temperature, before centrifugation at 12 000 xg for 15 min at 4˚C. The top aqueous layer was transferred to a new 1.7 mL microfuge tube, and RNA was precipitated with the addition of 500 μL isopropanol and 1 μL glycogen. Samples were mixed gently and incubated for 10 min at room temperature, before pelleting RNA by centrifugation at 12 000 xg for 10 min at 4˚C. Supernatant was removed by pipetting and the RNA pellet was washed with the addition of 1 mL of ice cold 75% ethanol and centrifugation at 7500 xg for 5 min at 4˚C. Supernatant was removed, samples were re-centrifuged and remaining supernatant also removed, and RNA pellet was briefly dried before resuspension in 20-50 μL of DEPC-treated water at 55˚C for 10 minutes.

RNA concentration was quantitated using a NanoDrop microvolume spectrophotometer (Thermo Fisher Scientific, Massachusetts, USA) , and cDNA was synthesised from 500 ng RNA using the SuperScript II First Strand Synthesis System for RT-PCR, according to manufacturer's protocols.

2.6.2 DNA extraction from cell lines

DNA was extracted from cell line material using the phenol chloroform extraction method. Up to $5x10^6$ cells were pelleted by centrifugation and washed with 1 mL PBS at 4˚C. Cell pellet was resuspended in 480 μL DNA Lysis Buffer by pipetting. SDS was added to a final concentration of 0.5%, as well as 10 μL of Proteinase K, and mixed by inversion 30 times. Samples were incubated overnight at 37˚C to complete cell lysis. 5 μL of RNase A was added and tubes were mixed by inversion 50 times, and incubated at 37˚C for 10 min. 10 μL of 5 M sodium chloride, 1 μL of glycogen, and 500 μL of buffer saturated phenol was added, and samples were mixed by shaking 50 times, before centrifugation at 16 000 xg for 5 min at room temperature, and the top aqueous later was transferred to a new 1.7 mL microfuge tube by

pipetting. 500 μL of phenol:chloroform:isoamyl alcohol mixture was added, and sample mixed by shaking 50 times, before centrifugation at 16 000 xg for 3 min. The top aqueous later was transferred to a new 1.7 mL microfuge tube, and Phenol:Chloroform:Isoamyl alcohol extraction was repeated as required for purity. DNA was precipitated with the addition of 1 mL of ethanol at -80˚C and mixing by inversion. Samples were centrifuged at 20 000 xg for 10 min at 4˚C, supernatant was removed, and DNA pellet was washed with 600 μL ice cold 70% ethanol. Ethanol was removed by centrifugation at 20 000 xg for 5 min at 4˚C, and DNA pellet was dried briefly at room temperature. DNA pellet was resuspended in 200 μL of DNA Hydration Solution at 55˚C for 2 h and quantitated using NanoDrop microvolume spectrophotometry, before use or storage at 4˚C.

2.6.3   *BCR-ABL1* RT-qPCR

For quantitation of the *BCR-ABL1* transcript levels, RT-qPCR was performed using the SYBR® Green Real-Time PCR Master Mix system. For quantitation of the typical e14a2 (p210) transcript, found in drug naïve K562 cells, the following primers were used:

Forward: 5'-GGG CTC TAT GGG TTT CTG AAT G-3'
Reverse: 5'-CGC TGA AGG GCT TTT GAA CT-3'

To our knowledge, quantitation of the *BCR-ABL1* e6a2 transcript had not been previously performed, requiring the design of RT-qPCR primers and experiments for this purpose. Using the Primer Express© Software for Real-Time PCR (Applied Biosystems), the following primers were designed for amplification of the BCR-ABL1 e6a2 breakpoint:

Forward: 5'-AAC GAC CAA GAA CTC TCT GGA AA-3'
Reverse: 5'-TGA GGC TCA AGT CAG ATG CT ACT-3'

For quantitation of *BCR-ABL1* e1a2 (p190) transcripts from transduced Ba/F3 cell lines, the commercially available BCR-ABL TaqMan Gene Expression Assay for e1-a2 was used according to manufacturer's protocol.

To normalise between samples, RT-qPCR was also performed for the control gene *GUSB*, using the following primers:

Forward: 5'-CTG AAC AGT CAC CGA CGA GA-3'
Reverse: 5'-GAA CGC TGC ACT TTT TGG TT-3'

Reactions were performed under standard 3 step SYBR Green qPCR protocol conditions, including melt curve analysis:

Cycle	Temp (˚C)	Time	Cycles
1	95	3 min	x1
2	95	10 sec	X40
	55	10 sec	
	72	30 sec	
4	95	10 sec	x1
5	65-95	5 sec per 0.5˚C	x1

In the K562 DasR cell line experiments, data were reported as a ddCt value, comparing gene expression levels with the K562 DMSO control line. In the Ba/F3 cell lines, data were reported as a dCt value against the *GUSB* control gene.

2.6.4   *BCR-ABL1* kinase domain Sanger sequencing

Sequencing of the *BCR-ABL1* kinase domain allowed the efficient detection of the kinase domain mutations commonly associated with TKI resistance. Briefly, a region of the *BCR-ABL1* e14a2 was amplified using the Expand Long Template PCR System, according to manufacturer's protocols, using the provided Expand Long Template Buffer 3 and the following primers:

Forward: 5'-ACT ATG AGC GTG CAG AGT GGA-3'
Reverse: 5'-GAG GGA GCA ATG GAG ACA CG-3'

The *BCR-ABL1* e6a2 transcript kinase domain was amplified using the following primers:

Forward: 5'-CAT GAA GCC TTT GAA AGC CG-3'

Reverse: 5'-GAG GGA GCA ATG GAG ACA CG-3'

These were amplified using the following PCR cycling conditions:

Cycle	Temp (˚C)	Time		Cycles
1	94	2 min		x1
2	94	10 sec		X10
	60	30 sec		
	68	2 min		
3	94	10 sec		x15
	60	30 sec		
	68	2 min, increasing by 20 sec each round		
4	68	7 min		x1
5	4	infinity		x1

Sequencing was performed by AGRF, using the following sequencing primers:

Forward: 5'-CGC AAC AAG CCC ACT GTC T-3'

Reverse: 5'-CAA GGT ACT CAC AGC CCC ACG GA-3'

Sequencing chromatogram files were aligned to *ABL1* sequences using Benchling or Mutation Surveyor® version 3.30 (SoftGenetics LLC, Pennsylvania, USA).

2.6.5   PCR validation and kinase domain sequencing of *BCR-ABL1* e6a2 transcript detection

Following the putative identification of the e6a2 fusion in FusionCatcher analysis of K562 DasR mRNA sequencing data, validation experiments were designed and performed. A PCR forward primer was designed within *BCR* exon 5 (ABLe5F):

Forward: 5'-CAT GAA GCC TTT GAA AGC CG-3'

Additionally, a forward primer straddling the *BCR-ABL1* e6a2 breakpoint was designed:

Forward 5'-CTC TCT GGA AAA AGC CCT TCA-3'

Both forward primers were used with the existing reverse primer for *BCR-ABL1* kinase domain amplification:

Reverse: 5'-GAG GGA GCA ATG GAG ACA CG-3'

Reactions were amplified using the Expand Long Template PCR System, as previously described for *BCR-ABL1* e14a2 transcript PCR. The PCR amplicons generated were resolved by 1% agarose gel electrophoresis. Additionally, amplicons were sequenced over the *ABL1* kinase domain, as per sequencing for *BCR-ABL1* kinase domain Sanger sequencing for e14a2 transcript mutations. Templates used were cDNA samples from the K562 DMSO, 10, and 200 nM DasR lines used in mRNAseq experiments.

2.6.6   MassARRAY sensitive *BCR-ABL1* kinase domain sequencing

The sensitivity of Sanger sequencing used for *BCR-ABL1* kinase domain mutation analysis was only 5-10%, therefore a more sensitive MALDI-TOF mass spectrometry based method of sequencing was also used (229), to determine whether cell populations with low T315I expression were present in K562 DasR dose escalation intermediates and single cell clones. The MassARRAY iPLEX System *BCR-ABL1* sequencing was performed with thanks to Mr Adrian Purins from the Leukaemia Unit at SA Pathology (Adelaide, Australia).

2.6.7   Target enrichment sequencing and validation for *BCR-ABL1* breakpoint detection

To identify the different *BCR-ABL1* fusions present in the K562 DasR cell lines dose escalation intermediates, target enrichment sequencing was performed using the SureSelect Target Enrichment System for Illumina Paired-End Multiplexed Library Sequencing, as per manufacturer's protocol. Briefly, DNA was extracted from selected K562 DasR dose escalation intermediate samples and single cell clones. A panel of capture probes spanning *ABL1* and

BCR genomic regions was designed by Dr Ilaria Pagani (SAHMRI Cancer Theme, Adelaide, Australia). Samples were hybridised with a fragmented and adaptor tagged genomic DNA library prepared from K562 samples, purified by magnetic bead wash, and sequenced on the Illumina NextSeq 500 platform (Illumina Inc., California, USA), generating 2x150 bp paired end reads. Sequencing data was uploaded to the Illumina BaseSpace Sequencing Hub.R Genomic breakpoints were determined using the FACTERA genomic fusion detection tool, and visualised using the NCBI Genome Data Viewer.

The *BCR-ABL1* e6a2 DNA breakpoint was–validated by PCR, gel electrophoresis, and Sanger sequencing in selected K562 DasR dose escalation intermediates, using the following primers flanking the breakpoint, designed using Primer3 version 1.1.4:

Forward: 5'-GTC CAG AGT TGC TGG GAA AG-3'
Reverse: 5'-GAA GAC CTT GAG TGC CAA GC-3'

2.6.8 *BCR-ABL1* DNA qPCR

Following identification of the *BCR-ABL1* e14a2 and e6a2 fusion breakpoints in the K562 DasR cell line, the genomic quantity of each fusion was determined using DNA qPCR. TaqMan FAM-TAMRA primers and probe were used to amplify the e14a2 genomic breakpoint:

Forward: 5'-TGA CCA CGG GAC ACC TTT G-3'
Reverse: 5'-AGG GTA TTT CTG TTT GGG TAT GGA-3'
Probe: 5'-CTG GCC GCT GTG GAG TGG GTT TTA TC-3'

MGB-TAMRA qPCR probes were designed over the e6a2 breakpoint:

Forward: 5'-AAG ATC TCA CAA CAG CTA TGA AGC A-3'
Reverse: 5'-GAG CAG GTC TCC CTC CAG AAT-3'
Probe: 5'-AGA CAG GAT TCC CC-3'

These were used in conjunction with TaqMan FAM-TAMRA control primers and probe amplifying genomic *GUSB* sequences:

Forward: 5'-ATT TTG CCG ATT TCA TGA CTG A-3'

Reverse: 5'-GAC GGG TAC GTT ATC CCA TGA G-3'

Probe: 5'-ATC CCA TGA GCC AAA CTG CCA CTT ACA C-3'

These primer/probe combinations were used with K562 DasR dose escalation intermediate DNA samples, as well as in serial dilutions of *GUSB* and *BCR-ABL1* e14a2 plasmid DNA, allowing relative quantitation of genomic *BCR-ABL1* copy numbers. This was reported as a percentage of *GUSB* quantity.

2.6.9   Cytogenetic *BCR-ABL1* analysis by fluorescence *in situ* hybridisation (FISH)

To investigate the genomic quantity and characteristics of *BCR-ABL1* fusions in K562 lines, cytogenetic analysis was performed. FISH analyses were performed with the assistance of Mr Jeffrey Suttle from the SA Cancer Cytogenetics Unit at IMVS, SA Pathology (Adelaide, Australia). Log phase K562 cells were cell cycle arrested by treatment with 10 µL/mL colcemid for 30 min at 37˚C, before centrifugation and aspiration of supernatant to 300 µL. Hypotonic potassium chloride (0.075 M) was added to a total volume of 9 mL, and cells were allowed to swell for 30 min at 37˚C. Carnoy's fixative was added to 10 mL total volume, and cells were pelleted by centrifugation for 10 min at 1000 rpm. Cells were repeatedly fixed and washed a further 2-3 times. Finally, fixative was aspirated to a minimal volume and ~0.5 mL of fixative was added to form a thin dispersion. Cells were dropped onto a glass slide from ~20 cm above and air dried, before immediate probing using 2 µL of the Vysis LSI BCR-/ABL Dual Color FISH probe. Samplers were sealed with a coverslip and sealed with Fixo Gum rubber cement, before performing probe denaturation / hybridisation by incubating in a Hybaid Omnislide thermal cycler (Thermo Fisher Scientific, Massachusetts, USA) at 72˚C for 4 minutes, then 37˚C overnight. Slides were stored in the dark from this point onwards. Slides were washed firstly with 0.4x saline sodium citrate + 0.1% NP-40 for 2 minutes at 72˚C, then 2x saline sodium citrate at room temperature for 1 minute. Slides were dried, and mounted with a small volume of Vectashield Antifade Mounting Medium with DAPI, and sealed with a cover slip. Cells were examined on a 100x oil lens using a red/green dual band pass filter.

2.6.10 *ABCG2* RT-qPCR

To determine the gene expression of ABC transporters, RT-qPCR was used. For quantitation of the *ABCG2* transcript, the following primers were used:

Forward: 5'-CAC CTT ATT GGC CTC AGG AA-3'
Reverse: 5'-CCT GCT TGG AAG GCT CTA TG-3'

For quantitation of the *ABCB1* transcript, the following primers were used:

Forward: 5'-AGA CAT GAC CAG GTA TGC CTA T-3'
Reverse: 5'-AGC CTA TCT CCT GTC GCA TTA-3'

Both of these primer pairs were used with a standard 3 step SYBR Green qPCR protocol, as per the *BCR-ABL1* RT-qPCR thermal cycling protocol.

To normalise between samples, RT-qPCR was also performed for the control gene *GUSB*, as per *BCR-ABL1* RT-qPCR protocol. Data were reported as a ddCt value, comparing gene expression levels with the K562 DMSO control line.

2.7 Protein and functional analysis of resistance mechanisms

2.7.1 Bcr-Abl and signalling partner western blot analysis

To visualise the level of Bcr-Abl protein in leukaemic cells, normal and phospho western blotting was performed. K562 cells were incubated in the presence of dasatinib or ponatinib for 2 h at 37˚C / 5% CO_2. Cells were washed in PBS and lysed by incubation with NP40 lysis buffer on ice for 20 min, followed by clarification of the lysate by centrifugation at 14000 rpm for 15 min at 4˚C. A sample of the supernatant was taken for protein quantification, and the remainder was added to 0.333 the volume of 4x LB, boiled in a 100˚C heat block for 12 minutes, and stored at -20˚C. Protein quantification for western blotting was performed using the DC Protein Assay, according to manufacturer's protocol. Lysates were equally loaded by total protein, typically at 40 µg. Lysates were separated by size exclusion SDS-PAGE gel electrophoresis on a Criterion TGX Precast gel, using the Precision Plus Protein Kaleidoscope

Standards or the BenchMark Protein Ladder. Protein was transferred to PVDF membrane using the Trans-Blot Turbo Transfer System (Bio-Rad Laboratories Inc., California, USA), using the high molecular weight setting. Membrane was cut appropriately and blocked using Li-Cor Odyssey Blocking Buffer for 1 h, then probed with anti-phospho-Bcr (1:1000), anti-phospho-Abl (1:1000), anti-Abl (1:1000), anti-phospho-STAT5 (1:1000), anti-phospho-STAT5 (1:1000), or β-Tubulin (1:2000) antibodies in Odyssey Blocking Buffer at 4˚C for 16-24 h. Membranes were washed 4x with TBST, then probed with donkey-anti-rabbit IRDye680LT (1:10000) and donkey-anti-mouse IRDye 800CW (1:10000) in Odyssey Blocking Buffer + 0.1% Tween20 + 0.01% SDS for 1 h at room temperature in darkness. Membranes were then washed 3x in TBST and 3x in TBS, before analysis on the Li-Cor Odyssey CLx Imaging System (Li-Cor Biosciences, Nebraska, USA). Image analysis was performed using supplied ImageStudio software version 5.2.5.

2.7.2 Flow cytometry for cell surface ABC transporter expression

To determine the cell membrane protein expression of ABC transporters, flow cytometric analyses were performed. Staining was performed on $5x10^5$ cells, which were pelleted by centrifugation and resuspended in 250 μL of flow cytometry blocking buffer on ice for 30 minutes. Cells were stained with either 20 μL of ABCG2 PE (with IgG2b PE isotype control) or ABCB1 PE (with IgG2a PE isotype control) antibodies, on ice for 40 min. Cells were washed twice with 1 mL HBSS + HEPES, and resuspended in PBS. Cells were analysed on either a BD FACSCanto™ II or BD LSRFortessa X-20 at the SAHMRI Flow Cytometry Core Facility, with the assistance of Dr Randall Grose. FCS files were analysed in FlowJo, gating ABC transporter positivity against known negative control samples.

2.7.3 BODIPY-prazosin efflux assay

To demonstrate the functional substrate transport activity of the ABCG2 transporter, leukaemic cells were analysed for uptake and/or efflux of the BODIPY-prazosin ABCG2 substrate. Cells were cultured in cell culture media at 37˚C for 1 h, in the presence and absence of the fluorescent marker BODIPY-prazosin, and in the presence and absence of the ABCG2 inhibitor Ko143, which effectively blocks ABCG2 function and BODIPY-prazosin efflux (230). Cells were subsequently washed of BODIPY-prazosin twice in PBS, and resuspended in

400 µL PBS supplemented with 5% BSA. BODIPY-prazosin fluorescence was detected by flow cytometry in the FITC channel; stain negativity was used as an indication of functional ABCG2.

2.7.4 Dasatinib intracellular uptake and retention assay

The IUR assay was performed with thanks to Mrs Sophie Watts, as previously described (163). Briefly, 2×10^5 cells were incubated with 0 or 2 µM C^{14}-dasatinib (kindly provided by Bristol Myers Squibb), in the presence or absence of 0.5 µM Ko143. This was performed for 2 h at 37^oC, in 2 mL of RPMI-1640 medium containing 10% FCS. Following incubation, cells were pelleted by centrifugation for 5 min at 6800 rpm then 30 sec at 13000 rpm. Radioactivity of C^{14}-dasatinib was determined independently in the supernatant and cell pellet using a Tri-Carb 2810R Liquid Scintillation Counter (Perkin Elmer, Inc.). The IUR was reported as ng of dasatinib incorporated per 200,000 cells, and results were expressed as mean +/- SEM.

2.8 Transcriptome sequencing and analysis

2.8.1 mRNA next generation sequencing

To explore the changes in the K562 DasR cell line associated with the acquisition of TKI resistance, sequencing of RNA transcripts from K562 DasR dose escalation intermediates was performed. Additionally, to explore the transcriptional diversity within the population of the cell line, previously generated single cell clones of the K562 200 nM Das line were sampled for mRNAseq experiments. RNA was extracted from 12 samples, which included K562 naïve and DMSO control lines, the 10, 15, 25, 50 and 200 nM K562 DasR lines, and the A8, C10, G5, E2 and F5 K562 200 nM Das single cell clones. Sequencing libraries were prepared using the NEXTFlex Rapid Directional RNA Seq Library Prep Kit. This kit utilises magnetic beads conjugated to oligo(dT) to isolate polyadenylated messenger RNA, depleting ribosomal and non-coding RNA. Initial quality control of RNA was performed using the Agilent 2100 Bioanalyzer (Agilent Technologies, California, USA), using the Bioanalyzer RNA 6000 Nano assay (Figure S14).

Libraries were sequenced on the Illumina MiSeq instrument (Illumina Inc., California, USA), using a 150 cycle to produce 2x75 bp paired end reads. Sequencing data was uploaded to the Illumina BaseSpace Sequencing Hub, which was used for FastQC quality control (Figure S15).

Read data was downloaded from BaseSpace for differential expression and fusion gene interrogation.

2.8.2   Differential expression analysis

To explore the differences in mRNA transcript expression in the K562 DasR samples, differential expression analysis was performed using the EdgeR pipeline (231), which was performed in RStudio version 1.1.447 using R version 3.5.0. The R script used can be found in the github repository found at: https://github.com/benleow/holy-grail

Sequencing reads were aligned to the hg19 reference genome using the STAR aligner (232). Lowly expressed reads (<10 counts per million) were filtered out, and samples were normalised based on library size. Gene symbol names were annotated from the NCBI database.

Hierarchical clustering dendrograms were generated based on the Euclidean distance between pooled sequencing samples, using Ward's minimum variance method (Figure S16). Based on these results, samples were clustered into discrete groupings to perform differential expression analysis. The K562 10, 15 and 25 nM Das cell lines were grouped together, for comparison with naïve and DMSO treated K562 control samples (Figure S17). Similarly, the K562 50 and 200 nM Das samples were grouped for analysis (Figure S18). Differential expression analysis was then performed using the Linear Models for Microarray and RNA-seq Data (limma) package for R. A heatmap of the 100 most differentially expressed genes, as ranked by p-value, was generated from each sample grouping compared with the K562 controls (Figures S19 and S20). Differentially expressed genes were also visualised with a volcano plot, highlighting genes with false discovery rate (FDR) <0.005, and log fold change (logFC) > 2 (Figure S21).

2.8.3   FusionCatcher analysis of fusion gene transcripts

To determine the novel genetic and transcriptional fusions associated with dasatinib resistance in the K562 DasR line, the FusionCatcher fusion gene detection tool was used, according to recommended guidelines (233). RNA sequencing reads were filtered, removing

reads aligning to ribosomal or transfer RNA, mitochondrial DNA, microorganism genomes, and the frequently spliced HLA genes. Adaptors and poly-nucleotide tails were trimmed. Reads were aligned to Ensemble genome annotations, and unmapped reads are kept for further analyses. Filtering steps enrich for reads which map to multiple genomic locations, such as fusion genes. To determine the fusion partners in the fusion gene, a list of candidate fusion partners is generated by aligning portions of the read to different genes. This preliminary list of candidate fusion genes is further filtered for paralogs, pseudogenes, micro RNA and transfer RNA, and other known false positive events such as conjoined HLA genes or overlapping genes. For increased sensitivity, the process is repeated four times using the Bowtie, BLAT, STAR and Bowtie2 aligners. A list of fusions and the amount of breakpoint supporting reads is provided as output. This output was manually interrogated for relevant fusions, and a figure of *BCR-ABL1* fusions and the supporting read numbers was generated.

2.9 Statistical analyses and generation of figures

Statistical analyses for comparative analysis of cell viability, IC50, and qPCR replicate experiments was performed in GraphPad Prism version 7.0, using unequal variance t-test to account for expected differences in variance and number of sample replication. Figures were prepared using Microsoft Powerpoint version 16.17, before transfer to Microsoft Word version 16.17. Tables were prepared using Microsoft Excel version 16.17.

3 Amplification and overexpression of the *BCR-ABL1* oncogene drives primary TKI resistance, and precedes development of the T315I mutation

3.1 Overview

Induced resistance to targeted chemotherapeutics in cell line models is a well-established method for the study of drug resistance mechanisms, including for kinase inhibition therapy in CML (182, 200). Using a K562 cell line model (K562 DasR), the gradual accumulation of TKI resistance was explored. Assays were performed to validate and quantify the level of dasatinib resistance. The K562 DasR cell line was previously generated in our laboratory (205). K562 cells were passaged over ~11 months, in concentrations of dasatinib increasing from 0.5 to 200 nM (Figure 3.1). At each increment of dasatinib concentration, cells were expanded and stored for subsequent analysis. The K562 DasR line was already known to exhibit *BCR-ABL1* overexpression and the T315I mutation as dasatinib resistance mechanisms, and the later intermediates in dasatinib dose escalation are highly resistant to dasatinib. These findings were thoroughly investigated at the beginning of this study, firstly by determining the level of TKI resistance of cells following prolonged dasatinib culture, then by exploring in detail the known TKI resistance mechanisms in the cells. *BCR-ABL1* expression was determined by RT-qPCR, and kinase domain mutations were determined by Sanger sequencing.

The level of dasatinib resistance was quantitated using the TKI-induced cell death assay, which utilises AnnexinV / 7-AAD staining of cell death markers, to ascertain the dose escalation intermediates in which resistance to therapeutic concentrations of dasatinib was acquired. It was hypothesised that positivity for the T315I mutation would be the biggest predictor of dasatinib resistance in the K562 DasR dose escalation intermediates. Dose escalation intermediate cell line samples were chosen before and after acquisition of T315I for viability analysis (10, 15, 25, 50, 200 nM Das, DMSO vehicle control). In order to link dasatinib resistance to Bcr-Abl activity in the presence of TKI, and demonstrate the cell line's dependence on Bcr-Abl for maintaining cell viability, selected dose escalation intermediates (2, 3.5, 5, 10, 15, 25, 50, 200 nM Das, DMSO control) were characterised by TKI pCrkL IC50 (IC50^{Das}). This was performed by utilising western blot analyses for phosphorylated CrkL, a marker of Bcr-Abl kinase activity (228).

Although *BCR-ABL1* (p210) transcript overexpression had previously been demonstrated in the K562 DasR line (Figure 3.1), the cellular aberrations causing this overexpression were unclear. Duplication of the Philadelphia chromosome is a recognised mechanism of treatment resistance and disease progression in CML (234). Chromosome duplication is reflected by increases in the gene expression and protein production of the *BCR-ABL1* gene, and excess oncoprotein can drive further proliferative signalling, leading to disease progression (10, 149). Understanding the mechanisms of *BCR-ABL1* gene and protein overexpression is beneficial from a disease prognosis standpoint, and may direct the design of therapeutic strategies. Therefore, studies were performed to quantify the genomic levels of *BCR-ABL1*. DNA amplification was determined by qPCR using a FAM-TAMRA primer/probe set designed for quantifying the typical K562 *BCR-ABL1* e14a2 genomic fusion breakpoint, and chromosomal abnormalities and *BCR-ABL1* gene amplification were observed by fluorescence *in situ* hybridisation (FISH) using a *BCR-ABL1* probe.

The presumed level of Bcr-Abl protein increases coinciding with DNA amplification and gene expression had not previously been measured, nor had the phosphorylation and activation of downstream signalling partner proteins such as STAT5. The predicted increases in Bcr-Abl protein levels, coinciding with rising *BCR-ABL1* transcript levels, were demonstrated by western blotting. Additionally, western blotting for phosphorylated Bcr-Abl (pAbl-Y245 and pBcr-Y177) was performed in selected intermediates to determine the association between gene expression and protein phosphorylation/activation. These were performed in gradient dasatinib and ponatinib. Expression and phosphorylation of the downstream signalling proteins STAT5 and CrkL was also simultaneously performed.

Mutation of the Bcr-Abl gatekeeper residue, T315I, was previously demonstrated as a resistance mechanism occurring in the K562 DasR line (Figure 3.1), conferring complete resistance to the TKIs dasatinib, nilotinib, and imatinib (134). The third generation TKI, ponatinib, is often used as salvage for therapy-resistant patients expressing the T315I mutation. Though it was designed to inhibit T315I-mutated Bcr-Abl, significantly higher concentrations of ponatinib are required to inhibit Bcr-Abl^{T315I}, when compared to Bcr-Abl^{wt}. There is also evidence that the gatekeeper residue mutation is kinase activating, resulting in increased transformative activity (160, 161). The T315I mutation was detected in the final 200

nM dasatinib line, with approximately 50% of *BCR-ABL1* (e14a2) transcripts expressing the C944T (T315I) base pair change. The mutation was retrospectively found at a low level in the 25 nM dasatinib intermediate (205). These data were replicated for validation. To detect presence of the T315I mutation at a low level, as might be expected with a minor population of T315I+ founder clones, additional Sequenom MassARRAY sequencing of the *BCR-ABL1* kinase domain was performed in selected K562 DasR intermediates. The Sequenom MassARRAY iPLEX platform utilises MALDI-TOF mass spectrometry to sensitively detect genetic mutations from PCR amplicons (235).

The acquisition of severely limits treatment options in CML, for which the only clinically available TKI is ponatinib. Loss of ponatinib efficacy in the cells of these patients often results in refractory disease. Hence, it was of clear importance to determine the sensitivity of the dasatinib resistant K562 cell lines to ponatinib induced cell death. To quantify the level of cross-resistance to ponatinib, ponatinib-induced cell death and ponatinib pCrkL IC50 assays (IC50^{Pon}) were performed in K562 DasR dose escalation intermediates. Again, K562 DasR intermediates before and after acquisition of T315I were analysed (10, 15, 25, 50, 200 nM Das, DMSO vehicle control).

While the K562 DasR cell line used in these analyses provides an adequate backbone for exploring emergent drug resistance mechanisms, the continually evolving nature of the cell line does not allow for determining the effect on kinase activity of isolated point mutations, such as T315I. A genetically purer model was therefore required to explore the effect of single point mutations of *BCR-ABL1*. To explore the effect of the T315I mutation on Bcr-Abl kinase function in the presence of dasatinib and ponatinib, the HL60 p210 and T315I cell lines were analysed by IC50^{Das} and IC50^{Pon}. These lines were previously generated by transducing HL60 cells with a pHIV-1SDm-based lentiviral vector containing both the *EGFP* gene and a *BCR-ABL1*^{wt} or *BCR-ABL1*^{T315I} gene, respectively. These were compared and contrasted with pCrkL IC50s calculated in the K562 DasR lines, to estimate the contribution of the T315I mutation to acquired TKI resistance.

3.2 Results

3.2.1 Dose escalation intermediates demonstrate gradual increases in resistance to dasatinib-mediated cell death

The dasatinib-induced cell death assay data demonstrated the gradual accrual of dasatinib resistance in the K562 DasR line, evidenced by increasing IC50^{Das} with ongoing passage in dasatinib. In the DMSO vehicle control line, cell viability was ablated by 100 nM dasatinib (Figure 3.3). However, this effect was attenuated in the K562 10 nM Das intermediate, and cells were significantly more viable that DMSO control (15% vs 48%, n=3, p=0.0057). Between the 10 and 15 nM Das intermediates, dasatinib resistance was significantly increased (48% viability vs 75%, n=3, p=0.0147). Complete dasatinib resistance was attained in the K562 25 nM Das and later intermediates, which exhibit stable cell viability in all dasatinib concentrations up to 5000 nM.

3.2.2 Bcr-Abl activity in K562 DasR resistance intermediates is maintained in the presence of dasatinib

To investigate the contribution of Bcr-Abl kinase activity to acquired dasatinib resistance, levels of phospho-CrkL (a surrogate marker of Bcr-Abl activity) were measured in K562 DasR dose escalation intermediates and control cells. Summary data of pCrkL IC50^{Das} demonstrate the gradual accrual of dasatinib resistance in the K562 DasR line (Figure 3.4). The dasatinib IC50 increases from 7.4 nM in the DMSO control to 37.5 nM in the K562 2 nM Das intermediate (n=4, p=0.0084). Between the 5 nM and 15 nM dasatinib intermediates, the IC50 increases significantly to over 700 nM (29.5 vs 743 nM, n=3, p=0.004). Confirming the findings of dasatinib cell death assay experiments, Bcr-Abl kinase activity in the 25 nM and higher intermediates cannot be inhibited, even in the presence of 5000 nM dasatinib, an unachievable clinical plasma concentration. Taken together with dasatinib cell death data, IC50 results indicate all K562 DasR cells remain dependent on Bcr-Abl activity for ongoing survival.

3.2.3 K562 DasR cells acquire the T315I mutation following long term culture in dasatinib, conferring complete dasatinib resistance

The presence of the Bcr-Abl T315I mutation in late-stage intermediates of the K562 DasR cell line correlated with complete dasatinib resistance. Sanger sequencing of the *BCR-ABL1* kinase domain in the K562 DasR dose escalation intermediates investigated the timeline of the emergence of T315I (Figure 3.5). The mutation was undetectable in K562 naïve and DMSO control lines, as well as all K562 DasR dose escalation intermediates up to the 50 nM Das, in which C944T was detectable in ~30% of amplified transcripts. Sequencing results from the *BCR-ABL1* transduced HL60 cell lines transcribing genetically pure *BCR-ABL1* mutants are included for reference.

Subsequent sequencing results from the more sensitive Sequenom MassARRAY platform demonstrated the emergence of the T315I mutation in the 25 nM Das intermediate, detected at very low frequency (0.5-2% of transcripts, Figure 3.5b). No other kinase domain mutations were detected. These data were consistent with previously published findings in the cell line (205). This suggests that a very low percentage of T315I expression is sufficient for the induction of dasatinib resistance.

To demonstrate the direct effect of the T315I mutation on dasatinib TKI efficacy, the pCrkL IC50 assay was performed on *BCR-ABL1* transduced HL60 lines harbouring wildtype (p210^{wt}) or mutated (p210^{T315I}) Bcr-Abl. HL60 cells expressing wildtype Bcr-Abl had a dasatinib IC50 of 8.9 nM, however, in the HL60 line expressing T315I mutated Bcr-Abl, kinase activity could not be inhibited, even in 5000 nM dasatinib (Figure 3.6).

3.2.4 *BCR-ABL1* e14a2 gene overexpression contributes to early dasatinib resistance

Data on expression levels of *BCR-ABL1* in K562 DasR dose escalation intermediates demonstrate transient fluctuations in *BCR-ABL1* gene expression (Figure 3.7). Over the course of dasatinib dose escalation, *BCR-ABL1* expression in K562 DasR cells trended upward, with the 2 nM Das intermediate expressing over 12-fold higher expression than DMSO control (n=3, p=0.0224). Of the dasatinib resistant intermediates tested, *BCR-ABL1* expression was highest in the 3.5 nM Das intermediate (13.9-fold increase over DMSO), however, due to large inter-assay variance, this did not reach statistical significance (n=3, p=0.0855). Interestingly,

over prolonged exposure to high concentration dasatinib, *BCR-ABL1* expression decreased, with the final 200 nM Das line expressing significantly lower transcript levels than the 2 nM Das intermediate (3.8 vs 12.1, n=3, p=0.0221). DMSO exposure did not significantly affect *BCR-ABL1* expression levels when compared with naïve K562 cells (1 vs 1.21, n=3, p=0.6809, data not shown).

3.2.5   Bcr-Abl protein levels are higher in K562 DasR lines; increased kinase signalling likely leads to resistance

Western blot analysis indicated an overexpression of Bcr-Abl protein in the K562 DasR dose escalation intermediates compared with control lines. Bcr-Abl protein levels increased in all intermediates compared with the DMSO-treated vehicle control (Figure 3.8). This was likely due to the increased *BCR-ABL1* mRNA expression levels observed (Figure 3.7). Also confirming RT-qPCR data, Bcr-Abl protein expression levels peaked early in the course of dose escalation, reducing after prolonged and increased dasatinib exposure. Intriguingly, a second protein band was identified, which migrated faster than the typical 210 kDa (e14a2) Bcr-Abl band observed in the control cells. This smaller Abl band was present in varying levels in all K562 DasR cells. The nature of this protein was further explored and is discussed in Chapter 4.

Bcr-Abl phosphorylation and activation typically results in the downstream phosphorylation of signalling proteins to elicit proliferative activity. To determine the effect of TKI exposure on Bcr-Abl signalling pathway activation, three K562 DasR dose escalation intermediates were selected for investigation of Bcr-Abl phosphorylation status (pBcr Y177 and pAbl Y245), STAT5a/b activation, and phosphorylation of the CrkL adaptor protein (Figure 3.9). K562 5 nM DasR, K562 200 nM DasR and K562 DMSO control cells were exposed to gradient TKI (5, 20, 200 nM dasatinib, 200 nM ponatinib, DMSO control). Results were concordant with pCrkL IC50^{Das} data, demonstrating the K562 DasR lines' continued activation of Bcr-Abl kinase signalling in the presence of TKI; this observation was particularly evident in the K562 200 nM DasR cells. In the 5 nM DasR intermediate, phosphorylation of Bcr Y177 was maintained in up to 20 nM dasatinib, although Abl (Y245) and CrkL (Y207) phosphorylation was inhibited with 5 nM dasatinib. Additionally, total Bcr-Abl expression was higher in K562 DasR lines than in the DMSO control line. Once again, the multiple apparent Bcr-Abl isoforms were observed in both K562 DasR lines, but not in the DMSO vehicle control. Total STAT5 protein levels

remained unchanged across all samples, however, phosphorylation of STAT5 was increased in DasR lines, likely indicative of increased Bcr-Abl signalling. Confirming dasatinib IC50 results, the 200 nM Das line remained kinase active in all dasatinib concentrations, however, kinase activity was ablated following two hours exposure to 200 nM ponatinib.

3.2.6 Genomic *BCR-ABL1* e14a2 copy increase coincides with increased *BCR-ABL1* e14a2 mRNA levels and acquisition of TKI resistance

DNA qPCR for *BCR-ABL1* copy number analysis showed a strong trend with both mRNA and protein expression levels, indicating that genomic amplification of the *BCR-ABL1* gene is likely causative of gene and protein overexpression (Figure 3.10). When normalised to PCR amplification of *GUSB*, the genomic level of *BCR-ABL1* quickly increased from 7.5% in the K562 DMSO line to 71% in the 2 nM DasR intermediate (n=3, p<0.0001). Note this is a relative expression level, and there is differential PCR amplification efficiency between *GUSB* and *BCR-ABL1*. *BCR-ABL1* copy number per cell is maximal in the 3.5 nM DasR intermediate, however, decreased significantly in the 5 nM DasR intermediate (102% vs 48.2%, n=3, p=0.001). *BCR-ABL1* DNA levels then fluctuated over the remainder of TKI dose escalation, transiently rising again in the 10 nM DasR intermediate, then falling with ongoing TKI exposure, such that *BCR-ABL1* levels were significantly lower in the final 200 nM DasR line (10 nM vs 200 nM, 69.7% vs 28.4%, n=3, p=0.014).

To investigate whether increased *BCR-ABL1* expression was associated with duplication of the Philadelphia chromosome or the addition of extrachromosomal elements, FISH analyses of *BCR-ABL1* gene fusions were performed in selected K562 DasR lines (Figure 3.11). Both interphase and metaphase spreads of K562 200 nM Das line indicated *BCR-ABL1* amplification occurred following prolonged dasatinib exposure. Notably, metaphase spreads revealed that gene amplification occurred within the original Philadelphia chromosome locus and was not present throughout the genome or on extrachromosomal elements.

3.2.7 Dasatinib resistant cells exhibit lowered ponatinib-induced cell death

Given ponatinib is often used as salvage therapy in dasatinib-resistant disease, cross-resistance to ponatinib was examined in K562 DasR. Data from ponatinib cell death assays in

dose escalation intermediates demonstrated decreases in ponatinib sensitivity coinciding with loss of dasatinib sensitivity (Figure 3.12). In the presence of 10 nM ponatinib, K562 10 nM DasR cells were significantly more viable than DMSO control cells (86% vs 23.6%, n=3, p=0.0007). However, unlike dasatinib sensitivity, decreases in ponatinib sensitivity did not occur linearly, and ponatinib resistance was not maximal in the 200 nM DasR line. Indeed, ponatinib resistance peaked in the 15 nM DasR intermediate, which upon culture in 50 nM ponatinib (a typical peak plasma concentration) was 63% viable, compared with 13% viable in the 200 nM DasR line in the same ponatinib concentration (n=3, p=0.0002). Importantly, all K562 DasR intermediates exhibited lower sensitivity to ponatinib than the DMSO vehicle control line, suggesting that the acquired dasatinib resistance mechanisms, such as overexpression of Bcr-Abl, also confer a loss of sensitivity to ponatinib.

3.2.8 K562 DasR dose escalation intermediates exhibit lower ponatinib IC50, and is not entirely dependent of %T315I

Ponatinib IC50 data in K562 DasR dose escalation intermediates supported cell death assay findings. All K562 DasR dose escalation intermediates exhibited ponatinib tolerance compared with vehicle control (Figure 3.13). As observed in cell death assay experiments, ponatinib sensitivity was lower in all K562 DasR lines when compared with DMSO control cells, and lowest in the 10 and 15 nM DasR intermediates (101 and 99 nM Das, respectively; $p < 0.01$). Correlating with ponatinib cell death assay data, the 25, 50 and 200 nM DasR lines trended towards higher ponatinib sensitivity than the 10 and 15 nM Das intermediates, however, this did not reach significance.

3.2.9 HL60 cells harbouring Bcr-Abl with the T315I mutation are less sensitive to ponatinib-based kinase inhibition

While ponatinib was designed to inhibit T315I mutated Bcr-Abl, it has been previously demonstrated that it does so with lesser activity (138). To quantify the effect of the T315I mutation on ponatinib efficacy, HL60 cells harbouring Bcr-Abl[T315I] were subjected to ponatinib IC50 (IC50[Pon]). Summary IC50[Pon] data from HL60 lines reiterated previous findings: while ponatinib was able to effectively inhibit T315I-mutated Bcr-Abl, it did so with lower efficacy

(Figure 3.14). Ponatinib IC50 calculated for wildtype Bcr-Abl was 9.4 nM ponatinib, compared with 59.3 nM for Bcr-Abl harbouring T315I (n=3, p=0.0095).

3.3 Discussion

The K562 DasR cell line was generated in our laboratory and preliminary experiments identified *BCR-ABL1* overexpression and the T315I mutation as mechanisms of resistance (205). In the current study, a comprehensive interrogation of dose escalation intermediates validated these findings, allowing confident use of the model.

The emergence of the T315I mutation in the 25 nM Das intermediate coincided with the gain of complete dasatinib resistance, as demonstrated by both dasatinib-induced cell death and pCrkL IC50^{Das} results. Furthermore, the lack of dasatinib response in the 25 nM Das intermediate indicated that each cell in the population harboured and expressed T315I mutated Bcr-Abl. Consistency between cell death assay and pCrkL IC50 assay results indicated that the cell line remained dependent on Bcr-Abl kinase activity for proliferation and survival.

3.3.1 Unknown mechanisms contribute to TKI resistance in the K562 10 and 15 nM DasR intermediates

In the DasR intermediate prior to acquisition of T315I (K562 15 nM DasR), the increased IC50^{Das} indicated a comparative decrease in sensitivity to dasatinib. Previously published *BCR-ABL1* RT-qPCR data (205) suggested this was a result of increased *BCR-ABL1* gene and protein expression. However, IC50^{Das} in the 10 and 15 nM DasR intermediates was significantly higher than the 2, 3.5 and 5 nM DasR intermediates, despite DNA *BCR-ABL1* qPCR and RT-qPCR data demonstrating no further increases in *BCR-ABL1* expression or genomic amplification. Additionally, IC50^{Pon} and cell death assays demonstrated that ponatinib sensitivity was lowest in the 10 and 15 nM DasR intermediates. IC50^{Pon} values calculated from retrovirally transformed HL60 p210^{wt} vs HL60 p210^{T315I} cells indicated that gatekeeper residue mutation conferred a significantly higher IC50^{Pon} compared with T315I mutation-harbouring cells. Based on these observations, it was expected that the K562 50 nM and 200 nM DasR lines would be less sensitive to ponatinib than earlier intermediates not harbouring T315I. The unexpectedly high IC50^{Pon} in the 10 and 15nM DasR intermediates suggested that resistance

mechanisms, in addition to either T315I or Bcr-Abl overexpression, were present in the intermediate lines, but not in the final resistant lines. While the IC50^{Pon} in the 50 and 200 nM Das intermediates were not significantly lower than the 10 and 15 nM Das intermediates, they were comparatively sensitive to ponatinib. The lack of significance may be attributable to the wide variance in individual IC50 values, due to a combination of fluctuating biological and experimental batch effects. To explore the resistance mechanisms at play in the dasatinib escalation intermediates, K562 DasR samples were selected for transcriptome sequencing analysis, the results of which are detailed in Chapters 4 and 5.

3.3.2   Bcr-Abl expression and TKI resistance

DNA qPCR, RT-qPCR, and western blotting experiments demonstrated early increases in Bcr-Abl gene and protein levels; prolonged and increased dasatinib exposure resulted in decreased Bcr-Abl expression levels. Correlation between increases in *BCR-ABL1* DNA content, and mRNA and protein expression levels, indicated that the primary mode of overexpression was driven by gene amplification. The mechanisms of gene duplication have been well studied (236, 237). The use of FISH analysis of K562 DasR cells revealed the tandem duplication of the *BCR-ABL1* gene within the original Philadelphia chromosome locus, which coincided with increased mRNA gene expression. However, to our knowledge, the rapid loss of *BCR-ABL1* DNA copy number has not been previously observed, and it is hypothesised that this was the result of the expansion and outgrowth of a leukaemic clone which had lower *BCR-ABL1* content, but which harboured an alternate, unknown dasatinib resistance mechanism. As the protein driver of oncogenesis and cellular proliferation in CML, Bcr-Abl levels often increase alongside disease progression, and there is a strong selective pressure for cells harbouring multiple copies of the fusion gene. However, our data suggest that while increased Bcr-Abl expression did contribute to TKI resistance, this effect was self-limiting; Bcr-Abl levels did not continue rising with prolonged TKI exposure. Our data also suggest there is an upper limit to the amount of Bcr-Abl a leukaemic clone can express and/or tolerate. Under dasatinib selective pressure, emergence of alternate resistance mechanisms such as T315I allowed these leukaemic clones to efficiently outcompete the *BCR-ABL1* overexpressing cells.

3.3.3 Bcr-Abl isoforms and TKI resistance

Western blot analyses of Bcr-Abl kinase and downstream signalling partners in K562 DasR dose escalation intermediates provided insight into Bcr-Abl activity in the presence and absence of TKI. As expected, Bcr-Abl kinase phosphorylation was associated with the phosphorylation of downstream partner, STAT5, as well as the adaptor protein CrkL. Additionally, a smaller band binding both Bcr and Abl antibodies was demonstrated in K562 DasR dose escalation intermediates. It was possible that this band represented a smaller Bcr-Abl fusion, similar to the p190 (e1a2) fusion observed in cases of Ph+ ALL, an aggressive lymphoid malignancy. There was a critical need to identify this Bcr-Abl isoform. While the contribution of this isoform to TKI resistance was not determined, the smaller fusion likely contributed to overall Bcr-Abl overexpression and kinase activity, even if the truncated fusion was not inherently less sensitive to TKI-based inhibition. Interestingly, phosphorylation of the smaller Bcr-Abl isoform would also allow Bcr-Abl harbouring the T315I mutation to phosphorylate wildtype Bcr-Abl, thereby maintaining protein kinase activation. In addition, the smaller Bcr-Abl fusion may confer the protein an alternate cell signalling profile. The delineation of this Bcr-Abl isoform and its contribution to TKI resistance was explored further in Chapter 4.

3.3.4 Chapter summary

The experiments presented here demonstrate that the K562 DasR model of TKI resistance accurately represents clinical observations TKI resistance mechanisms. *BCR-ABL* gene overexpression was validated in dose escalation intermediates, and correlated with gene duplication within the Philadelphia chromosome. The resultant Bcr-Abl protein overexpression allowed continuing activation of downstream signalling in moderate TKI concentrations, and protein visualisation identified a smaller Bcr-Abl fusion which was further explored. Determination of T315I mutation status was associated with loss of dasatinib sensitivity, as well as lowered ponatinib sensitivity, however the concurrent measurement of TKI sensitivity suggested alternate resistance mechanisms in the K562 10 and 15 nM DasR intermediates. Clonal selection of the cell line was observed and indicated that while Bcr-Abl overexpression is sufficient in lower TKI concentrations, other resistance mechanisms were more advantageous or necessary in higher concentrations. Experimental repetition will

determine whether these are stochastic events, or whether the selective pressures consistently result in clonal dominance of certain cell populations.
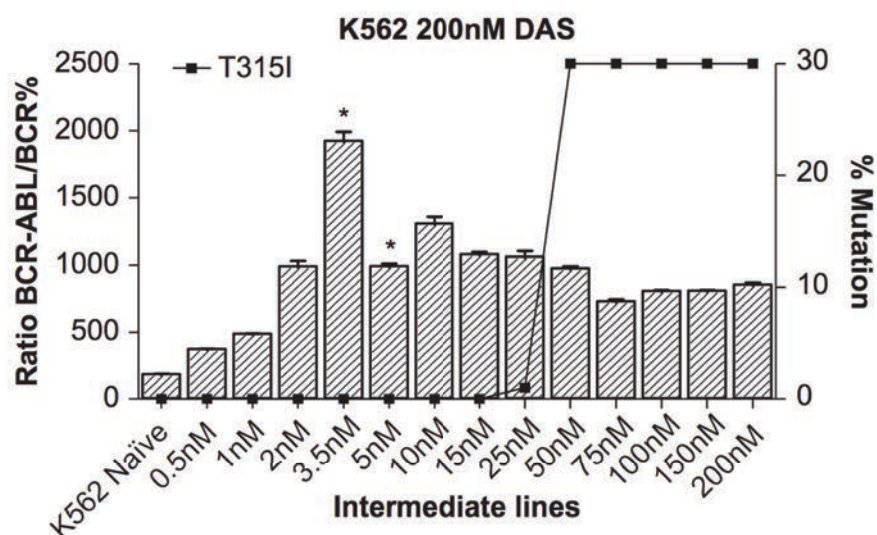
3.4 Chapter 3: Figures

Figure 3.1: Previously identified resistance mechanisms in the K562 200 nM Das resistant cell line. Bars represent mRNA expression of the *BCR-ABL1* fusion typically expressed by K562 cells, e14a2. Results demonstrate the gradual increase of *BCR-ABL1* expression, peaking in the 3.5 nM Das intermediate, before falling significantly in the 5 nM Das intermediate. Unpaired t-test was performed between dose escalation intermediates; significance is denoted by (*) for $p < 0.05$. Additionally, the percentage of T315I mutated *BCR-ABL1* e14a2 transcripts is shown on the line graph. First detected in the 25 nM Das intermediate, %T315I quickly rises with prolonged dasatinib dose escalation. Reproduced with permission from (205).
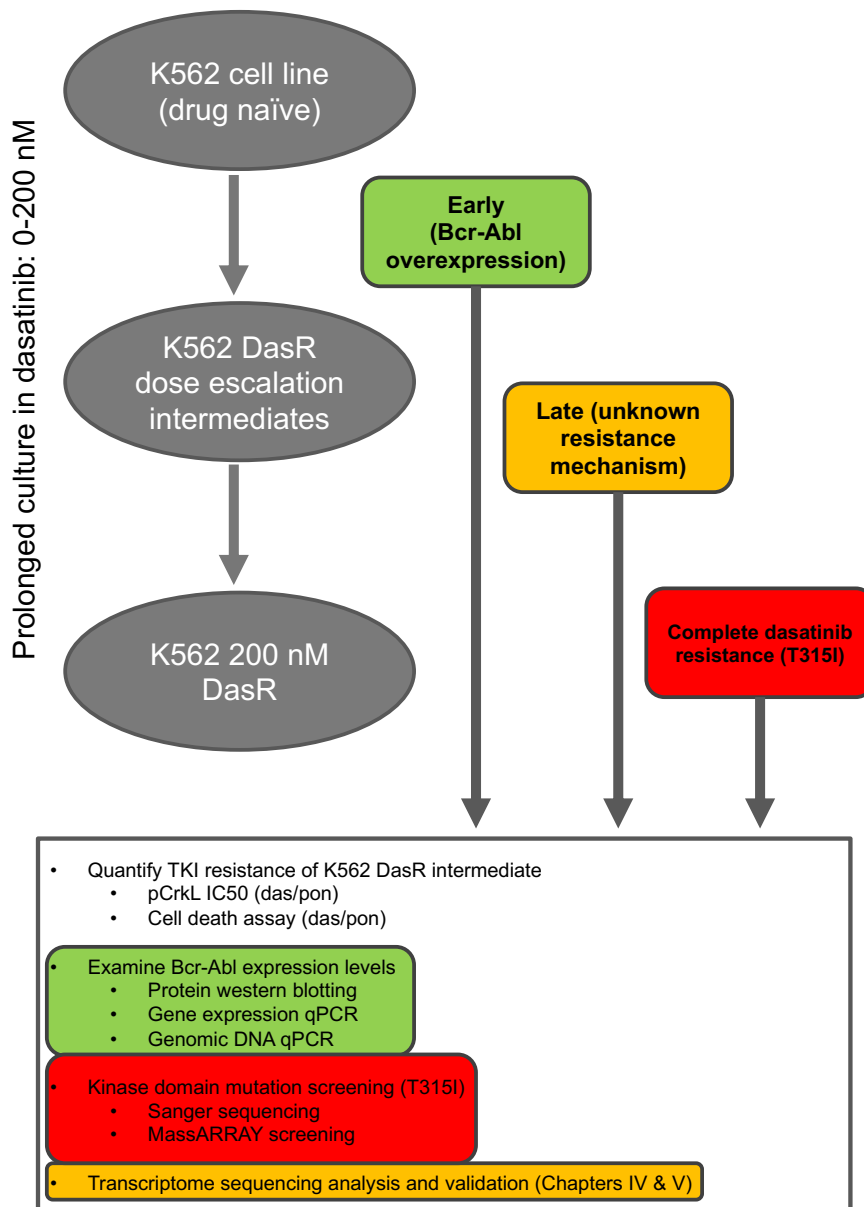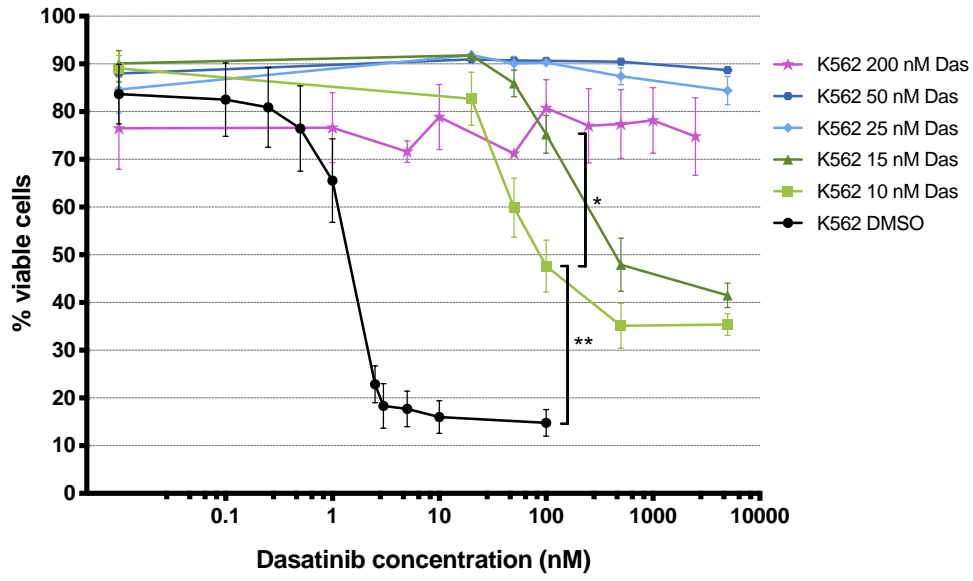
Figure 3.2: Flow chart of the generation of the K562 DasR cell line and dasatinib dose escalation intermediates, and experiments performed for quantitation of TKI resistance, and analyses for potential TKI resistance mechanisms. Das = dasatinib, pon = ponatinib.
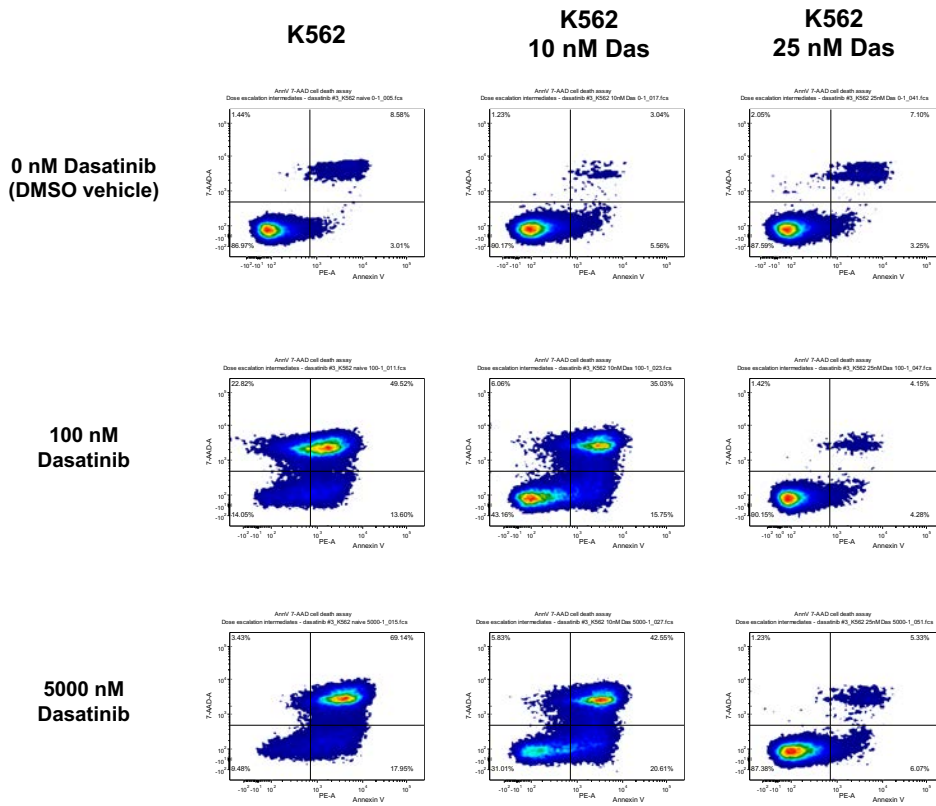
a)

b)

Figure 3.3: K562 cells cultured in dasatinib exhibit decreased sensitivity to dasatinib induced cell apoptosis. a) Cell viability of K562 DasR dose escalation intermediates cultured in gradient dasatinib for 72 h. Values indicate mean -/+ SEM of at least 3 independent replicate experiments. Unequal variances t-test was performed between dose escalation intermediates at each dasatinib concentration; significance is denoted by (*) for $p < 0.05$, (**) for $p < 0.01$. b) Representative data of AnnexinV (x-axis) / 7-AAD (y-axis) co-staining for cell viability in 0, 100 and 5000 nM dasatinib. Percent viable cells (AnnexinV / 7-AAD negative) from three separate experiments were plotted in a).
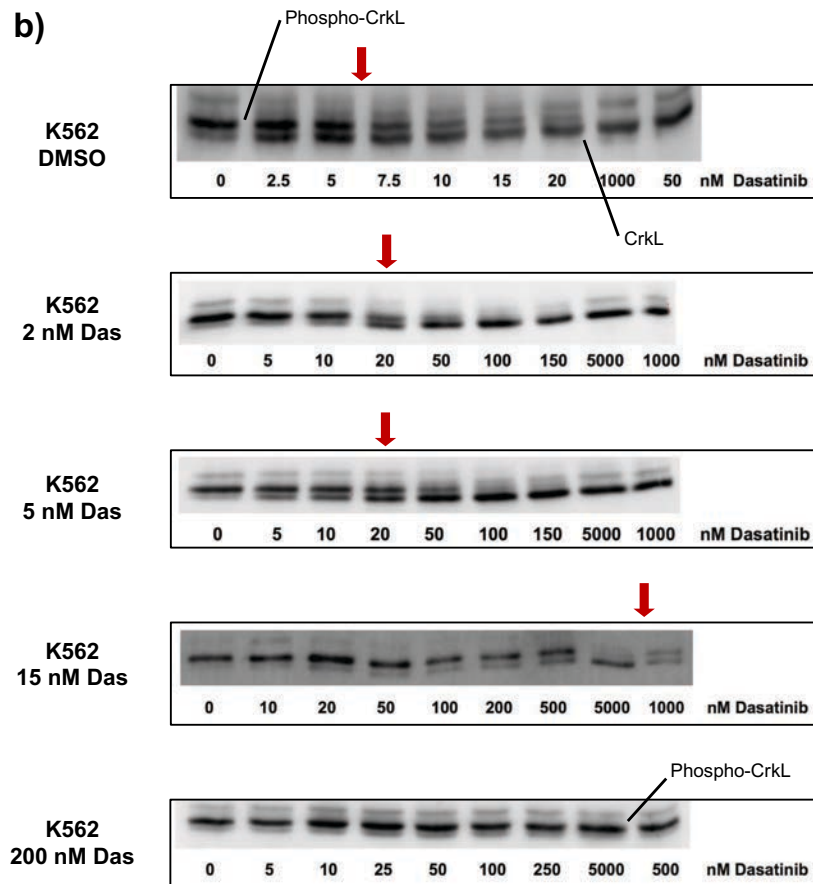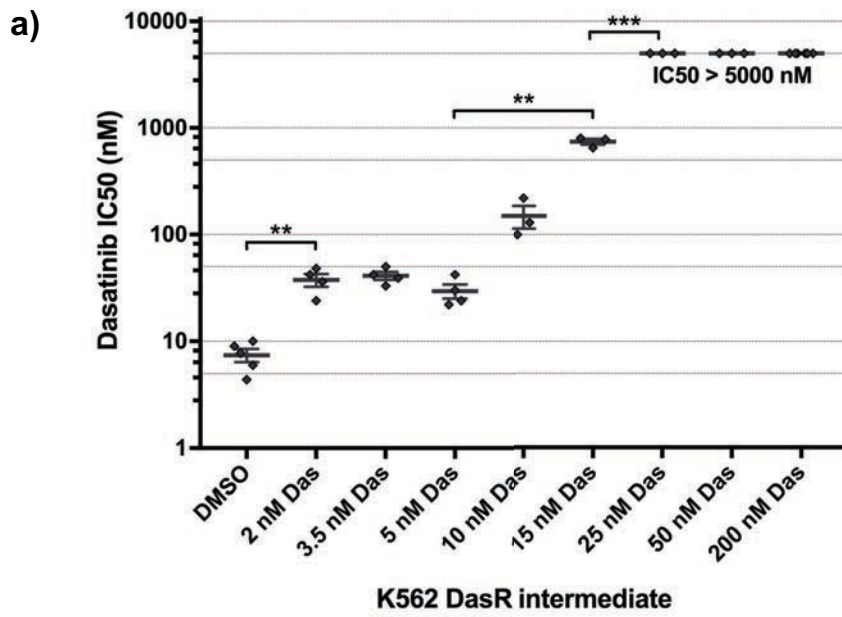
a)

b)

K562 DMSO

K562 2 nM Das

K562 5 nM Das

K562 15 nM Das

K562 200 nM Das

Figure 3.4: a) Dasatinib IC50 data for K562 dose escalation intermediates, based on loss of phosphorylated (Phospho-) CrkL. Data confirms that prolonged culture in increasing doses of dasatinib coincides with a decrease in dasatinib sensitivity. Whiskers indicate mean -/+ SEM of at least 3 independent replicate experiments. Unequal variances t-test was performed between dose escalation intermediates; significance is denoted by (**) for $p < 0.01$, (***) for $p < 0.001$. b) Representative dasatinib pCrkL IC50 western blotting. Samples are selected K562 DasR dose escalation intermediates; red arrows indicate the approximate point of 50% Bcr-Abl kinase inhibition (IC50^{Das}).

a)

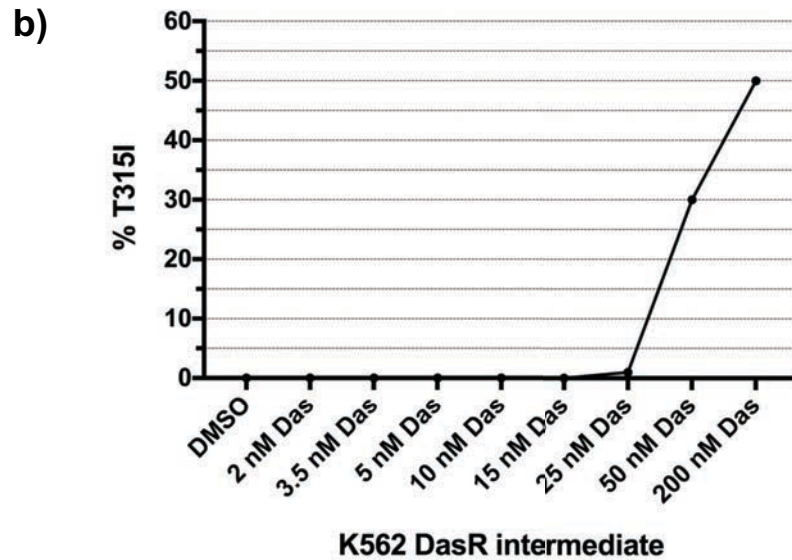| Lane label	
HL60 p210^wt	

b)

Figure 3.5: a) *BCR-ABL1* (e14a2) kinase domain mutation screening using the Sanger sequencing platform for selected TKI resistant and control cell lines. Highlighted region indicates cytosine 944 which, upon mutation to thymine, gives rise to the protein sequence mutation, T315I. b) Summary data of percentage T315I mutated *BCR-ABL1* (e14a2) transcripts from K562 dose escalation intermediates using the Sequenom MassARRAY platform. Results demonstrate the gain of the T315I mutation in the K562 25 nM Das intermediate, which is strongly selected for upon ongoing dasatinib dose escalation. wt=wildtype.
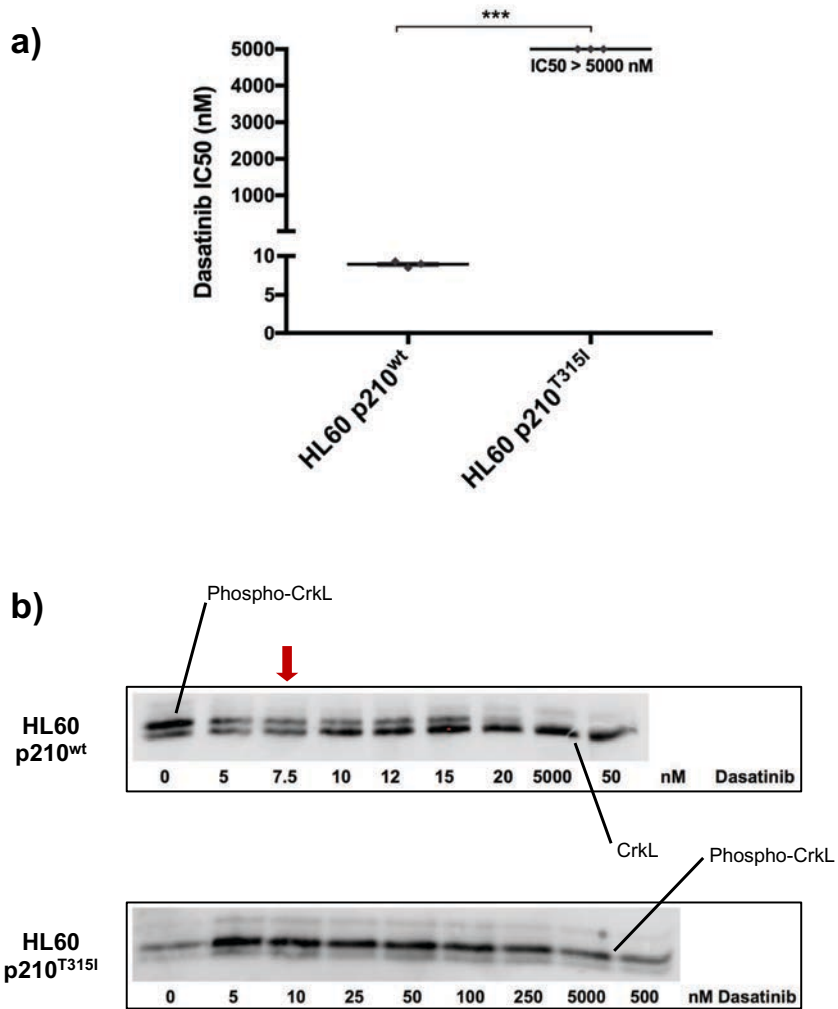
Figure 3.6: a) Dasatinib IC50 values for HL60 lines transfected with wildtype (wt) or T315I mutat *BCR-ABL1*, based on loss of phosphorylated (Phospho-) CrkL. Values indicate mean -/+ SEM of 3 independent experiments. Unequal variances t-test was performed between dose escalation intermediates; significance is denoted by (***) for p<0.001. b) Representative dasatinib IC50 western blotting; red arrow indicates the approximate point of 50% Bcr-Abl kinase inhibition (IC50[Das]), which was not achievable in the HL60 p210[T315I] line.

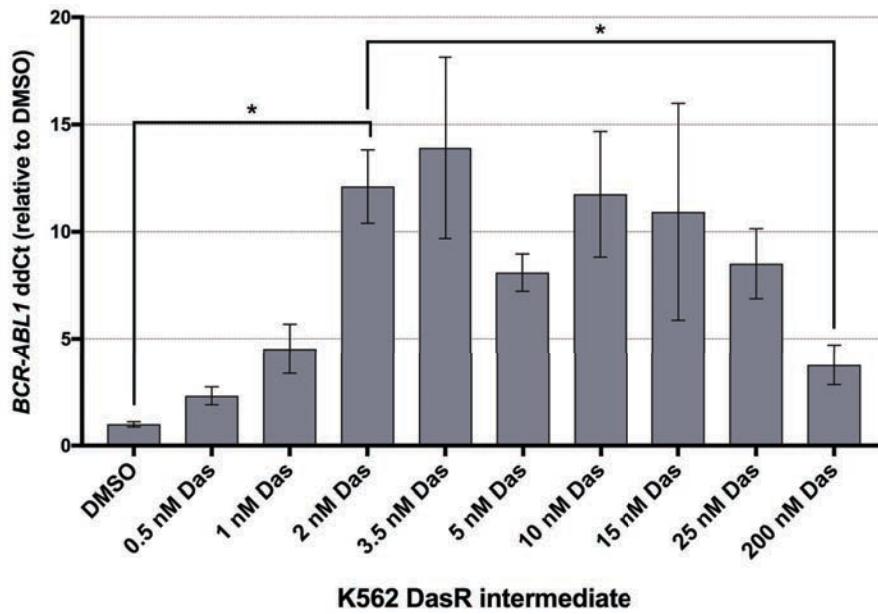Figure 3.7: *BCR-ABL1* (e14a2 transcript) mRNA expression levels in K562 DasR dose escalation intermediates rise transiently with increasing dasatinib exposure. Data represent mean -/+ SEM of 3 independent experiments. Unequal variances t-test was performed between dose escalation intermediates; significance is denoted by (*) for $p < 0.05$.
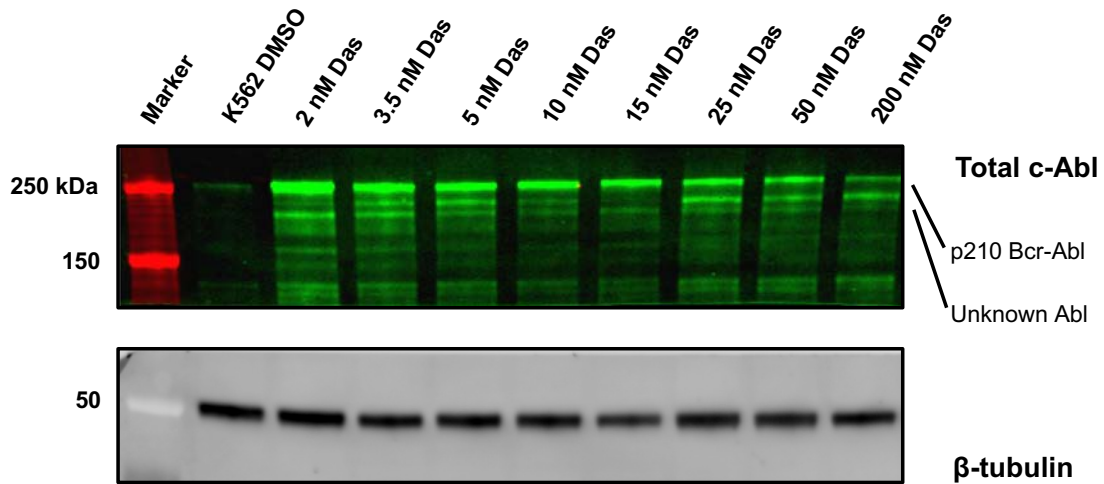
Figure 3.8: Western blotting analysis of total c-Abl from NP40 lysates in K562 DasR dose escalation intermediates. Results indicate an increase in Bcr-Abl expression concurrent with increasing dasatinib concentration levels, as well as the emergence of at least one additional Bcr-Abl isoform, appearing ~10-20 kDa smaller than the typical 210 kDa (*BCR-ABL1* e14a2) protein harboured in drug naïve K562 cells.
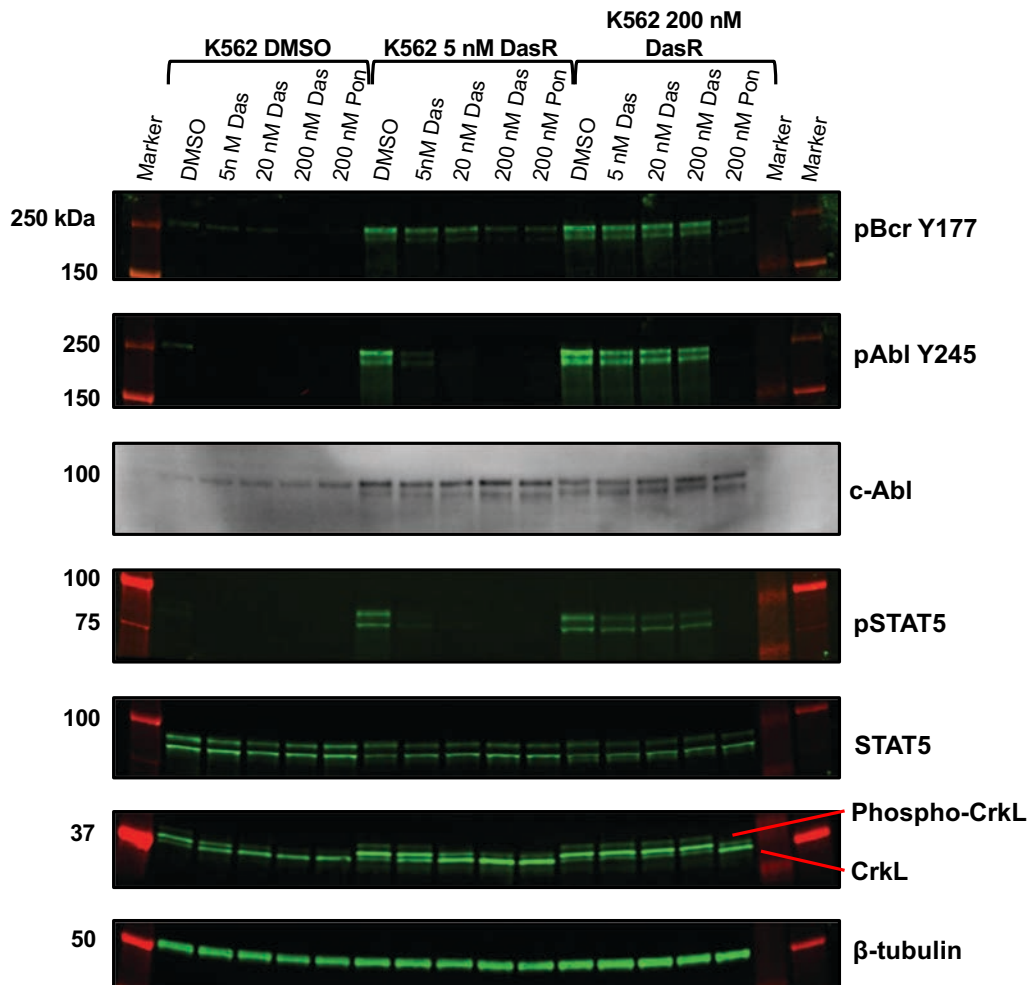
Figure 3.9: Western blotting analysis of Bcr-Abl and downstream signalling proteins. Results confirm an increase in Bcr-Abl expression concurrent with increasing dasatinib concentration levels, as well as the presence of two Bcr-Abl isoforms. Phospho-protein analysis demonstrate the acquired resistance to dasatinib in the K562 DasR lines relies on ongoing signalling protein phosphorylation, which is ablated by 200 nM ponatinib.
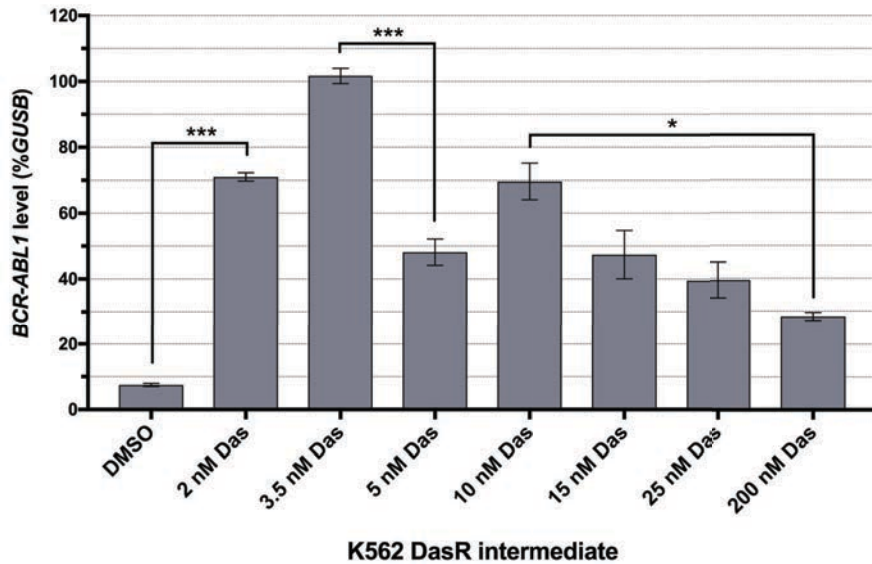
Figure 3.10: DNA qPCR results for genomic quantity of *BCR-ABL1*, normalised to *GUSB*. Results indicate a significant increase in cellular *BCR-ABL1* content, acquired early in the course of dose escalation, which falls significantly with prolonged and increasing TKI exposure. Data represent mean -/+ SEM of 3 independent experiments. Unequal variances t-test was performed between dose escalation intermediates; significance is denoted by (*) for p<0.05, (**) for p<0.01, (***) for p<0.001.

K562 DMSO   **K562 200 nM Das**
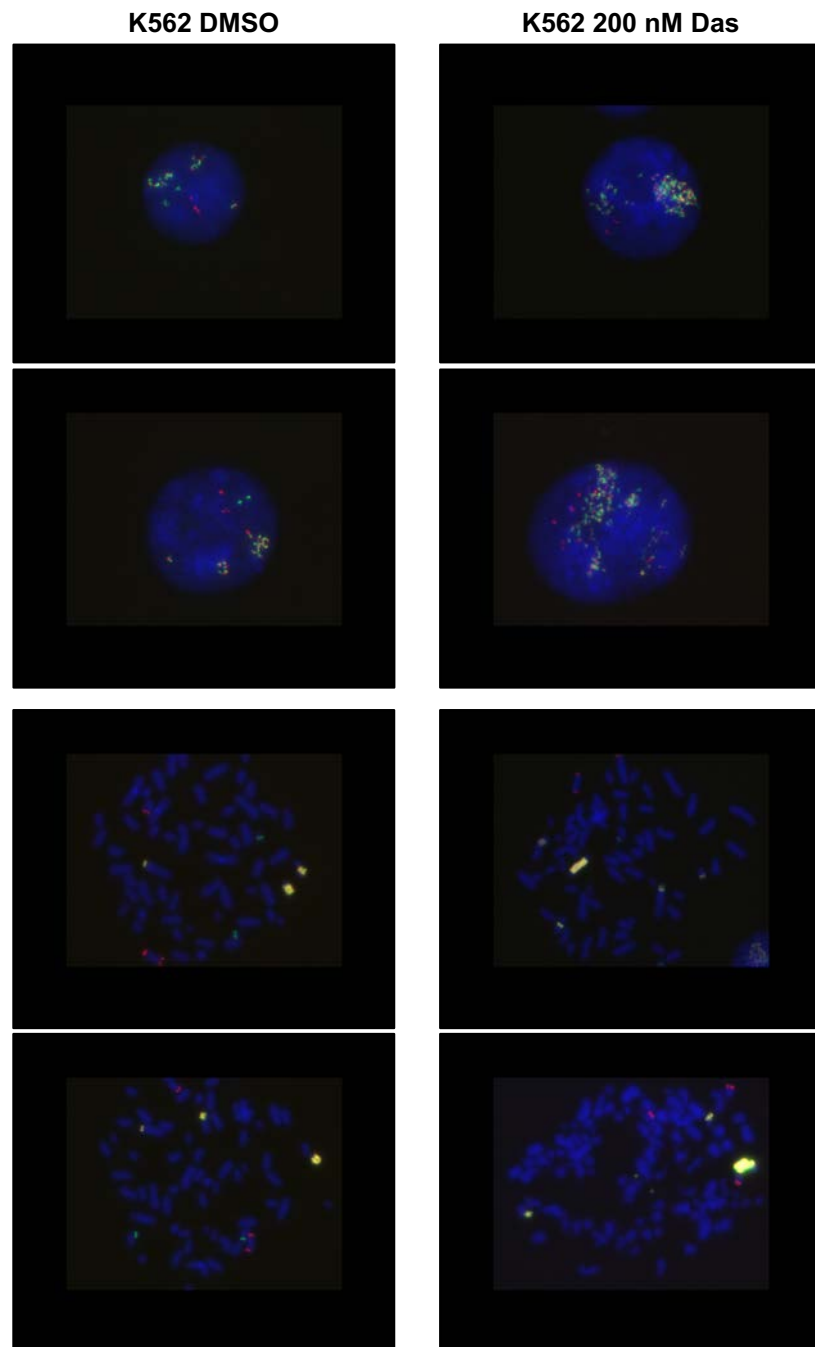
Figure 3.11: Representative interphase (upper half) and metaphase (lower half) FISH analyses of K562 200 nM Das and DMSO control lines revealed genomic *BCR-ABL1* amplification. Increased *BCR-ABL1* signal in metaphase spreads of K562 200 nM Das line (lower right) indicate that gene amplification has occurred. The condensed signal suggests that amplification occurred within the original *BCR-ABL1* locus on the Philadelphia chromosome, and not on extrachromosomal elements. Green = *BCR*, red = *ABL1*.
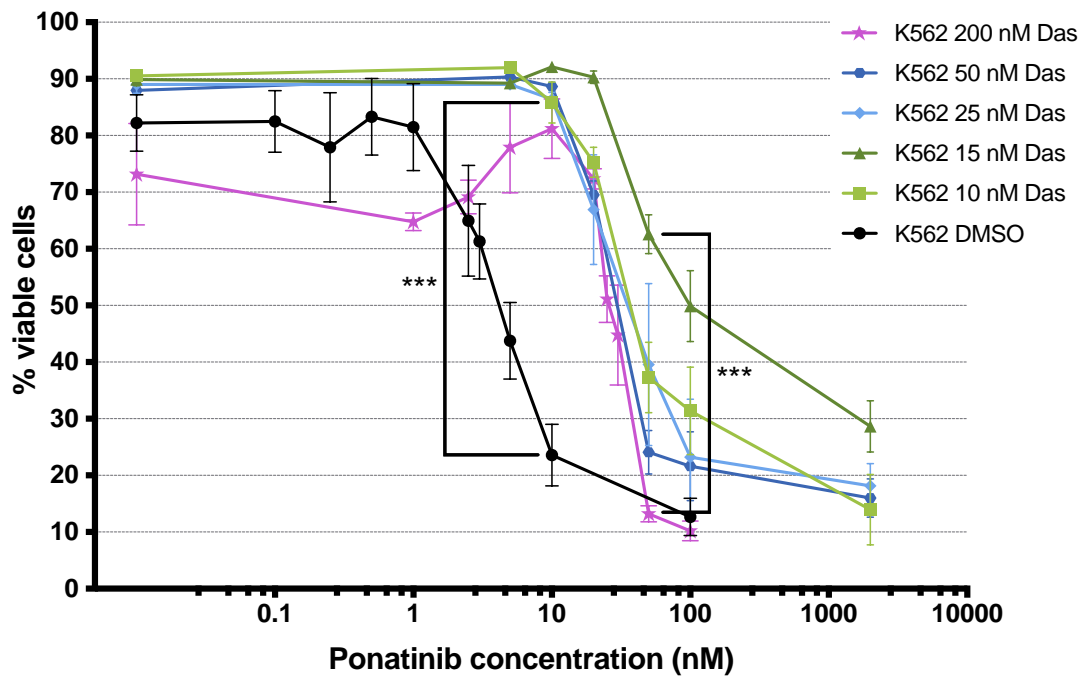
Figure 3.12: K562 cells cultured in ponatinib exhibit decreased sensitivity to ponatinib induced cell apoptosis. Cell viability of K562 DasR dose escalation intermediates cultured in gradient ponatinib for 72 h as determined by Annexin V / 7-AAD staining. Values indicate mean -/+ SEM of at least 3 independent experiments. Unequal variances t-test was performed between dose escalation intermediates at each ponatinib concentration; significance is denoted by (***) for p<0.001.
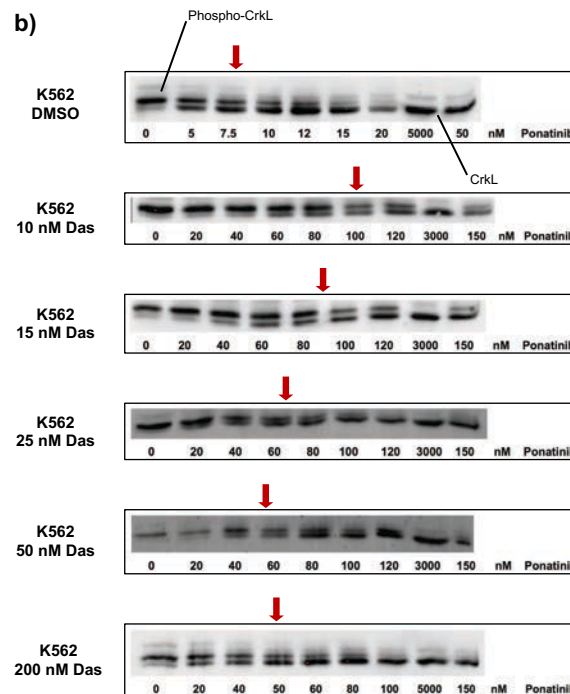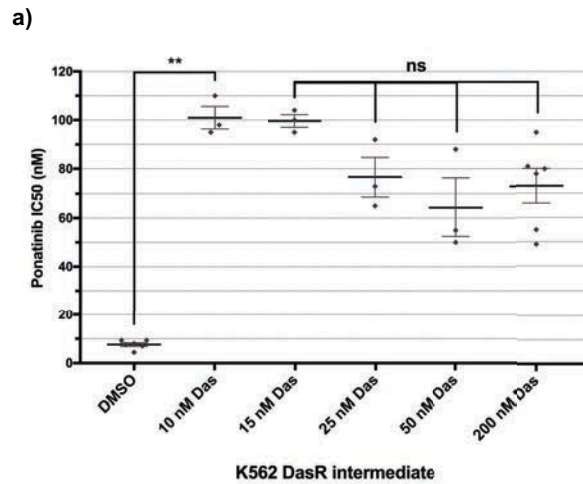
Figure 3.13: a) Ponatinib IC50 data for K562 dose escalation intermediates, based on loss of phosphorylated (Phospho-) CrkL. Data indicate a decrease in ponatinib sensitivity in K562 DasR lines, which unexpectedly peaks in the 10 and 15 nM DasR intermediates. Whiskers indicate mean -/+ SEM of at least 3 independent replicate experiments. Unequal variances t-test was performed between dose escalation intermediates; significance is denoted by (ns) for $p>0.05$, (*) for $p<0.05$, (**) for $p<0.01$. b) Representative IC50^{Pon} western blotting. Samples are selected K562 DasR dose escalation intermediates; red arrows indicate the approximate point of 50% Bcr-Abl kinase inhibition.
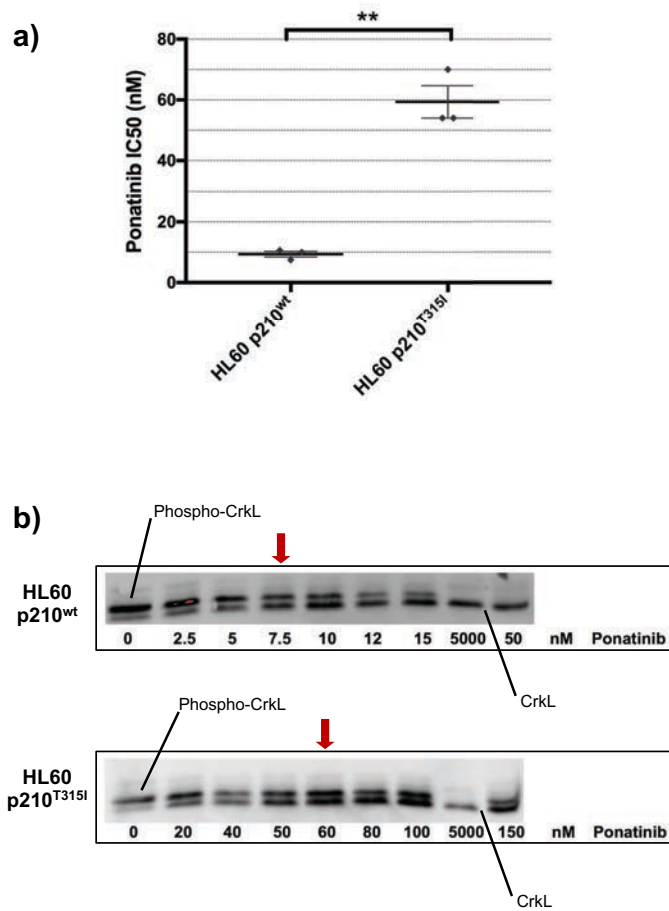
Figure 3.14: a) Ponatinib IC50 values for HL60 cell lines transfected with wildtype (wt) or T315I mutated *BCR-ABL1*, based on loss of phosphorylated (Phospho-) CrkL. Whiskers indicate mean -/+ SEM of 3 independent replicate experiments. Unequal variances t-test was performed between dose escalation intermediates; significance is denoted by (*) for $p < 0.05$, (**) for $p < 0.01$. b) Representative ponatinib IC50 western blotting; red arrows indicate the approximate point of 50% Bcr-Abl kinase inhibition (IC50^{pon}).

4 The e6a2 *BCR-ABL1* isoform arises in response to dasatinib exposure; cells expressing e6a2 are less sensitive to dasatinib-induced cell death

4.1 Introduction

Results from the previous chapter indicated that in addition to Bcr-Abl overexpression and T315I, the K562 DasR cell line harboured resistance mechanisms which had not yet been elucidated. Transcriptome sequencing has been described as the gold standard for the determination of the cellular adaptations involved in drug resistance (238). This method can reveal the genetic mechanisms of drug resistance, as well as suggest novel drug targets to re-sensitise leukaemic cells to treatment (239). To determine the cellular adaptations occurring over dasatinib dose escalation, the K562 10, 15, 25, 50, and 200 nM Das intermediates were sampled for exploratory mRNAseq experiments, along with the DMSO treated and TKI naïve K562 controls.

The mRNAseq data generated was interrogated using several analytical methods, including measurement of global gene expression changes, identification of single nucleotide variants, and identification of chimeric fusion gene transcripts, such as *BCR-ABL1* and its isoforms. To determine the fusion genes present in transcriptome analysis samples, the FusionCatcher fusion gene finder software tool was used. The FusionCatcher algorithm aligns reads using Bowtie, BLAT, STAR and Bowtie2 programs, compiling unmapped reads as evidence for candidate gene fusions, mapping the two gene halves of the read to separate genetic elements (233). A summarised list of genetic fusions and the number of supporting reads is provided as output. Using this method, the *BCR-ABL1* e6a2 fusion was identified. Presence of the fusion was detected in all of the K562 DasR intermediate lines sampled for transcriptome sequencing, however, was not present in the drug naïve controls.

Following identification of the e6a2 fusion, the following research questions regarding e6a2 required addressing:

1. What is the transcriptional expression of BCR-ABL1 e6a2 in the K562 DasR cell line?

2. Is the e6a2 transcript the result of a gene splicing isoform or a de novo genomic breakpoint?

3. Does the e6a2 isoform harbour kinase domain mutations?

4. What is the contribution of e6a2 to TKI resistance? Does expression of e6a2 confer a selective advantage from increased kinase activity in the presence of dasatinib?

Prior to the identification of e6a2 in K562 DasR resistant lines, only the typical isoform of e14a2 (b3a2, p210), had been quantitated by standard diagnostic tests. The *BCR-ABL1* RT-qPCR performed previously was specific for the e14a2 transcript, and PCR for *BCR-ABL1* kinase domain sequencing amplified only e14a2. Bcr-Abl western blot analysis of K562 DasR dose escalation intermediates had suggested an alternate and distinct Bcr-Abl fusion, and identification of the e6a2 fusion transcript allowed genetic analyses to be performed. To validate the presence of the e6a2 transcript, PCR forward primers were designed within *BCR* exon 5, as well as spanning the e6a2 breakpoint junction, designed for use with the existing reverse primer used in *BCR-ABL1* e14a2 kinase domain amplification. Primers were used with K562 DasR dose escalation cDNA samples to amplify e6a2 transcripts present. The PCR products were sequenced for detection of *ABL1* kinase domain mutations. To quantify mRNA expression of the alternate e6a2 transcript, RT-qPCR primers were designed to amplify e6a2. These were used in a SYBR Green qPCR system to quantify the relative *BCR-ABL1* expression in K562 DasR dose escalation intermediates. Ct values were normalised to the endogenous control gene, *GUSB*.

The expression of the e6a2 transcript may have resulted from a number of different cellular events, i.e. an alternative splicing product, a *de novo* chromosomal fusion, or intra-chromosomal deletion of an existing *BCR-ABL1* fusion. Determination of the DNA breakpoint location would provide evidence for the origin of the e6a2 transcript, and furthermore, allow the qPCR determination of relative copy number levels. To achieve this, target enrichment DNA sequencing was performed in selected K562 DasR samples, using the Agilent SureSelect Target Enrichment system (240). Genomic DNA was extracted from K562 DasR samples and fragmented to ~300 bp, and fragments harbouring *BCR-ABL1* sequences were pulled down using a panel of probes spanning genomic *ABL1* and *BCR* sequences, designed by Dr Ilaria Pagani (SAHMRI Cancer Theme). 150 bp paired end read sequencing was performed by Mark Vanderhoek (SAHMRI Genomics Core Facility). Data generated was analysed using the FACTERA program (241) with the assistance of Dr Chung Kok and Dr Benjamin Mayne (SAHMRI Cancer Theme). In this method, discordant reads are used to locate genomic regions involved in potential fusions, followed by an *in silico* validation whereby the number of supporting reads gives confidence to the determined breakpoints. The determination of the e6a2 *BCR-ABL1* DNA fusion breakpoint allowed the subsequent qPCR quantification of the

genomic *BCR-ABL1* levels. To achieve this, a TaqMan MGB primer/probe combination spanning the e6a2 junction was designed, with the assistance of Dr Ilaria Pagani. PCR Ct values were normalised to amplification of the endogenous control gene *GUSB*. A standard curve was generated using a plasmid harbouring the *GUSB* sequence, such that absolute genomic volumes could be quantified. *BCR-ABL1* e6a2 levels are reported as a percentage of *GUSB* genetic quantities.

The determination of *BCR-ABL1* expression and amplification levels suggested that expression of the e6a2 *BCR-ABL1* isoform was selected over dasatinib dose escalation. This may be due to the e6a2 isoform having inherently elevated TKI resistance, or providing an associated proliferative advantage due to differential signalling pathway activation. To further explore these possibilities, we tested the *BCR-ABL1* isoforms: e14a2, e6a2, and e1a2, using the Ba/F3 transformation assay popularised by Daley and Baltimore (14). Attempts to clone the e14a2 and e6a2 sequences from K526 DasR cDNA samples were unsuccessful, thus the *BCR-ABL1* e14a2 sequence was purchased from the plasmid repository, Addgene (225). The e6a2 sequence was generated via site directed mutagenesis and inserted into the multiple cloning site of the lentiviral pRuf-iG-2 lentiviral expression vector (242). Lentiviral vectors were transfected into HEK-293T cells and viral particle supernatant was used to infect Ba/F3 murine pro-B cells. The Ba/F3 cell line is typically dependent on a source of murine IL-3 for growth factor-dependent survival and proliferation (226). Transduction with an oncogenic driver gene, such as *BCR-ABL1*, confers the cell line growth factor-independent survival. Validation of *BCR-ABL1* expression was performed by *BCR-ABL1* RT-qPCR using a SYBR green PCR platform. This was again normalised to expression of the endogenous control gene, *GUSB*. Bcr-Abl kinase activity in the cell lines were validated using western blotting for phosphorylation of Bcr-Abl kinase substrate, CrkL. To test for TKI resistance associated with expression of *BCR-ABL1* e6a2, the pCrkL IC50 and TKI-induced cell death assays were performed using the TKI dasatinib.

4.2 Results

4.2.1 Identification of an alternate *BCR-ABL1* transcript in K562 DasR cell line transcriptome samples

To determine potential resistance mechanisms in the K562 DasR cell line, transcriptome analysis of K562 DasR dose escalation intermediates was performed. Using the FusionCatcher fusion detection program, several fusion gene transcript breakpoints were detected over several genes. After filtering the detected transcripts for *BCR-ABL1* breakpoints, several transcript isoforms were identified in the various K562 DasR and control lines (Table 4.1). Among those identified was the *BCR-ABL1* e14a2 transcript, which as expected, was found in all K562 samples. Additionally, a *BCR-ABL1* breakpoint corresponding with the rare e6a2 transcript was also identified, however only in the dasatinib resistant samples tested (K562 10, 15, 25, 50, 200 nM Das). The number of e6a2 breakpoint spanning reads was comparable to that of e14a2, indicating that this was not a spurious, lowly expressed transcript. To confirm the presence of the e6a2 transcript, primers were designed flanking the breakpoint for use with PCR, qPCR, and sequencing validation.

4.2.2 The *BCR-ABL1* e6a2 fusion is expressed in the K562 DasR cell line

Validation of the e6a2 *BCR-ABL1* fusion transcript was performed by PCR and gel electrophoresis (Figure 4.1). Unlike the LongF0810 forward primer used in PCR amplification of the *BCR-ABL1* e14a2 fusion in Chapter 3, the primer pair used here were designed specifically to amplify e6a2. Primers were based on sequencing information derived from mRNAseq experiments (ABLe5F, LongR0510). Amplification products indicated a 1994 bp band corresponding to the presence of the e6a2 fusion in K562 DasR lines, and a 2855 bp band corresponding to the typical *BCR-ABL1* e14a2 fusion. Interestingly, an unidentified band of approximately 2500 bp was also identified in DasR lines; the significance of this band is discussed. The K562 DMSO control line harboured only the e14a2 fusion. Amplification products from alternate primers (e6a2breakpoint, LongR0510) resulted in a single 1652 bp band in both 10 and 200 nM DasR lines, corresponding to presence of e6a2. Again, the K562 DMSO line demonstrated no evidence of the e6a2 isoform.

Following successful demonstration of the presence of the e6a2 fusion in two K562 DasR dose escalation intermediates, the presence of this isoform was ascertained in all remaining K562 DasR intermediates. PCR amplicon analysis indicated that the e6a2 fusion first appeared in the K562 2 nM DasR intermediate, and remained in all later K562 DasR intermediates, including the final 200 nM Das line (Figure 4.2). Again, the naïve and DMSO control K562 lines demonstrated no expression of *BCR-ABL1* e6a2.

4.2.3 The *BCR-ABL1* e6a2 fusion expressed by K562 DasR lines does not harbour kinase domain mutations

Kinase domain sequencing previously performed was specific to e14a2 transcripts (Chapter 3). Following validation of the presence of e6a2 in K562 DasR lines it was necessary to ascertain whether the *BCR-ABL* e6a2 transcripts also harboured kinase domain mutations. However, sequence analyses demonstrated the complete absence of kinase domain mutations, including the already identified T315I mutation (Figure 4.3), in e6a2 transcripts from any of the K562 DasR lines.

4.2.4 Expression of the *BCR-ABL1* e6a2 fusion gene transcript is selected for following prolonged culture in dasatinib

Similarly, transcriptional mRNA expression was previously measured in e14a2 *BCR-ABL* transcripts only (Chapter 3.2.4). Therefore, it was also necessary to quantify the expression of *BCR-ABL1* e6a2 transcripts in K562 DasR dose escalation intermediates. As the e6a2 fusion was not expressed by the K562 naïve or DMSO vehicle control lines, a ddCt value (fold change) could not be calculated. As such, data are reported as a -dCt value, normalised to *GUSB* expression; the background e6a2 amplification in K562 controls was set at 0 (Figure 4.4). RT-qPCR results demonstrated the first significant expression of the e6a2 fusion in the 2 nM Das intermediate, with higher relative expression than DMSO control (0 vs 8.7, n=3, p<0.001). Expression continued to rise with ongoing dasatinib dose escalation, peaking in the K562 10 nM DasR line (8.7 vs 16.4, n=3, p=0.027). However, further dasatinib dose escalation did not result in consistent increases in e6a2 gene expression, and no further significant differences were observed beyond the 10 nM DasR intermediate.

4.2.5 Expression of the *BCR-ABL1* e6a2 transcript is due to a genomic e6a2 fusion

To determine the origin of the e6a2 transcript, target enrichment DNA sequencing of *ABL1* and *BCR* sequences was performed in genomic samples from K562 DasR samples (15 and 200 nM Das, naïve K562 control). FACTERA analysis for gDNA breakpoint analysis revealed that expression of the e6a2 fusion transcript was due to unique chromosomal fusion, distinct from the e14a2 fusion in the dasatinib naïve K562 control line (Table 4.2). K562 15 and 200 nM DasR lines both harboured two distinct *BCR-ABL1* fusions, corresponding to e14a2 and e6a2 genomic breakpoints, whereas the drug naïve K562 line harboured only e14a2. Whereas the e14a2 5' *BCR* breakpoint is in *BCR* intron 14, the e6a2 *BCR* breakpoint is in intron 6. Both e14a2 and e6a2 3' *ABL1* breakpoint locations are within *ABL1* intron 1, however, at different locations (Figure 4.5). Due to regions of homology between the *BCR* and *ABL1* breakpoint regions, FACTERA analysis called different breakpoints between the lines, differing in location by 1-5 nucleotides; an inherent caveat of the program. Two alternate *BCR* fusions were also identified, fused 5' to *VWF* and *XKR3*, however these were not further explored due to the low supporting read numbers.

To validate the e6a2 DNA breakpoint location, PCR primers were designed flanking the breakpoint, amplifying a predicted 741 bp product. Gel electrophoresis of selected K562 DasR lines identified the fusion in dasatinib resistant lines, but not in K562 control (Figure 4.6). The e6a2 PCR amplicon was verified by Sanger sequencing, aligning to genomic *BCR* and *ABL1* sequences (Figure 4.7), which identified the breakpoint to single nucleotide specificity. This sequence was used for the design of primers in follow up experiments.

4.2.6 Increased expression of the *BCR-ABL1* e6a2 fusion in K562 DasR cells is driven by genomic amplification of the fusion gene

Following identification of the e6a2 genomic *BCR-ABL1* breakpoint, the relative genomic copy number of *BCR-ABL1* e6a2 was quantified in K562 DasR dose escalation intermediates. Following confirmation that the nucleotide sequence did not occur elsewhere in the genome, DNA samples from K562 DasR dose escalation intermediates were interrogated for genomic *BCR-ABL1* e6a2 expression (Figure 4.8). Normalised to the amplification of *GUSB*, the genomic quantity of *BCR-ABL1* e6a2 increased significantly, from undetectable levels in the K562 DMSO control line to 57% in the 5 nM DasR intermediate (p=0.006, n=3). Genomic *BCR-ABL1*

e6a2 levels again significantly increased to 92% in the 10 nM DasR line (p=0.006, n=3), before significantly falling to 5% in the 15 nM DasR intermediate (p<0.001, n=3). However, with increasing dasatinib escalation, genomic levels of *BCR-ABL1* e6a2 again rose to 37% in the final 200 nM DasR resistant line (p=0.001, n=3).

Taken in conjunction with *BCR-ABL1* e6a2 RT-qPCR analysis, as well as Bcr-Abl western blotting (Chapter 3), results suggest that expression of e6a2 is clonally selected for, though only during some stages of dasatinib dose escalation.

4.2.7 Expression of the *BCR-ABL1* e6a2 fusion is transforming in Ba/F3 cells

To assess the inherent TKI resistance of the Bcr-Abl e6a2 fusion product, Ba/F3 cells transformed with vectors containing e14a2 or e6a2 *BCR-ABL1* were studied using TKI sensitivity assays. Empty pRuf-iG2 vector and *BCR-ABL1* e1a2 transformed lines were concurrently generated as experimental controls. An outline of the generation of the Ba/F3 *BCR-ABL1* e14a2, procedure can be found in Chapter 2.4. The correct size of the *BCR-ABL1* insert in each vector was confirmed by restriction enzyme digest, and the full length *BCR-ABL1* sequence was validated by Sanger sequencing.

Fluorescence of eGFP, indicative of gene of interest expression, was measured in cells by light and eGFP microscopy (Figure 4.9). Results indicated the eGFP positivity of all pRuf-iG2 transduced Ba/F3 lines, indicative of successful gene transduction. Transformation of Ba/F3 cells was confirmed by the withdrawal of WEHI-3B conditioned media containing IL-3. Cells transformed with *BCR-ABL1* constructs maintained viability in the absence of IL-3. Conversely, IL-3 withdrawal from the empty vector control cells resulted in a complete loss of viability. Cells were enriched by flow assisted cell sorting (FACS) for eGFP positivity.

Transformation was further confirmed by western blot analyses assessing phosphorylation of the Bcr-Abl kinase substrate, CrkL (Figure 4.10). In the Ba/F3 empty vector control line, no phosphorylation of CrkL was evident; conversely, CrkL in *BCR-ABL1* transduced Ba/F3 cell lines was almost fully phosphorylated. Unfortunately, Bcr-Abl protein levels were unable to be directly measured, with c-Abl western blotting not demonstrating detectable Bcr-Abl in Ba/F3 lines. However, levels of *BCR-ABL1* transcript expression were quantified by RT-qPCR for the

e14a2, e6a2 and e1a2 transcripts (Table 4.3). Results demonstrated the purity of expression for each cell line, with appropriate amplification of transcripts.

4.2.8 Ba/F3 cells expressing *BCR-ABL1* e6a2 are more resistant to dasatinib-induced cell death than those expressing *BCR-ABL1* e14a2

To determine whether the e6a2 fusion conferred an inherent dasatinib resistance advantage over e14a2, Ba/F3 cells expressing *BCR-ABL1* e14a2, e6a2, or e1a2, or an empty vector control, were cultured in dasatinib for 72 h, before co-staining with AnnexinV / 7-AAD and flow cytometric analysis. Results demonstrated that while all three cell lines were sensitive to some level of dasatinib induced cell death, Ba/F3 cells harbouring *BCR-ABL1* e6a2 were less sensitive to dasatinib induced cell death than Ba/F3 harbouring e14a2 (Figure 4.11). In the absence of dasatinib, there were no significant differences between cell viability between all three *BCR-ABL1* expressing lines. However, following culture in 3 nM dasatinib, the Ba/F3 *BCR-ABL1* e6a2 line was significantly more viable than Ba/F3 *BCR-ABL1* e14a2 (71.2 vs 32.8% n=3, p=0.023). In dasatinib concentrations above this, no significant differences in cell viability were observed, as the cell lines approached 100% cell death. The level of dasatinib susceptibility in *BCR-ABL1* e6a2 expressing cells was similar to those expressing *BCR-ABL1* e1a2 (p190), with no significant differences in viability between e6a2 and e1a2 at any dasatinib concentration tested.

4.2.9 The Bcr-Abl e6a2 fusion is not more resistant to dasatinib-induced kinase inhibition than Bcr-Abl e14a2

Having demonstrated that cells expressing e6a2 are more resistant to dasatinib induced cell death, the phospho-CrkL IC50 assay was performed to determine whether the variations in resistance were due to differences in TKI induced kinase inhibition. Results indicated that the e6a2 kinase was not more resistant to dasatinib than e14a2 (Figure 4.12). The IC50^{Das} for Bcr-Abl e6a2 was in fact lower than that for Bcr-Abl e14a2, though this did not reach significance (7.43 vs 12.5 nM, n=4, p=0.122). A wide variance was noted in the Ba/F3 e14a2 IC50 replicates, which may result in the lack of significant difference. Conversely, the IC50 for the Bcr-Abl e1a2 fusion was significantly higher than e6a2 (17.3 vs 7.43 nM, n=4, p=0.013). These

results demonstrate that the decreased dasatinib induced cell death of e6a2 expressing cells is not mediated by phosphorylation signalling through CrkL. This shall be further discussed.

4.3 Chapter discussion

The identification of cells expressing the *BCR-ABL1* e6a2 transcript in K562 DasR cells is a novel finding, which suggested a replicative advantage of these cells in the context of TKI exposure. Some hypotheses suggest certain Bcr-Abl isoforms may confer more aggressive disease, however, in this model the mechanism was unknown by which e6a2 harbouring cells maintained a selective advantage. The positive selection for high *BCR-ABL1* e6a2 transcript and protein expression may be due to differences in kinase activation and signalling, altered TKI binding interactions to the protein, or differential phosphatase binding and interaction, which each could lead to maintained kinase signalling and cell proliferation in the presence of dasatinib. However, the presence of additional copies of *BCR-ABL1*, regardless of the isoform, likely contributes to Bcr-Abl protein overexpression and resultant clonal dominance in these cells; tracking the genomic quantities and expression of *BCR-ABL1* can only hint at the molecular mechanisms of resistance. Additionally, due to its rarity, the e6a2 transcript may be overlooked in diagnostic tests, resulting in incorrect disease prognosis and poorer associated patient outcomes. An exploration of the association between resistance and the expression of the e6a2 fusion was performed here using several overlapping approaches; the clinical implications and limitations are here discussed.

4.3.1   Clinical identification of the e6a2 *BCR-ABL1* fusion

The clinical identification of the Bcr-Abl e6a2 isoform has been previously discussed (Chapter 1), and has been associated with several leukaemic phenotypes, including CML, AML, chronic myelomonocytic leukaemia, B- and T-ALL, and basophilic myeloid leukaemia (69-79, 82-88). The presence of e6a2 in several leukaemic subtypes, and the fact that patient outcomes following treatment differed, indicated that this isoform does not necessarily confer a particular disease fate. It has been suggested, however not demonstrated, that the presence of e6a2 results in a more aggressive disease and poorer patient outcome (71, 74, 89). Several patients with e6a2 responded to TKI therapy, demonstrating that the use of TKI is still

indicated for *BCR-ABL1* e6a2 positive disease. However, relapse and progression during TKI therapy was still evident in some patients (75).

A key difference between the commonly observed e13a2/e14a2 transcripts and e6a2 and other rare isoforms is how the fusions are detected from a patient biopsy. A diagram of the *BCR-ABL1* transcript isoforms can be found in Figure 1.3.2. PCR for the more common e13a2 and e14a2 transcripts does not amplify the e6a2 transcript. RT-qPCR for *BCR-ABL1* transcripts is now routine for the diagnosis of CML, however, as was the case in our study, rare transcripts are not typically investigated following the identification of a *BCR-ABL1* driver gene. Several of the patient case studies only detected e6a2 via weak PCR amplification using e1a2 (p190) specific primers, subsequently using Sanger sequencing to validate the fusion breakpoint. In these cases, cytogenetic analyses provides only relatively vague description of the *BCR-ABL1* fusion location. More importantly, following identification of a *BCR-ABL1* transcript in a patient, exploratory searches for alternate fusions is not usually performed in follow up examinations of molecular response. If a rare transcript were to arise in response to TKI treatment, as it did in our model, this would likely go unnoticed in a patient's molecular analysis using typical *BCR-ABL1* qPCR methods. Therefore, disease recurrence would only be detectable by increased white cell count or other diagnostic measures. This, in addition to potentially slower disease diagnosis due to difficulty in identifying the isoform, may hinder effective treatment strategy design. These confounding factors may all contribute to the poorer outcome observed in patients expressing rare *BCR-ABL1* drivers. The data presented here suggests that in TKI resistant patients, diagnosticians should determine whether the presence of rare a Bcr-Abl isoform is affecting treatment.

4.3.2   Expansion of the e6a2 positive clone in the K562 DasR cell line

The expansion of leukaemic cells expressing Bcr-Abl e6a2 under the selective pressure of dasatinib exposure suggested a selective advantage held by these cells. Thus, efforts were directed at characterising the kinase function and TKI resistance profile of Bcr-Abl e6a2 in relation to e14a2 and e1a2. RT-qPCR analyses demonstrated the emergence of detectable levels of e6a2 transcripts occurring early in dasatinib dose escalation. While the K562 2 nM DasR dose escalation intermediate was the first to exhibit significantly higher relative expression than the DMSO control, a trend of increasing e6a2 transcript expression was

observed in dose escalation intermediates from 0.5 nM to 10 nM Das. This suggests the existence of a minor clone expressing e6a2 in the drug naïve K562 line, which was selected for under dasatinib exposure. DNA qPCR for genomic e6a2 quantities recapitulated the trend of increasing e6a2 levels until the K562 10 nM DasR intermediate, as well as a significant reduction in e6a2 amplification between the 10 and 15 nM DasR intermediates, suggesting that in this model, genomic *BCR-ABL1* levels drive increases in protein expression. Amplification of *BCR-ABL1* is a known mechanism of increased gene expression, and amplification of *BCR-ABL1* by tandem duplication or Philadelphia chromosome duplication has been associated with disease aggression, TKI resistance, and poor outcome (148, 149, 243). However, decreases in gene amplification and expression have not been extensively documented, and a mechanism for the loss of *BCR-ABL1* copies and the selection of these cells, as was observed here, is not readily apparent. Therefore, it is postulated that the loss of genomic *BCR-ABL1* in the cell population was due to the selection and outgrowth of a dasatinib resistant clone which harboured relatively lower *BCR-ABL1* levels, and which gained TKI resistance by other mechanisms. Subsequent increases in *BCR-ABL1* quantity in the K562 25 nM DasR and later intermediates may have been due to re-selection for *BCR-ABL1* overexpressing cells, though as these cells already harboured T315I, there are no immediately apparent reasons for this selective pressure.

4.3.3   The pleckstrin homology (PH) domain and intracellular signalling of Bcr-Abl

Compared with the typical e14a2 fusion, e6a2 exhibits truncation of the PH domain (*BCR* exons 5-10), however, retains the Dbl homology (DH) domain (exons 3-5), the serine/threonine kinase domain, and N-terminal coiled coil oligomerisation regions (exon 1) (Figure 1.4). The PH domain is present in a diverse range of >285 proteins involved in cellular signalling, cytoskeletal organisation and membrane trafficking (244-246). The domain has well characterised roles in phospholipid binding, holding the positive electrostatic polarisation necessary for interactions with negatively charged phospholipids (247). The strong affinity of the PH domain with phospholipids can allow localisation of the protein to the plasma membrane and actin cytoskeleton (248). It has been demonstrated that p190 Bcr-Abl, which lacks the DH and PH domains of Bcr, interacts with a different protein subset than p210 (249, 250). Thus, lack of the PH domain in Bcr-Abl e6a2 may result in protein localisation to the cytosol, where it would interact with a different subset of protein cofactors.

The DH-PH domain juxtaposition is also responsible for Rho GTPase and GEF activity: the catalytic exchange of GTP for GDP on Rho substrates, effected by an increased rate of GDP dissociation (251). GEF-mediated activation of Cdc42, Rac1 and RhoA is involved in cytoskeletal remodelling, modulation of proliferation and apoptosis, and myeloid differentiation (252). Native Bcr has been demonstrated to stimulate the GEF activity of Cdc42, RhoA, Rac1 and Rac2 (35); these protein interactions are conserved in Bcr-Abl (253, 254). The loss of the DH domain in the translated p190 is hypothesised to interrupt RhoGEF activity and G-protein interactions (223), and localisation of the protein complex (250, 255). Alterations in the p190 kinase activation profile are likely to affect cellular signalling, possibly worsening disease prognosis and treatment response. Studies of p190 Bcr-Abl have determined that due to the lack of the DH domain, p190 is unable to activate RhoA, however does still activate Rac1 and Cdc42; it has been theorised that p190 activation of Rac1 and Cdc42 occurs via GEF interactions with the Dbl family GEF, Vav (256, 257). Authors hypothesised that progenitor cell differentiation by p210 activation of RhoA conferred a less aggressive leukaemic phenotype. Demehri *et al* compared the transforming effects of p210 and p190 with a naturally occurring "p200" Bcr-Abl fusion, lacking the PH domain (258, 259). While all constructs used resulted in oncogenic transformation of 32D and Ba/F3 cells, there was a marked increase in the kinase activity of the p190 and p200 isoforms, with higher STAT6 phosphorylation and shorter disease latency in engrafted mice. Taken together, the studies of signalling and functional differences between cells expressing Bcr-Abl lacking DH-PH GEF functionality suggest this deficiency will significantly alter the conferred disease phenotype.

As the study presented here used a murine pro-B Ba/F3 cell line as the transformative backbone, we were not able to thoroughly explore the myeloid differentiation which may have been induced by the different Bcr-Abl isoforms. However, no obvious cellular morphology differences were observed between the transformed Ba/F3 lines or indeed in the K562 DasR line where the e6a2 isoform was originally identified. Nevertheless, a deeper analysis of the Ba/F3 lines may determine the differences in GEF functionality, and determine cell signalling perturbations due to Bcr-Abl truncation.

4.3.4   Molecular formation of the genomic *BCR-ABL1* e6a2 fusion

Patient case studies involving e6a2 reported the presence of only the e6a2 fusion in isolation (69, 70, 79, 260). This is in contrast to the concurrent expression of e14a2 with e6a2 observed in this model, and the interactions facilitated by co-expression of the two isoforms has not previously been studied. The K562 cell line harbours multiple genomic copies of *BCR-ABL1*, and target enrichment sequencing experiments performed here suggest a mechanism for the formation of the additional e6a2 fusion observed in dasatinib resistant variants of this line. The location of the e6a2 breakpoint in intronic regions suggests a deletion between *BCR* introns 7-13 juxtaposing *BCR* exon 6 with *ABL1* exon 2. FISH analysis previously demonstrated that K562 DasR intermediates harbouring the e6a2 fusion maintained intact native *BCR* and *ABL1* genes, indicating that e6a2 did not form via their fusion (Chapter 3). Intrachromosomal deletion may have occurred during chromosomal replication during the S phase of cell cycle, however, as amplification of the *BCR-ABL1* locus was previously demonstrated in Chapter 3, it is more likely that the deletion occurred during a gene duplication event. Interestingly, intronic regions within *BCR* have been demonstrated to act as transcriptional repressors (261), and the deletion of *BCR* introns may have also resulted in the relative increased expression of the e6a2 fusion. This would significantly contribute to overall Bcr-Abl levels, and the TKI resistant phenotype observed in these cells.

4.3.5   Dasatinib sensitivity of the e6a2 Bcr-Abl fusion

Experiments elucidating differences in dasatinib sensitivity between *BCR-ABL1* transduced Ba/F3 lines were complex to interpret. Consistent with predictions, the e6a2 transduced line was less sensitive to dasatinib induced cell death, compared with Ba/F3 *BCR-ABL1* e14a2. Dasatinib sensitivity of e6a2 was similar to that of e1a2 Bcr-Abl. These results are in line with hypotheses about the GEF function of the PH-DH domains in Bcr-Abl, and how a proliferative loss of function may occur. IC50 assays for CrkL phosphorylation demonstrated that the e6a2 kinase was not more resistant to kinase inhibition by dasatinib; while not significant, the IC50 was lower than that of other kinase isoforms. The hypothesis that the e6a2 fusion conferred increased kinase activity in the presence of dasatinib was thus disproven. This indicated that the observed decrease in dasatinib cell sensitivity in e6a2 and e1a2 was not due to increased kinase activation in the presence of dasatinib. Altered GEF activity and/or protein cofactor recruitment of e6a2 and e1a2 may have resulted in this loss of dasatinib sensitivity, in the

absence of increased kinase activation. However, it should be noted that the e1a2 isoform also maintained an increased dasatinib pCrkL IC50, which may have been due to kinase activity of the isoform.

One limitation of the model is the random insertion location of the transgene, which may result in these non-congruous results. While it is known that lentiviral transduction integrates transgenes into highly expressed transcriptional units (262), there is random and stochastic variance in the integration site. Therefore, transgene insertion may be disruptive to endogenous gene function and homeostasis, potentially leading to altered proliferative potential or apoptosis resistance. Additionally, the variance in transcription and translation of the different *BCR-ABL1* isoforms could lead to differential levels of TKI sensitivity. However, high levels of *BCR-ABL1* gene and protein expression would likely increase both dasatinib IC50 and dasatinib induced cell death. The decreased dasatinib induced cell death, but increased pCrkL IC50 in the Ba/F3 *BCR-ABL1* e6a2 line, suggests that the decreased dasatinib induced cell death is not due to increased kinase activity. The effect could be further explored with functional studies investigating phosphoprotein differences between the cell lines, for example using co-immunoprecipitation of Bcr-Abl isoforms to identify protein cofactors. Differential GEF activity could result in the increased proliferation and/or decreased apoptosis in e6a2 harbouring cells. Methods of assessing GEF and GTPase activity *in vitro* have been previously documented (263), which could delineate differences between Bcr-Abl isoforms. However, these methodologies were not within the scope of this project.

4.3.6   Clinical implications and further study

An aspect of the emergence of e6a2 mediated TKI resistance that remains to be investigated was the co-expression of both e6a2 and e14a2 *BCR-ABL1* in each cell of the resistant population. Protein characterisation of the K562 DasR cell line detailed in Chapter 3 demonstrated the expression of both Bcr-Abl isoforms in the cell line. Phosphorylation of both isoforms appeared to be linked, and it was likely that transphosphorylation occurred between e14a2 and e6a2. In the K562 DasR line, the T315I mutation was identified only in e14a2 transcripts, however, e6a2 protein also remained phosphorylated in the presence of inhibitory levels of dasatinib, demonstrating the ability of different isoforms of Bcr-Abl to interact with and phosphorylate each other, in addition to regular transphosphorylation

between identical Bcr-Abl molecules (Figure 3.9). In the Ba/F3 transformation model presented here, only e14a2, or e6a2, or e1a2 Bcr-Abl was present in each line, and the interactions between isoforms was not investigated. There may be signalling pathway and kinase activity perturbation of Bcr-Abl transphosphorylation between isoforms, due to differential binding of protein co-factors, which could be explored using a cell line model expressing both e14a2 and e6a2/e1a2. However, outside of e13a2 and e14a2 co-occurring as splice variants, the identification of multiple Bcr-Abl isoforms within a leukaemic clone is rare, with most patient case studies identifying only a single expressed Bcr-Abl isoform, thus limiting the translational relevance of this line of investigation.

The identification of the rare e6a2 *BCR-ABL1* fusion in a TKI resistant context is a novel finding, and has significant clinical implications. Modern methodology for diagnosis of Ph+ leukaemia typically involves the identification of a common *BCR-ABL1* transcript isoform in leukaemic cells by targeted PCR, and disease monitoring over the course of treatment by *BCR-ABL1* RT-qPCR. However, subsequent exploration for alternate *BCR-ABL1* fusions is not typically performed, and in this case, the emergence of e6a2 in response to TKI exposure would go undetected. Haematological relapse associated with rare *BCR-ABL1* transcripts, expanding under TKI exposure, may be a significant contributor to poor treatment response and patient mortality, and the outcomes of this study support the ongoing determination of leukaemic driver genes, particularly in the case of refractory disease of unknown origin.

The study performed here is the first to identify the emergence of *BCR-ABL1* e6a2 coinciding with dasatinib treatment. Quantification of the transcript determined that e6a2 expression was selected for, rising with increasing dasatinib exposure, but falling with the acquisition of alternate resistance mechanisms. The induced expression of e6a2 resulted in the malignant transformation of Ba/F3 cells, resulting in a disease which was less sensitive to TKI-based inhibition than that of *BCR-ABL1* e14a2. This reduced sensitivity was not due to kinase signalling through phosphorylation of CrkL. This study provides evidence for the expression of e6a2 as a resistance mechanism, and warrants the exploration of e6a2 mediated resistance in a patient setting.

BCR breakpoint	ABL1 breakpoint	K562 naïve	K562 DMSO	10 nM Das	15 nM Das	25 nM Das	50 nM Das	200 nM Das
22:23632600:+	9:133729451:+	14	14	23	26	21	21	18
22:23613779:+	9:133729451:+			22	12	13	18	18
22:23632600:+	9:133729454:+			4		2	4	
22:23613779:+	9:133729454:+			2				2
22:23632600:+	9:133655756:+	3	8	21	19	15	15	8
22:23632600:+	9:133638585:+	2		2	2			
22:23632600:+	9:133657191:+		4	6	8	6	4	2
22:23632737:+	9:133607147:+		2	7	6	4	4	3
22:23632738:+	9:133607148:+		2	8	6	4	4	3
22:23613779:+	9:133655756:+			11	2	2	3	4
22:23613779:+	9:133638585:+			8		2	3	4
22:23632600:+	9:133706197:+			4	3	2		
22:23632599:+	9:133729451:+			3	2			
22:23632600:+	9:133678445:+			2		2		
22:23632600:+	9:133614295:+				2			
22:23613779:+	9:133672194:+							2

Table 4.1: FusionCatcher analysis of transcriptome expression data demonstrated the presence of the *BCR-ABL1* e14a2 transcript (red) in all K562 samples, as well as the e6a2 transcript (blue) in dasatinib resistant cells. Additionally, several other *BCR-ABL1* fusion breakpoints (black) were identified sporadically, possibly due to transcriptional error or partial/unfinished splicing of transcripts.
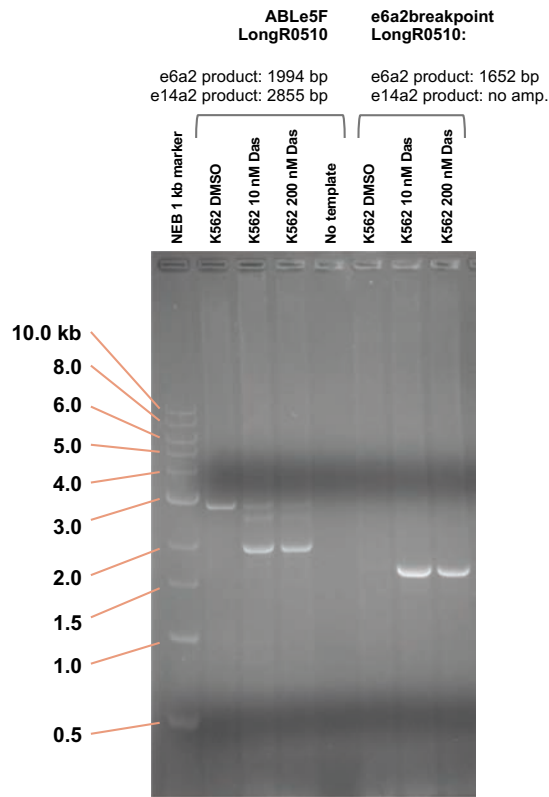
Figure 4.1: Gel electrophoresis of PCR amplicons from selected K562 DasR dose escalation intermediate cDNA samples, amplified using *BCR-ABL1* primers both within *BCR* exon 5 ABLe5F, and spanning the e6a2 breakpoint (e6a2breakpoint). Results validate the presence of an e6a2 *BCR-ABL1* fusion expressed by K562 DasR lines, but not in DMSO control line. An unidentified product of around ~2500 bp amplified in K562 DasR lines, which may correspond with the presence of other *BCR-ABL1* fusions or rare splice variants. Forward (ABLe5F, e6a2breakpoint) and reverse (LongR0510) primers are indicated. amp=amplification; bp=base pairs
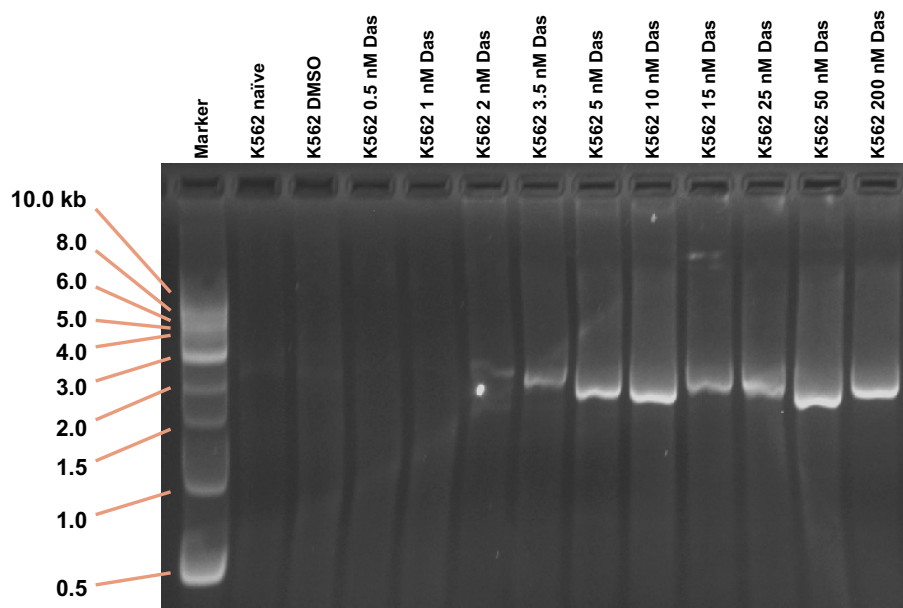
Figure 4.2: PCR amplicons from K562 DasR dose escalation intermediate cDNA samples, using *BCR-ABL1* primers spanning the e6a2 breakpoint junction (e6a2breakpoint, LongR0510). Results demonstrate the emergence of an e6a2 specific amplicon in K562 2 nM DasR intermediate which is retained in subsequent dose escalation intermediates; there is a visible band at the expected 1652 bp size. The e6a2 fusion was not detected in drug naïve or DMSO vehicle control lines or early dose escalation intermediates <2 nM Das.
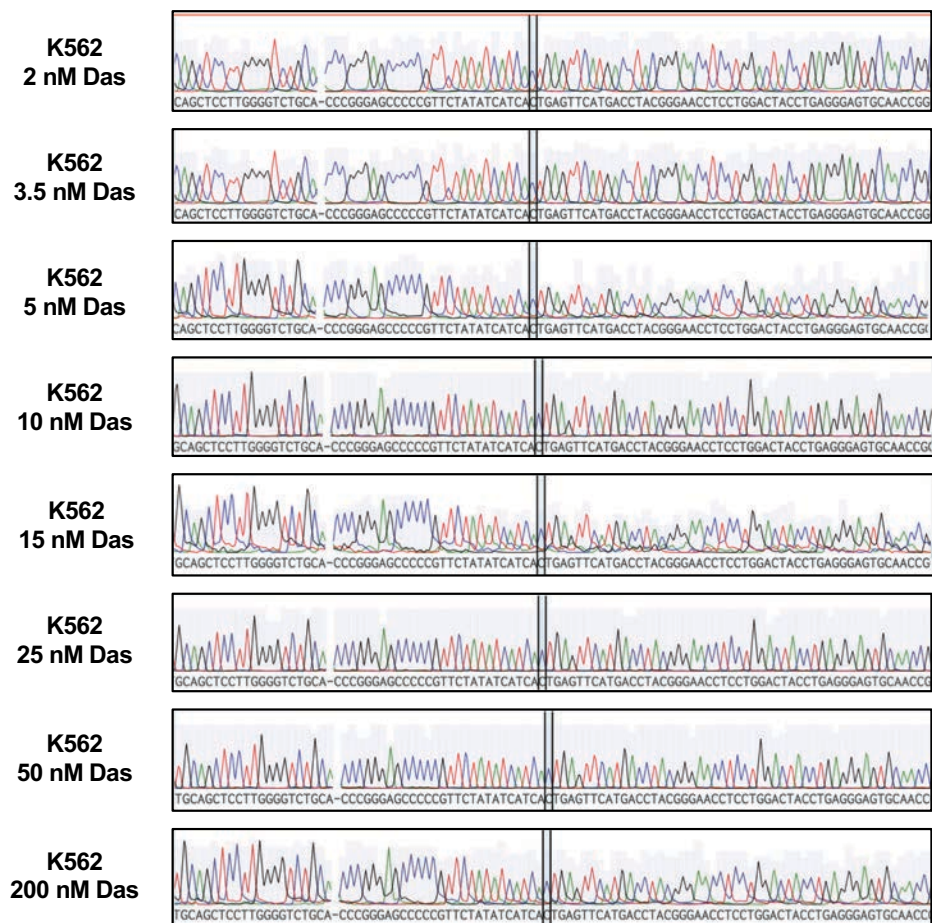
Figure 4.3: K562 DasR dose escalation intermediates do not harbour kinase domain mutations in the *BCR-ABL1* e6a2 fusion. Sequencing of the kinase domain of e6a2 mRNA transcripts was conducted and compared with the GenBank *ABL1* reference sequence. The nucleotide sequences exactly match the reference sequence, with none of the common kinase domain mutations present, including T315I (highlighted above), which was detected in *BCR-ABL1* e14a2 transcripts.
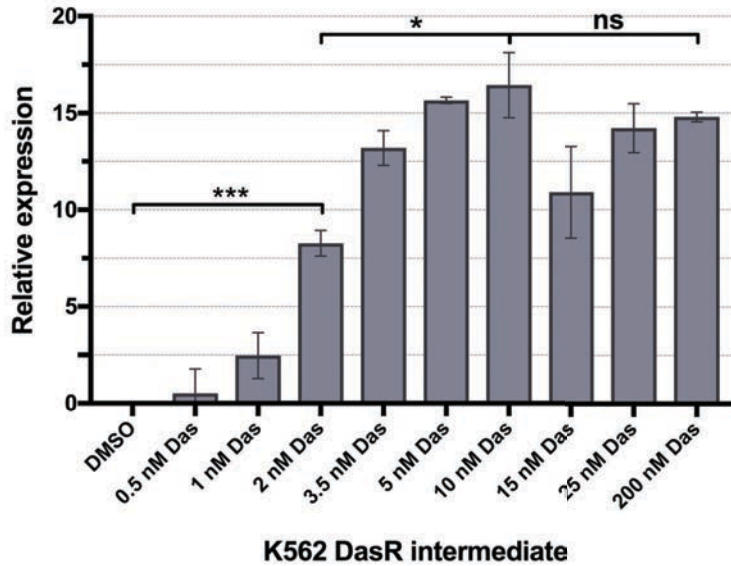
Figure 4.4: *BCR-ABL1* e6a2 transcript levels initially increase during dasatinib dose escalation, peaking in the 10 nM DasR intermediate, before expression plateaus. RT-q PCR specific for *BCR-ABL* e6a2 transcripts was performed in the K562 DasR intermediates, and expression was normalised to the control gene *GUSB*. K562 DMSO control cells expressed no e6a2, thus expression was set at zero, with all other intermediates reported as a relative –dCt. Bars indicate mean transcript expression -/+ SEM of 3 independent experiments. Unequal variances t-test was performed between cell lines; significance is denoted by (*) for p<0.05, (***) for p<0.001. ns=not significant.

Cell line	Region1	Region2	Break1	Break2	Supporting_reads1	Supporting_reads2
K562 naïve	BCR	ABL1	chr22:23632737	chr9:133607147	194	153
K562 15 nM Das	BCR	ABL1	chr22:23614939	chr9:133627619	260	282
	BCR	ABL1	chr22:23632737	chr9:133607147	200	162
K562 200 nM Das	BCR	ABL1	chr22:23614938	chr9:133627618	327	361
	BCR	ABL1	chr22:23632742	chr9:133607152	213	178
	BCR	VWF	chr22:23612611	chr12:6119636	26	5
	BCR	XKR3	chr22:23612611	chr22:17169850	26	8

Table 4.2: FACTERA analysis of target enrichment sequencing for *BCR* and *ABL1* breakpoint fusion locations identified the *BCR-ABL1* DNA breakpoints in selected K562 DasR lines. The e14a2 breakpoint (chr22:23632737 / chr9:133607147 and chr22:23632742 / chr9:133607152) was identified in all K562 DasR and control lines. Additionally, an e6a2 breakpoint (chr22:23614939 / chr9:133627619 and chr22:23614938 / chr9:133627618, highlighted in purple) was identified, exclusively in dasatinib resistant lines.
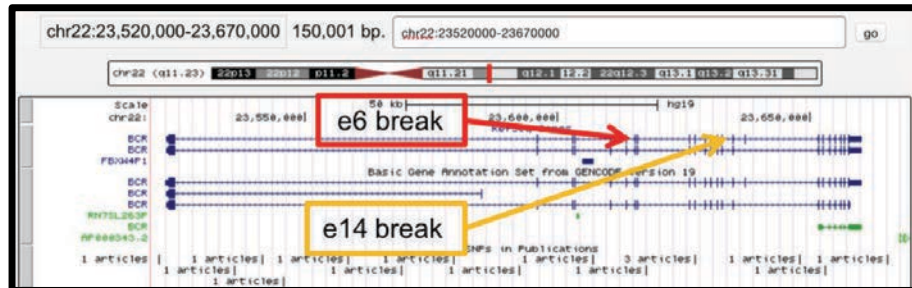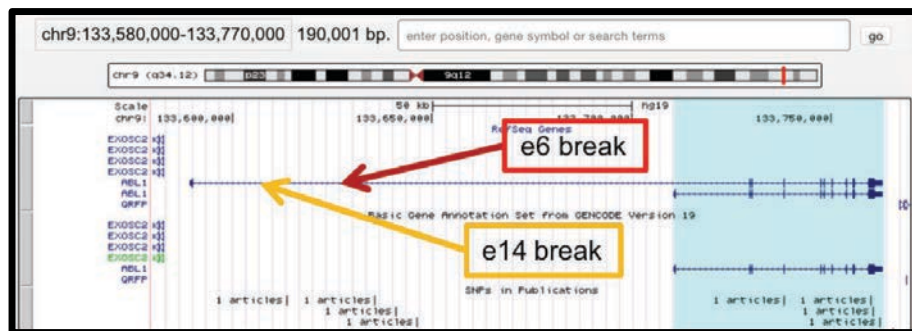
Figure 4.5: NCBI Genome Data Viewer visualising the locations of the *BCR-ABL1* e14a2 and e6a2 breakpoint locations identified in DNA enrichment sequencing experiments. Top: 5' *BCR* breakpoint locations; bottom: 3' *ABL1* breakpoints. The e14a2 *BCR* break is located in *BCR* intron 14, whereas the e6a2 *BCR* break is within intron 6. Both *ABL1* breakpoints are within *ABL1* intron 1, in two distinct locations. The identified breakpoints are consistent with the fusion of *BCR* exon 6 and *ABL1* exon 2 resulting from an intrachromosomal deletion of a region within an existing *BCR-ABL1* e14a2 fusion. Thick lines indicate exonic regions; thin lines indicate intronic regions.
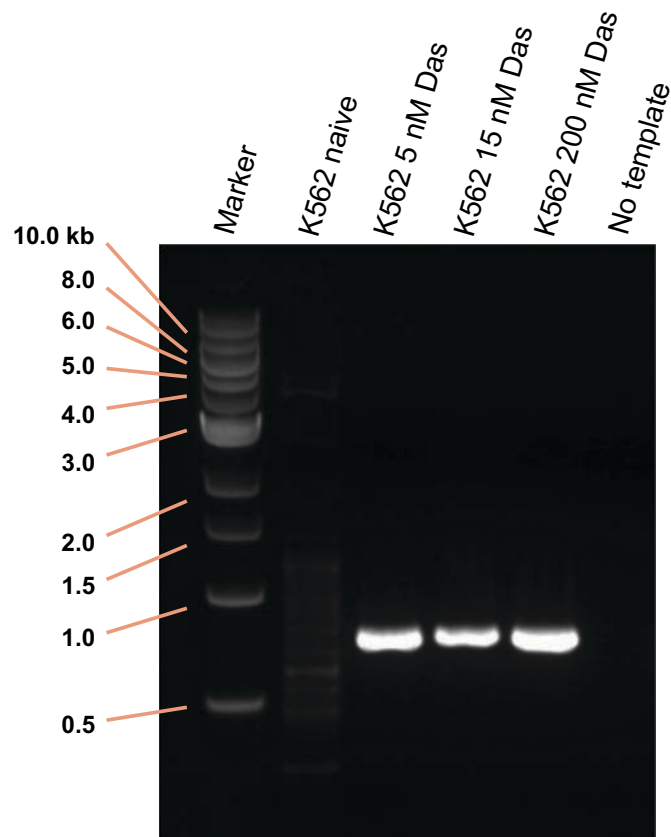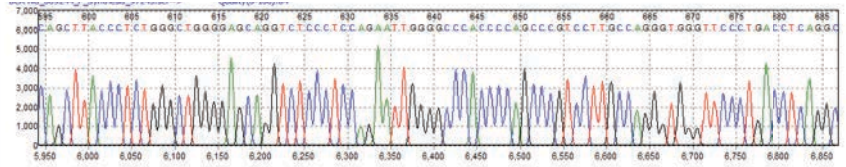
Figure 4.6: PCR amplification validated the presence of a genomic *BCR-ABL1* breakpoint, resulting in a 741 bp product, harboured by K562 DasR cell lines, but not drug naïve controls.
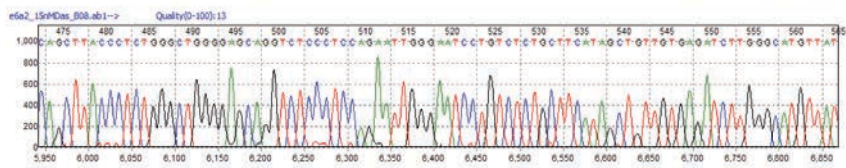
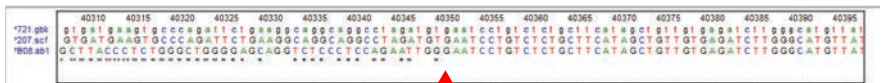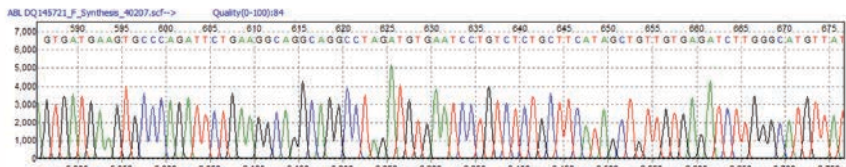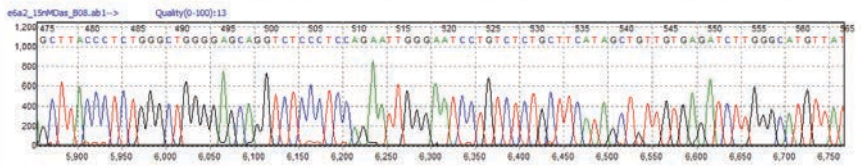Figure 4.7: Sanger sequencing confirmation of the e6a2 DNA breakpoint PCR product, aligned to both *BCR* and *ABL1* sequences. Asterisks under the sequence indicate misalignment, which was used to identify the breakpoint location, highlighted with the red arrow.
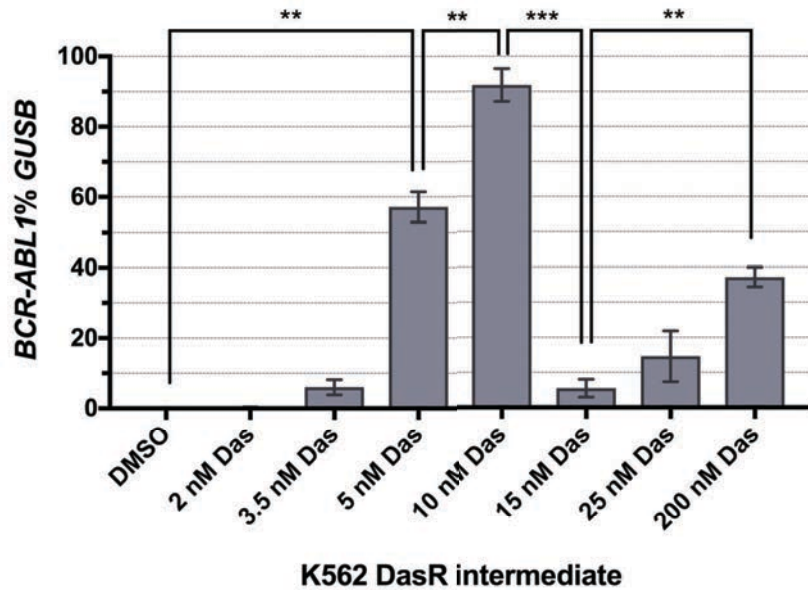
Figure 4.8: DNA qPCR of genomic *BCR-ABL1* highlights an increase in the genomic quantity of e6a2 *BCR-ABL1* fusions, indicative of gene amplification. This increase fluctuated continuously over the course of dose escalation, including a significant *BCR-ABL1* copy loss between the 10 and 15 nM Das intermediates. High genomic *BCR-ABL1* quantities were not consistently selected for in higher dasatinib concentrations. Bars indicate mean -/+ SEM of 3 independent experiments. Unequal variances t-test was performed between cell lines; significance is denoted by (**) for $p < 0.01$, (***) for $p < 0.001$.
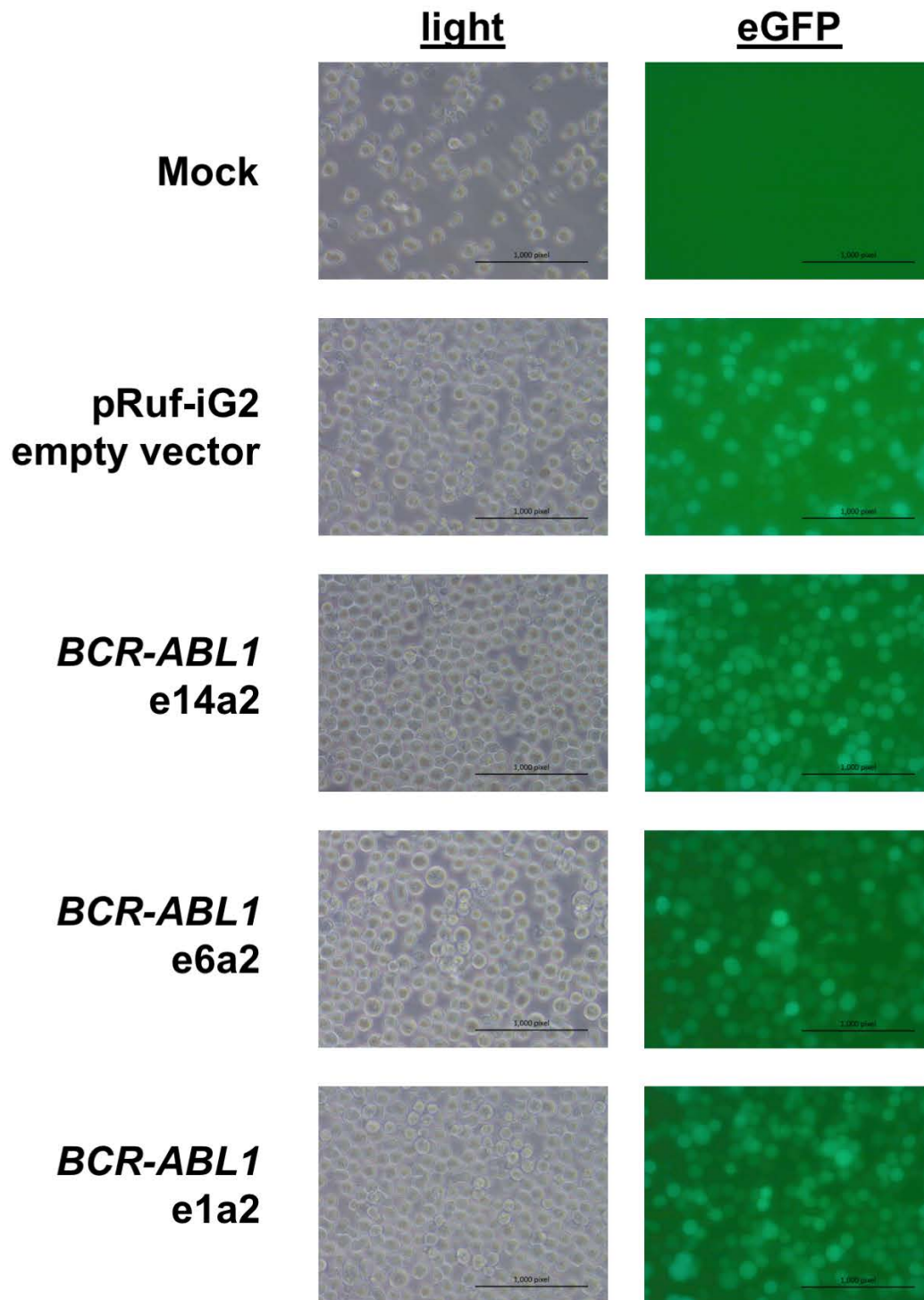
Figure 4.9: Figure 4.9: Photos of lentivirally transduced Ba/F3 lines confirmed successful transduction. The mock transduction produced no eGFP positive cells. All cells transduced with pRuf-iG2 constructs produced a strong eGFP signal, allowing subsequent enrichment by FACS. Images were taken using a Zeiss Axiocam Erc 5s at 40x magnification; scale bar indicates 1000 pixels = 55 μm.
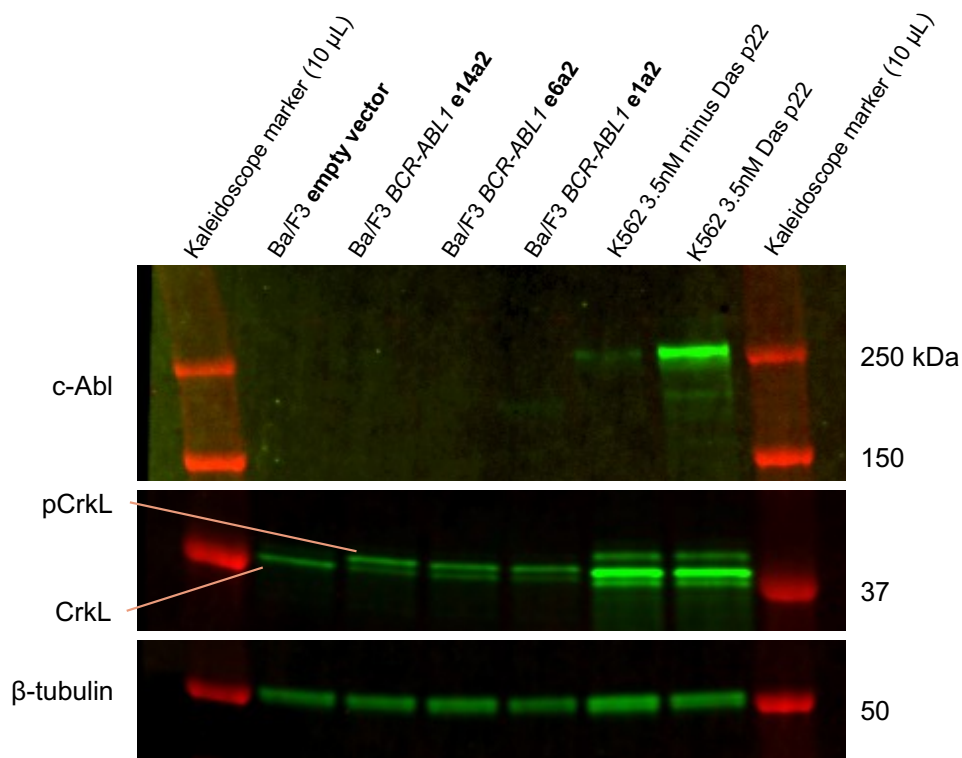
Figure 4.10: Western blotting assessing phosphorylation of the Bcr-Abl kinase substrate, CrkL, demonstrated the successful malignant transformation of *BCR-ABL1* harbouring Ba/F3 lines. The empty vector transduced line exhibited no phosphorylation of CrkL (Phospho-CrkL), whilst all *BCR-ABL1* transduced lines exhibited almost complete phosphorylation of CrkL. K562 DasR lines overexpressing Bcr-Abl were used as positive control. Lysates were loaded equally by protein at 40 μg; blots are representative of two independent experiments.

Sample	BCR-ABL1 e14a2 (SYBR)	BCR-ABL1 e6a2 (SYBR)	BCR-ABL1 e1a2 (TaqMan)	BCR (TaqMan)
Ba/F3 EV #1	undetermined	undetermined	undetermined	33.91
Ba/F3 EV #2	undetermined	undetermined	undetermined	35.22
Ba/F3 EV #3	undetermined	undetermined	undetermined	35.09
Ba/F3 e14a2 #1	18.34	31.05	34.22	34.08
Ba/F3 e14a2 #2	16.14	29.79	35.21	34.60
Ba/F3 e14a2 #3	16.34	29.50	34.54	33.88
Ba/F3 e6a2 #1	undetermined	18.64	33.31	33.92
Ba/F3 e6a2 #2	undetermined	17.21	33.71	36.35
Ba/F3 e6a2 #3	undetermined	16.99	33.94	33.98
Ba/F3 e1a2 #1	undetermined	undetermined	16.96	33.84
Ba/F3 e1a2 #2	undetermined	undetermined	15.96	34.27
Ba/F3 e1a2 #3	undetermined	undetermined	16.03	33.91
K562 DMSO e14a2+	25.14	undetermined	37.42	24.44
K562 3.5 nM Das e14a2/e6a2+	20.00	25.46	22.32	24.18
Patient e1a2+	undetermined	undetermined	34.16	24.16

Table 4.3: RT-qPCR Ct values from *BCR-ABL1* quantitation of Ba/F3 cell lines demonstrated that transduced lines were expressing the correct *BCR-ABL1* transcript isoforms. The empty vector transduced line did not amplify any *BCR-ABL1* products. Conversely, *BCR-ABL1* transduced lines amplified their appropriate isoforms at < 20 cycle numbers. As primers flanked breakpoints, e6a2 primers weakly amplify e14a2 transcripts, and e1a2 primers amplify e14a2 and e6a2 transcripts, however only following many amplification cycles. K562 samples harbouring e14a2 and e6a2 were included as positive controls, as was an e1a2 positive patient sample. Experimental samples were run in triplicate; undetermined = no amplification.
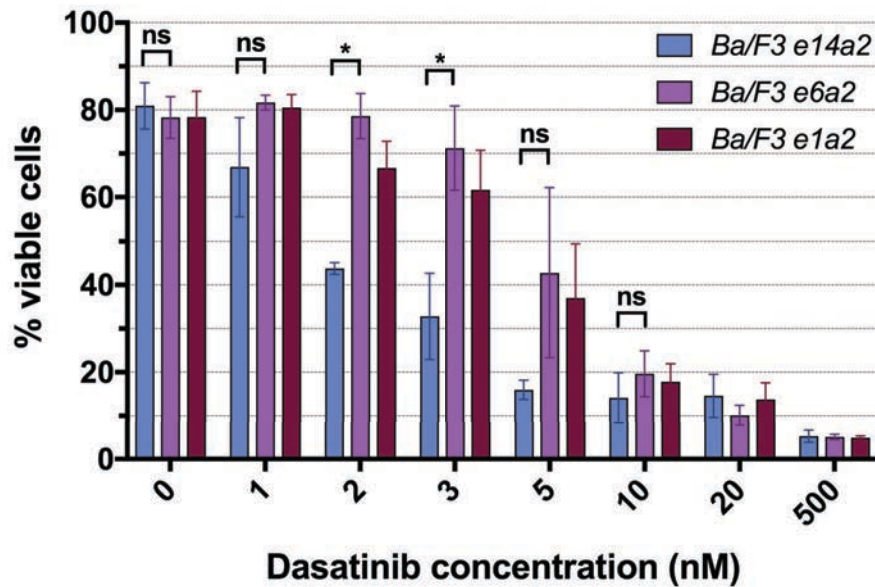
Figure 4.11: Results from dasatinib induced cell death assay in *BCR-ABL1* transduced Ba/F3 cells demonstrated the lower sensitivity to dasatinib of e6a2 harbouring cells, compared with cells expressing the typical e14a2 fusion. Interestingly, cells expressing the e1a2 fusion, typically associated with poor TKI response, exhibited similar dasatinib sensitivity to cells expressing e6a2. Values indicate mean -/+ SEM of 3 independent experiments. Unequal variances t-test was performed between cell lines at each dasatinib concentration; significance is denoted by (*) for $p < 0.05$, (ns=not significant).
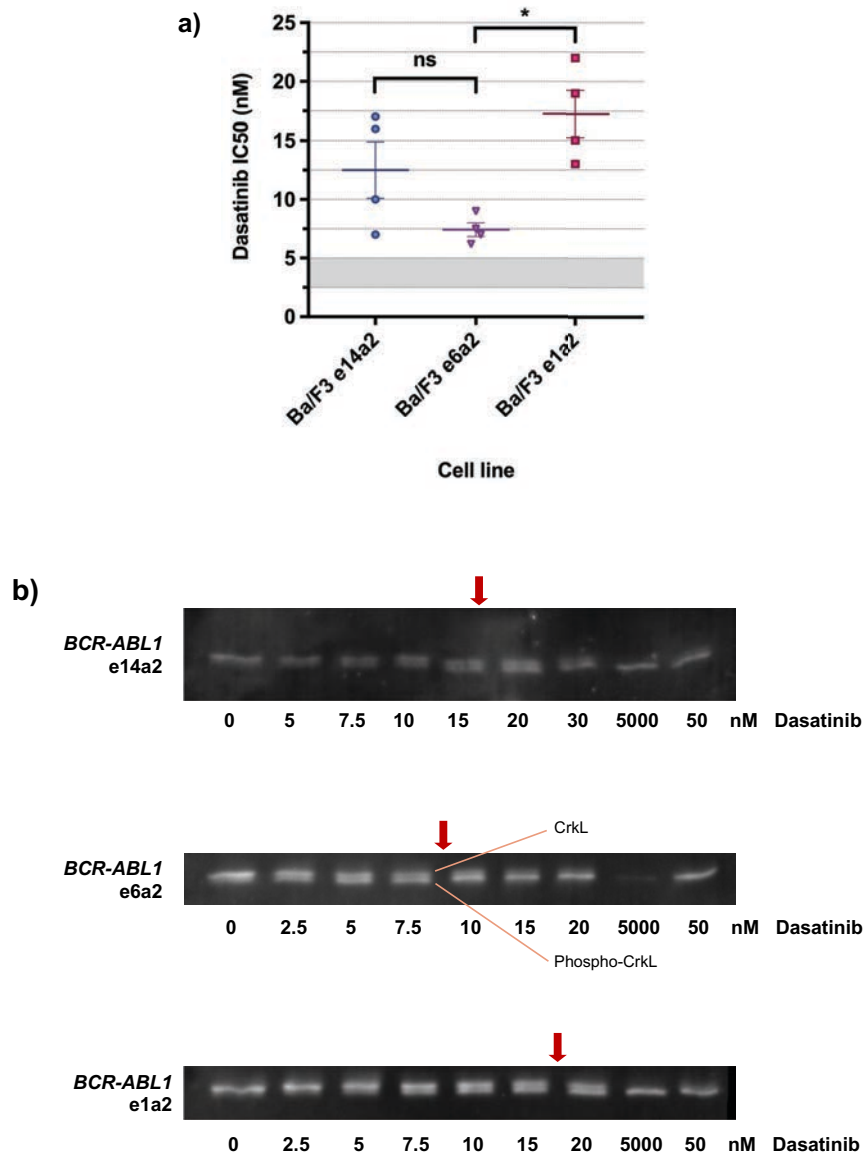
Figure 4.12: a) Results of dasatinib IC50 experiments in Ba/F3 *BCR-ABL1* cell lines indicated that differences in dasatinib mediated cell death were not due to inherent differences in kinase inhibition sensitivity. Approaching statistical significance, the average dasatinib IC50 of Bcr-Abl e6a2 was lower than that of Bcr-Abl e14a2. Conversely, the IC50 of Bcr-Abl e1a2 was higher than e6a2. Bars indicate mean -/+ SEM of 4 independent experiments. Unequal variances t-test was performed between cell lines; significance is denoted by (*) for $p<0.05$, ns=not significant b) Representative dasatinib pCrkL IC50 western; red arrows indicate the approximate point of 50% Bcr-Abl kinase inhibition (dasatinib IC50).

5 The expression of the drug transporter ABCG2 contributes to dasatinib and ponatinib resistance

5.1 Introduction

The identification of the *BCR-ABL1* e6a2 transcript expression in the K562 DasR cell line helped establish the contribution of e6a2 to TKI resistance. However, was not sufficient to explain the loss of TKI sensitivity observed in some K562 DasR dose escalation intermediates. Observed resistance to dasatinib was higher in the 10 and 15 nM DasR intermediates than could be explained by Bcr-Abl expression or kinase domain mutations alone (Chapter 3.2.1, Figure 3.3); in these intermediates, the *BCR-ABL1* expression did not significantly increase, while TKI resistance did increase. Indeed, the highest ponatinib tolerance observed was in the 15 nM Das cell line. Clearly, undefined resistance mechanisms were present in these cells. As part of the interrogation of TKI resistance mechanisms present in this model, RNA sequencing data was explored for global gene expression, and fluctuations in expression over the course of increasing dasatinib exposure. mRNAseq differential gene expression analyses comparing control and dasatinib-resistant cell lines were filtered for significance and large fold differences in transcription, and a shortlist of differentially expressed genes was generated. This method identified the increased expression of the ABCG2 transporter gene.

Expression of the *ABCG2* gene had not been examined in the other K562 DasR dose escalation intermediates, and it was unknown whether the gene was being translated into a functional transporter. Importantly, the effect of increased ABCG2 expression on the dasatinib and ponatinib sensitivity of the cell line had not been established. To further explore the role of ABCG2 in the K562 DasR line, experiments were designed to validate the findings of the transcriptome analysis and the following research questions were posed:

1. What was the level of ABCG2 expressed during dasatinib escalation in the K562 DasR intermediates?

2. Was ABCG2 functional in these lines, and could efflux function be chemically inhibited?

3. Could inhibition of ABCG2 mediated efflux sensitise K562 DasR cells to TKI therapy?

Sequencing of RNA transcripts from dose escalation intermediate samples of the K562 DasR line, revealed the overexpression of the *ABCG2* gene, correlating with the acquisition of dasatinib resistance. This result was validated by RT-qPCR for *ABCG2*, against the control gene *GUSB*, and reported as a ddCt value normalised to the K562 DMSO vehicle control. The effect

of *ABCG2* transcript overexpression on the levels and function of ABCG2 protein was determined. Cell surface ABCG2 expression was measured in K562 DasR lines by flow cytometry. As the ABC transporter ABCB1 is commonly associated with chemotherapy resistance, ABCB1 surface expression was concurrently measured. Using the BODIPY-prazosin efflux assay (264-266), the transporter function of the ABCG2 protein was interrogated, and the effectiveness of the ABCG2 inhibitor Ko143 was tested.

Dasatinib transport by ABCG2 was measured using the dasatinib intracellular uptake and retention assay (IUR) assay, which was performed in the K562 15 nM DasR intermediate and K562 control cells by Mrs Sophie Watts in the SAHMRI leukaemia laboratory. Cells were cultured in radiolabelled C^{14}-dasatinib in the presence of Ko143, and drug uptake-retention was measured by scintillation.

To determine whether inhibition of transporter function sensitised leukaemic cells to TKI induced apoptosis, the dasatinib pCrkL IC50 (IC50^{Das}) and TKI induced cell death assays were repeated in the presence of the ABCG2 transport inhibitor Ko143. Additionally, as ponatinib is often prescribed for patients who are resistant to 1st and 2nd generation TKIs, the role of ABCG2 in mediating ponatinib efflux was determined. Ponatinib pCrkL IC50 (IC50^{Pon}) and cell death assays were performed in the presence of Ko143.

5.2 Results

5.2.1 Transcriptome sequencing identifies *ABCG2* transcript overexpression in K562 DasR dose escalation intermediates

We performed RNA sequencing differential expression analysis of K562 DasR samples. The 10, 15 and 25 nM DasR intermediates were pooled as a comparative group based on hierarchical clustering analysis, as were the K562 naïve and DMSO vehicle control lines (Figures S16). Each sample was run in singlicate, thus differential expression analysis could not be performed between the two control groups, however, biological differences between the two samples would add to overall variance, and therefore increase confidence in the shortlisted differentially expressed genes. Plots identifying the top most differentially regulated genes can be found in Figures S19 and S20. Volcano plot visualisation of

differentially expressed genes identified the ABCG2 gene as both significantly (FDR=1.01x10^{-11}) and highly expressed (logFC=9.978) compared with drug naïve controls (Figure 5.1).

5.2.2 The ABCG2 gene and protein is overexpressed in K562 DasR dose escalation intermediates

The RNAseq gene expression results were validated by RT-qPCR; additional K562 DasR intermediates were also assessed to complete the full spectrum of TKI resistant intermediates. A significant increase in *ABCG2* expression in all K562 DasR lines was observed when compared with control cells (Figure 5.2). Compared with K562 DMSO control, increased *ABCG2* expression was first observed in the 2 nM DasR intermediate (fold change (ΔΔCt)=1 vs 332.5, p=0.0017), after which expression plateaued until the 5 nM DasR intermediate. *ABCG2* expression subsequently increased further and reached a peak in the 15 nM DasR intermediate (fold change=332.5 vs 14670.1, p=0.0023), before a significant decrease in the 200 nM DasR line (fold change=14670.1 vs 5.3, p=0.0039). However, *ABCG2* expression in the 200 nM DasR line remained significantly higher than in DMSO control (fold change=5.3 vs 1, p=0.0316).

The *ABCB1* transporter is commonly associated with therapeutic drug resistance. Therefore, gene expression of *ABCB1* was determined concurrently with *ABCG2*. Results demonstrated no significant changes in *ABCB1* expression associated with dasatinib resistance in the K562 DasR lines (Figure 5.2).

To determine if increased *ABCG2* gene expression translated to a rise in ABCG2 surface protein expression, flow cytometric analysis of ABCG2 expression was performed. The percentage of ABCG2-positive cells demonstrated a transient elevation in ABCG2 protein expression, consistent with mRNA levels (Figure 5.3). When compared with the K562 DMSO control line, significant overexpression of ABCG2 was first detected in the 10 nM DasR intermediate (63.0 vs 15.7% positive, p=0.0005, n=4). ABCG2 expression rose significantly to 87.7% in the 15 nM DasR intermediate (p=0.0025, n=7), before significantly falling to 28.1% in the K562 200 nM Das line (p=0.0054, n=3). Further interrogation of ABCG2 expression in K562 DasR dose escalation intermediates indicated the early emergence of a small population

of cells with high ABCG2 expression (Figure 5.3b). With continued dasatinib exposure, the minor population of ABCG2 overexpressing cells in the 2 nM DasR intermediate became the dominant clonal population, with the majority of cells in the 15 nM DasR intermediate demonstrating a high level of ABCG2 expression. However, in the 25 nM DasR intermediate, a population of cells with low ABCG2 expression re-emerged, and in K562 200 nM DasR cells, ABCG2 expression fell close to baseline levels.

5.2.3 ABCG2 is functional in K562 DasR intermediates

In order to demonstrate ABCG2 functionality in K562 DasR intermediates, and to confirm adequate concentrations of Ko143 required to inhibit transport activity, the BODIPY-prazosin efflux assay was performed. Results demonstrated ABCG2 substrate efflux in the K562 10 nM and 15 nM DasR intermediates, indicated by stain negativity following 30 minutes incubation in BODIPY-prazosin (Figure 5.4, blue peak). The K562 DMSO vehicle control line, as well as K562 5 nM and 25 nM DasR intermediates stained positive for BODIPY-prazosin, indicating an absence of ABCG2 mediated substrate efflux. In these lines, the addition of 500 nM Ko143 had no effect on BODIPY-prazosin fluorescence. At this concentration, Ko143 exhibits specific inhibition of ABCG2 (267). However, in the 10 and 15 nM DasR cell populations, addition of 500 nM Ko143 resulted in retention of BODIPY-prazosin, demonstrating that: 1) the ABCG2 expressed by these resistant cell lines was functionally active and 2) the concentration of Ko143 used was sufficient for ABCG2 inhibition. Thus, this concentration of Ko143 was used in subsequent IC50 and cell death assays.

In addition to the BODIPY-prazosin efflux assay, the dasatinib IUR assay was performed in the K562 15 nM DasR intermediate (greatest expression of ABCG2), along with the drug naïve K562 control (Figure 5.5). Comparison indicated that the 15 nM DasR intermediate retained significantly less C^{14}-dasatinib than the naïve control (24.6 vs 12.1 ng / $2x10^5$ cells, n=5, p<0.001). The addition of 500 nM Ko143 to the K562 naïve control line did not alter dasatinib retention (22.1 vs 24.6 ng / $2x10^5$ cells, n=5, p=0.234), however, in the 15 nM DasR line Ko143 addition resulted in significantly elevated intracellular dasatinib concentrations (19.4 vs 12.1 ng / $2x10^5$ cells, n=5, p=0.004); Ko143 treated 15 nM DasR cells did not have significantly lower dasatinib IUR than drug naïve K562 cells in the absence of Ko143 (p=0.06). Taken

together, these data suggest variable increases in ABCG2 functionality during intermediate stages of dasatinib resistance generation.

5.2.4 Inhibition of ABCG2 sensitises ABCG2 overexpressing K562 DasR cells to dasatinib-mediated Bcr-Abl inhibition and induces cell death

To demonstrate the causative role of ABCG2 transporter function in reducing dasatinib sensitivity, dasatinib-induced cytotoxicity assays were repeated in the presence and absence of the ABCG2 inhibitor Ko143. Results (Figure 5.6) demonstrated a key role of ABCG2 in the acquisition of dasatinib resistance. When cultured in a concentration gradient of dasatinib, the addition of Ko143 did not significantly lower the viability of K562 DMSO control cells at any dasatinib concentration. However, in the 10 nM DasR intermediate, cells were significantly less viable when Ko143 was used in addition to 50 nM dasatinib (28.4 vs 51.9% viable, n=3, p=0.003). Indeed, in the majority of dasatinib concentrations tested, addition of Ko143 was found to increase the cell death in K562 10 nM DasR cells. This trend was also observed in the 15 nM DasR intermediate, however, due to large variance between assays, differences in cellular viability due to Ko143 were not statistically significant. Interestingly, in the 10 and 15 nM DasR intermediates, a proportion of cells remained viable even in 5000 nM dasatinib. In the K562 25 nM DasR cells and all higher dose escalation intermediates, cell viability remained high in any dasatinib concentration, regardless of whether cells were cultured in the presence or absence of Ko143, suggesting ABCG2 was not required for dasatinib resistance in later intermediates.

Sensitivity of Bcr-Abl to inhibition by dasatinib was measured in the presence of Ko143 using the pCrkL IC50 assay (Figure 5.7). IC50^{Das} data confirmed previously generated IC50 data (Figure 3.4); the IC50^{Das} increased with prolonged dasatinib exposure, eventually peaking at over 5000 nM in the 25 nM and later DasR intermediates, coinciding with the cell lines' acquisition of T315I (Figure 3.5). Addition of Ko143 in the K562 DMSO line did not significantly alter the IC50^{Das} (6.97 vs 7.44 nM, p=0.778, n=3). However, in the 10 and 15 nM DasR intermediates, addition of Ko143 significantly lowered the IC50^{Das}, sensitising the cells to dasatinib induced Bcr-Abl inhibition. In the 15 nM DasR intermediate, addition of Ko143 reduced the IC50^{Das} from 743 to 22.3 nM (p<0.0001, n=3); a similar effect was observed in the 10 nM DasR intermediate (150 vs 16 nM, p=0.021, n=3). Intriguingly, in the presence of Ko143,

the IC50^{Das} in the K562 15 nM DasR line was not significantly higher than the K562 DMSO control (22.3 vs 6.97, p=0.101, n=3), indicating that the predominant mode of dasatinib resistance in the 15 nM DasR intermediate was ABCG2 overexpression. Ko143 also induced a small dasatinib sensitising effect in early dose escalation intermediates, though this only reached significance in the 3.5 nM DasR intermediate (41 vs 21.3 nM, p=0.006, n=3). As expected, late dose escalation intermediates, expressing the T315I mutation, exhibited no dasatinib sensitivity in the presence or absence of Ko143.

5.2.5 ABCG2 contributes to ponatinib cross resistance

Following confirmation of the involvement of ABCG2 overexpression in dasatinib resistance, the contribution of ABCG2 overexpression to ponatinib resistance was also assessed. TKI induced cytotoxicity and pCrkL IC50 assays were performed in the presence of Ko143 (Figure 5.8). In the absence of Ko143, sensitivity to ponatinib in K562 DasR cells was consistent with previously generated data (Figure 3.13). In the K562 DMSO control line, addition of Ko143 did not result in significant changes to cell viability in the presence of gradient ponatinib. While a modest reduction in cell viability was observed when K562 10 nM DasR intermediate cells were cultured with Ko143 (Figure 5.8b), the addition of Ko143 significantly lowered 15 nM DasR cell viability in several of the ponatinib concentrations tested (Figure 5.8c); in 10 nM ponatinib, the addition of Ko143 reduced viability from 88% to 52% (p<0.001); in 50 nM ponatinib, Ko143 reduced viability from 52% to 28% (p=0.003). Previously, the K562 25, 50 and 200 nM DasR lines were demonstrated as completely resistant to dasatinib induced cell death (Figure 3.3a); in contrast, these lines were susceptible to ponatinib induced cell death (Figure 5.8d-f). Ko143 did not significantly alter the cell viability in these lines, presumably attributable to the loss of ABCG2 expression.

Bcr-Abl ponatinib IC50 experiments performed in the presence of Ko143 (Figure 5.9) was consistent with ponatinib cell death assays. The Bcr-Abl kinase activity in cells overexpressing ABCG2 was significantly less sensitive to ponatinib induced inhibition. Addition of Ko143 restored ponatinib sensitivity and significantly lowered the ponatinib IC50 in the 10 nM (101 vs 47 nM, n=3, p=0.006) and 15 nM (99.7 vs 58.7 nM, n=3, p=0.015) DasR intermediates. This effect was not observed in the K562 DMSO control line, or the 50 or 200 nM DasR lines. Interestingly, Ko143 had a marginal ponatinib sensitising effect in the 25 nM DasR line (bulk

population of cells contained ABCG2 +ve and -ve cells, Figure 5.3a), though this did not reach statistical significance (55.7 vs 76.7 nM, n= 3, p=0.109).

5.3 Chapter discussion

Acquired resistance to TKI therapy often results in treatment failure for CML patients, and there is a well-recognised role of ABC transporters in conferring resistance. A greater understanding of different substrate transport profiles will direct the appropriate administration of therapeutic agents. This study demonstrates that the drug transporter ABCG2 contributes to dasatinib and ponatinib efflux *in vitro*, and that inhibition of ABCG2 efflux activity can re-sensitise leukaemic cells to TKI. Additionally, the emergence, selection and de-selection of leukaemic cells overexpressing ABCG2 as a resistance mechanism was assessed over long-term dasatinib exposure. Determining the circumstances under which this cell population undergoes clonal evolution provides insight into the forces affecting leukaemic cell clonal dynamics. This is an important consideration for defining novel therapeutic strategies for leukaemia patients who are resistant or intolerant to TKI treatment.

5.3.1 Dasatinib and ponatinib efflux by ABC transporters

The efflux of dasatinib by ABCG2 was first demonstrated by our laboratory (184). This has been subsequently validated in a number of *in vitro* studies, which have cumulatively demonstrated that ABCG2 expression increases the dasatinib pCrkL IC50, lowers dasatinib cellular uptake and retention, and is involved in *in vivo* brain barrier transport of dasatinib (173). The results presented here, using the K562 DasR cell line and its ABCG2 overexpressing intermediates, have corroborated these findings. This study thoroughly demonstrated that ABCG2 overexpressing cells have higher dasatinib pCrkL IC50, lower dasatinib-mediated cell death, and lower dasatinib uptake and intracellular retention. Furthermore, all the observed effects of ABCG2 mediated resistance can be reversed by administration of the small molecule inhibitor of ABCG2, Ko143.

The 3rd generation TKI, ponatinib, is indicated as a second/third line treatment for CML and Ph+ ALL patients that are resistant or intolerant to previous TKI treatment. As discussed previously, upregulation of small molecule transporters such as ABCB1 has been

demonstrated to confer a multidrug resistant phenotype, due to the broad substrate specificity. This is the first demonstration of resistance to ponatinib occurring via upregulation of ABCG2 due to previous exposure to dasatinib treatment. Previously, studies in our laboratory studying ponatinib-ABCG2 interactions have demonstrated that ABCG2 does not mediate ponatinib transport (268, 269). Further studies have demonstrated that ponatinib is a potent inhibitor of ABCG2 transport (270). This is at odds with the current findings, which have demonstrated that high ABCG2 expression results in ponatinib resistance, and that inhibition of ABCG2 transport can sensitise these cells to ponatinib treatment. Similar to my project, previous studies have used Ko143, as well as the less specific ABC transporter inhibitor pantoprazole, to inhibit ABCG2 activity. However, possible points of difference between the studies include the absolute levels of ABCG2 expression in the cell lines. The K562 15 nM DasR dose escalation intermediate exhibited the highest ABCG2 expression, as demonstrated by flow cytometric analysis. It is possible that ABCG2 mediated transport of ponatinib is not as efficient as for dasatinib, and that a high level of expression is necessary for detectable increases in ponatinib IC50 in ABCG2-overexpressing cells; ABCG2 expression levels may not have been as high in previous studies. Substrate transport assays could definitively demonstrate ponatinib transport by ABCG2. To our knowledge, no study of ponatinib intracellular uptake and retention have been performed. This could demonstrate the transport of ponatinib by ABC transporters, and could be performed in future studies.

5.3.2   Clinical use of ABCG2 inhibitors

This study has demonstrated the effective *in vitro* use of Ko143 to sensitise ABCG2 overexpressing cells to both dasatinib and ponatinib treatment. While ABC transporter inhibition has potential as an effective therapeutic strategy, to date, ABCG2 transporter inhibitors have not been used with clinical efficacy (271). Initial attempts to clinically translate this strategy used the ABCG2 inhibitor fumitremorgin C (a Ko143 analogue). In an *in vitro* study by Nakanishi *et al.*, ABCG2 overexpressing K562 cells were 2-3 fold more resistant to imatinib than parental controls, however, ABCG2 inhibition with fumitremorgin C restored imatinib induced cell death. However, these findings did not translate effectively, and the clinical use of fumitremorgin was associated with severe neurotoxicity (271). In the experiments presented here, the fumitremorgin C predecessor, Ko143 was used. While Ko143 was developed over a decade ago (230, 272), there has been limited clinical success with the

drug. Physiological ABCG2 expression occurs in the mammary gland, testis, intestine, colon, liver, kidney, venules, brain endothelium, and placental tissue, playing an important role in xenobiotic efflux, folate and uric acid homeostasis, and protection from toxic porphyrin build up (273-276). Significant toxicity can result from ABC inhibitor treatment, and the titration for clinically relevant dosages will likely prove difficult. Nevertheless, ABC transporter inhibition remains a clinically relevant avenue. Our laboratory has previously demonstrated the ABC transporter inhibitors pantoprazole and esomeprazole to sensitise leukaemic cells to TKI treatment (277), and transporter inhibition has successfully been used concomitantly with traditional chemotherapies (278).

As previously stated, many TKIs, including imatinib, nilotinib and ponatinib, demonstrate inhibition of ABC transporters. This transport inhibiting effect could be exploited to sensitise leukaemic cells to drug induced toxicity. The co-treatment of imatinib or nilotinib with dasatinib has been demonstrated to increase the dasatinib sensitivity via inhibition of ABCG2 activity (279). Ponatinib has also been demonstrated to inhibit the activity of ABCG2, enhancing the intracellular uptake of ABCG2 efflux substrates (270). The addition of ponatinib to ABCG2 transported chemotherapeutics resulted in synergistic cytotoxicity. However, this effect may only occur at TKI concentrations several times higher than what is clinically achievable (173, 197). A strategy using low doses of several TKIs could be utilised to circumvent this (271, 279). Using combinatorial treatment strategies, different TKIs may maximise the inhibition of Bcr-Abl mutants and inhibit ABC transporter mediated efflux, while also allowing lower dosing of individual drugs, therefore limiting off target drug toxicity (128). Alternatively, switching to different classes of chemotherapeutic agents which are not substrates of ABC transporters, ABC transporter-mediated resistance could be circumvented (280).

5.3.3   ABCG2 and the stem cell phenotype

Evidence indicates a critical role for ABCG2 in the protection of haematopoietic stem cell populations, and a stem cell 'side population' can be purified based on the activity of ABCG2 (281). High levels of gene expression are observed in areas of low oxygen, such as the stem cell niche (282). The expression of ABCG2 is highly conserved in primitive stem cells from bone marrow, skeletal muscle, cultured embryonic stem cells, and the enforced expression of

ABCG2 in normal murine bone marrow cells increases the stem cell population proportion, inhibiting haematopoietic development (283). ABCG2 expression is crucial for stem cell survival, and ABCG2-null progenitor cells demonstrate impaired survival under hypoxic conditions (282). ABCG2 also plays a role in cancer stem cell maintenance, with inhibition of ABCG2 activity reducing the expression of stem cell markers and self-renewal capacity of glioma stem cells (284). In the model presented here, ABCG2 expression may be maintaining a stem cell-like population in the K562 10 and 15 nM DasR intermediates. The lower cell cycling rate of stem cells limits their sensitivity to drug treatments such as TKIs. However, the ABCG2 overexpressing K562 DasR cells did not exhibit a slower growth cycle in routine cell culture, requiring subculture at the same rate of other K562 lines. Other unknown functions of ABCG2 expression in determining the stem cell subtype may be causative of decreased dasatinib and ponatinib sensitivity, however, the primary route of cellular TKI defence is most likely through TKI export from the cell. It may be worthwhile to determine the expression and function of ABCG2 in the stem cell (CD34+) population of diagnostic CML sample, to determine their inherent TKI resistance, and to establish whether inhibition of ABCG2 function will sensitise these cells to TKI.

5.3.4 Selective pressure of dasatinib on ABCG2 expression

Following identification of *ABCG2* overexpression from mRNAseq of K562 DasR samples, qPCR and flow cytometric expression analyses were used to track gene and protein expression over the course of dasatinib dose escalation. A population of ABCG2 overexpressing cells was identified early in dose escalation, detectable in the 2, 3.5 and 5 nM Das intermediates, however, high ABCG2 expression was not strongly selected for until escalation to 10-15 nM dasatinib. Findings elaborated on in Chapters 3 and 4 indicated that *BCR-ABL1* overexpression was highest in these early intermediates, and reached a maximum in the 3.5-5 nM Das lines. I hypothesise that in lower concentrations of dasatinib, *BCR-ABL1* overexpression alone is sufficient for cells to maintain viability and proliferative activity, and high ABCG2 expression does not confer a selective advantage under these circumstances. However, at higher dasatinib concentrations, ABCG2 overexpression confers significantly greater dasatinib resistance, thus allowing ABCG2 overexpressing cells to proliferate. Alternatively, there may be a molecular switch in the control of ABCG2 gene expression, whereby higher intracellular TKI concentrations induce drug transporter expression. However, this remains difficult to test,

as a 10-15 nM dose of dasatinib to a TKI naïve *BCR-ABL1*+ve cell line population will typically result in cell death.

Upon continued dasatinib dose escalation above 25 nM, ABCG2 expression significantly decreased. Preliminary results demonstrated that cells expressing the highly resistant T315I mutation first arose in the 25 nM intermediate; it is possible that a minor population of T315I positive clones were selected for, outcompeting the cells that overexpress ABCG2 as a resistance mechanism. Curiously, analysis of cell viability assay data identified a subpopulation of the 15 nM DasR intermediate, highly resistant to dasatinib in both the presence and absence of Ko143 (Figure 5.6c). This suggests that a significant proportion of the cell population was expressing T315I at a low level, only being selected for in higher dasatinib concentrations. Additionally, this finding highlights the failure of aggregate/pooled cell population experiments for determining cell population heterogeneity. The observed loss of ABCG2 expression with prolonged dasatinib escalation is likely due to an increase in the T315I positive, ABCG2 expression low, fraction of the cell population.

Alternatively, cellular ABCG2 expression may provide the and environment conducive to development of a kinase domain mutation, in which there is low intracellular concentration of TKI and insufficient Bcr-Abl inhibition to prevent cellular proliferation. Our laboratory has previously demonstrated that ABC transporter overexpression precedes kinase domain mutation (182), however, in the current study it is unknown whether the T315I founder clones were also ABCG2 overexpressing. The association between T315I and ABCG2 expression could have been determined by sorting K562 DasR cells for ABCG2 expression, and sequencing the T315I region in the ABCG2 high and low populations, to establish and correlations between expression of these resistance mechanisms.

5.3.5   Future work

The fluctuations in ABCG2 expression dynamics and its effects on dasatinib and ponatinib resistance underlie a convoluted biological complexity. There remain several research questions regarding the stochastic induction of ABCG2 expression and TKI resistance, and as discussed, a number of experimental assays which could elucidate this. The translation of ABC transporter inhibitors into clinical use is ongoing, and molecular characterisation of ABC

transporter substrate transport will likely indicate potential therapeutic drug combinations. The results presented here demonstrate how ABCG2 can contribute to TKI resistance and cross resistance. However, we have demonstrated that perturbation of ABCG2 expression primarily occurs within a particular drug concentration window, and as such, the targeting of ABC transporter expression early in the course of TKI treatment may halt the progression of disease and drug resistance.

Volcano plot: 10/15/25nM Das vs naive/DMSO Ctrls

Figure 5.1: Volcano plot diagram indicating genes differentially expressed in the K562 10, 15 and 25 nM DasR intermediates, compared with drug naïve controls. Green dots / labeled genes indicate genes with expression logFC>2, and FDR<0.005 as a significance cutoff. Note the ABCG2 gene towards the far right of the diagram, indicating a high level of expression in K562 DasR intermediates.
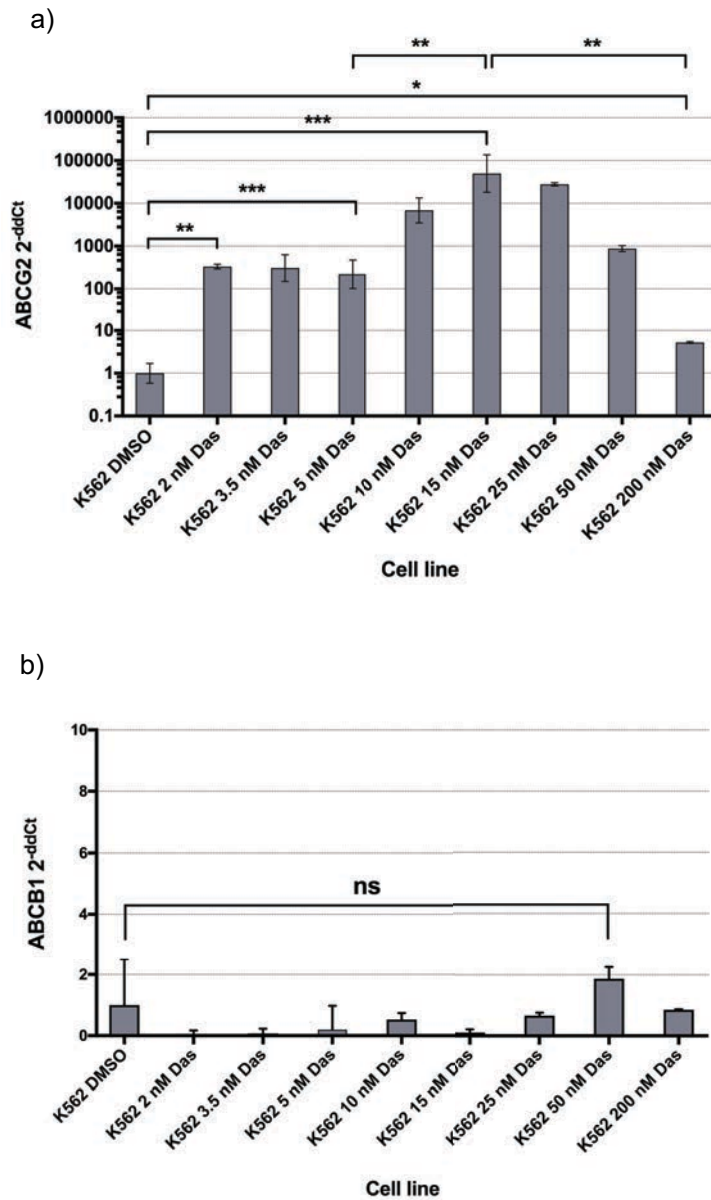
a)

b)

Figure 5.2: RT-qPCR gene expression data for a) ABCG2 and b) ABCB1 from K562 DasR dose escalation intermediates, normalised to internal control gene GUSB. Data is reported as 2^{-ddCt} value. ABCG2 gene expression rises over the course of dasatinib dose escalation, with expression peaking in the 15 nM Das intermediate, however with increasing dasatinib exposure, ABCG2 expression significantly falls. No significant changes were observed in ABCB1 expression over the course of dasatinib exposure. Bars indicate mean of independent experiments performed in triplicate; error bars indicate $2^{-ddCt\ -/+\ SD}$. Unequal variances t-test was performed between samples; significance is denoted by (*) for $p<0.05$, (**) for $p<0.01$, (***) for $p<0.001$.
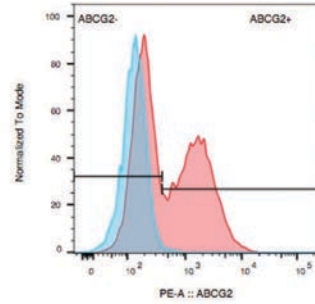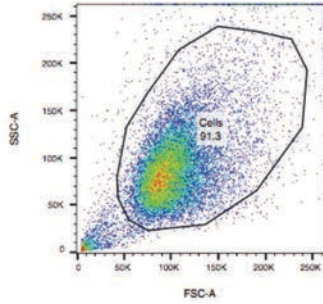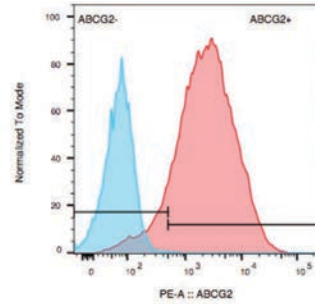
a)

b)

K562 DMSO

K562 2 nM Das

K562 3.5 nM Das
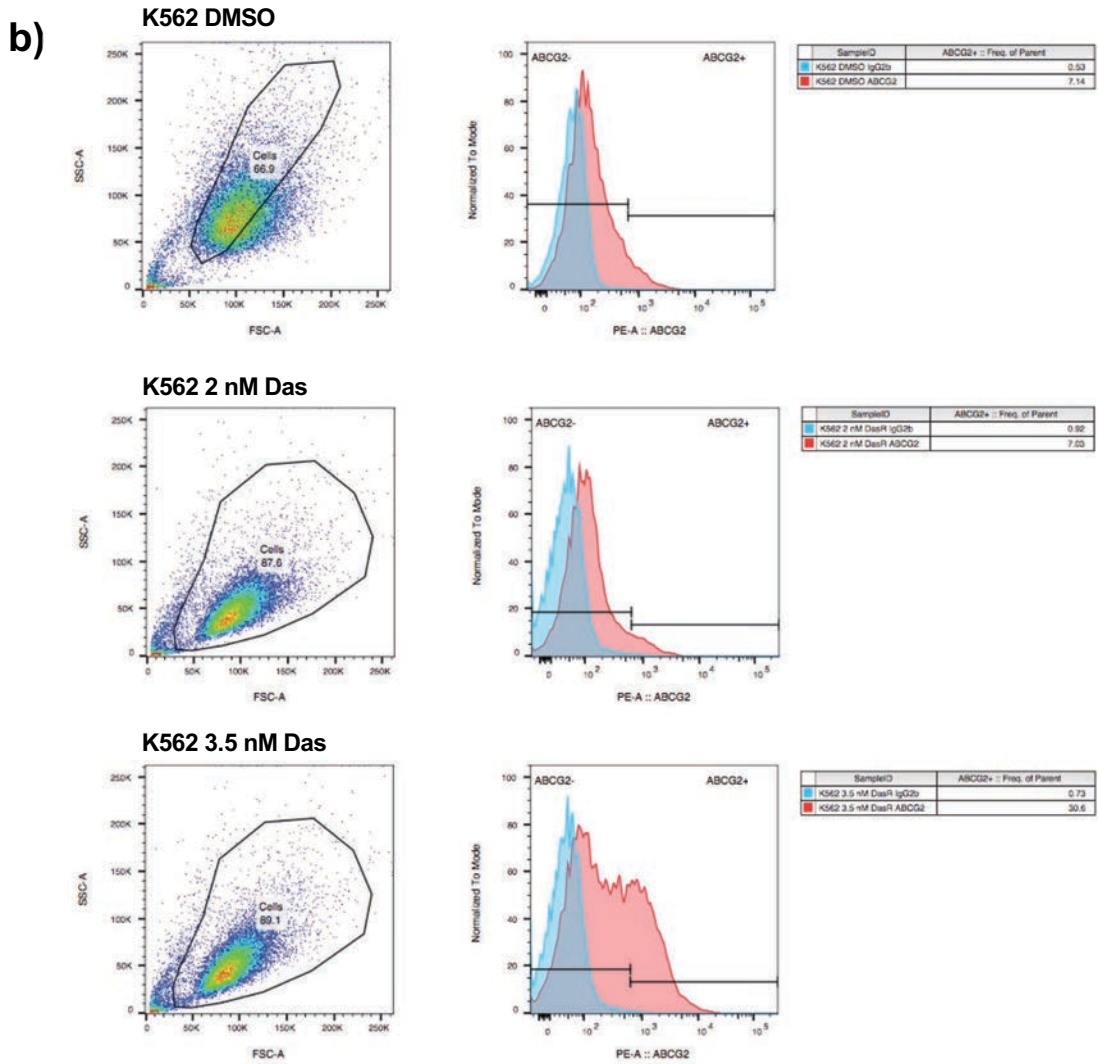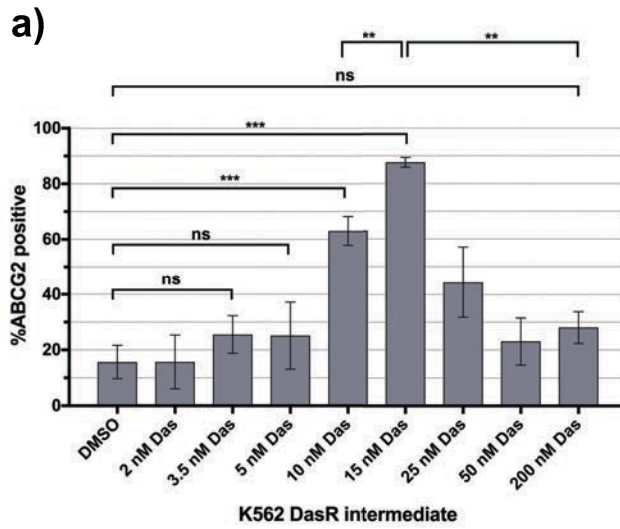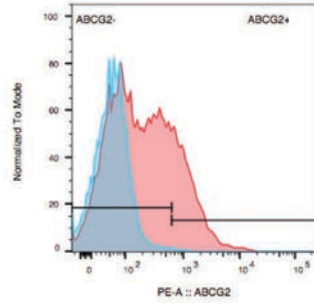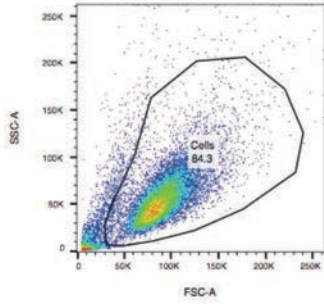
K562 5 nM Das

SampleID	ABCG2+ :: Freq. of Parent
K562 5 nM DasR IgG2b	1.01
K562 5 nM DasR ABCG2	23.4

K562 10 nM Das

SampleID	ABCG2+ :: Freq. of Parent
K562 10 nM DasR IgG2b	1.82
K562 10 nM Das ABCG2	50.3

K562 15 nM Das
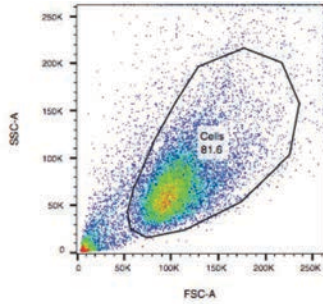
SampleID	ABCG2+ :: Freq. of Parent
K562 15 nM DasR IgG2b	0.34
K562 15 nM DasR ABCG2	90.3

K562 25 nM Das
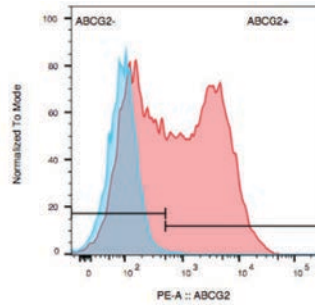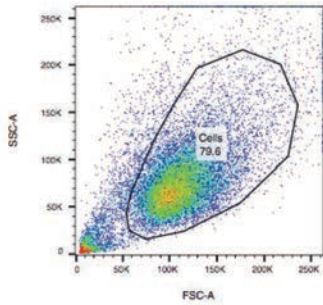
SampleID	ABCG2+ :: Freq. of Parent
K562 25 nM DasR IgG2b	0.88
K562 25 nM DasR ABCG2	55.9
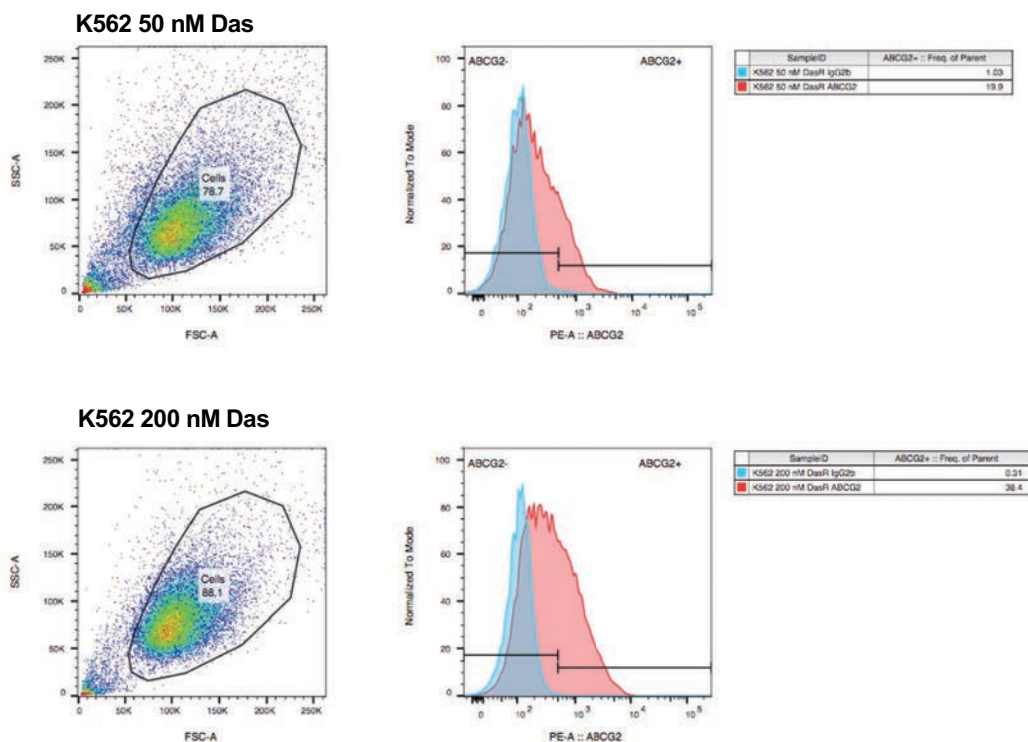
Figure 5.3: a) Flow cytometry results for ABCG2 cell surface expression indicate the protein expression of ABCG2 transiently increasing, correlating with RT-qPCR data. Again, ABCG2 expression rises, peaking in the 15 nM Das intermediate, before significantly falling with ongoing dasatinib escalation. Bars represent mean of at least three independent experiments, error bars denote SEM. Unequal variances t-test was performed between dose escalation intermediates; significance is denoted by (*) for p<0.05, (**) for p<0.01, (***) for p<0.001. b) Representative flow cytometry data of ABCG2 cell surface expression. Dot plots were gated for live cells based on forward/side scatter. Grey peak in ABCG2 histogram represents isotype control IgG2b; red peak is ABCG2 antibody stained.
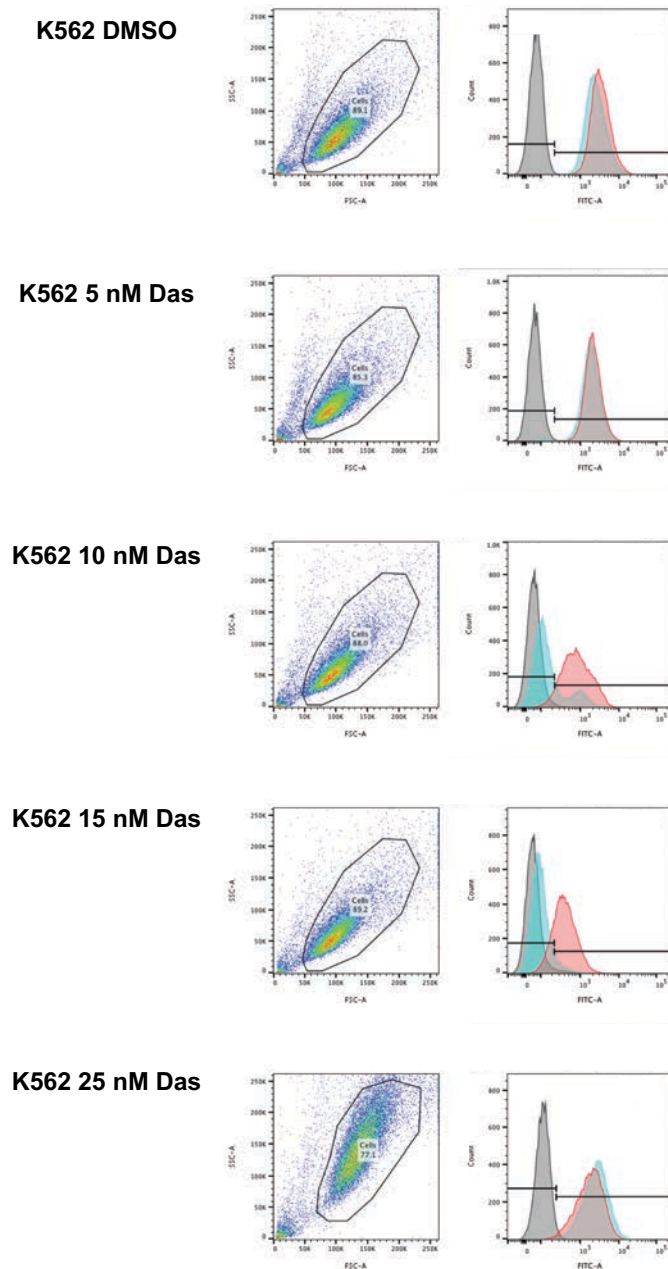
Figure 5.4: BODIPY-prazosin efflux assay in selected K562 DasR dose escalation intermediates demonstrate the functionality of the ABCG2 transporter in the 10 and 15 nM Das cells, but not before or after these intermediates. FITC fluorescence (blue peak) is indicative of BODIPY-prazosin retention, demonstrating a lack of transporter function when gated against unstained control (grey peak). Non-staining in 10 and 15 nM Das intermediate samples demonstrate transporter functionality. Addition of 500 nM Ko143 (red peak) resulted in retention of BODIPY-prazosin, indicating this dosage of Ko143 was sufficient for ABCG2 inhibition.
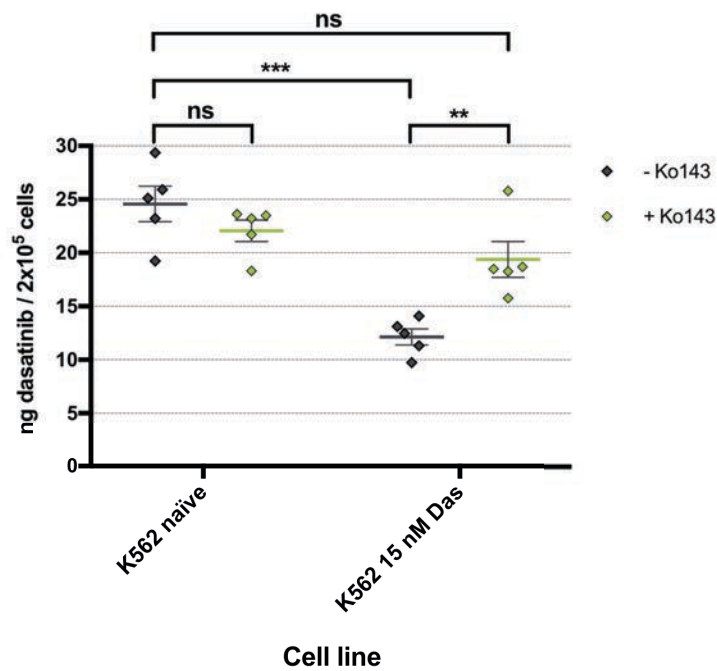
Figure 5.5: Dasatinib intracellular uptake and retention (IUR) assay data for the K562 DasR 15 nM Das intermediate, with drug naïve control. Results demonstrate that the K562 15 nM Das intermediate, which overexpresses ABCG2, has significantly lower dasatinib retention than the naïve K562 line from which it was derived. However, the addition of 500 nM Ko143 significantly increased the retention of dasatinib in the 15 nM Das intermediate. Lines represent the mean of 5 replicate experiments and dots represent the data from individual replicates; error bars indicate SEM. Unequal variances t-test was performed between dose escalation intermediates; significance is denoted by (ns) for $p > 0.05$, (**) for $p < 0.01$, (***) for $p < 0.001$.
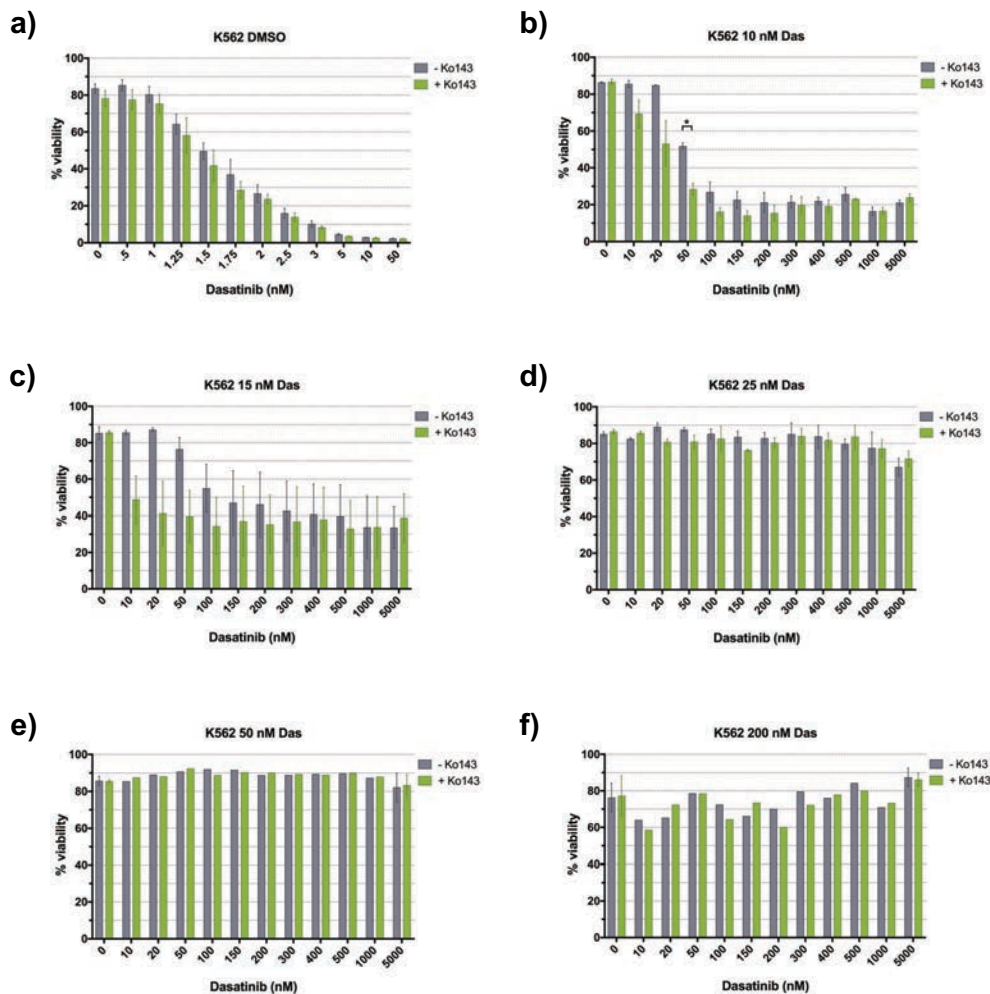
Figure 5.6: Dasatinib-induced cytoxicity data for K562 DasR dose escalation intermediates: b) 10 nM, c) 15 nM, d) 25 nM, e) 50 nM, f) 200 nM, and a) DMSO control. Experiments were performed in the presence (green bars) and absence (grey bars) of the ABCG2 inhibitor, Ko143. In the 10 nM and 15 nM intermediates, addition of Ko143 lowered cell viability in the presence of dasatinib at most concentrations of dasatinib, although this only reached significance in a single dasatinib concentration. No significant differences were observed with the addition of Ko143 in the 25, 50 or 200 nM Das lines, which remained viable regardless of the dasatinib or Ko143 dosage. Addition of Ko143 to K562 DMSO control line did not significantly affect cell viability. Data for the K562 DMSO, 10 and 15 nM Das lines represent the mean of three independent replicate experiments; error bars represent SEM. In the K562 25, 50 and 200 nM Das lines, it was clear that cell viability was not affected by dasatinib exposure, and experiments were terminated after two replicates. Unequal variances t-test was performed between -/+ Ko143 samples; significance is denoted by (*) for p<0.05.

a)

b)

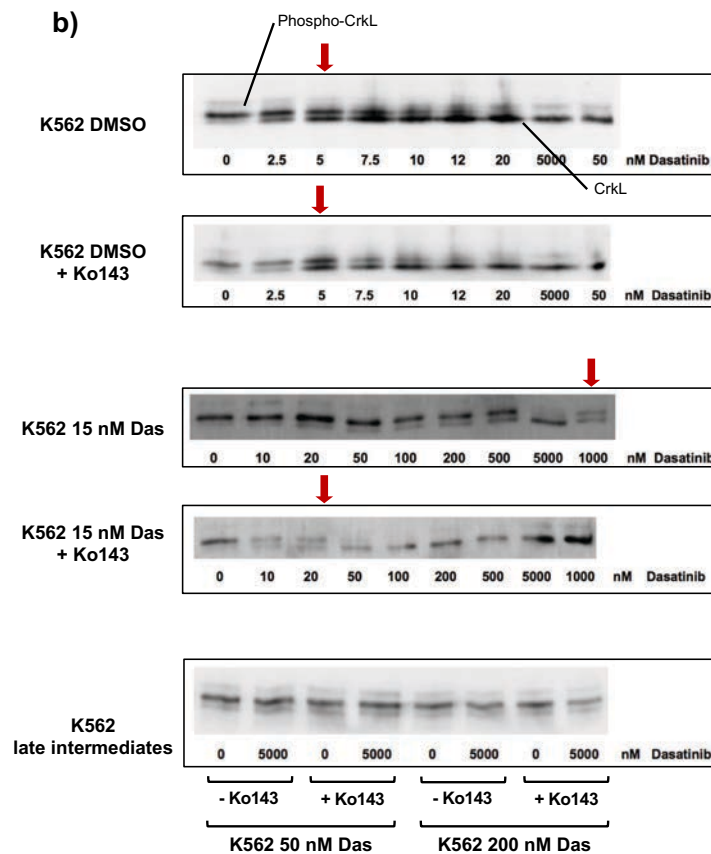Figure 5.7: a) Dasatinib IC50 of selected K562 DasR dose escalation intermediates, in the presence of ABCG2 inhibitor Ko143. Addition of Ko143 significantly lowered the dasatinib IC50 in the 10 and 15 nM DasR intermediates, demonstrating the contribution of ABCG2 to acquired dasatinib resistance. Interestingly, the Ko143 also significantly lowered the IC50[Das]

in the 3.5 nM Das intermediate, which only exhibited marginal ABCG2 expression. No effect of Ko143 was observed in the 25, 50 and 200 nM DasR lines, in which an $IC50^{Das}$ could not be obtained ($IC50^{Das}$ > 5000 nM). Bars represent the mean of at least three independent experiments, with diamonds denoting IC50 calculated from individual replicates; error bars represent SEM. Unequal variances t-test was performed between -/+ Ko143 samples; significance is denoted by (ns) for $p > 0.05$, (*) for $p < 0.05$, (**) for $p < 0.01$, (***) for $p < 0.001$. b) Representative dasatinib IC50 western blotting. Samples are selected K562 DasR dose escalation intermediates; red arrows indicate the approximate point of 50% inhibition. In the 50 and 200 nM Das lines, no concentration of dasatinib was able to inhibit Bcr-Abl activity, whether in the presence of absence of Ko143, demonstrating that ABCG2 was not required for dasatinib resistance in these cell lines.
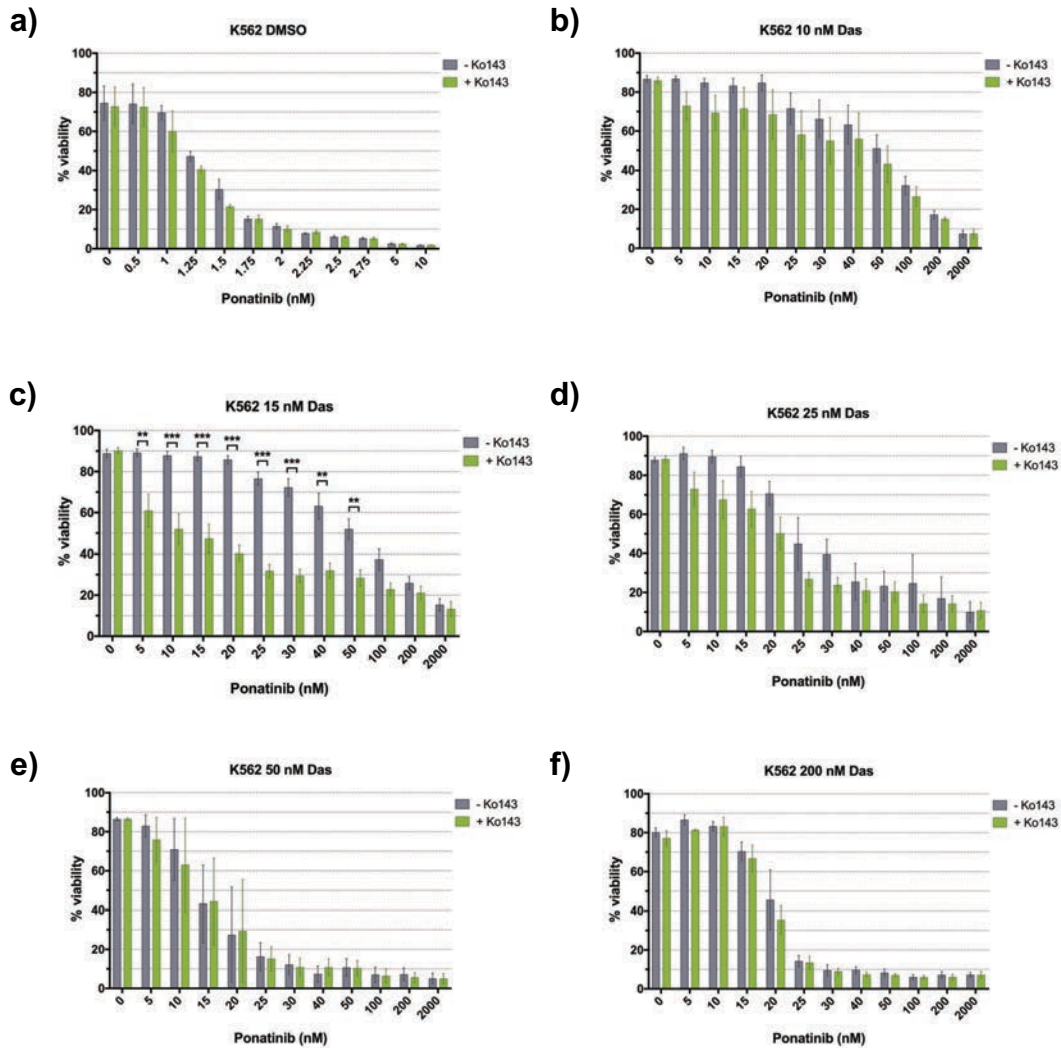
Figure 5.8: Ponatinib-induced cytoxicity data for K562 DasR dose escalation intermediates: b) 10 nM, c) 15 nM, d) 25 nM, e) 50 nM, f) 200 nM, and a) DMSO control. Experiments were performed in the presence (green bars) and absence (grey bars) of the ABCG2 inhibitor, Ko143. In the 15 nM intermediate, addition of Ko143 significantly lowered cell viability at most concentrations of dasatinib, demonstrating the key role of ABCG2 in ponatinib cross-resistance. No significant differences were observed with the addition of Ko143 in the 25, 50 or 200 nM Das lines, No significant differences were observed with the addition of Ko143 in the 25, 50 or 200 nM Das lines, where ponatinib was still effective at inducing cytoxicity. Addition of Ko143 to K562 DMSO control line did not significantly affect cell viability. Data represent the mean of at least three independent replicate experiments; error bars represent SEM. Unequal variances t-test was performed between -/+ Ko143 samples; significance is denoted by (*) for p<0.05, (**) for p<0.01, (***) for p<0.001.
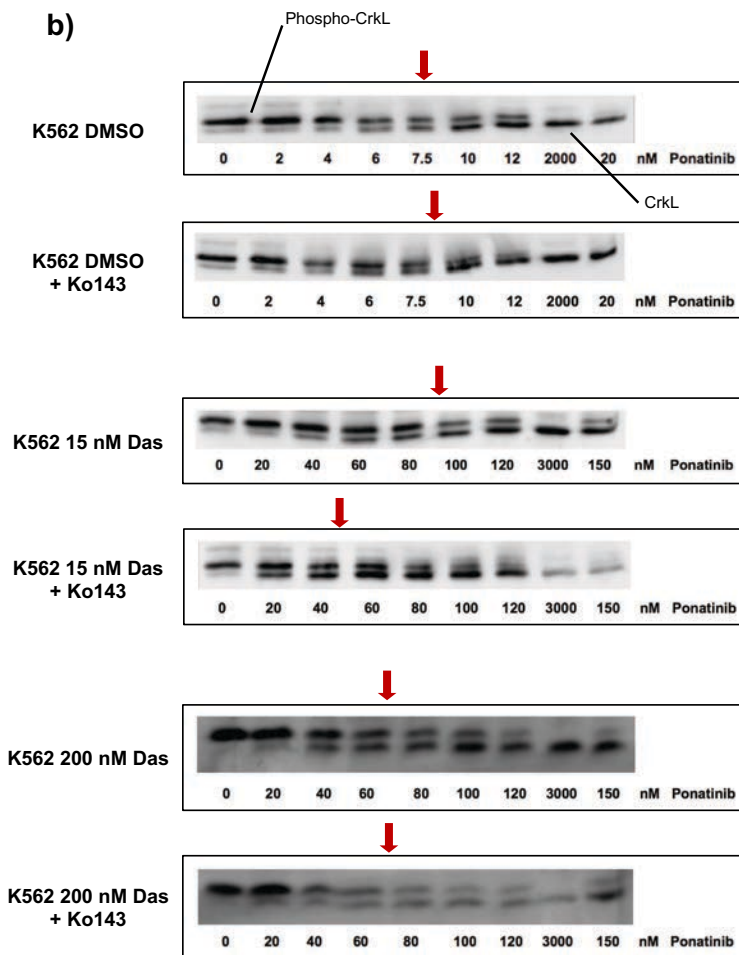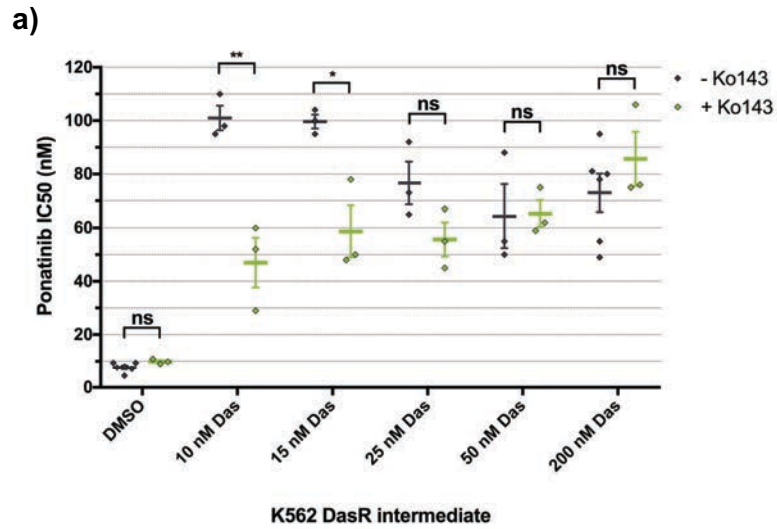
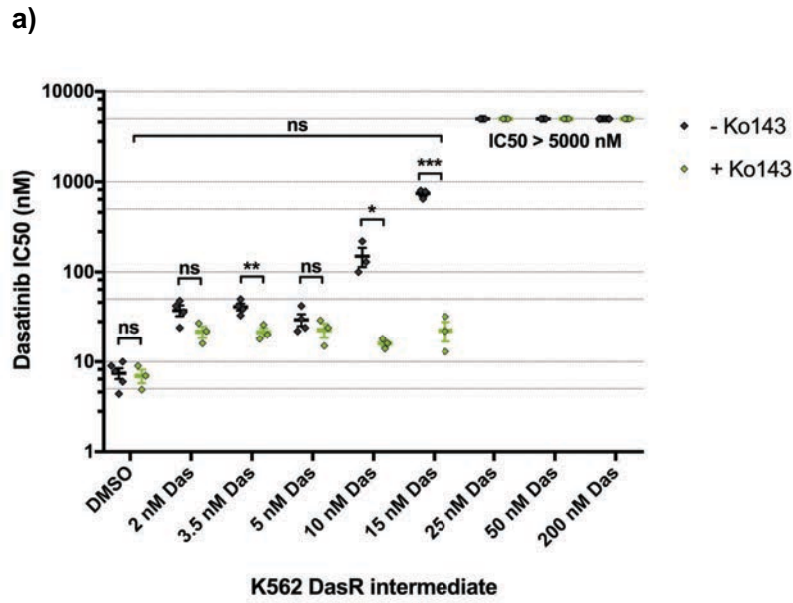Figure 5.9: a) Summary data of ponatinib IC50 of selected K562 DasR dose escalation intermediates, in the presence of ABCG2 inhibitor Ko143. Addition of Ko143 significantly lowered the ponatinib IC50 in the 10 and 15 nM DasR intermediates, demonstrating the

contribution of ABCG2 to lowered ponatinib sensitivity. Addition of Ko143 lowered ponatinib IC50 in the 25 nM Das intermediate, although this did not reach significance. No significant differences were observed in the presence of Ko143 in the 50 and 200 nM DasR lines. Data represent the mean of at least three independent replicate experiments; error bars represent SEM. Unequal variances t-test was performed between -/+ Ko143 samples; significance is denoted by (n.s.) for p>0.05, (*) for p<0.05, (**) for p<0.01. b) Representative ponatinib IC50 western blotting. Samples are selected K562 DasR dose escalation intermediates; red arrows indicate the approximate point of 50% inhibition.

6 Discussion

6.1 TKI exposure and the emergence of TKI resistance mechanisms

The selective pressure of TKI exposure in CML results in the emergence of leukaemic cells with TKI resistant characteristics as the clonally dominant population. This effect was first identified in CML patients who became resistant to imatinib, with researchers identifying amplification and/or mutation of the *BCR-ABL1* gene and protein as resistance mechanisms (146). This was subsequently replicated by *in vitro* models of treatment resistant CML (144). While some of these cell line models have identified multiple resistance mechanisms fluctuating in an evolving cell population (182, 200), the majority of studies identify a single TKI resistance mechanism as causative of treatment resistance. Often, this cause of resistance is identified as a Bcr-Abl kinase domain mutation, *BCR-ABL1* overexpression, or increased efflux transporter expression, with each resistance mechanism observed in the absence of another. This also reflects what is generally observed in clinical studies; the T315I mutation is frequently described in patients as solely causative of dasatinib resistance (285). However, this may also be an experimental artefact, due to the approach with which patient and cell line studies are undertaken. Studies of TKI resistant patients typically investigate resistance mechanisms following the detection of TKI failure, where the leukaemic cell population has already expanded when symptoms re-emerge or leukaemic cell presence is detected by routine blood examination. While this 'snapshot' approach is necessitated for practical reasons , there is a lack of understanding of how and why complete elimination of the leukaemic cell population does not occur; it is possible, if not likely, that undetected resistance mechanisms are present in these circumstances, allowing repopulation of the leukaemic cells. Similarly, the majority of *in vitro* cell line model analyses of TKI resistance have been performed only following long-term drug treatment, with samples taken only at a single point in time (145, 178, 243, 286, 287). Rarely have studies investigated the dynamics of leukaemic cells during the critical period at the induction of drug resistance, and thus documentation of the fluctuations of resistance mechanisms in leukaemic cell populations is lacking. Indeed, patient studies have demonstrated that high levels of *BCR-ABL1* expression predict and predispose cells to the gain of alternate imatinib resistance mechanisms (147, 182). Furthermore, previous performed analyses of TKI resistance mechanisms is often not exploratory, but targeted, to already known and expected resistance mechanisms (144, 200, 288). Again, these studies likely neglect many of the cellular changes occurring over prolonged

TKI treatment. The project presented here has detailed the fluctuations in the K562 DasR leukaemic cell population occurring over months of incrementally increasing dasatinib exposure. Three distinct TKI resistance mechanisms were identified and validated; overexpression of Bcr-Abl, upregulation of the ABCG2 membrane transporter, and mutation of the Bcr-Abl gatekeeper residue, T315I. While each resistance mechanism has been independently observed in isolation by other studies, to date, no other study has observed their sequential emergence, thus this project serves an insight to the selective pressure of TKI exposure and how it influences the evolution of the malignancy. The observed fluctuations in the cell population can be explained by a model of selection by which leukaemic cells with the most energy efficient TKI resistance mechanisms are selected, a theory for which evidence has been provided by this project.

6.2 Factors influencing the selection of dasatinib resistant leukaemic cell populations

The transition from Bcr-Abl overexpression, to increased ABCG2 expression, and finally development of the T315I mutation, the principal TKI resistance mechanism in the K562 DasR cell line, is reflective of the selective forces contributed by dasatinib. Models of TKI resistance have previously been generated and examined; the different methodologies used to generate TKI resistance have resulted in a different spectrum of observed and identified resistance mechanisms, which can be compared with our model.

The overexpression of the *BCR-ABL1* gene and protein product is a well characterised mechanism of resistance to TKI treatment (146, 147, 149, 205, 207). In the K562 DasR cell line model, *BCR-ABL1* overexpression was identified when our laboratory first described *in vitro* TKI resistance mechanisms (205); in the current study it was demonstrated that genomic amplification is causative of gene transcript overexpression. *BCR-ABL1* overexpression has been noted in other cell line models of TKI resistance (144, 207). However, *BCR-ABL1* amplification is not universally identified as a resistance mechanism, even with other K562 models; a K562 line generated by Okabe *et al* resistant to ~15 nM dasatinib observed lower Bcr-Abl levels in resistant lines (289, 290). Therefore, it is hypothesised that the level of Bcr-Abl expression in leukaemic cells is maintained with random, stochastic variance, and does

not consistently rise. Instead, it is selected for upon prolonged dasatinib exposure. Indeed, this is the case for resistance to other TKIs. A study by our laboratory generating subsequent ponatinib resistance from the K562 200 nM DasR cell line described here, demonstrated a continuing rise in *BCR-ABL1* gene expression upon increasing ponatinib exposure (288, 291). However, in this study of dasatinib resistance, the loss of *BCR-ABL1* expression was also identified, concurrent with the gain of the ABCG2 overexpression (Figure 6.1). The loss of *BCR-ABL1* expression with TKI treatment is normally indicative of lowered patient disease burden and the death of leukaemic cells, however, in this case, the loss of *BCR-ABL1* expression was not concomitant with cell death. Instead, the reductions in *BCR-ABL1* expression were associated with a loss of genomic *BCR-ABL1* in the bulk population, which was likely due to expansion of cells with lower *BCR-ABL1* copy numbers. This population flux was presumably driven by the selective advantage of ABCG2 overexpressing cells, however, the unexpected reduction in *BCR-ABL1* expression suggests that with the gain of an alternate resistance mechanism, the high level expression of *BCR-ABL1* does not confer a selective advantage, and is instead a cellular burden driving deselection.

With ongoing dasatinib dose escalation, fluctuations in the expression of resistance mechanisms are again observed, with the loss of ABCG2 expression following the gain of the T315I mutation. The loss of ABC transporter expression with prolonged TKI exposure has previously been described (200). Indeed, a similar effect has been observed by our laboratory, whereby initial TKI resistance was driven by ABC transporter expression, however, expression was lost with the gain of alternate resistance mechanisms and prolonged TKI escalation (182). In this model, the de-selection of *BCR-ABL1* and ABCG2 overexpressing cells concurrent with the gain of an alternate resistance mechanism suggests that there is a cellular expenditure associated with the expression of these resistance mechanisms. Indeed, there is a significant energy cost involved in the synthesis of a gene transcript and protein. In order for leukaemic cells to overcome TKI exposure by Bcr-Abl expression alone, a full length protein must be synthesised to 'mop up' each TKI molecule, making it a highly inefficient process. Comparatively, TKI resistance mediated by ABC transporter expression is more energy efficient; although the ABC transporters are ATP-dependent, following protein synthesis, a single transporter protein can exclude many TKI molecules from the cell. Conversely, gain of a mutation in the Bcr-Abl kinase domain, such as T315I, has no associated energy expenditure,

while rendering the TKI completely ineffective and providing the leukaemic cell a clear selective advantage, in the presence of TKI. However, this begs the question as to why T315I is not strongly selected for earlier on during dasatinib dose escalation. The lack of early emergence of kinase domain mutations during dasatinib dose escalation is likely due to decreased kinase efficiency due to T315I, which would then only be selected for in the presence of a TKI. Withdrawal of dasatinib from the 200 nM Das cell line, over several passages, has been demonstrated to coincide with the loss of T315I mutant expression (unpublished data). Furthermore, in CML patients T315I is rarely identified in the absence of prior TKI exposure, and the gatekeeper residue is highly conserved across patients and protein species alike (159). Thus, it seems that it is only under the selective pressure of high dasatinib concentrations, that T315I consistently emerges.

6.3 Therapeutic implications and future prospects

There are several therapeutic and scientific implications of the thesis here presented. This research aimed to investigate the evolution of resistance to TKI therapy in a cell line model of CML, utilising exploratory and functional methods to identify the mechanisms of resistance. The findings suggest that TKI resistance is not static, but dynamic, with the alterations in leukaemic cells possibly exposing them to therapeutic intervention. This identified several mechanisms of resistance to the TKI dasatinib, namely: Bcr-Abl overexpression, the T315I mutation, and overexpression of ABCG2. Critically, the ABCG2 inhibitor Ko143 was able to sensitise leukaemic cells to dasatinib treatment. While Ko143 has not been translated clinically, ABC transporter inhibition using other drugs may provide a therapeutic avenue. The exploitation of the ABC transporter-inhibiting effect of certain TKIs may prove useful. Concurrent treatment with low doses of several TKIs may simultaneously block transporter mediated resistance, while effectively inhibiting Bcr-Abl. Similarly, early treatment with a T315I inhibitor may prevent the spontaneous development and selective emergence of the mutation. Concurrent TKI treatment may also limit the side effects of the individual TKIs, which are linked to patient trough plasma concentrations (292). However, currently available T315I inhibitors have severe side effects, and the efficacy and safety of this strategy remains to be explored.

This study marks the first time the transport of ponatinib by ABCG2 has been described. Ponatinib is currently indicated for treatment resistant Ph+ leukaemia, particularly following the detection of the T315I mutation. The tolerance of ponatinib by certain K562 DasR cells, conferred by the same resistance mechanisms, will likely result in a lack of efficacy of ponatinib salvage therapy. These observations presented here suggest that when available, patient leukaemic material be thoroughly examined for all known resistance mechanisms, such that ponatinib treatment efficacy may be predicted.

There is an ATP / GTP expenditure associated with certain mechanisms of drug resistance. TKI resistance mechanisms allows a selective advantage under TKI exposure, however, expression of the resistance mechanism may confer a disadvantage in the absence of TKI selective pressure. Thus, the addition and withdrawal of TKI results in fluctuations in cell population numbers and cellular traits. Studies have demonstrated that the intermittent use of chemotherapy cycles can allow repeated drug responses, and alleviates the strong selective pressure chemotherapy resistant mutations and mechanisms, which can occur over continuous treatment regimens (293). This also holds true for TKI treatment; if upon imatinib treatment withdrawal there is subsequent disease recurrence, patients typically respond to imatinib reintroduction (294, 295). Nevertheless, exactly how to manipulate the balance of leukaemic cell population, drug side effects, and the selective pressure towards TKI resistance, remains a case-by-case affair.

The project presented here has significantly added to the understanding of therapeutic resistance in the treatment of Ph+ leukaemia. Exploration of the TKI resistance mechanisms in a CML disease model highlighted the selective advantages conferred by leukaemic cell expression of Bcr-Abl, ABC efflux transport, and kinase domain mutations, and emphasised the complexity of their interactions. For the first time, the active transport of ponatinib by ABCG2 has been demonstrated. Furthermore, this study underlines the exploratory power of transcriptome sequencing for the determination of transitory cellular adaptations which occur during the accrual of TKI resistance. Overall the data presented here confirm the complex evolution of CML and support early interrogation of resistance mechanisms in order to eradicate leukaemic cells prior to disease progression.
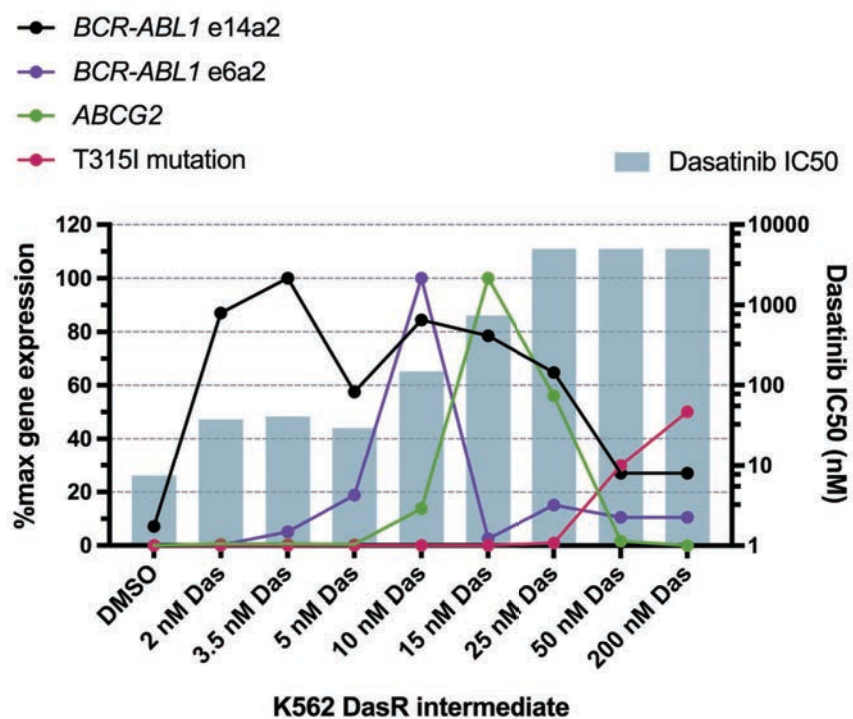
Figure 6.1: A composite graph of the TKI resistance mechanisms identified in the K526 DasR dose escalation intermediates, and their fluctuations over the course of increasing dasatinib exposure. Resistance mechanisms are shown on the left axis; *BCR-ABL1* e14a2 (black line), e6a2 (purple line), and *ABCG2* gene expression levels are plotted as a percentage of the maximal expressing lines, and the T315I mutation (red line) is shown as a percentage of *BCR-ABL1* transcripts. The dasatinib IC50 (blue bars), a marker of dasatinib resistance, is shown on the right axis. Data demonstrate the flux in the dominance of dasatinib resistant K562 populations, suggesting that *ABCG2* expression is a preferential resistance mechanism to *BCR-ABL1* overexpression, and the T315I mutation supplants the need for any other resistance mechanism.

7 Supplementary data

LENTIVIRAL EXPRESSION VECTOR CONSTRUCTION
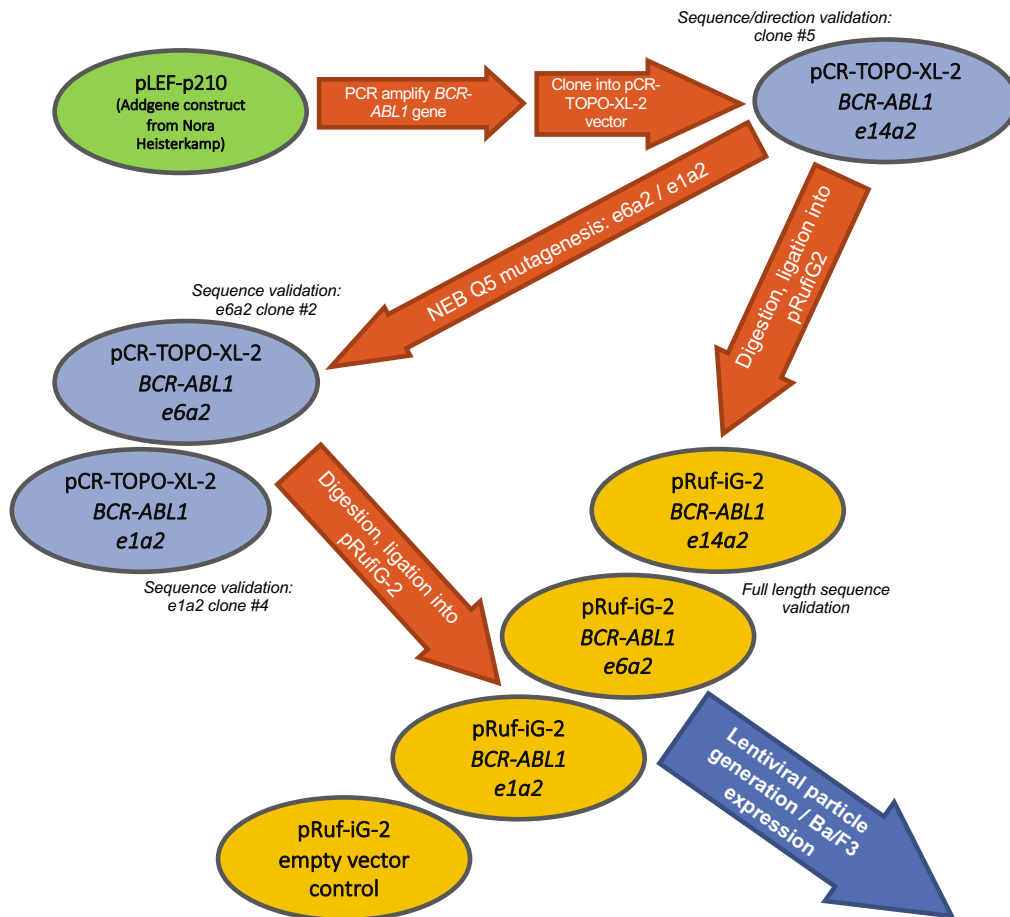
Figure S1: Flow diagram for the construction of the lentiviral expression vector for Ba/F3 transduction. A vector containing the *BCR-ABL1* e14a2 sequence (pLEF-p210) was purchased, and cloned into the pCR-XL-2-TOPO vector for site directed mutagenesis, to generate the e6a2 and e1a2 sequences. *BCR-ABL1* constructs were then cloned into the pRuf-iG2 vector for lentiviral transduction into the Ba/F3 line.

a)

```
        GST                    Thrombin
        ProLysSerAspLeuValProArgGlySer
5'  CCAAAATCGGATCTGGTTCCGCGTGGATCCGGGAATTCCCCGGGTCTAGA
                             BamHI   EcoRI        XbaI
        GGGCCCTATTCTATAGTGTCACCTAAATGCTAGAGCTCGCTGA  3'
                         SP6
```
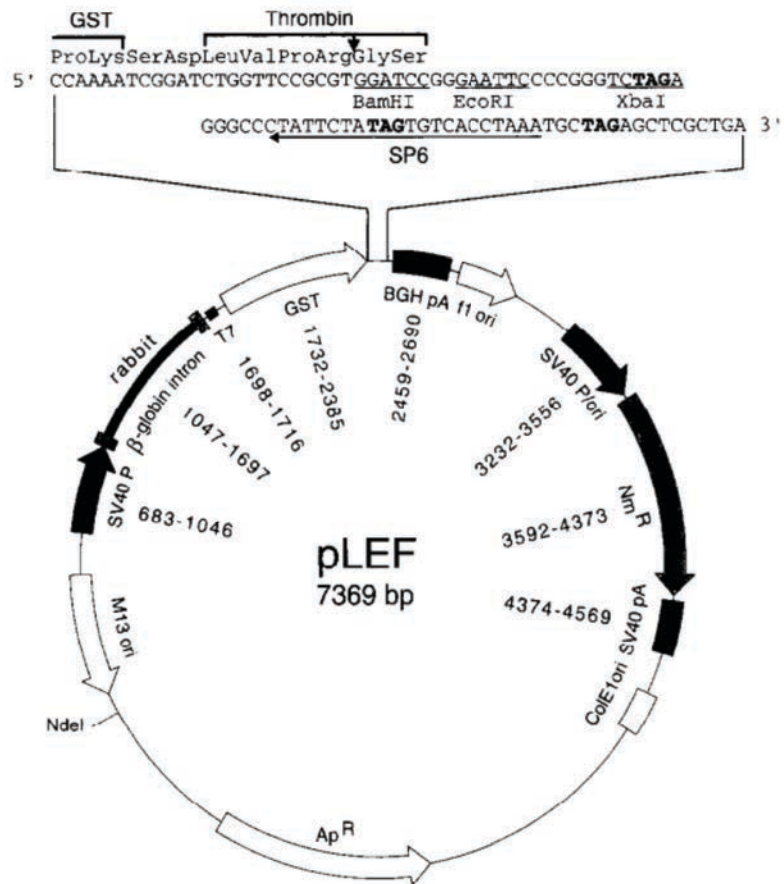
pLEF
7369 bp

b)
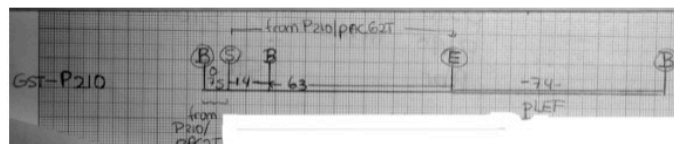
Figure S2: a) A diagram of the pLEF vector backbone previously generated by Rudert *et al* (296). This was used by Kweon *et al* for cloning and expression of *BCR-ABL1* constructs (225). b) A diagram of the pLEF-p210 vector purchased from Addgene. The *BCR-ABL1* sequence was inserted into the pLEF backbone via the 5' BamHI and 3' EcoRI cut sites. The diagram was kindly provided by Addgene depositor Professor Nora Heisterkamp.
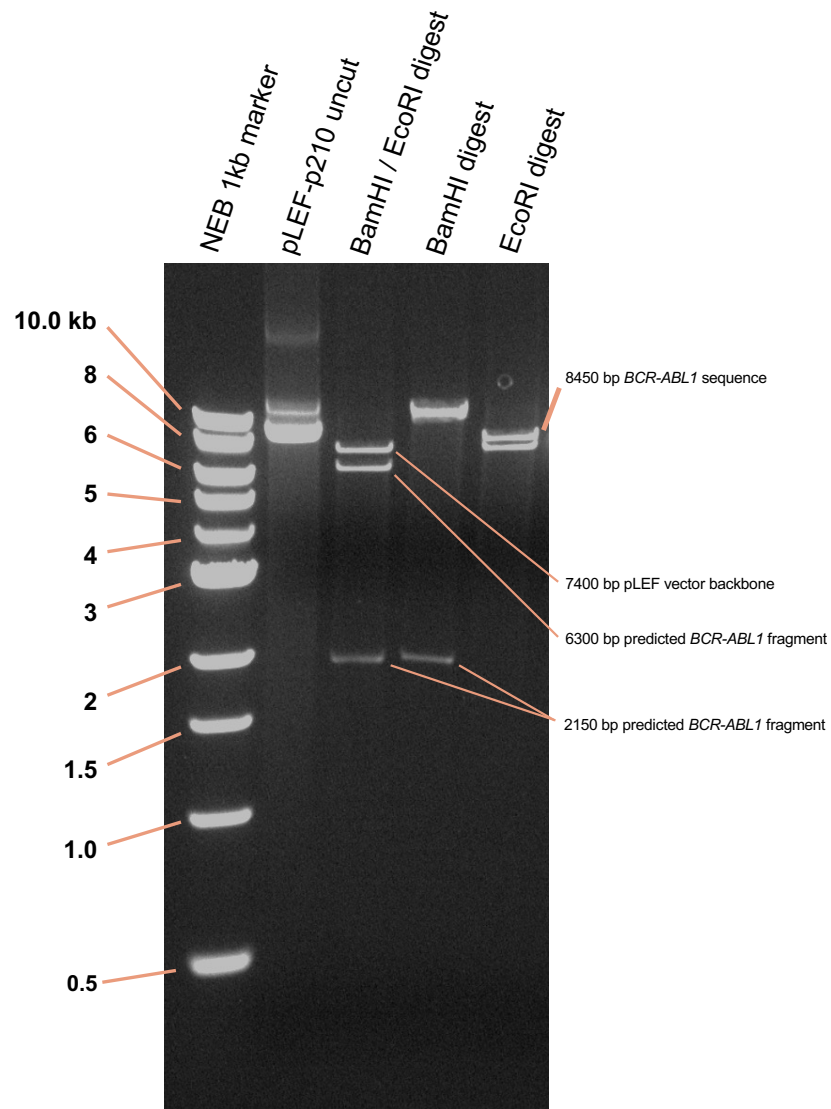
Figure S3: Gel electrophoresis of test digest of the ~15850 bp pLEF-p210 vector using the restriction enzymes BamHI and EcoRI. Double digest demonstrated the presence of a ~7400 bp band, indicative of the ~7400 bp pLEF plasmid backbone, as well as ~6300 and 2150 bp predicted bands from digest of *BCR-ABL1*.

a)
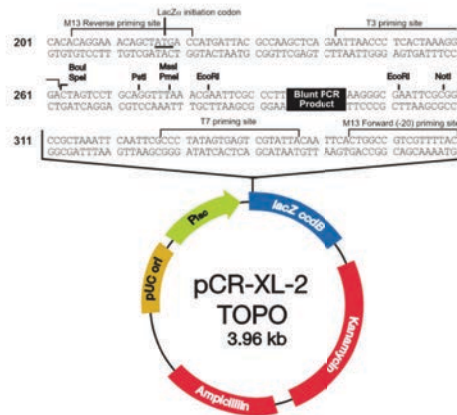
b)
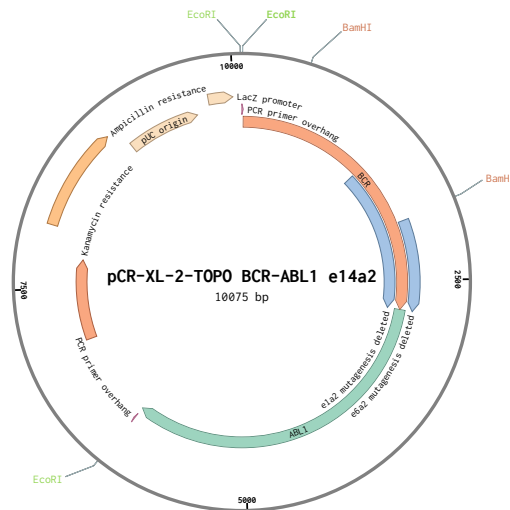
Figure S4: a) Diagram depicting the backbone of the pCR-XL-2-TOPO vector, which was used as an easily modifiable backbone for mutagenesis and plasmid expansion. Map was provided with TOPO-XL2 Complete Cloning Kit. b) The blunt end *BCR-ABL1* e14a2 (red and green) construct was cloned in using kit manufacturers' protocols. The blue regions indicate the sequences excised in e6a2 and e1a2 mutagenesis reactions. Plasmid map was made in the Benchling web application.
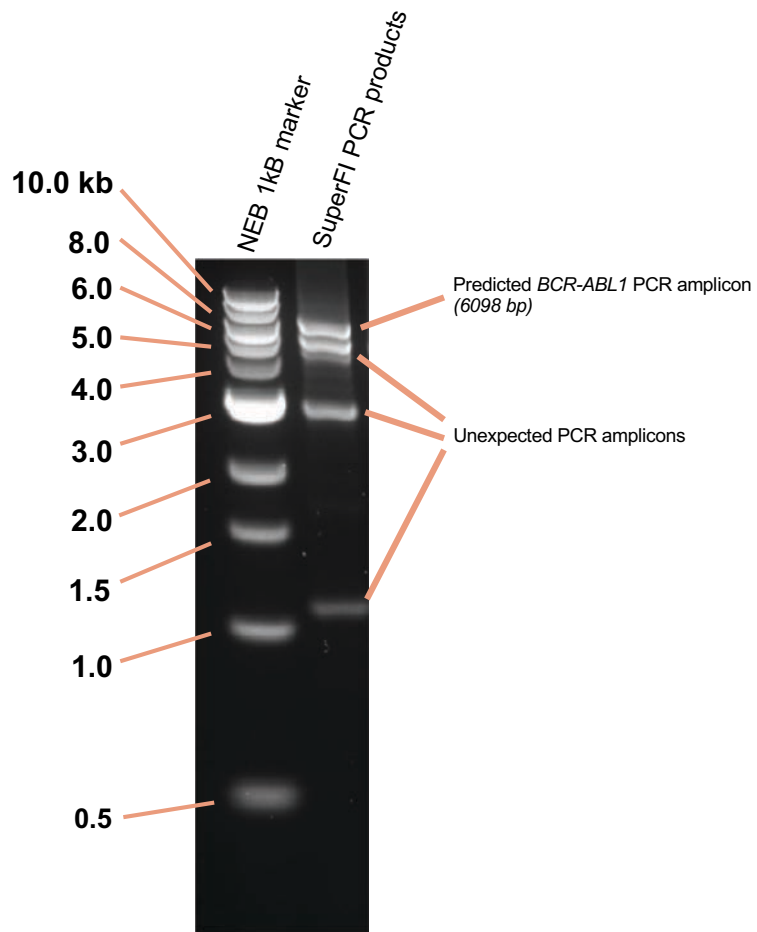
Figure S5: Using the TOPO XL-2 Complete Cloning Kit, the *BCR-ABL1* sequence was amplified from the pLEF-p210 vector. The predicted *BCR-ABL1* PCR amplicon was gel excised and column purified for cloning into the pCR-XL-2-TOPO vector.
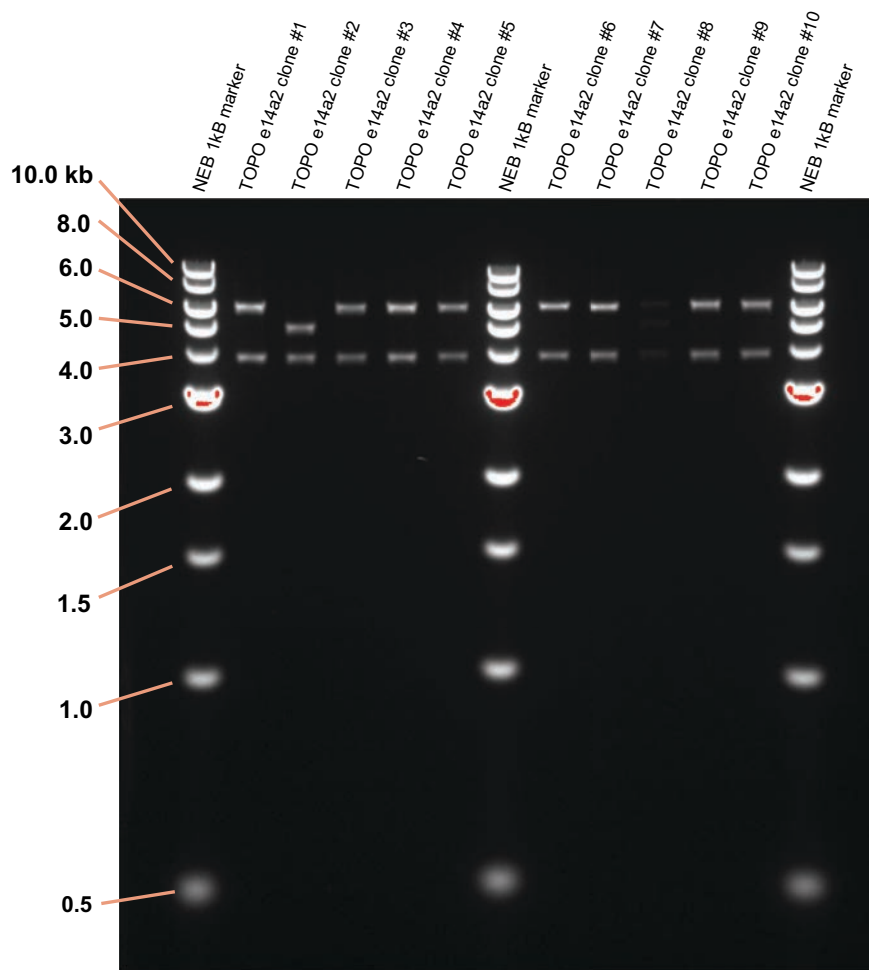
Figure S6: pCR-XL-2-TOPO vector with *BCR-ABL1* e14a2 insert was transformed into *E. coli*, and colonies were selected for plasmid miniprep. Digested with EcoRI, plasmids with the correctly sized insert were sequenced for the direction of the insert. Based on this, TOPO *BCR-ABL1* e14a2 clone #5 was fully sequenced for *BCR-ABL1*, and used as a template for mutagenesis reactions.
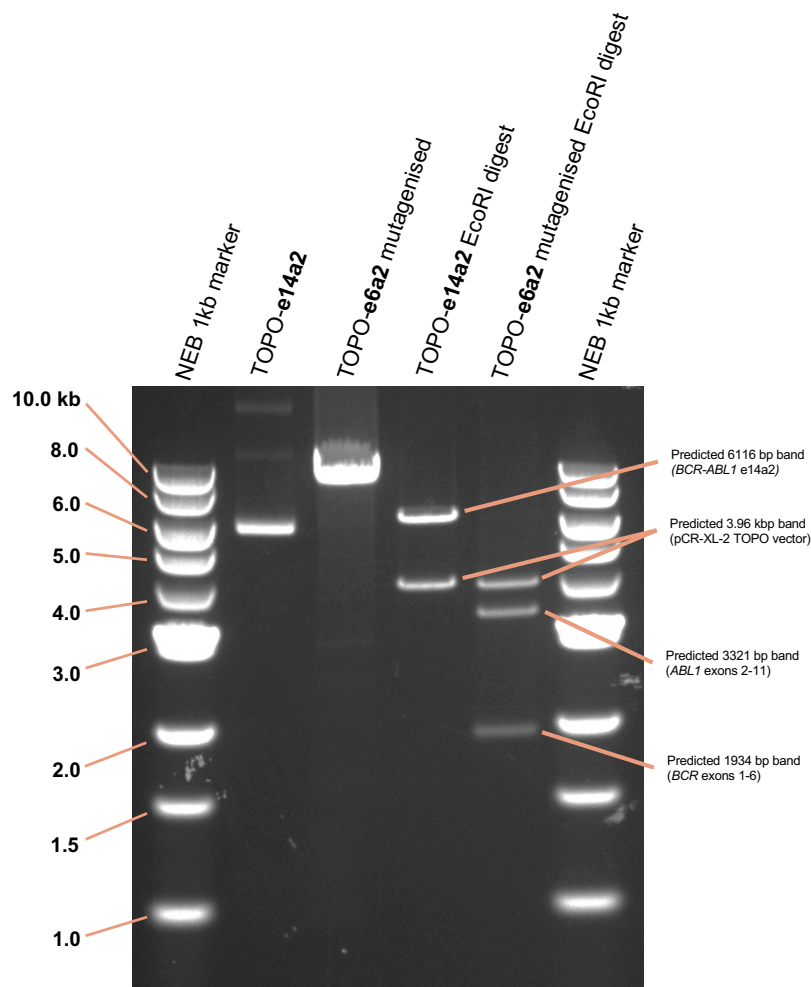
Figure S7: The *BCR-ABL1* e14a2 PCR amplified sequence was cloned into the 3.96 kb pCR-XL-2-TOPO vector for mutagenesis. The e6a2 mutagenised, linearised vector was electrophoresed alongside the original e14a2 construct, undigested (left) and digested using EcoRI (right). EcoRI cut sites lie on either side of the pCR-XL-2-TOPO PCR-product insert point, with EcoRI restriction digest releasing the *BCR-ABL1* e14a2 sequence (lane 4), and the ~1.9 kb and ~3.3 kb bands predicted following e6a2 mutagenesis (lane 5). The mutagenised and ligated plasmid was transformed into *E. coli*, and 10 colonies were selected for miniprep and validation.
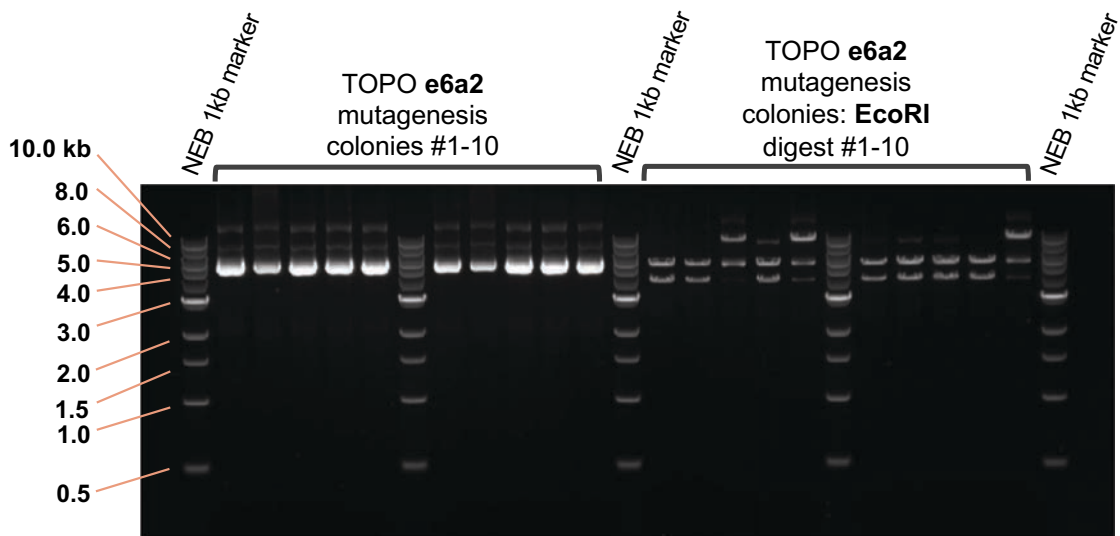
Figure S8: Colonies isolated following e6a2 mutagenesis and transformation into *E. coli* were expanded for miniprep plasmid extraction and purification, and digested using EcoRI to determine the size of the plasmid insert. Colonies #1, #2, #4, #6, #7, #8 and #9 were selected and sequenced over the *BCR-ABL1* breakpoint.
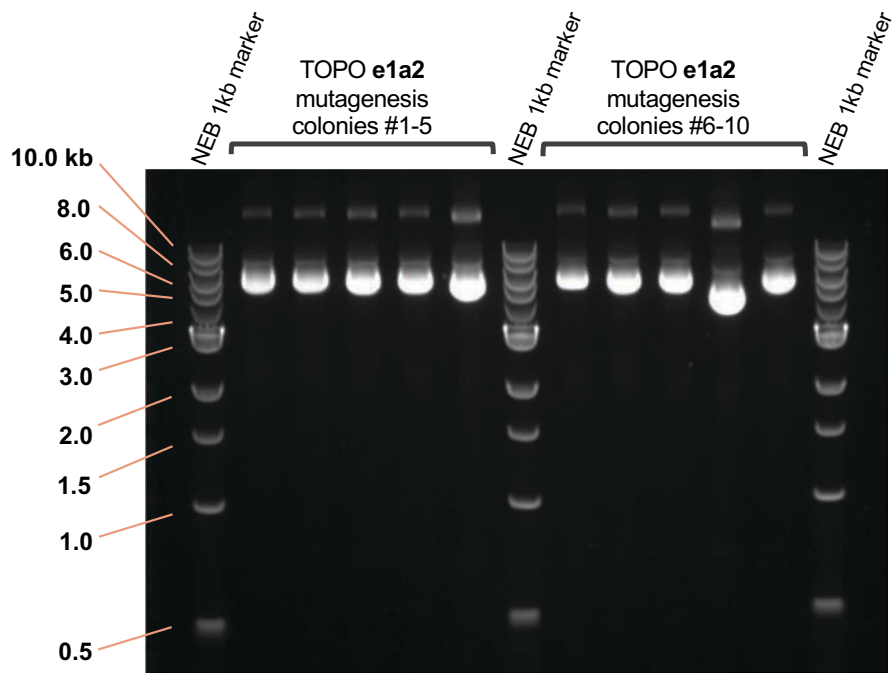
Figure S9: Colonies isolated following e1a2 mutagenesis and transformation into *E. coli* were expanded for miniprep plasmid extraction and purification to determine the size of the plasmid insert. All colonies except colony #9 were sequenced over the *BCR-ABL1* breakpoint.
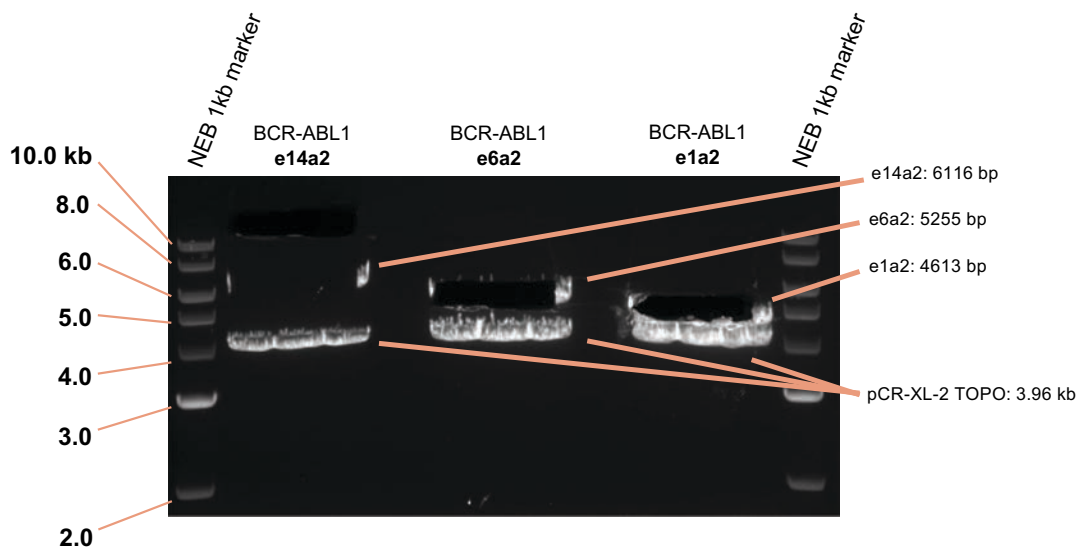
Figure S10: TOPO plasmids were digested with EcoRI and electrophoresed for band excision and gel purification of the *BCR-ABL1* insert sequences. Photo was taken following band excision to avoid UV damage of DNA sequences.
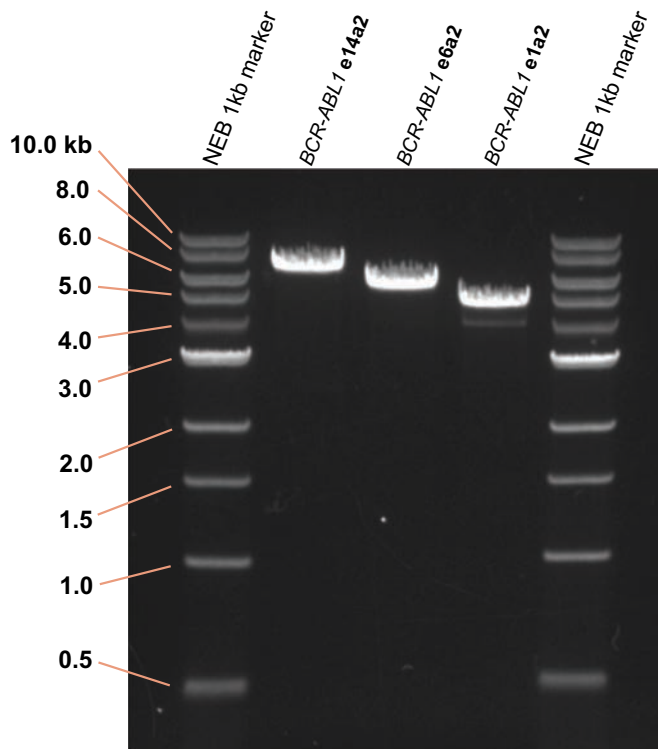
Figure S11: Gel purified *BCR-ABL1* e14a2, e6a2 and e1a2 sequences for cloning into pRuf-iG2 vector. A small amount of the pCR-XL-2-TOPO vector was found in the e1a2 product, however the impurity was low enough to continue with ligation into the pRuf-iG2 vector.
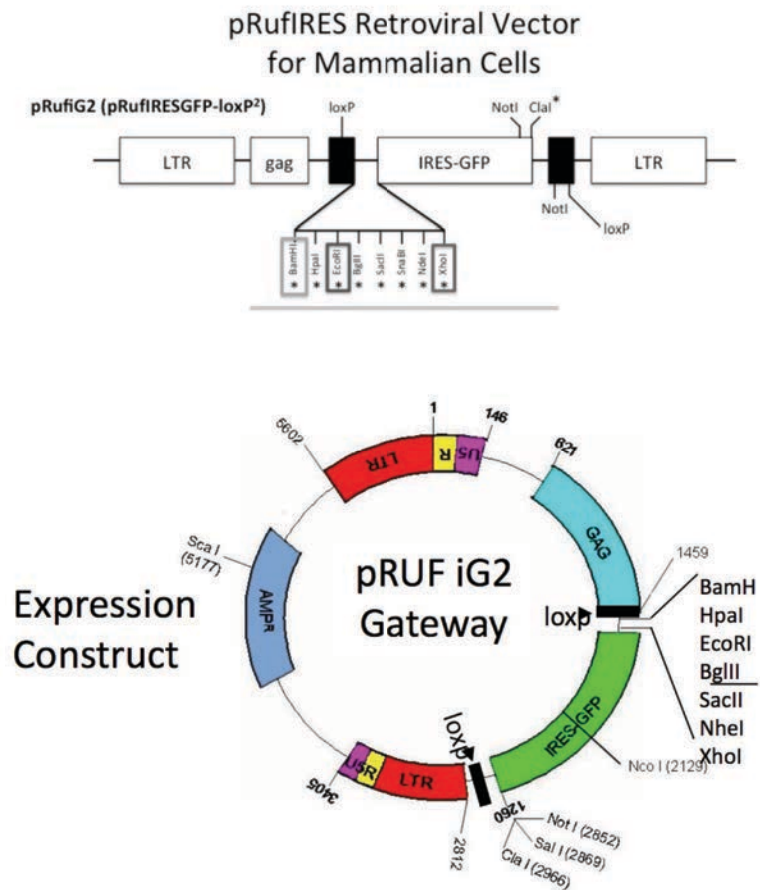
Figure S12: Diagram depicting the pRuf-iG2 vector used for lentiviral transduction of Ba/F3 cells. *BCR-ABL1* constructs were cloned into the multiple cloning site using the enzymes BamHI and EcoRI.
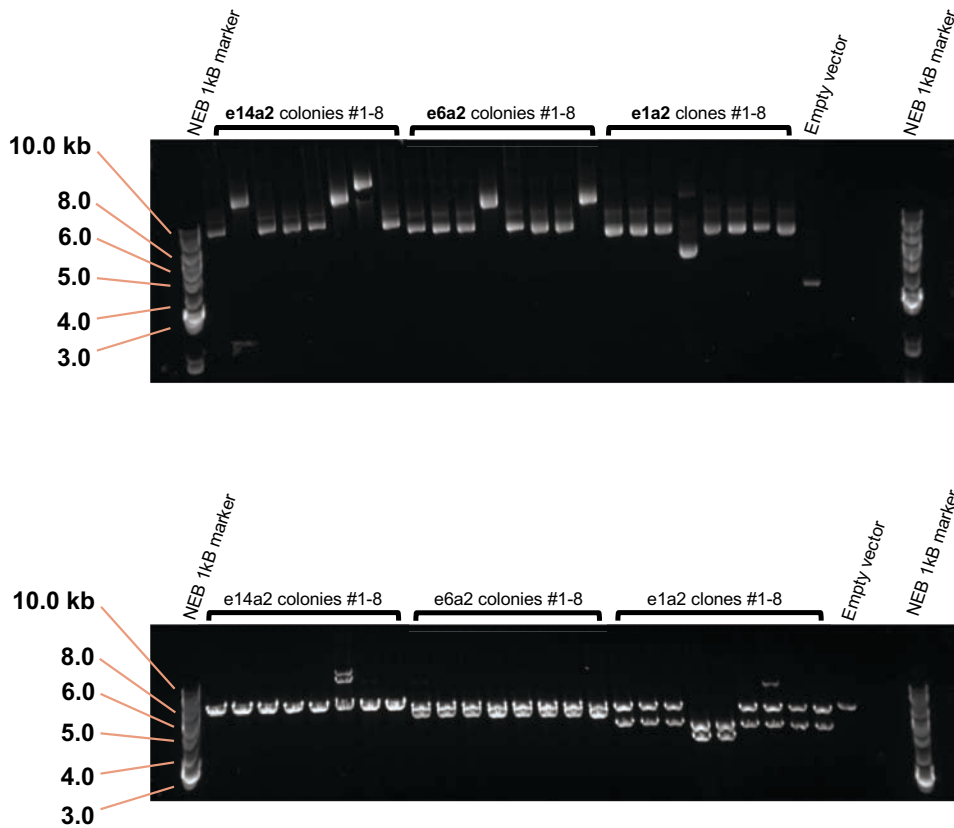
Figure S13: Following ligation of *BCR-ABL1* sequences into the pRuf-iG2 expression vector, plasmids were transformed into chemically competent *E. coli* DH5α under ampicillin selection. Eight colonies were picked for each construct for plasmid miniprep. Plasmid sizes were estimated by gel electrophoresis (upper gel). Restriction digest with EcoRI (lower gel) was used to determine the size of the ligated sequence, to exclude plasmids with incorrect insertion.

a)
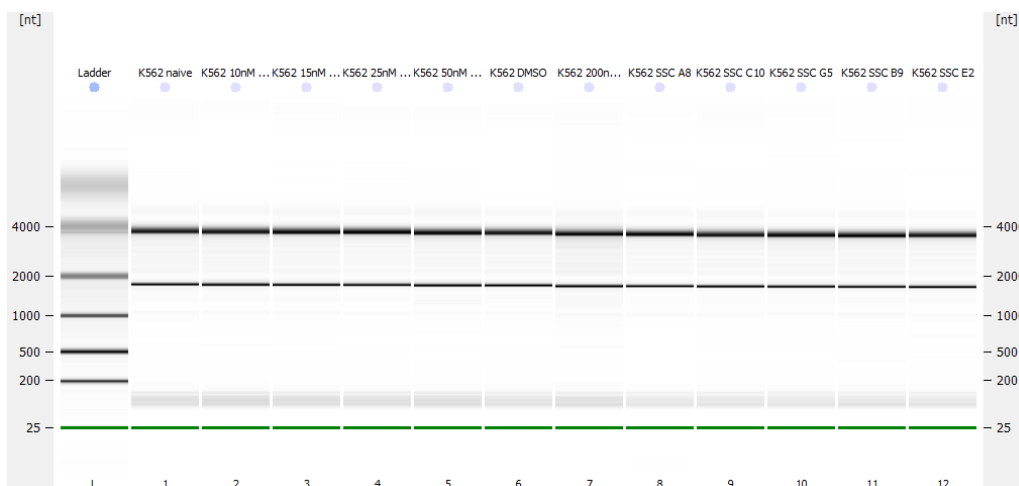
b)
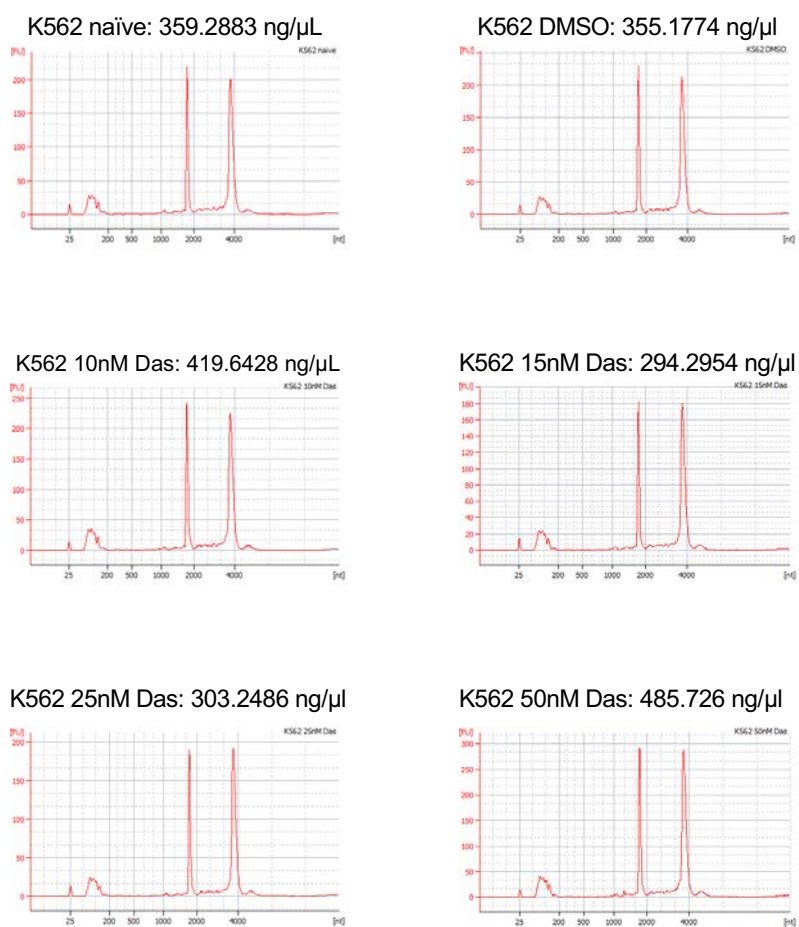
b) cont.
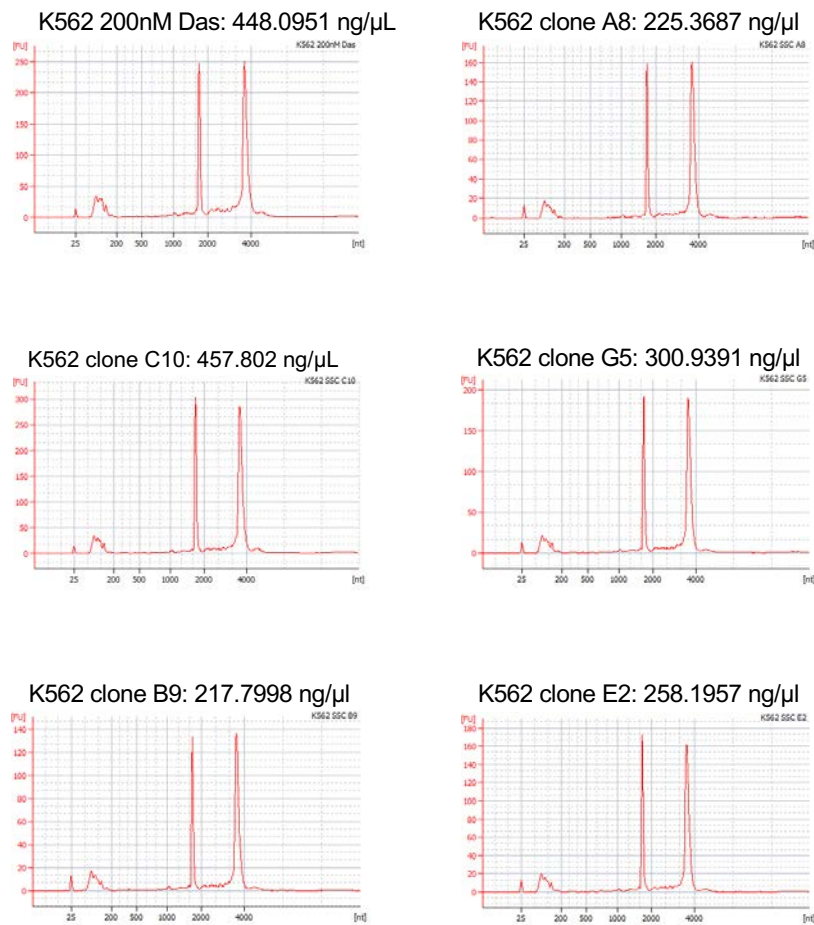
Figure S14: a) Bioanalyzer electrophoresis of RNA samples used for RNA sequencing experiments was analysed to generate b), which demonstrated the integrity and concentration of samples. The two larger peaks in each sample are indicative of ribosomal RNA, whereas the smaller peak at ~150 nucleotides indicates fragmented mRNA used for sequencing.

% Reads Identified (PF) vs Index Number

Lane 1

b)
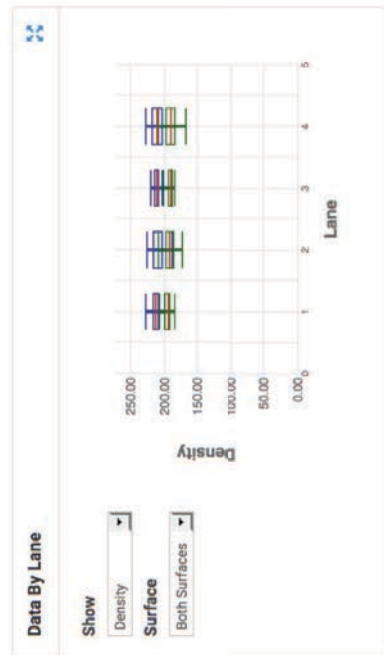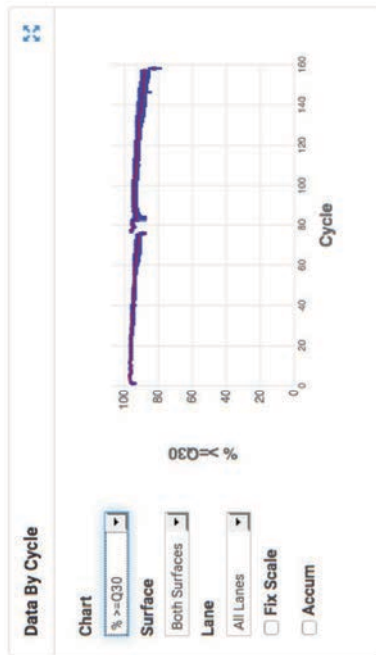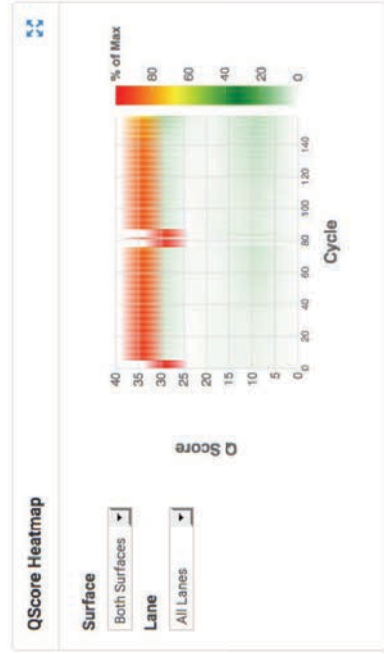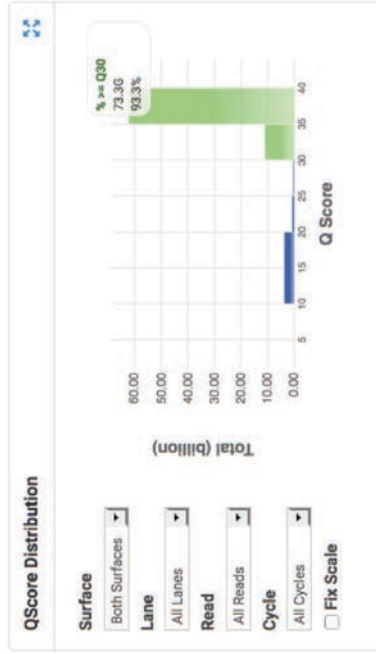
TOTAL READS	PF READS		% READS IDENTIFIED (PF)	CV	MIN	MAX
275,638,000	253,205,302		90.7379	0.1569	5.5291	9.0292

INDEX	SAMPLE ID	PROJECT	INDEX 1 (I7)	INDEX 2 (I5)	% READS IDENTIFIED (PF)
1	K562_Clone_C10	default	ACTTGA	n/a	8.7946
2	K562_Clone_B9	default	TAGCTT	n/a	8.4621
3	K562_Clone_G5	default	GATCAG	n/a	9.0292
4	K562_Clone_A8	default	TTAGGC	n/a	5.5291
5	K562_15_DAS	default	GCCAAT	n/a	8.6723
6	K562_200_DAS	default	ATCACG	n/a	6.6507
7	K562_50_DAS	default	CTTGTA	n/a	6.5432
8	K562_25_DAS	default	CAGATC	n/a	6.3524
9	K562_10_DAS	default	ACAGTG	n/a	8.7592
10	K562_N	default	CGATGT	n/a	6.7184
11	K562_DMSO	default	TGACCA	n/a	7.3423
12	K562_Clone_E2	default	GGCTAC	n/a	7.8845
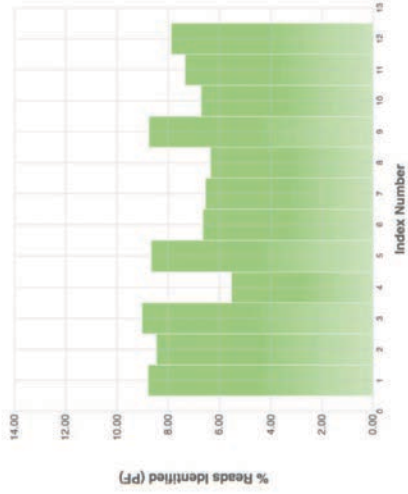
Figure S15: a) Quality control data from RNA sequencing experimental data demonstrated the accuracy of sequencing base calls. Q score (phred score) was greater than 30 (99.9% accuracy). b) Quality control data from RNA sequencing experimental data demonstrated an appropriate distribution of sequenced reads across the samples. This data was used to normalise for read sequencing depth between samples for differential expression analysis.
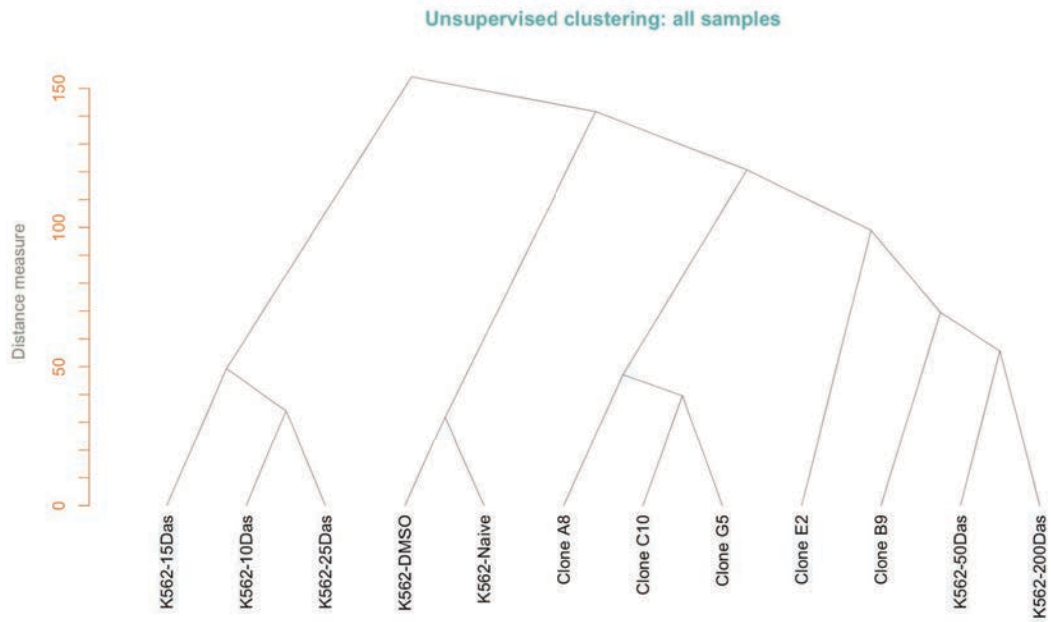
Figure S16: Unsupervised hierarchical clustering plot for all K562 DasR cell line samples used in RNA sequencing experiments, with drug naïve K562 controls. Results demonstrate the degree of clustering of selected DasR samples compared with controls.
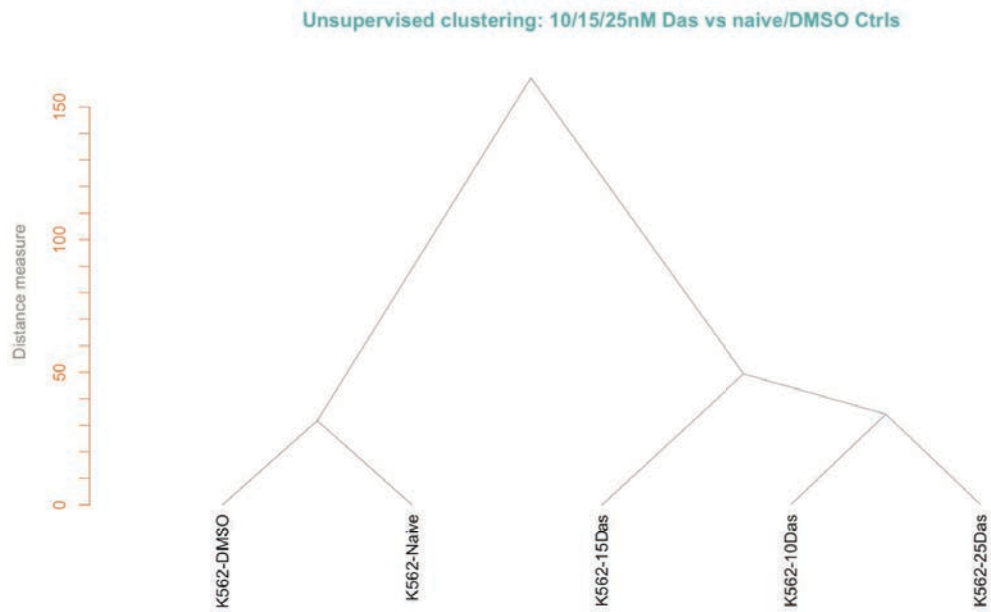
Figure S17: Unsupervised hierarchical clustering plot for K562 DasR 10, 15 and 25 nM dose escalation intermediates, and drug naïve K562 controls. Results demonstrate the degree of clustering of selected DasR samples compared with controls, which were subsequently grouped for differential expression analysis.
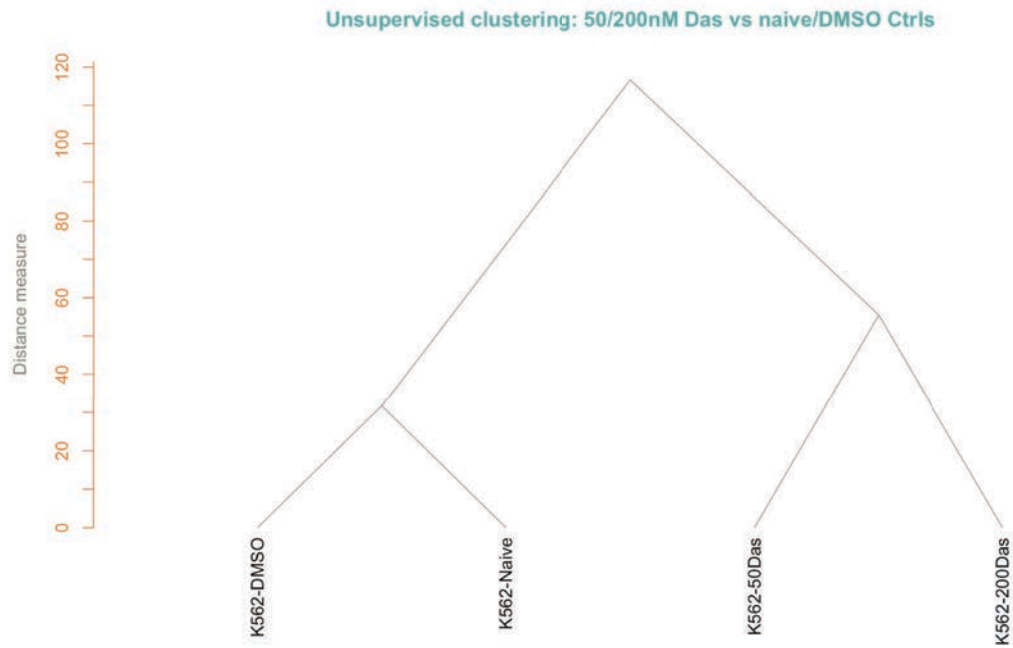
Figure S18: Unsupervised hierarchical clustering plot for the K562 50 and 200 nM DasR dose escalation intermediates, and drug naïve K562 controls. Results demonstrate the degree of clustering of selected DasR samples compared with controls, which were subsequently grouped for differential expression analysis.

Figure S19: Differential expression heatmap of the 100 most significantly differentially regulated genes in the 10, 15, and 25 nM DasR dose escalation intermediates.
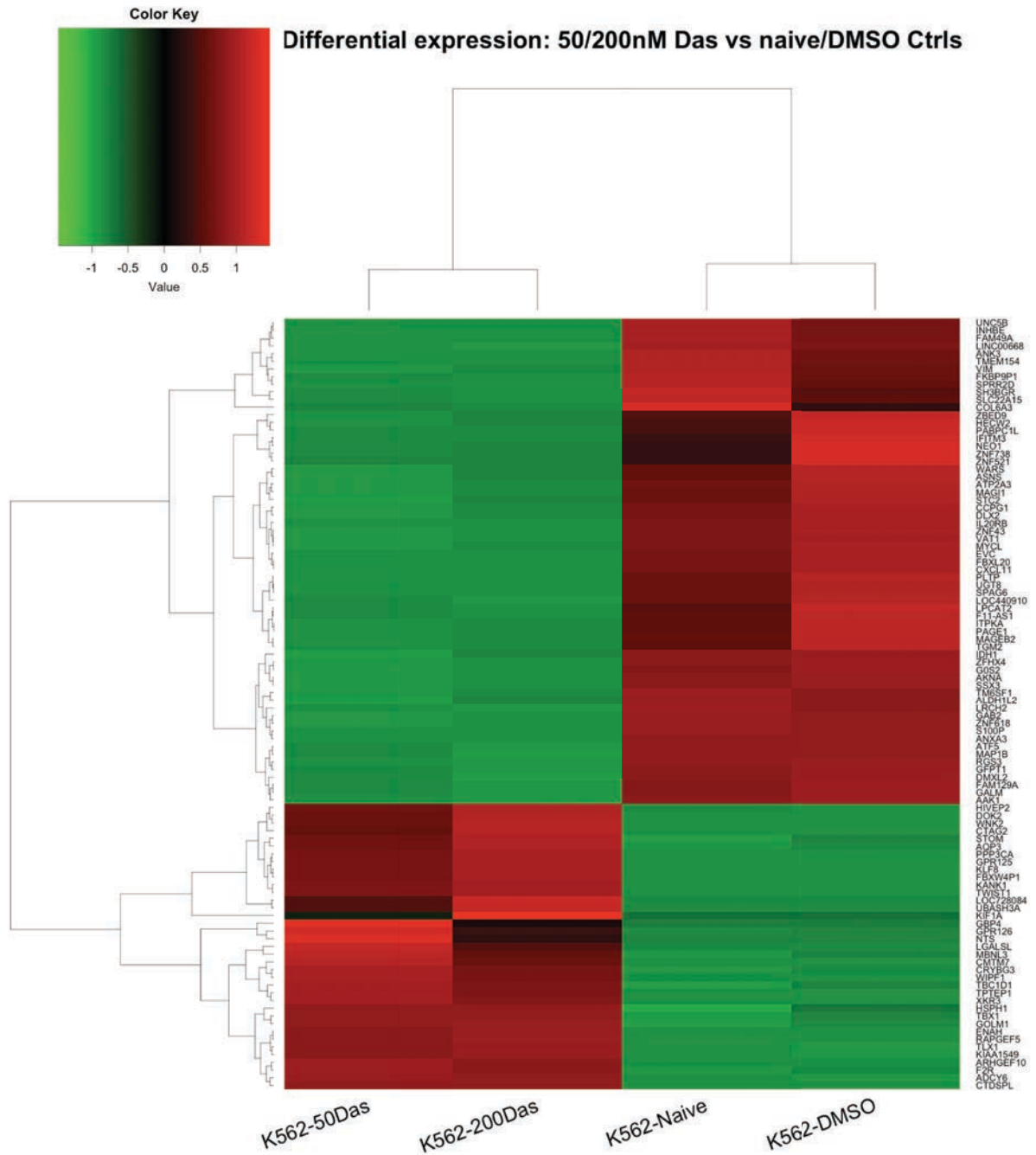
Figure S20: Differential expression heatmap of the 100 most significantly differentially regulated genes in the 50 and 200 nM DasR dose escalation intermediates.

Volcano plot: 50/200nM Das vs naive/DMSO Ctrls

Figure S21: Volcano plot diagram indicating genes differentially expressed in the K562 50 and 200 nM DasR intermediates, compared with drug naïve controls. Green dots / labeled genes indicate genes with expression logFC>2, and FDR<0.005 as a significance cutoff.

8 References

1.   Bennett JH. Case of Hypertrophy of the Spleen and Liver: In which Death Took Place from Suppuration of the Blood: Edinburgh Med Sug J; 1845.

2.   Geary CG. The story of chronic myeloid leukaemia. Br J Haematol. 2000;110(1):2-11.

3.   Piller GJ. Leukaemia – a brief historical review from ancient times to 1950. Br J Haematol. 2001;112(2):282-92.

4.   Union for International Cancer Control U. Medicines for treatment of the following cancers – review – EML and EMLc: World Health Organization; 2015 [cited 2018 11/09/2018]. Available   from: http://www.who.int/selection_medicines/committees/expert/20/applications/cancer/en/.

5.   Sawyers CL. Chronic myeloid leukemia. N Engl J Med. 1999;340(17):1330-40.

6.   Thompson PA, Kantarjian HM, Cortes JE. Diagnosis and Treatment of Chronic Myeloid Leukemia in 2015. Mayo Clin Proc. 2015;90(10):1440-54.

7.   Jabbour E, Kantarjian H. Chronic myeloid leukemia: 2016 update on diagnosis, therapy, and monitoring. Am J Hematol. 2016;91(2):252-65.

8.   NSW CC. Chronic myeloid leukaemia (CML): Cancer Council NSW; 2016. Available from: https://www.cancercouncil.com.au/chronic-myeloid-leukaemia/.

9.   Tanaka K, Takechi M, Hong J, Shigeta C, Oguma N, Kamada N, et al. 9; 22 translocation and bcr rearrangements in chronic myelocytic leukemia patients among atomic bomb survivors. J Radiat Res. 1989;30(4):352-8.

10.   Radich JP. The Biology of CML blast crisis. Hematology Am Soc Hematol Educ Program. 2007:384-91.

11.   Nowell PC. A minute chromosome n human chronic granualocytic leukemia. Science. 1960;132:1497-501.

12.   Rowley JD. Letter: A new consistent chromosomal abnormality in chronic myelogenous leukaemia identified by quinacrine fluorescence and Giemsa staining. Nature. 1973;243(5405):290-3.

13.   Gollin SM, editor Mechanisms leading to nonrandom, nonhomologous chromosomal translocations in leukemia. Semin Cancer Biol; 2007: Elsevier.

14.   Daley GQ, Baltimore D. Transformation of an interleukin 3-dependent hematopoietic cell line by the chronic myelogenous leukemia-specific P210bcr/abl protein. Proc Natl Acad Sci USA. 1988;85(23):9312-6.

15.   Daley GQ, Van Etten RA, Baltimore D. Induction of chronic myelogenous leukemia in mice by the P210bcr/abl gene of the Philadelphia chromosome. Science. 1990;247(4944):824-30.

16.   Pear WS, Miller JP, Xu L, Pui JC, Soffer B, Quackenbush RC, et al. Efficient and rapid induction of a chronic myelogenous leukemia-like myeloproliferative disease in mice receiving P210 bcr/abl-transduced bone marrow. Blood. 1998;92(10):3780-92.

17.   Li S, Ilaria RL, Jr., Million RP, Daley GQ, Van Etten RA. The P190, P210, and P230 forms of the BCR/ABL oncogene induce a similar chronic myeloid leukemia-like syndrome in mice but have different lymphoid leukemogenic activity. J Exp Med. 1999;189(9):1399-412.

18.   Hariharan IK, Harris AW, Crawford M, Abud H, Webb E, Cory S, et al. A bcr-v-abl oncogene induces lymphomas in transgenic mice. Mol Cell Biol. 1989;9(7):2798-805.

19.   Scott S, Travis D, Whitby L, Bainbridge J, Cross NC, Barnett D. Measurement of BCR-ABL 1 by RT-qPCR in chronic myeloid leukaemia: findings from an International EQA Programme. Br J Haematol. 2017;177(3):414-22.

20.   Zhu Q-S, Heisterkamp N, Groffen J. Unique organization of the human BCR gene promoter. Nucleic Acids Res. 1990;18(23):7119-25.

21.   Shah N, Witte O, Denny C. Characterization of the BCR promoter in Philadelphia chromosome-positive and-negative cell lines. Mol Cell Biol. 1991;11(4):1854-60.

22.   Pane F, Intrieri M, Quintarelli C, Izzo B, Muccioli GC, Salvatore F. BCR/ABL genes and leukemic phenotype: from molecular mechanisms to clinical correlations. Oncogene. 2002;21(56):8652.

23.   Alam A, al Qawasmeh K, Kanbar J, Syed MH, Lal A, Hussain S, et al. Philadelphia Positive Acute Lymphoblastic Leukemia (Ph+ ALL), Tawam Experience. Blood; 2015. p. 4867.

24.   Heisterkamp N, Groffen J. Philadelphia-positive leukemia: a personal perspective. Oncogene. 2002;21(56):8536.

25.   Gambacorti-Passerini C, Le Coutre P, Mologni L, Fanelli M, Bertazzoli C, Marchesi E, et al. Inhibition of the ABL kinase activity blocks the proliferation of BCR/ABL+ leukemic cells and induces apoptosis. Blood Cell Mol Dis. 1997;23(3):380-94.

26.   Sirvent A, Benistant C, Roche S. Cytoplasmic signalling by the c-Abl tyrosine kinase in normal and cancer cells. Biology of the Cell. 2008;100(11):617-31.

27.   Nagar B, Hantschel O, Young MA, Scheffzek K, Veach D, Bornmann W, et al. Structural basis for the autoinhibition of c-Abl tyrosine kinase. Cell. 2003;112(6):859-71.

28.   Feller SM, Knudsen B, Hanafusa H. c-Abl kinase regulates the protein binding activity of c-Crk. EMBO J. 1994;13(10):2341-51.

29.   Van Etten RA. Cycling, stressed-out and nervous: cellular functions of c-Abl. Trends Cell Biol. 1999;9(5):179-86.

30.   Greuber EK, Smith-Pearson P, Wang J, Pendergast AM. Role of ABL family kinases in cancer: from leukaemia to solid tumours. Nat Rev Cancer. 2013;13(8):nrc3563.

31.   Pluk H, Dorey K, Superti-Furga G. Autoinhibition of c-Abl. Cell. 2002;108(2):247-59.

32.   Hantschel O, Nagar B, Guettler S, Kretzschmar J, Dorey K, Kuriyan J, et al. A myristoyl/phosphotyrosine switch regulates c-Abl. Cell. 2003;112(6):845-57.

33.   Maru Y, Witte ON. The BCR gene encodes a novel serine/threonine kinase activity within a single exon. Cell. 1991;67(3):459-68.

34.   Laurent E, Talpaz M, Wetzler M, Kurzrock R. Cytoplasmic and nuclear localization of the 130 and 160 kDa Bcr proteins. Leukemia. 2000;14(11):1892.

35.   Chuang T, Xu X, Kaartinen V, Heisterkamp N, Groffen J, Bokoch G. Abr and Bcr are multifunctional regulators of the Rho GTP-binding protein family. P Natl Acad Sci USA. 1995;92(22):10282-6.

36.   Bustelo XR, Sauzeau V, Berenjeno IM. GTP-binding proteins of the Rho/Rac family: regulation, effectors and functions in vivo. Bioessays. 2007;29(4):356-70.

37.   Mahon GM, Wang Y, Korus M, Kostenko E, Cheng L, Sun T, et al. The c-Myc oncoprotein interacts with Bcr. Curr Biol. 2003;13(5):437-41.

38.   Reuther GW, Fu H, Cripe LD, Collier RJ, Pendergast AM. Association of the protein kinases c-Bcr and Bcr-Abl with proteins of the 14-3-3 family. Science. 1994;266(5182):129-33.

39.   Meng J, Jiang J-J, Atsumi T, Bando H, Okuyama Y, Sabharwal L, et al. Breakpoint Cluster Region–Mediated Inflammation Is Dependent on Casein Kinase II. J Immunol. 2016;197(8):1601082.

40.   McWhirter JR, Galasso DL, Wang J. A coiled-coil oligomerization domain of Bcr is essential for the transforming function of Bcr-Abl oncoproteins. Mol Cell Biol. 1993;13(12):7587-95.

41.   Zhao X, Ghaffari S, Lodish H, Malashkevich VN, Kim PS. Structure of the Bcr-Abl oncoprotein oligomerization domain. Nature structural biology. 2002;9(2):117-20.

42.   Zhang X, Subrahmanyam R, Wong R, Gross AW, Ren R. The NH2-terminal coiled-coil domain and tyrosine 177 play important roles in induction of a myeloproliferative disease in mice by Bcr-Abl. Mol Cell Biol. 2001;21(3):840-53.

43.   Cilloni D, Saglio G. Molecular pathways: BCR-ABL. Clin Cancer Res. 2011:930-637.

44.   Kharas MG, Fruman DA. ABL oncogenes and phosphoinositide 3-kinase: mechanism of activation and downstream effectors. Cancer Res. 2005;65(6):2047-53.

45.   Danhauser-Riedl S, Warmuth M, Druker BJ, Emmerich B, Hallek M. Activation of Src kinases p53/56lyn and p59hck by p210bcr/abl in myeloid cells. Cancer Res. 1996;56(15):3589-96.

46.   Klejman A, Schreiner SJ, Nieborowska-Skorska M, Slupianek A, Wilson M, Smithgall TE, et al. The Src family kinase Hck couples BCR/ABL to STAT5 activation in myeloid leukemia cells. EMBO J. 2002;21(21):5766-74.

47.   Carlesso N, Frank DA, Griffin JD. Tyrosyl phosphorylation and DNA binding activity of signal transducers and activators of transcription (STAT) proteins in hematopoietic cell lines transformed by Bcr/Abl. J Exp Med. 1996;183(3):811-20.

48.   Melo JV, Deininger MW. Biology of chronic myelogenous leukemia—signaling pathways of initiation and transformation. Hematol Oncol Clin N. 2004;18(3):545-68.

49.   Wingelhofer B, Neubauer HA, Valent P, Han X, Constantinescu SN, Gunning PT, et al. Implications of STAT3 and STAT5 signaling on gene regulation and chromatin remodeling in hematopoietic cancer. Leukemia. 2018;32:1713-26.

50.   Sonoyama J, Matsumura I, Ezoe S, Satoh Y, Zhang X, Kataoka Y, et al. Functional cooperation among Ras, STAT5, and phosphatidylinositol 3-kinase is required for full oncogenic activities of BCR/ABL in K562 cells. J Biol Chem. 2002;277(10):8076-82.

51.   Kim JH, Chu SC, Gramlich JL, Pride YB, Babendreier E, Chauhan D, et al. Activation of the PI3K/mTOR pathway by BCR-ABL contributes to increased production of reactive oxygen species. Blood. 2005;105(4):1717-23.

52.   Deininger MW, Goldman JM, Melo JV. The molecular biology of chronic myeloid leukemia. Blood. 2000;96(10):3343-56.

53.   Sawyers CL, Callahan W, Witte ON. Dominant negative MYC blocks transformation by ABL oncogenes. Cell. 1992;70(6):901-10.

54.   Skorski T, Bellacosa A, Nieborowska-Skorska M, Majewski M, Martinez R, Choi JK, et al. Transformation of hematopoietic cells by BCR/ABL requires activation of a PI-3k/Akt-dependent pathway. Embo J. 1997;16(20):6151-61.

55.   Sharma N, Magistroni V, Piazza R, Citterio S, Mezzatesta C, Khandelwal P, et al. BCR/ABL1 and BCR are under the transcriptional control of the MYC oncogene. Molecular cancer. 2015;14(1):132.

56.   Hehlmann R. How I treat CML blast crisis. Blood. 2012;120(4):737-47.

57.   Sattler M, Verma S, Shrikhande G, Byrne CH, Pride YB, Winkler T, et al. The BCR/ABL Tyrosine Kinase Induces Production of Reactive Oxygen Species in Hematopoietic Cells. J Biol Chem. 2000;275(32):24273-8.

58.   Slupianek A, Hoser G, Majsterek I, Bronisz A, Malecki M, Blasiak J, et al. Fusion tyrosine kinases induce drug resistance by stimulation of homology-dependent recombination repair,

prolongation of G(2)/M phase, and protection from apoptosis. Mol Cell Biol. 2002;22(12):4189-201.

59.   Bedi A, Zehnbauer BA, Barber JP, Sharkis SJ, Jones RJ. Inhibition of apoptosis by BCR-ABL in chronic myeloid leukemia. Blood. 1994;83(8):2038-44.

60.   Wilson G, Vandenberghe E, Pollitt R, Rees D, Goodeve A, Peake I, et al. Are aberrant BCR–ABL transcripts more common than previously thought? Br J Haematol. 2000;111(4):1109-11.

61.   Barnes DJ, Melo JV. Cytogenetic and molecular genetic aspects of chronic myeloid leukaemia. Acta Haematol-Basel. 2002;108(4):180-202.

62.   Chan LC, Karhi KK, Rayter SI, Heisterkamp N, Eridani S, Powles R, et al. A novel abl protein expressed in Philadelphia chromosome positive acute lymphoblastic leukaemia. Nature. 1987;325(6105):635-7.

63.   Gong Z, Medeiros L, Cortes J, Zheng L, Khoury J, Wang W, et al. Clinical and prognostic significance of e1a2 BCR-ABL1 transcript subtype in chronic myeloid leukemia. Blood Cancer J. 2017;7(7):e583.

64.   Martínez-Laperche C, Jiménez-Gámiz P, Collado R, Minguela-Puras A, Piñán-Francés M, Bellosillo B, et al. Chronic myeloid leukemia (CML) patients with atypical e1a2 P190 BCR-ABL translocation show a poor response to therapy with tyrosine kinase inhibitors (TKI). Am Soc Hematology; 2013.

65.   Verstovsek S, Lin H, Kantarjian H, Saglio G, De Micheli D, Pane F, et al. Neutrophilic-chronic myeloid leukemia: Low levels of p230 BCR/ABL mRNA and undetectable p230 BCR/ABL protein may predict an indolent course. Cancer: Interdisciplinary International Journal of the American Cancer Society. 2002;94(9):2416-25.

66.   Melo JV. The diversity of BCR-ABL fusion proteins and their relationship to leukemia phenotype. Blood. 1996;88(7):2375-84.

67.   Kelliher M, Knott A, McLaughlin J, Witte ON, Rosenberg N. Differences in oncogenic potency but not target cell specificity distinguish the two forms of the BCR/ABL oncogene. Mol Cell Biol. 1991;11(9):4710-6.

68.   Voncken JW, Kaartinen V, Pattengale PK, Germeraad WT, Groffen J, Heisterkamp N. BCR/ABL P210 and P190 cause distinct leukemia in transgenic mice. Blood. 1995;86(12):4603.

69.   Hochhaus A, Reiter A, Skladny H, Melo JV, Sick C, Berger U, et al. A novel BCR-ABL fusion gene (e6a2) in a patient with Philadelphia chromosome-negative chronic myelogenous leukemia. Blood. 1996;88(6):2236-40.

70.   Dupont M, Jourdan E, Chiesa J. Identification of E6A2 BCR-ABL fusion in a Philadelphia-positive CML. Leukemia. 2000;14(11):2011-2.

71.   Colla S, Sammarelli G, Voltolini S, Crugnola M, Sebastio P, Giuliani N. e6a2 BCR-ABL transcript in chronic myeloid leukemia: is it associated with aggressive disease? Haematologica. 2004;89(5):611-3.

72.   Vefring HK, Gruber FX, Wee L, Hovland R, Hjorth-Hansen H, Gedde Dahl T, et al. Chronic myelogenous leukemia with the e6a2 BCR-ABL and lacking imatinib response: presentation of two cases. Acta Haematol. 2009;122(1):11-6.

73.   Torres F, Ivanova-Dragoeva A, Pereira M, Veiga J, Rodrigues AS, Sousa AB, et al. An e6a2 BCR-ABL fusion transcript in a CML patient having an iliac chloroma at initial presentation. Leukemia Lymphoma. 2007;48(5):1034-7.

74.   Schultheis B, Wang L, Clark RE, Melo JV. BCR-ABL with an e6a2 fusion in a CML patient diagnosed in blast crisis. Leukemia. 2003;17(10):2054-5.

75.   Schnittger S, Bacher U, Kern W, Haferlach T, Hertenstein B, Haferlach C. A new case with rare e6a2 BCR-ABL fusion transcript developing two new resistance mutations during imatinib mesylate, which were replaced by T315I after subsequent dasatinib treatment. Leukemia. 2008;22(4):856-8.

76.   Roti G, La Starza R, Gorello P, Gottardi E, Crescenzi B, Martelli MF, et al. e6a2 BCR/ABL1 fusion with cryptic der(9)t(9;22) deletions in a patient with chronic myeloid leukemia. Haematologica. 2005;90(8):1139-41.

77.   Popovici C, Cailleres S, David M, Lafage-Pochitaloff M, Sainty D, Mozziconacci MJ. E6a2 BCR-ABL fusion with BCR exon 5-deleted transcript in a Philadelphia positive CML responsive to Imatinib. Leukemia Lymphoma. 2005;46(9):1375-7.

78.   Langabeer SE, Crampe M, Kelly J, Fadalla K, Connaghan G, Conneally E. Nilotinib and allogeneic stem cell transplantation in a chronic myeloid leukemia patient with e6a2 and e1a2 BCR-ABL transcripts. Leuk Res. 2010;34(8):e204-5.

79.   Zagaria A, Anelli L, Coccaro N, Tota G, Casieri P, Cellamare A, et al. BCR-ABL1 e6a2 transcript in chronic myeloid leukemia: biological features and molecular monitoring by droplet digital PCR. Virchows Arch. 2015;467(3):357-63.

80.   Yao J, Douer D, Wang L, Arcila ME, Nafa K, Chiu A. A case of acute myeloid leukemia with e6a2 BCR-ABL fusion transcript acquired after progressing from chronic myelomonocytic leukemia. Leuk Res Rep. 2017;7:17-9.

81.   Ritchie DS, McBean M, Westerman DA, Kovalenko S, Seymour JF, Dobrovic A. Complete molecular response of e6a2 BCR-ABL-positive acute myeloid leukemia to imatinib then dasatinib. Blood. 2008;111(5):2896-8.

82.   Hayette S, Tigaud I, Thomas X, French M, Perrin MC, Nicolini F, et al. Identification of a rare e6a2 BCR-ABL fusion gene during the disease progression of chronic myelomonocytic leukemia: a case report. Leukemia. 2004;18(10):1735-6.

83.   Burmeister T, Schwartz S, Taubald A, Jost E, Lipp T, Schneller F, et al. Atypical BCR-ABL mRNA transcripts in adult acute lymphoblastic leukemia. Haematologica. 2007;92(12):1699-702.

84.   Quentmeier H, Cools J, Macleod RA, Marynen P, Uphoff CC, Drexler HG. e6-a2 BCR-ABL1 fusion in T-cell acute lymphoblastic leukemia. Leukemia. 2005;19(2):295-6.

85.   Kumar D, Panigrahi MK, Saikia KK, Kapoor G, Mehta A. Molecular analysis of childhood B-acute lymphoblastic leukemia: Identification and prognosis of rare breakpoints. Mol Biol. 2015;49(6):944-8.

86.   Staal-Viliare A, Latger-Cannard V, Rault JP, Didion J, Gregoire MJ, Bologna S, et al. [A case of de novo acute basophilic leukaemia: diagnostic criteria and review of the literature]. Ann Biol Clin (Paris). 2006;64(4):361-5.

87.   Rohon P, Divoka M, Calabkova L, Mojzikova R, Katrincsakova B, Rusinakova Z, et al. Identification of e6a2 BCR-ABL fusion in a Philadelphia-positive CML with marked basophilia: implications for treatment strategy. Biomed Pap Med Fac Univ Palacky Olomouc Czech Repub. 2011;155(2):187-90.

88.   Gregoire MJ, Latger-Cannard V, Staal A, Bologna S, Leotard B, Rault JP, et al. Identification of an acute basophilic leukaemia carrying a rare e6a2 BCR-ABL transcript. Acta Haematol. 2006;116(3):216-8.

89.   Beel KA, Lemmens J, Vranckx H, Maertens J, Vandenberghe P. CML with e6a2 BCR-ABL1 transcript: an aggressive entity? Ann Hematol. 2011;90(10):1241-3.

90.   Branford S, Rudzki Z, Hughes T. A novel BCR–ABL transcript (e8a2) with the insertion of an inverted sequence of ABL intron 1b in a patient with Philadelphia-positive chronic myeloid leukaemia. Brit J Haematol. 2000;109(3):635-7.

91.   Cayuela J-M, Rousselot P, Nicolini F, Espinouse D, Ollagnier C, Bui-Thi M, et al. Identification of a rare e8a2 BCR-ABL fusion gene in three novel chronic myeloid leukemia patients treated with imatinib. Leukemia. 2005;19(12):2334.

92.   Demehri S, Paschka P, Schultheis B, Lange T, Koizumi T, Sugimoto T, et al. e8a2 BCR–ABL: more frequent than other atypical BCR–ABL variants? Leukemia. 2005;19(4):681.

93.   Tchirkov A, Couderc J-L, Périssel B, Goumy C, Regnier A, Uhrhammer N, et al. Major molecular response to imatinib in a patient with chronic myeloid leukemia expressing a novel form of e8a2 BCR-ABL transcript. Leukemia. 2006;20(1):167.

94.   Qin YZ, Jiang B, Jiang Q, Zhang Y, Jiang H, Li JL, et al. Imatinib mesylate resistance in a chronic myeloid leukemia patient with a novel e8a2 BCR-ABL transcript variant. Acta Haematol. 2008;120(3):146-9.

95.   Park IJ, Lim YA, Lee WG, Park JS, Kim HC, Lee H-J, et al. A case of chronic myelogenous leukemia with e8a2 fusion transcript. Cancer Genet Cytogenet. 2008;185(2):106-8.

96.   Mühlmann J, Thaler J, Hilbe W, Bechter O, Erdel M, Utermann G, et al. Fluorescence in situ hybridization (FISH) on peripheral blood smears for monitoring Philadelphia chromosome-positive chronic myeloid leukemia (CML) during interferon treatment: A new strategy for remission assessment. Gene Chromosome Canc. 1998;21(2):90-100.

97.   Branford S, Hughes T, Rudzki Z. Monitoring chronic myeloid leukaemia therapy by real-time quantitative PCR in blood is a reliable alternative to bone marrow cytogenetics. Brit J Haematol. 1999;107(3):587-99.

98.   Marum JE, Branford S. Current developments in molecular monitoring in chronic myeloid leukemia. Ther Adv Hematol. 2016;7(5):237-51.

99.   Hughes T, Deininger M, Hochhaus A, Branford S, Radich J, Kaeda J, et al. Monitoring CML patients responding to treatment with tyrosine kinase inhibitors: review and recommendations for harmonizing current methodology for detecting BCR-ABL transcripts and kinase domain mutations and for expressing results. Blood. 2006;108(1):28-37.

100.   Baccarani M, Deininger MW, Rosti G, Hochhaus A, Soverini S, Apperley JF, et al. European LeukemiaNet recommendations for the management of chronic myeloid leukemia: 2013. Blood. 2013;122(6):872-84.

101.   Hughes TP, Ross DM. Moving treatment-free remission into mainstream clinical practice in CML. Blood. 2016;128(1):17-23.

102.   Goldman JM, Apperley JF, Jones L, Marcus R, Goolden AW, Batchelor R, et al. Bone marrow transplantation for patients with chronic myeloid leukemia. New Engl J Med. 1986;314(4):202-7.

103.   Radich J. Stem cell transplant for chronic myeloid leukemia in the imatinib era. Semin Hematol. 2010;47(4):354-61.

104.   Talpaz M, Hehlmann R, Quintas-Cardama A, Mercer J, Cortes J. Re-emergence of interferon-α in the treatment of chronic myeloid leukemia. Leukemia. 2013;27(4):803.

105.   Bonifazi F, de Vivo A, Rosti G, Guilhot F, Guilhot J, Trabacchi E, et al. Chronic myeloid leukemia and interferon-α: a study of complete cytogenetic responders. Blood. 2001;98(10):3074-81.

106.   Druker BJ, Tamura S, Buchdunger E, Ohno S, Segal GM, Fanning S, et al. Effects of a selective inhibitor of the Abl tyrosine kinase on the growth of Bcr–Abl positive cells. Nat Med. 1996;2(5):561.

107. Furet P, Caravatti G, Lydon N, Priestle JP, Sowadski JM, Trinks U, et al. Modelling study of protein kinase inhibitors: binding mode of staurosporine and origin of the selectivity of CGP 52411. J Comput Aid Mol Des. 1995;9(6):465-72.

108. Deininger MW, Goldman JM, Lydon N, Melo JV. The tyrosine kinase inhibitor CGP57148B selectively inhibits the growth of BCR-ABL–positive cells. Blood. 1997;90(9):3691-8.

109. Oetzel C, Jonuleit T, Götz A, van der Kuip H, Michels H, Duyster J, et al. The tyrosine kinase inhibitor CGP 57148 (ST1 571) induces apoptosis in BCR-ABL-positive cells by down-regulating BCL-X. Clin Cancer Res. 2000;6(5):1958-68.

110. Cortes J, Giles F, O'Brien S, Thomas D, Albitar M, Rios MB, et al. Results of imatinib mesylate therapy in patients with refractory or recurrent acute myeloid leukemia, high-risk myelodysplastic syndrome, and myeloproliferative disorders. Cancer Am Cancer Soc. 2003;97(11):2760-6.

111. Heinrich MC, Griffith DJ, Druker BJ, Wait CL, Ott KA, Zigler AJ. Inhibition of c-kit receptor tyrosine kinase activity by STI 571, a selective tyrosine kinase inhibitor. Blood. 2000;96(3):925-32.

112. Hughes TP, Kaeda J, Branford S, Rudzki Z, Hochhaus A, Hensley ML, et al. Frequency of major molecular responses to imatinib or interferon alfa plus cytarabine in newly diagnosed chronic myeloid leukemia. New Engl J Med. 2003;349(15):1423-32.

113. Apperley JF. Part I: mechanisms of resistance to imatinib in chronic myeloid leukaemia. Lancet Oncol. 2007;8(11):1018-29.

114. Druker BJ, Talpaz M, Resta DJ, Peng B, Buchdunger E, Ford JM, et al. Efficacy and safety of a specific inhibitor of the BCR-ABL tyrosine kinase in chronic myeloid leukemia. New Engl J Med. 2001;344(14):1031-7.

115. Lee S, Kim Y-J, Min C-K, Kim H-J, Eom K-S, Kim D-W, et al. The effect of first-line imatinib interim therapy on the outcome of allogeneic stem cell transplantation in adults with newly diagnosed Philadelphia chromosome–positive acute lymphoblastic leukemia. Blood. 2005;105(9):3449-57.

116. Druker BJ, Guilhot F, O'brien SG, Gathmann I, Kantarjian H, Gattermann N, et al. Five-year follow-up of patients receiving imatinib for chronic myeloid leukemia. New Engl J Med. 2006;355(23):2408-17.

117. Nicolini FE, Balsat M, Lekieffre M, Alcazer V, Labussière-wallet H, Huet S, et al. Very Long-Term Follow-up (> 80 months) of Imatinib (IM) First-Line for Chronic Phase (CP) CML Patients. Blood; 2015. p. 2774.

118. Nagar B, Bornmann WG, Pellicena P, Schindler T, Veach DR, Miller WT, et al. Crystal structures of the kinase domain of c-Abl in complex with the small molecule inhibitors PD173955 and imatinib (STI-571). Cancer Res. 2002;62(15):4236-43.

119. Hantschel O. Structure, regulation, signaling, and targeting of abl kinases in cancer. Genes Cancer. 2012;3(5-6):436-46.

120. O'Hare T, Eide CA, Deininger MW. New Bcr-Abl inhibitors in chronic myeloid leukemia: keeping resistance in check. Expert Opin Investig Drugs. 2008;17(6):865-78.

121. Weisberg E, Manley PW, Breitenstein W, Brüggen J, Cowan-Jacob SW, Ray A, et al. Characterization of AMN107, a selective inhibitor of native and mutant Bcr-Abl. Cancer Cell. 2005;7(2):129-41.

122. Rix U, Hantschel O, Durnberger G, Remsing Rix LL, Planyavsky M, Fernbach NV, et al. Chemical proteomic profiles of the BCR-ABL inhibitors imatinib, nilotinib, and dasatinib reveal novel kinase and nonkinase targets. Blood. 2007;110(12):4055-63.

123.   Kantarjian HM, Giles F, Quintás-Cardama A, Cortes J. Important therapeutic targets in chronic myelogenous leukemia. Clin Cancer Res. 2007;13(4):1089-97.

124.   Kantarjian H, Giles F, Wunderle L, Bhalla K, O'brien S, Wassmann B, et al. Nilotinib in imatinib-resistant CML and Philadelphia chromosome–positive ALL. New Engl J Med. 2006;354(24):2542-51.

125.   Saglio G, Kim D-W, Issaragrisil S, Le Coutre P, Etienne G, Lobo C, et al. Nilotinib versus imatinib for newly diagnosed chronic myeloid leukemia. New Engl J Med. 2010;362(24):2251-9.

126.   Tokarski JS, Newitt JA, Chang CYJ, Cheng JD, Wittekind M, Kiefer SE, et al. The structure of Dasatinib (BMS-354825) bound to activated ABL kinase domain elucidates its inhibitory activity against imatinib-resistant ABL mutants. Cancer Res. 2006;66(11):5790-7.

127.   Shah NP, Nicoll JM, Bleickardt E, Nicaise C, Paquette RL, Sawyers CL. Potent Transient Inhibition of BCR-ABL by Dasatinib Leads to Complete Cytogenetic Remissions in Patients with Chronic Myeloid Leukemia: Implications for Patient Management and Drug Development. Blood; 2006.

128.   Bradeen HA, Eide CA, O'Hare T, Johnson KJ, Willis SG, Lee FY, et al. Comparison of imatinib mesylate, dasatinib (BMS-354825), and nilotinib (AMN107) in an N-ethyl-N-nitrosourea (ENU)–based mutagenesis screen: high efficacy of drug combinations. Blood. 2006;108(7):2332-8.

129.   Conchon M, Freitas CMBdM, Rego MAdC, Junior B, Ramos JW. Dasatinib: clinical trials and management of adverse events in imatinib resistant/intolerant chronic myeloid leukemia. Rev Bras Hematol Hemoter. 2011;33(2):131-9.

130.   Phan C, Jutant EM, Tu L, Thuillet R, Seferian A, Montani D, et al. Dasatinib increases endothelial permeability leading to pleural effusion. The European respiratory journal. 2018;51(1):1701096.

131.   Talpaz M, Shah NP, Kantarjian H, Donato N, Nicoll J, Paquette R, et al. Dasatinib in imatinib-resistant Philadelphia chromosome–positive leukemias. New Engl J Med. 2006;354(24):2531-41.

132.   Kantarjian H, Shah NP, Hochhaus A, Cortes J, Shah S, Ayala M, et al. Dasatinib versus imatinib in newly diagnosed chronic-phase chronic myeloid leukemia. New Engl J Med. 2010;362(24):2260-70.

133.   Cortes JE, Kim DW, Pinilla-Ibarz J, le Coutre PD, Paquette R, Chuah C, et al. Ponatinib efficacy and safety in Philadelphia chromosome-positive leukemia: final 5-year results of the phase 2 PACE trial. Blood. 2018;132(4):393-404.

134.   O'Hare T, Shakespeare WC, Zhu X, Eide CA, Rivera VM, Wang F, et al. AP24534, a pan-BCR-ABL inhibitor for chronic myeloid leukemia, potently inhibits the T315I mutant and overcomes mutation-based resistance. Cancer Cell. 2009;16(5):401-12.

135.   Omar Al Ustwani M, Wetzler M. Novel Therapies for T315I-Mutant CML. Target Oncol. 2014.

136.   Cortes JE, Kantarjian H, Shah NP, Bixby D, Mauro MJ, Flinn I, et al. Ponatinib in refractory Philadelphia chromosome–positive leukemias. New Engl J Med. 2012;367(22):2075-88.

137.   Karaman MW, Herrgard S, Treiber DK, Gallant P, Atteridge CE, Campbell BT, et al. A quantitative analysis of kinase inhibitor selectivity. Nature Biotechnol. 2008;26(1):127.

138.   Zabriskie MS, Eide CA, Tantravahi SK, Vellore NA, Estrada J, Nicolini FE, et al. BCR-ABL1 compound mutations combining key kinase domain positions confer clinical resistance to ponatinib in Ph chromosome-positive leukemia. Cancer Cell. 2014;26(3):428-42.

139.   Wylie AA, Schoepfer J, Jahnke W, Cowan-Jacob SW, Loo A, Furet P, et al. The allosteric inhibitor ABL001 enables dual targeting of BCR–ABL1. Nature. 2017;543(7647):733.

140.   Adrián FJ, Ding Q, Sim T, Velentza A, Sloan C, Liu Y, et al. Allosteric inhibitors of Bcr-abl–dependent cell proliferation. Nat Chem Biol. 2006;2(2):95-102.

141.   Hughes TP, Goh Y-T, Ottmann OG, Minami H, Rea D, Lang F, et al. Expanded phase 1 study of ABL001, a potent, allosteric inhibitor of BCR-ABL, reveals significant and durable responses in patients with CML-chronic phase with failure of prior TKI therapy. Am Soc Hematol; 2016. p. 625.

142.   Eadie LN, Saunders VA, Branford S, White DL, Hughes TP. The new allosteric inhibitor asciminib is susceptible to resistance mediated by ABCB1 and ABCG2 overexpression in vitro. Oncotarget. 2018;9(17):13423.

143.   Wylie A, Schoepfer J, Berellini G, Cai H, Caravatti G, Cotesta S, et al. ABL001, a potent allosteric inhibitor of BCR-ABL, prevents emergence of resistant disease when administered in combination with nilotinib in an in vivo murine model of chronic myeloid leukemia. Blood; 2014. p. 398.

144.   Mahon FX, Deininger MW, Schultheis B, Chabrol J, Reiffers J, Goldman JM, et al. Selection and characterization of BCR-ABL positive cell lines with differential sensitivity to the tyrosine kinase inhibitor STI571: diverse mechanisms of resistance. Blood. 2000;96(3):1070-9.

145.   Weisberg E, Griffin JD. Mechanism of resistance to the ABL tyrosine kinase inhibitor STI571 in BCR/ABL–transformed hematopoietic cell lines. Blood. 2000;95(11):3498-505.

146.   Gorre ME, Mohammed M, Ellwood K, Hsu N, Paquette R, Rao PN, et al. Clinical resistance to STI-571 cancer therapy caused by BCR-ABL gene mutation or amplification. Science. 2001;293(5531):876-80.

147.   Barnes DJ, Palaiologou D, Panousopoulou E, Schultheis B, Yong AS, Wong A, et al. Bcr-Abl expression levels determine the rate of development of resistance to imatinib mesylate in chronic myeloid leukemia. Cancer Res. 2005;65(19):8912-9.

148.   Radich JP, Dai H, Mao M, Oehler V, Schelter J, Druker B, et al. Gene expression changes associated with progression and response in chronic myeloid leukemia. Proc Natl Acad Sci USA. 2006;103(8):2794-9.

149.   Gadzicki D, von Neuhoff N, Steinemann D, Just M, Busche G, Kreipe H, et al. BCR-ABL gene amplification and overexpression in a patient with chronic myeloid leukemia treated with imatinib. Cancer Genet Cytogenet. 2005;159(2):164-7.

150.   Andrews DF, 3rd, Collins SJ. Heterogeneity in expression of the bcr-abl fusion transcript in CML blast crisis. Leukemia. 1987;1(10):718-24.

151.   Collins SJ, Groudine MT. Chronic myelogenous leukemia: amplification of a rearranged c-abl oncogene in both chronic phase and blast crisis. Blood. 1987;69(3):893-8.

152.   Shah NP, Nicoll JM, Nagar B, Gorre ME, Paquette RL, Kuriyan J, et al. Multiple BCR-ABL kinase domain mutations confer polyclonal resistance to the tyrosine kinase inhibitor imatinib (STI571) in chronic phase and blast crisis chronic myeloid leukemia. Cancer Cell. 2002;2(2):117-25.

153.   Skaggs BJ, Gorre ME, Ryvkin A, Burgess MR, Xie Y, Han Y, et al. Phosphorylation of the ATP-binding loop directs oncogenicity of drug-resistant BCR-ABL mutants. Proc Natl Acad Sci USA. 2006;103(51):19466-71.

154.   O'Hare T, Eide CA, Deininger MW. Bcr-Abl kinase domain mutations, drug resistance, and the road to a cure for chronic myeloid leukemia. Blood. 2007;110(7):2242-9.

155.   Branford S, Rudzki Z, Walsh S, Parkinson I, Grigg A, Szer J, et al. Detection of BCR-ABL mutations in patients with CML treated with imatinib is virtually always accompanied by clinical resistance, and mutations in the ATP phosphate-binding loop (P-loop) are associated with a poor prognosis. Blood. 2003;102(1):276-83.

156.   Corbin AS, Buchdunger E, Pascal F, Druker BJ. Analysis of the structural basis of specificity of inhibition of the Abl kinase by STI571. J Biol Chem. 2002;277(35):32214-9.

157.   Zhou T, Parillon L, Li F, Wang Y, Keats J, Lamore S, et al. Crystal structure of the T315I mutant of Abl kinase. Chem Biol Drug Des. 2007;70(3):171-81.

158.   Soverini S, Iacobucci I, Baccarani M, Martinelli G. Targeted therapy and the T315I mutation in Philadelphia-positive leukemias. Haematologica; 2007. p. 437-9.

159.   Azam M, Seeliger MA, Gray NS, Kuriyan J, Daley GQ. Activation of tyrosine kinases by mutation of the gatekeeper threonine. Nat Struct Mol Biol. 2008;15(10):1109.

160.   Griswold IJ, MacPartlin M, Bumm T, Goss VL, O'Hare T, Lee KA, et al. Kinase domain mutants of Bcr-Abl exhibit altered transformation potency, kinase activity, and substrate utilization, irrespective of sensitivity to imatinib. Mol Cell Biol. 2006;26(16):6082-93.

161.   Härtel N, Klag T, Hanfstein B, Mueller MC, Schenk T, Erben P, et al. Enhanced ABL-inhibitor-induced MAPK-activation in T315I-BCR-ABL-expressing cells: a potential mechanism of altered leukemogenicity. J Cancer Res Clin. 2012;138(2):203-12.

162.   Desterke C, Aggoune D, Bonnet ML, Prade N, Chomel J-C, Delabesse E. T315I-Mutated BCR-ABL Induces a Distinct and Specific Molecular Signature With High Expression Of Zinc Finger (ZNF) Transcription Factors. Am Soc Hematology; 2013. p. 4899.

163.   White DL, Saunders VA, Dang P, Engler J, Zannettino AC, Cambareri AC, et al. OCT-1–mediated influx is a key determinant of the intracellular uptake of imatinib but not nilotinib (AMN107): reduced OCT-1 activity is the cause of low in vitro sensitivity to imatinib. Blood. 2006;108(2):697-704.

164.   Watkins D, Hughes T, White D. OCT1 and imatinib transport in CML: is it clinically relevant? Leukemia. 2015;29(10):1960.

165.   Dean M, Hamon Y, Chimini G. The human ATP-binding cassette (ABC) transporter superfamily. J Lipid Res. 2001;42(7):1007-17.

166.   Theodoulou FL, Kerr ID. ABC transporter research: going strong 40 years on. Biochem Soc Trans. 2015;43(5):1033-40.

167.   Vasiliou V, Vasiliou K, Nebert DW. Human ATP-binding cassette (ABC) transporter family. Hum Genomics. 2009;3(3):281-90.

168.   ter Beek J, Guskov A, Slotboom DJ. Structural diversity of ABC transporters. J Gen Physiol. 2014;143(4):419-35.

169.   Juliano RL, Ling V. A surface glycoprotein modulating drug permeability in Chinese hamster ovary cell mutants. Biochim Biophys Acta. 1976;455(1):152-62.

170.   Chen CJ, Chin JE, Ueda K, Clark DP, Pastan I, Gottesman MM, et al. Internal duplication and homology with bacterial transport proteins in the mdr1 (P-glycoprotein) gene from multidrug-resistant human cells. Cell. 1986;47(3):381-9.

171.   Thomas H, Coley HM. Overcoming multidrug resistance in cancer: an update on the clinical strategy of inhibiting p-glycoprotein. Cancer Control. 2003;10(2):159-65.

172.   Gottesman MM, Fojo T, Bates SE. Multidrug resistance in cancer: role of ATP-dependent transporters. Nat Rev Cancer. 2002;2(1):48-58.

173.   Eadie LN, Hughes TP, White DL. Interaction of the efflux transporters ABCB1 and ABCG2 with imatinib, nilotinib, and dasatinib. Clin Pharmacol Ther. 2014;95(3):294-306.

174.	Gottesman MM. Mechanisms of cancer drug resistance. Annu Rev Med. 2002;53:615-27.

175.	Mahon FX, Belloc F, Lagarde V, Chollet C, Moreau-Gaudry F, Reiffers J, et al. MDR1 gene overexpression confers resistance to imatinib mesylate in leukemia cell line models. Blood. 2003;101(6):2368-73.

176.	Illmer T, Schaich M, Platzbecker U, Freiberg-Richter J, Oelschlagel U, von Bonin M, et al. P-glycoprotein-mediated drug efflux is a resistance mechanism of chronic myelogenous leukemia cells to treatment with imatinib mesylate. Leukemia. 2004;18(3):401-8.

177.	Thomas J, Wang L, Clark RE, Pirmohamed M. Active transport of imatinib into and out of cells: implications for drug resistance. Blood. 2004;104(12):3739-45.

178.	Hirayama C, Watanabe H, Nakashima R, Nanbu T, Hamada A, Kuniyasu A, et al. Constitutive overexpression of P-glycoprotein, rather than breast cancer resistance protein or organic cation transporter 1, contributes to acquisition of imatinib-resistance in K562 cells. Pharm Res. 2008;25(4):827-35.

179.	Widmer N, Colombo S, Buclin T, Decosterd LA. Functional consequence of MDR1 expression on imatinib intracellular concentrations. Blood. 2003;102(3):1142.

180.	Park SH, Park CJ, Kim DY, Lee BR, Kim YJ, Cho YU, et al. MRP1 and P-glycoprotein expression assays would be useful in the additional detection of treatment non-responders in CML patients without ABL1 mutation. Leuk Res. 2015;39(10):1109-16.

181.	Eadie LN, Dang P, Saunders VA, Yeung DT, Osborn MP, Grigg AP, et al. The clinical significance of ABCB1 overexpression in predicting outcome of CML patients undergoing first-line imatinib treatment. Leukemia. 2017;31(1):75-82.

182.	Eadie LN, Hughes TP, White DL. ABCB1 Overexpression Is a Key Initiator of Resistance to Tyrosine Kinase Inhibitors in CML Cell Lines. PLoS One. 2016;11(8):e0161470.

183.	Hegedus C, Ozvegy-Laczka C, Apati A, Magocsi M, Nemet K, Orfi L, et al. Interaction of nilotinib, dasatinib and bosutinib with ABCB1 and ABCG2: implications for altered anti-cancer effects and pharmacological properties. Br J Pharmacol. 2009;158(4):1153-64.

184.	Hiwase DK, Saunders V, Hewett D, Frede A, Zrim S, Dang P, et al. Dasatinib cellular uptake and efflux in chronic myeloid leukemia cells: therapeutic implications. Clin Cancer Res. 2008;14(12):3881-8.

185.	Hamada A, Miyano H, Watanabe H, Saito H. Interaction of imatinib mesilate with human P-glycoprotein. J Pharmacol Exp Ther. 2003;307(2):824-8.

186.	Dohse M, Scharenberg C, Shukla S, Robey RW, Volkmann T, Deeken JF, et al. Comparison of ATP-binding cassette transporter interactions with the tyrosine kinase inhibitors imatinib, nilotinib and dasatinib. Drug Metab Dispos. 2010;38(8):1371-80.

187.	Hiwase DK, Saunders VA, Nievergall E, Ross DD, White DL, Hughes TP. Dasatinib targets chronic myeloid leukemia-CD34+ progenitors as effectively as it targets mature cells. Haematologica. 2013;98(6):896-900.

188.	Allikmets R, Schriml LM, Hutchinson A, Romano-Spica V, Dean M. A human placenta-specific ATP-binding cassette gene (ABCP) on chromosome 4q22 that is involved in multidrug resistance. Cancer Res. 1998;58(23):5337-9.

189.	Damiani D, Tiribelli M, Geromin A, Michelutti A, Cavallin M, Sperotto A, et al. ABCG2 overexpression in patients with acute myeloid leukemia: Impact on stem cell transplantation outcome. Am J Hematol. 2015;90(9):784-9.

190.	Meyer zu Schwabedissen HE, Kroemer HK. In vitro and in vivo evidence for the importance of breast cancer resistance protein transporters (BCRP/MXR/ABCP/ABCG2). Handb Exp Pharmacol. 2011(201):325-71.

191.   Polgar O, Robey RW, Bates SE. ABCG2: structure, function and role in drug response. Expert Opin Drug Metab Toxicol. 2008;4(1):1-15.

192.   McDevitt CA, Collins RF, Conway M, Modok S, Storm J, Kerr ID, et al. Purification and 3D structural analysis of oligomeric human multidrug transporter ABCG2. Structure. 2006;14(11):1623-32.

193.   Taylor NMI, Manolaridis I, Jackson SM, Kowal J, Stahlberg H, Locher KP. Structure of the human multidrug transporter ABCG2. Nature. 2017;546(7659):504-9.

194.   Jackson SM, Manolaridis I, Kowal J, Zechner M, Taylor NM, Bause M, et al. Structural basis of small-molecule inhibition of human multidrug transporter ABCG2. Nat Struct Mol Biol. 2018;25(4):333.

195.   Beretta GL, Cassinelli G, Pennati M, Zuco V, Gatti L. Overcoming ABC transporter-mediated multidrug resistance: the dual role of tyrosine kinase inhibitors as multitargeting agents. Eur J Med Chem. 2017;142:271-89.

196.   Fletcher JI, Williams RT, Henderson MJ, Norris MD, Haber M. ABC transporters as mediators of drug resistance and contributors to cancer cell biology. Drug Resist Update. 2016;26:1-9.

197.   Hegedűs C, Szakács G, Homolya L, Orbán TI, Telbisz Á, Jani M, et al. Ins and outs of the ABCG2 multidrug transporter: an update on in vitro functional assays. Adv Drug Deliver Rev. 2009;61(1):47-56.

198.   Özvegy-Laczka C, Hegedűs T, Várady G, Ujhelly O, Schuetz JD, Váradi A, et al. High-Affinity Interaction of Tyrosine Kinase Inhibitors with the ABCG2 Multidrug Transporter. Mol Pharmacol. 2004;65(6):1485-95.

199.   de Lima LT, Vivona D, Bueno CT, Hirata RD, Hirata MH, Luchessi AD, et al. Reduced ABCG2 and increased SLC22A1 mRNA expression are associated with imatinib response in chronic myeloid leukemia. Med Oncol. 2014;31(3):851.

200.   Gromicho M, Dinis J, Magalhaes M, Fernandes AR, Tavares P, Laires A, et al. Development of imatinib and dasatinib resistance: dynamics of expression of drug transporters ABCB1, ABCC1, ABCG2, MVP, and SLC22A1. Leukemia Lymphoma. 2011;52(10):1980-90.

201.   Eadie LN, Saunders VA, Hughes TP, White DL. Degree of kinase inhibition achieved in vitro by imatinib and nilotinib is decreased by high levels of ABCB1 but not ABCG2. Leukemia Lymphoma. 2013;54(3):569-78.

202.   Kim Y-K, Lee S-S, Jeong S-H, Ahn J-S, Yang D-H, Lee J-J, et al. OCT-1, ABCB1, and ABCG2 expression in imatinib-resistant chronic myeloid leukemia treated with dasatinib or nilotinib. Chonnam Med J. 2014;50(3):102-11.

203.   Donato NJ, Wu JY, Stapley J, Gallick G, Lin H, Arlinghaus R, et al. BCR-ABL independence and LYN kinase overexpression in chronic myelogenous leukemia cells selected for resistance to STI571. Blood. 2003;101(2):690-8.

204.   Wu J, Meng F, Kong LY, Peng Z, Ying Y, Bornmann WG, et al. Association between imatinib-resistant BCR-ABL mutation-negative leukemia and persistent activation of LYN kinase. J Natl Cancer Inst. 2008;100(13):926-39.

205.   Tang C, Schafranek L, Watkins DB, Parker WT, Moore S, Prime JA, et al. Tyrosine kinase inhibitor resistance in chronic myeloid leukemia cell lines: investigating resistance pathways. Leukemia Lymphoma. 2011;52(11):2139-47.

206.   Dai Y, Rahmani M, Corey SJ, Dent P, Grant S. A Bcr/Abl-independent, Lyn-dependent form of imatinib mesylate (STI-571) resistance is associated with altered expression of Bcl-2. J Biol Chem. 2004;279(33):34227-39.

207. Mahon F-X, Hayette S, Lagarde V, Belloc F, Turcq B, Nicolini F, et al. Evidence that resistance to nilotinib may be due to BCR-ABL, Pgp, or Src kinase overexpression. Cancer Res. 2008;68(23):9809-16.

208. Hentschel J, Rubio I, Eberhart M, Hipler C, Schiefner J, Schubert K, et al. BCR-ABL- and Ras-independent activation of Raf as a novel mechanism of Imatinib resistance in CML. International journal of oncology. 2011;39(3):585-91.

209. Ma L, Shan Y, Bai R, Xue L, Eide CA, Ou J, et al. A therapeutically targetable mechanism of BCR-ABL-independent imatinib resistance in chronic myeloid leukemia. Sci Transl Med. 2014;6(252):252ra121.

210. Peng B, Lloyd P, Schran H. Clinical pharmacokinetics of imatinib. Clin Pharmacokinet. 2005;44(9):879-94.

211. van Erp NP, Gelderblom H, Guchelaar HJ. Clinical pharmacokinetics of tyrosine kinase inhibitors. Cancer treatment reviews. 2009;35(8):692-706.

212. Gschwind H-P, Pfaar U, Waldmeier F, Zollinger M, Sayer C, Zbinden P, et al. Metabolism and disposition of imatinib mesylate in healthy volunteers. Drug Metab Dispos. 2005;33(10):1503-12.

213. Clevers H. The cancer stem cell: premises, promises and challenges. Nat Med. 2011;17(3):313.

214. O'Hare T, Corbin AS, Druker BJ. Targeted CML therapy: controlling drug resistance, seeking cure. Curr Opin Genetics Dev. 2006;16(1):92-9.

215. Eiring AM, Deininger MW. Individualizing kinase-targeted cancer therapy: the paradigm of chronic myeloid leukemia. Genome Biol. 2014;15(9):461.

216. Hiwase DK, White DL, Powell JA, Saunders VA, Zrim SA, Frede AK, et al. Blocking cytokine signaling along with intense Bcr-Abl kinase inhibition induces apoptosis in primary CML progenitors. Leukemia. 2010;24(4):771-8.

217. Liu J, Joha S, Idziorek T, Corm S, Hetuin D, Philippe N, et al. BCR-ABL mutants spread resistance to non-mutated cells through a paracrine mechanism. Leukemia. 2008;22(4):791-9.

218. Zahreddine H, Borden K. Mechanisms and insights into drug resistance in cancer. Front Pharmacol. 2013;4:28.

219. Foo J, Leder K, Mumenthaler SM. Cancer as a moving target: understanding the composition and rebound growth kinetics of recurrent tumors. Evol Appl. 2013;6(1):54-69.

220. Hanahan D, Weinberg RA. Hallmarks of cancer: the next generation. Cell. 2011;144(5):646-74.

221. Donnenberg VS, Donnenberg AD. Multiple drug resistance in cancer revisited: the cancer stem cell hypothesis. J Clin Pharmacol. 2005;45(8):872-7.

222. Mughal TI, Radich JP, Deininger MW, Apperley JF, Hughes TP, Harrison CJ, et al. Chronic myeloid leukemia: reminiscences and dreams. Haematologica. 2016;101(5):541-58.

223. Laurent E, Talpaz M, Kantarjian H, Kurzrock R. The BCR gene and philadelphia chromosome-positive leukemogenesis. Cancer Res. 2001;61(6):2343-55.

224. Kamens J. Addgene: Making Materials Sharing "Science As Usual". PLoS Biol. 2014;12(11).

225. Kweon SM, Cho YJ, Minoo P, Groffen J, Heisterkamp N. Activity of the Bcr GTPase-activating domain is regulated through direct protein/protein interaction with the Rho guanine nucleotide dissociation inhibitor. J Biol Chem. 2008;283(6):3023-30.

226. Warmuth M, Kim S, Gu XJ, Xia G, Adrian F. Ba/F3 cells and their use in kinase drug discovery. Curr Opin Oncol. 2007;19(1):55-60.

227.   Persons DA, Mehaffey MG, Kaleko M, Nienhuis AW, Vanin EF. An improved method for generating retroviral producer clones for vectors lacking a selectable marker gene. Blood Cell Mol Dis. 1998;24(2):167-82.

228.   White D, Saunders V, Lyons AB, Branford S, Grigg A, To LB, et al. In vitro sensitivity to imatinib-induced inhibition of ABL kinase activity is predictive of molecular response in patients with de novo CML. Blood. 2005;106(7):2520-6.

229.   Syrmis M, Moser R, Whiley D, Vaska V, Coombs G, Nissen M, et al. Comparison of a multiplexed MassARRAY system with real-time allele-specific PCR technology for genotyping of methicillin-resistant Staphylococcus aureus. Clin Microbiol Infect. 2011;17(12):1804-10.

230.   Allen JD, van Loevezijn A, Lakhai JM, van der Valk M, van Tellingen O, Reid G, et al. Potent and specific inhibition of the breast cancer resistance protein multidrug transporter in vitro and in mouse intestine by a novel analogue of fumitremorgin C. Mol Cancer Ther. 2002;1(6):417-25.

231.   Robinson MD, McCarthy DJ, Smyth GK. edgeR: a Bioconductor package for differential expression analysis of digital gene expression data. Bioinformatics. 2010;26(1):139-40.

232.   Dobin A, Davis CA, Schlesinger F, Drenkow J, Zaleski C, Jha S, et al. STAR: ultrafast universal RNA-seq aligner. Bioinformatics. 2013;29(1):15-21.

233.   Nicorici D, Satalan M, Edgren H, Kangaspeska S, Murumagi A, Kallioniemi O, et al. FusionCatcher-a tool for finding somatic fusion genes in paired-end RNA-sequencing data. BioRxiv. 2014:011650.

234.   Jabbour EJ, Hughes TP, Cortés JE, Kantarjian HM, Hochhaus A. Potential mechanisms of disease progression and management of advanced-phase chronic myeloid leukemia. Leukemia Lymphoma. 2014;55(7):1451-62.

235.   Gabriel S, Ziaugra L, Tabbaa D. SNP genotyping using the Sequenom MassARRAY iPLEX platform. Curr Protoc Hum Genet. 2009;Chapter 2:Unit 2 12.

236.   Magadum S, Banerjee U, Murugan P, Gangapur D, Ravikesavan R. Gene duplication as a major force in evolution. J Genet. 2013;92(1):155-61.

237.   Reams AB, Roth JR. Mechanisms of Gene Duplication and Amplification. CSH Perspect Biol. 2015;7(2):a016592.

238.   Wacker SA, Houghtaling BR, Elemento O, Kapoor TM. Using transcriptome sequencing to identify mechanisms of drug action and resistance. Nat Chem Biol. 2012;8(3):235-7.

239.   Roberts KG, Mullighan CG. Genomics in acute lymphoblastic leukaemia: insights and treatment implications. Nat Rev Clin Oncol. 2015;12(6):344-57.

240.   Giuffre A, Pabon-Pena C, Novak B, Joshi S, Ong J, Visitacion M, et al. The Agilent Technologies' SureSelect™ All Exon Product Portfolio: High Performance Target Enrichment System for Human and Mouse Exome Sequencing on Illumina and SOLiD Platforms. J Biomol Tech. 2011;22(Supplement):S41-S.

241.   Newman AM, Bratman SV, Stehr H, Lee LJ, Liu CL, Diehn M, et al. FACTERA: a practical method for the discovery of genomic rearrangements at breakpoint resolution. Bioinformatics. 2014;30(23):3390-3.

242.   Noll JE, Hewett DR, Williams SA, Vandyke K, Kok C, To LB, et al. SAMSN1 Is a Tumor Suppressor Gene in Multiple Myeloma. Neoplasia. 2014;16(7):572-85.

243.   le Coutre P, Tassi E, Varella-Garcia M, Barni R, Mologni L, Cabrita G, et al. Induction of resistance to the Abelson inhibitor STI571 in human leukemic cells through gene amplification. Blood. 2000;95(5):1758-66.

244.   Mayer BJ, Ren R, Clark KL, Baltimore D. A putative modular domain present in diverse signaling proteins. Cell. 1993;73(4):629-30.

245.   Haslam RJ, Koide HB, Hemmings BA. Pleckstrin domain homology. Nature. 1993;363(6427):309-10.

246.   Lenoir M, Kufareva I, Abagyan R, Overduin M. Membrane and protein interactions of the pleckstrin homology domain superfamily. Membranes. 2015;5(4):646-63.

247.   Blomberg N, Baraldi E, Nilges M, Saraste M. The PH superfold: a structural scaffold for multiple functions. Trends Biochem Sci. 1999;24(11):441-5.

248.   Zheng Y. Dbl family guanine nucleotide exchange factors. Trends Biochem Sci. 2001;26(12):724-32.

249.   Reckel S, Gehin C, Tardivon D, Georgeon S, Kükenshöner T, Löhr F, et al. Structural and functional dissection of the DH and PH domains of oncogenic Bcr-Abl tyrosine kinase. Nat Commun. 2017;8:2101.

250.   Cutler JA, Tahir R, Sreenivasamurthy SK, Mitchell C, Renuse S, Nirujogi RS, et al. Differential signaling through p190 and p210 BCR-ABL fusion proteins revealed by interactome and phosphoproteome analysis. Leukemia. 2017;31(7):1513-24.

251.   Viaud J, Gaits-Iacovoni F, Payrastre B. Regulation of the DH–PH tandem of guanine nucleotide exchange factor for Rho GTPases by phosphoinositides. Adv Biol Regulat. 2012;52(2):303-14.

252.   Zohn IM, Campbell SL, Khosravi-Far R, Rossman KL, Der CJ. Rho family proteins and Ras transformation: the RHOad less traveled gets congested. Oncogene. 1998;17(11 Reviews):1415-38.

253.   Adams J, Houston H, Allen J, Lints T, Harvey R. The hematopoietically expressed vav proto-oncogene shares homology with the dbl GDP-GTP exchange factor, the bcr gene and a yeast gene (CDC24) involved in cytoskeletal organization. Oncogene. 1992;7(4):611-8.

254.   Sahay S, Pannucci NL, Mahon GM, Rodriguez PL, Megjugorac NJ, Kostenko EV, et al. The RhoGEF domain of p210 Bcr-Abl activates RhoA and is required for transformation. Oncogene. 2007;27:2064.

255.   Kawai T, Sanjo H, Akira S. Duet is a novel serine/threonine kinase with Dbl-Homology (DH) and Pleckstrin-Homology (PH) domains. Gene. 1999;227(2):249-55.

256.   Harnois T, Constantin B, Rioux A, Grenioux E, Kitzis A, Bourmeyster N. Differential interaction and activation of Rho family GTPases by p210bcr-abl and p190bcr-abl. Oncogene. 2003;22:6445.

257.   Daubon T, Chasseriau J, El Ali A, Rivet J, Kitzis A, Constantin B, et al. Differential motility of p190bcr-abl- and p210bcr-abl-expressing cells: respective roles of Vav and Bcr-Abl GEFs. Oncogene. 2008;27(19):2673-85.

258.   Demehri S, O'Hare T, Eide CA, Smith CA, Tyner JW, Druker BJ, et al. The function of the pleckstrin homology domain in BCR-ABL-mediated leukemogenesis. Leukemia. 2010;24(1):226-9.

259.   Demehri S, O'Hare T, Wood LJ, Loriaux M, Druker BJ, Deininger MW. BCR-ABL Lacking the Pleckstrin Homology (PH) Domain of BCR Induces a More Aggressive Leukemia Than P210BCR-ABL in a Murine Model of CML. Am Soc Hematology; 2004. p. 2564.

260.   Crampe M, Haslam K, Groarke E, Kelleher E, O'Shea D, Conneally E, et al. Chronic Myeloid Leukemia with an e6a2 BCR-ABL1 Fusion Transcript: Cooperating Mutations at Blast Crisis and Molecular Monitoring. Case Rep Hematol. 2017;2017:9071702.

261.   Stewart MJ, Cox G, Reifel-Miller A, Kim SY, Westbrook CA, Leibowitz DS. A novel transcriptional suppressor located within a downstream intron of the BCR gene. J Biol Chem. 1994;269(14):10820-9.

262.   Ciuffi A. Mechanisms governing lentivirus integration site selection. Curr Gene Ther. 2008;8(6):419-29.

263.   Eberth A, Ahmadian MR. In vitro GEF and GAP assays. Curr Protoc Cell Biol. 2009;Chapter 14:Unit 14 9.

264.   Robey RW, Honjo Y, Morisaki K, Nadjem TA, Runge S, Risbood M, et al. Mutations at amino-acid 482 in the ABCG2 gene affect substrate and antagonist specificity. Br J Cancer. 2003;89:1971.

265.   Takara K, Yamamoto K, Matsubara M, Minegaki T, Takahashi M, Yokoyama T, et al. Effects of alpha-adrenoceptor antagonists on ABCG2/BCRP-mediated resistance and transport. PLoS One. 2012;7(2):e30697.

266.   Henrich CJ, Robey RW, Bokesch HR, Bates SE, Shukla S, Ambudkar SV, et al. New inhibitors of ABCG2 identified by high-throughput screening. Mol Cancer Ther. 2007;6(12 Pt 1):3271-8.

267.   Weidner LD, Zoghbi SS, Lu S, Shukla S, Ambudkar SV, Pike VW, et al. The Inhibitor Ko143 Is Not Specific for ABCG2. J Pharmacol Exp Ther. 2015;354(3):384-93.

268.   White DL, Lu L, Clackson TP, Saunders VA, Hughes TP. ATP dependent efflux transporters ABCB1 and ABCG2 are unlikely to impact the efficacy, or mediate resistance to the tyrosine kinase inhibitor, ponatinib. Blood; 2011. p. 2745.

269.   Lu L, Saunders V, Leclercq T, Hughes T, White D. Ponatinib is not transported by ABCB1, ABCG2 or OCT-1 in CML cells. Leukemia. 2015;29(8):1792.

270.   Sen R, Natarajan K, Bhullar J, Shukla S, Fang HB, Cai L, et al. The novel BCR-ABL and FLT3 inhibitor ponatinib is a potent inhibitor of the MDR-associated ATP-binding cassette transporter ABCG2. Mol Cancer Ther. 2012;11(9):2033-44.

271.   Westover D, Li F. New trends for overcoming ABCG2/BCRP-mediated resistance to cancer therapies. J Exp Clin Cancer Res. 2015;34:159.

272.   Burger H, van Tol H, Boersma AW, Brok M, Wiemer EA, Stoter G, et al. Imatinib mesylate (STI571) is a substrate for the breast cancer resistance protein (BCRP)/ABCG2 drug pump. Blood. 2004;104(9):2940-2.

273.   Shukla S, Wu C-P, Ambudkar SV. Development of inhibitors of ATP-binding cassette drug transporters – present status and challenges. Expert Opin Drug Metab Toxicol. 2008;4(2):205-23.

274.   Robey RW, To KK, Polgar O, Dohse M, Fetsch P, Dean M, et al. ABCG2: a perspective. Adv Drug Deliv Rev. 2009;61(1):3-13.

275.   Vlaming ML, Lagas JS, Schinkel AH. Physiological and pharmacological roles of ABCG2 (BCRP): recent findings in Abcg2 knockout mice. Adv Drug Del Rev. 2009;61(1):14-25.

276.   Matsuo H, Takada T, Ichida K, Nakamura T, Nakayama A, Ikebuchi Y, et al. Common defects of ABCG2, a high-capacity urate exporter, cause gout: a function-based genetic analysis in a Japanese population. Science Transl Med. 2009;1(5):5ra11.

277.   Hiwase DK, Eadie L, Saunders V, Hughes T, White DL. Proton pump inhibitors augment nilotinib and dasatinib mediated Bcr-Abl kinase inhibition. Am Soc Hematology; 2010. p. 3991.

278.   Leonard GD, Fojo T, Bates SE. The role of ABC transporters in clinical practice. Oncologist. 2003;8(5):411-24.

279.   D'Cunha R, Bae S, Murry DJ, An G. TKI combination therapy: strategy to enhance dasatinib uptake by inhibiting Pgp- and BCRP-mediated efflux. Biopharm Drug Dispos. 2016;37(7):397-408.

280.   Selbo PK, Weyergang A, Eng MS, Bostad M, Maelandsmo GM, Hogset A, et al. Strongly amphiphilic photosensitizers are not substrates of the cancer stem cell marker ABCG2 and

provides specific and efficient light-triggered drug delivery of an EGFR-targeted cytotoxic drug. J Control Release. 2012;159(2):197-203.

281.   Wolf N, Kone A, Priestley G, Bartelmez S. In vivo and in vitro characterization of long-term repopulating primitive hematopoietic cells isolated by sequential Hoechst 33342-rhodamine 123 FACS selection. Exp Hematol. 1993;21(5):614-22.

282.   Krishnamurthy P, Schuetz JD. Role of ABCG2/BCRP in biology and medicine. Annu Rev Pharmacol Toxicol. 2006;46:381-410.

283.   Zhou S, Schuetz JD, Bunting KD, Colapietro AM, Sampath J, Morris JJ, et al. The ABC transporter Bcrp1/ABCG2 is expressed in a wide variety of stem cells and is a molecular determinant of the side-population phenotype. Nat Med. 2001;7(9):1028-34.

284.   Wee B, Pietras A, Ozawa T, Bazzoli E, Podlaha O, Antczak C, et al. ABCG2 regulates self-renewal and stem cell marker expression but not tumorigenicity or radiation resistance of glioma cells. Sci Rep. 2016;6:25956.

285.   Soverini S, Colarossi S, Gnani A, Castagnetti F, Rosti G, Bosi C, et al. Resistance to dasatinib in Philadelphia-positive leukemia patients and the presence or the selection of mutations at residues 315 and 317 in the BCR-ABL kinase domain. Haematologica. 2007;92(3):401-4.

286.   Camgoz A, Gencer EB, Ural AU, Baran Y. Mechanisms responsible for nilotinib resistance in human chronic myeloid leukemia cells and reversal of resistance. Leukemia Lymphoma. 2013;54(6):1279-87.

287.   Wang Z, Chen W. A convenient cell culture model for CML acquired resistance through BCR-ABL mutations. Chronic Myeloid Leukemia: Springer; 2016. p. 149-57.

288.   Lu L, Saunders V, Kok CH, Leclercq T, Hughes TP, White DL. Modeling Ponatinib Resistance in BCR-ABL1+ Cell Lines: Implications for Ponatinib Resistance in TKI-Resistant and TKI-naïve Patients. Blood. 2014;124(21):4515.

289.   Okabe S, Tauchi T, Ohyashiki K. Characteristics of dasatinib-and imatinib-resistant chronic myelogenous leukemia cells. Clin Cancer Res. 2008;14(19):6181-6.

290.   Okabe S, Tauchi T, Broxmeyer HE, Ohyashiki K. Mechanism of Drug Resistance to Dasatinib (BMS-354825) and Imatinib in Chronic Myelogenous Leukemia Cells. Blood; 2006. p. 1386.

291.   Lu L, Kok CH, Saunders VA, Wang J, McLean JA, Hughes TP, et al. Modelling ponatinib resistance in tyrosine kinase inhibitor-naive and dasatinib resistant BCR-ABL1+ cell lines. Oncotarget. 2018;9(78):34735-47.

292.   Mizuta S, Sawa M, Tsurumi H, Matsumoto K, Miyao K, Hara T, et al. Plasma concentrations of dasatinib have a clinical impact on the frequency of dasatinib dose reduction and interruption in chronic myeloid leukemia: an analysis of the DARIA 01 study. Int J Clin Oncol. 2018;23(5):1-9.

293.   Kuczynski EA, Sargent DJ, Grothey A, Kerbel RS. Drug rechallenge and treatment beyond progression—implications for drug resistance. Nat Rev Clin Oncol. 2013;10(10):571.

294.   Mahon F-X, Réa D, Guilhot J, Guilhot F, Huguet F, Nicolini F, et al. Discontinuation of imatinib in patients with chronic myeloid leukaemia who have maintained complete molecular remission for at least 2 years: the prospective, multicentre Stop Imatinib (STIM) trial. Lancet Oncol. 2010;11(11):1029-35.

295.   Goh H-G, Kim Y-J, Kim D-W, Kim H-J, Kim S-H, Jang S-E, et al. Previous best responses can be re-achieved by resumption after imatinib discontinuation in patients with chronic myeloid leukemia: implication for intermittent imatinib therapy. Leukemia Lymphoma. 2009;50(6):944-51.

296.   Rudert F, Visser E, Gradl G, Grandison P, Shemshedini L, Wang Y, et al. pLEF, a novel vector for expression of glutathione S-transferase fusion proteins in mammalian cells. Gene. 1996;169(2):281-2.